LANDSCAPE OF TEMPERATE ICE CAPS

by

Tómas Jóhannesson

A dissertation submitted in partial fulfillment
of the requirements for the degree of

Doctor of Philosophy

University of Washington

1992

Approved by Charles F. Raymond

(Chairperson of Supervisory Committee)

Program Authorized
to Offer Degree Geophysics Program

Date 30 April, 1992

Doctoral Dissertation

In presenting this dissertation in partial fulfillment of the requirements for the Doctoral degree at the University of Washington, I agree that the Library shall make its copies freely available for inspection. I further agree that extensive copying of this dissertation is allowable only for scholarly purposes, consistent with "fair use" as prescribed in the U.S. Copyright Law. Requests for copying or reproduction of this dissertation may be referred to University Microfilms, 300 North Zeeb Road, Ann Arbor, Michigan 48106, to whom the author has granted "the right to reproduce and sell (a) copies of the manuscript in microform and/or (b) printed copies of the manuscript made from microform."

Signature Tómas Jóhannesson

Date 30 April, 1992

University of Washington

Abstract

Landscape of Temperate Ice Caps

by Tómas Jóhannesson

Chairperson of the Supervisory Committee: Professor Charles F. Raymond
Geophysics Program

The landscape of temperate ice caps is analyzed starting with a linearization of the non-linear ice flow equations. The theoretical treatment is based on *ice flux filters* which describe how localized bedrock and ice surface perturbations affect the ice flux. The filters are used to derive steady state ice surface undulations corresponding to given bedrock undulations and to formulate a time-dependent theory describing non-steady ice flow.

The time-dependent theory indicates that observed glacier landscape is mainly a result of steady ice flow over the bedrock topography. The theory implies that the differential equations describing time-dependent glacier flow are primarily diffusive in nature. Non-steady glacier waves are in general predicted to disappear by diffusion before they have propagated one wavelength. Too much emphasis has been placed on propagation of glacier waves by earlier authors on glacier dynamics.

Steady ice surface undulations are computed from a filter (Green's function) which describes the ice surface perturbation corresponding to a sharp basal spike (δ-function). For two-dimensional flow, this perturbation has the following features. (1) There is a "standing wave" in the ice surface above the basal spike with a peak on the upstream side and a trough on the downstream side. It's wavelength is 1.5-3 ice thicknesses. (2) There is a long exponentially decaying tail on the upstream side of the standing wave. (3) The total volume of ice in the ice surface perturbation is exactly equal to the volume of the basal spike. The standing wave explains the many observations of ice surface

undulations on ice caps and ice sheets with wavelengths on the order of 3-4 ice thicknesses which are reported in the glaciological literature and which have not been adequately explained before.

Glacier landscape along flow lines from the Hofsjökull ice cap, Central Iceland, is in good accordance with the two-dimensional theory. It appears that the geometry of the ice surface is mostly determined by ice flow *over* the bedrock undulations rather than *around* them. Detailed comparison of measured and predicted surface undulations verifies the prediction of a standing wave in the ice surface geometry corresponding to a basal spike.

TABLE OF CONTENTS

		Page
LIST OF FIGURES		viii
LIST OF TABLES		xiii
LIST OF SYMBOLS		xiv
CHAPTER 1: INTRODUCTION		1
1.1	GLACIER LANDSCAPE	1
1.2	GOALS OF DISSERTATION	6
1.3	ORGANIZATION OF DISSERTATION	8
CHAPTER 2: PREVIOUS WORK		10
2.1	OBSERVATIONS OF SURFACE UNDULATIONS	10
2.2	ANALYSIS BASED ON LOCAL ICE THICKNESS AND SURFACE SLOPE	13
2.3	ANALYTICAL ANALYSIS FOR LINEAR NEWTONIAN RHEOLOGY	15
2.4	LONGITUDINAL STRESS GRADIENTS	17
2.5	NUMERICAL SOLUTION OF THE FULL PROBLEM	19
2.6	LONGITUDINAL AVERAGING	21
2.7	BOUNDARY LAYER AT THE SURFACE	23
2.8	SUMMARY AND DISCUSSION	23
CHAPTER 3: ICE DYNAMICS		26
3.1	INTRODUCTION	26
3.2	NOTATION	26
	3.2.1 Vector notation	26
	3.2.2 Dimensional and non-dimensional variables	27
	3.2.3 List of symbols	28
3.3	MATHEMATICAL PRELIMINARIES	28

3.3.1 Perturbation expansions 28
3.3.2 Fourier transforms 29
3.3.3 Transfer functions 30
3.3.4 Green's functions 30
3.3.5 Continuous analysis — discrete data 31
3.4 FIELD EQUATIONS 32
3.4.1 Conservation of mass 32
3.4.2 Conservation of momentum 32
3.4.3 Constitutive relations for ice 32
3.5 BOUNDARY CONDITIONS 34
3.5.1 Kinematic boundary condition at the upper surface 34
3.5.2 Stress boundary condition at the upper surface 34
3.5.3 Kinematic boundary condition at the base 34
3.5.4 Basal sliding 35
3.6 ICE FLUX 36
3.6.1 General 36
3.6.2 Time-dependent evolution of surface geometry 36
3.6.3 Steady state 37
3.7 LAMINAR FLOW APPROXIMATION 37
3.7.1 General 37
3.7.2 Linearization of ice flux for laminar flow 39

CHAPTER 4: TWO-DIMENSIONAL THEORY 41
4.1 INTRODUCTION 41
4.2 LONG SCALE DATUM FLOW 41
4.2.1 General 41
4.2.2 Non-dimensional formulation 42
4.2.3 Boundary layer at the surface 44
4.2.4 Derivation of the long scale datum flow 45
4.2.5 Datum long scale solution 52
4.2.6 Failure for short scales 55

4.3 SHORT SCALE FLOW 56
4.3.1 General 56
4.3.2 Non-dimensional formulation 57
4.3.3 Linearized field equations for small perturbations 59
4.3.4 Datum ice flow 62
4.3.5 Datum viscosity 63
4.3.6 Linearization of boundary conditions 67
4.3.7 Ice flux perturbations 69
4.3.8 Steady state ice surface undulations 71
4.4 LAMINAR FLOW APPROXIMATION 72
4.4.1 General 72
4.4.2 Transfer functions 74
4.4.3 Green's functions 75
4.4.4 Transfer of long undulations 79
4.5 LINEAR NEWTONIAN FLOW 80
4.5.1 General 80
4.5.2 The stream function 81
4.5.3 Field equations 81
4.5.4 Boundary conditions 82
4.5.5 Transformation into the wave number domain 83
4.5.6 Ice flux filters 84
4.5.7 Steady state ice surface undulations 89
4.5.8 Transfer functions 90
4.5.9 Green's functions 94
4.5.10 Slope filters 98
4.5.11 Discussion 101
4.6 NON-LINEAR FLOW — FLUX PERTURBATIONS 103
4.6.1 General 103
4.6.2 Stream and stress functions 106
4.6.3 Field equations 107

4.6.4 Boundary conditions 108
4.6.5 Numerical formulation 112
4.6.6 Verification of numerical computations 116
4.6.7 Flux filters 117
4.6.8 Simplified theory 124
4.6.9 Length-scales for longitudinal flow variations 133
4.6.10 Total flux 136
4.6.11 Relation to previous work 140
4.7 NON-LINEAR FLOW — PERTURBATIONS IN THE STEADY STATE SURFACE GEOMETRY 141
4.7.1 General 141
4.7.2 Transfer functions 143
4.7.3 Green's functions 146
4.7.4 Effect of longitudinal strain rate 153
4.7.5 Effect of basal sliding 154
4.7.6 Slope filters 154
4.7.7 How far can a glacier flow uphill? 157
4.7.8 Effect of mass balance variations 157
4.7.9 Relation to previous work 159

CHAPTER 5: THREE-DIMENSIONAL THEORY 165
5.1 INTRODUCTION 165
5.2 DATUM ICE FLOW AND PRELIMINARY ANALYSIS 165
5.2.1 General 165
5.2.2 Non-dimensional variables 166
5.2.3 Long scale datum flow 166
5.2.4 Datum viscosity for two-dimensional flow perturbations 169
5.2.5 Ice flux perturbations 171
5.2.6 Steady state ice surface undulations 172
5.2.7 Undulations along the direction of the datum flow 172
5.3 LAMINAR FLOW APPROXIMATION 176

5.3.1 General 176
5.3.2 Transfer functions 178
5.3.3 Green's functions 181
5.3.4 Transfer of undulations which are almost aligned with the datum flow 183
5.4 LINEAR NEWTONIAN FLOW 189
5.4.1 General 189
5.4.2 Stream function for three dimensional flow 189
5.4.3 Field equations 191
5.4.4 Boundary conditions 192
5.4.5 Ice flux divergence 195
5.4.6 Steady state ice surface undulations 195

CHAPTER 6: TIME-DEPENDENT GLACIER FLOW 204
6.1 INTRODUCTION 204
6.2 TIME-SCALES FOR GLACIER FLOW 205
6.3 MODIFIED KINEMATIC WAVE EQUATION 206
6.4 DIFFUSION TIME-SCALE 210
6.5 RELATIVE IMPORTANCE OF PROPAGATION AND DIFFUSION 213
6.6 DIFFUSION OF WAVE OGIVES 215
6.7 PROPAGATION OF KINEMATIC WAVES 218

CHAPTER 7: LANDSCAPE OF HOFSJÖKULL 220
7.1 INTRODUCTION 220
7.2 HOFSJÖKULL 220
7.2.1 General 220
7.2.2 Geometry 220
7.2.3 Mass balance 221
7.2.4 Datum velocity and strain rate 222
7.3 DIGITAL MAPS OF HOFSJÖKULL 224

7.4 ANALYSIS ALONG APPROXIMATE FLOW LINES 225
7.4.1 General 225
7.4.2 Blautukvíslarjökull 225
7.4.3 Þjórsárjökull 229
7.4.4 Sátujökull 231
7.4.5 Detrending 233
7.4.6 Ice surface filters 234
7.4.7 Slope filters 236
7.4.8 Results for laminar flow 236
7.4.9 Effect of detrending length scale 238
7.4.10 Results for full ice flow equations 239
7.4.11 Results for Blautukvíslarjökull 242
7.4.12 Results for Þjórsárjökull 245
7.4.13 Results for Sátujökull 248
7.5 ANALYSIS USING THREE-DIMENSIONAL LAMINAR FLOW THEORY 250
7.5.1 General 250
7.5.2 Detrending 250
7.5.3 Ice surface filters 251
7.5.4 Results 251
7.6 DISCUSSION AND SUMMARY OF RESULTS 256

CHAPTER 8: SYNOPSIS 259

LIST OF REFERENCES 265

APPENDIX 1: DISCRETE AND CONTINUOUS FILTERS 272
A1.1 INTRODUCTION 272
A1.2 ONE DIMENSION 273
A1.3 TWO DIMENSIONS 277

APPENDIX 2: STREAM FUNCTION FOR LINEAR RHEOLOGY — 2D 280

APPENDIX 3: STREAM FUNCTION FOR LINEAR RHEOLOGY — 3D 283

LIST OF FIGURES

Number Page

1.1.1. Surface and bedrock profiles along a flow line from Þjórsárjökull 2

1.1.2. Perspective views of the surface and bedrock of Þjórsárjökull 4

4.2.1. Coordinate system and length-scales for long scale analysis 42

4.3.1. Coordinate system for short scale analysis 57

4.3.2. Viscosity distribution predicted by Glen's flow law 64

4.3.3. Graphical interpretation of viscosity components 66

4.4.1. Transfer functions predicted by the laminar flow approximation 76

4.4.2. Green's functions predicted by the laminar flow approximation 77

4.5.1. Flux filters for linear Newtonian rheology and no basal sliding 87

4.5.2. Flux filters for linear Newtonian rheology and non-zero basal sliding 89

4.5.3. Transfer functions for linear Newtonian rheology and no basal sliding 91

4.5.4. Transfer functions for linear Newtonian rheology and non-zero basal sliding 92

4.5.5. Scaled Green's functions for linear Newtonian rheology and no basal sliding 95

4.5.6. Green's functions for linear Newtonian rheology and no basal sliding 96

4.5.7. Green's functions for linear Newtonian rheology and non-zero basal sliding 97

4.5.8. Steady state ice surface geometry above Gaussian basal mountains (with volume equal to 1) for linear Newtonian rheology 98

4.5.9. Steady state ice surface geometry above Gaussian basal mountains (with center height equal to 1) for linear Newtonian rheology 99

4.5.10. Surface slope filters for linear Newtonian rheology and no basal sliding 100

4.5.11. Surface slope filters for linear Newtonian rheology and non-zero basal sliding 101

4.6.1. Flux filters for linear Newtonian rheology, comparison of analytical and numerical results 116

4.6.2. Fourier transforms of flux filters for non-linear rheology, no basal sliding, $e = 0.01$ 120

4.6.3. Flux filters for non-linear rheology, no basal sliding, $e = 0.01$ 121

4.6.4. Flux filters for non-linear rheology, no basal sliding, $e = 0.001$ 122

4.6.5. Flux filters for non-linear rheology, non-zero basal sliding, $e = 0.01$ 123

4.6.6. Length-scale of longitudinal stress gradients for non-linear rheology 128

4.7.1. Transfer functions for non-linear rheology, no basal sliding 143

4.7.2. Transfer functions for non-linear rheology, non-zero basal sliding 144

4.7.3. Scaled Green's functions for non-linear rheology, no basal sliding, $e = 0.01$ 147

4.7.4. Green's functions for non-linear rheology, no basal sliding, $e = 0.01$ 148

4.7.5. Steady state ice surface geometry above Gaussian basal mountains (with volume equal to 1) for non-linear rheology 152

4.7.6. Green's functions for non-linear rheology, no basal sliding, $e = 0.001$ 154

4.7.7. Green's functions for non-linear rheology, non-zero basal sliding, $e = 0.01$ 155

4.7.8. Surface slope filters for non-linear rheology, no basal sliding 156

4.7.9. Transfer functions for non-linear rheology compared with transfer functions corresponding to the analyses of Kamb and Echelmeyer (1986a) and Robin (1967) 161

5.3.1. Perspective views of the transfer amplitude predicted by the laminar flow approximation for 3D glacier flow 180

5.3.2. Perspective views of the Green's function predicted by the laminar flow approximation for 3D glacier flow 182

5.3.3. Perspective views of the modified transfer amplitude predicted by the laminar flow approximation for 3D glacier flow 188

5.4.1. Perspective views of the transfer amplitude predicted by linear Newtonian rheology for 3D glacier flow 197

5.4.2. Perspective views of the modified transfer amplitude predicted by linear Newtonian rheology for 3D glacier flow 198

5.4.3. Perspective views of the modified Green's function predicted by linear Newtonian rheology for 3D glacier flow 199

5.4.4. Longitudinal and transverse sections through the Green's function predicted by linear Newtonian rheology for no basal sliding 201

5.4.5. Longitudinal and transverse sections through the Green's function predicted by linear Newtonian rheology for non-zero basal sliding 202

6.3.1. Wavelength dependent kinematic wave velocity for linear and non-linear rheology 208

6.3.2. Wavelength dependent diffusion coefficient for linear and non-linear rheology 209

6.5.1. Wavelength dependent ''quality factor'' $Q(\lambda)$ for linear and non-linear rheology 214

7.2.1. Location map for Hofsjökull 221

7.4.1. Perspective views of the surface and bedrock of Blautukvíslarjökull 226

7.4.2. Surface and bedrock profiles along flow lines from Blautukvíslarjökull 228

7.4.3. Surface and bedrock profiles along flow lines from Þjórsárjökull 230

7.4.4. Surface and bedrock profiles along flow lines from Sátujökull 232

7.4.5. Discrete filters for Blautukvíslarjökull, Þjórsárjökull and Sátujökull 235

7.4.6. Ice surface undulations predicted by the laminar flow approximation 237

7.4.7. Ice surface undulations predicted by the full ice flow equations 240

7.4.8. Ice surface undulations on Blautukvíslarjökull predicted by the full ice flow equations 243

7.4.9. Ice surface undulations on Þjórsárjökull predicted by the full ice flow equations 246

7.4.10. Ice surface undulations on Sátujökull predicted by the full ice flow equations 248

7.5.1. Ice surface undulations along flow lines on Þjórsárjökull predicted by the laminar flow approximation for 3D glacier flow 252

7.5.2. Ice surface undulations perpendicular to flow lines on Þjórsárjökull predicted by the laminar flow approximation for 3D glacier flow 254

LIST OF TABLES

Number Page

7.4.1. Flow lines from Blautukvíslarjökull 229

7.4.2. Flow lines from Þjórsárjökull 231

7.4.3. Flow lines from Sátujökull 233

7.4.4. Statistics of ice surface undulations for flow lines from Blautukvíslarjökull 244

7.4.5. Statistics of ice surface undulations for flow lines from Þjórsárjökull 245

7.4.6. Statistics of ice surface undulations for flow lines from Sátujökull 249

7.5.1. Statistics of ice surface undulations on Hofsjökull 255

LIST OF SYMBOLS

Symbols used in Chapter 3 and the following chapters are listed below. Physical variables, scales for physical variables, physical parameters and constants, and mathematical symbols are listed separately.

The notation of Chapter 2 describing previous work is different from the notation which is used in the rest of the dissertation. Symbols used in Chapter 2 are listed separately at the end of the list of symbols used in the other chapters.

PHYSICAL VARIABLES

Dimensional variables (but not physical constants) are indicated by the "~" sign, such that $\tilde{u}_i$ is a velocity vector in units of m/s or m/a. Variables without the "~" sign are non-dimensional, so that u_i is a non-dimensional velocity vector. Small perturbations are denoted by the "Δ" symbol, *e.g.* $\Delta\alpha$ for surface slope perturbations.

b	mass balance
d	depth below ice surface, $d = z_s - z$
d_b	thickness of boundary layer near the ice surface
g_i	acceleration of gravity vector
h	ice thickness, $h = z_s - z_b$
p	pressure, $p = -\sigma_{ii}/3$
q_d, q_s	ice flux contributions from internal deformation and basal sliding for laminar flow
q_i	ice flux vector, $i = x,y$
r	radio of ice flux contributions, $r = \tilde{q}_s/\tilde{q}_d$
t	time
u_i	ice velocity vector
u,v,w	velocity components

u_b	sliding velocity
x_i	position vector
x,y,z	space coordinates
z_b	z coordinate of the bedrock
z_s	z coordinate of the ice surface
α	surface slope
β	bedrock slope
γ	angle between the z-axis the vertical
Δq_e,Δq_n,Δq_a,Δq_b	ice flux perturbation components, Δq_e is called the shear stress component, Δq_n the normal stress component, Δq_a the advection component, and Δq_b the basal component
$\dot{\varepsilon}$	effective strain rate, $2\dot{\varepsilon}^2 = \dot{\varepsilon}_{ij}\dot{\varepsilon}_{ij}$
$\dot{\varepsilon}_{ij}$	strain rate tensor, $\dot{\varepsilon}_{ij} = \frac{1}{2}(\partial u_i/\partial x_j + \partial u_j/\partial x_i)$
η	viscosity
η_1,η_2,η_3	viscosities derived from a linearization of Glen's flow law
θ	angle between the x-axis and the bedrock profile
θ	two-dimensional stress function
σ_{ij}	stress tensor
σ_s	length scale of smoothing
τ	effective shear stress, $2\tau^2 = \tau_{ij}\tau_{ij}$
τ_{ij}	deviatoric stress tensor, $\tau_{ij} = \sigma_{ij} + p$
τ_b	basal shear stress
ξ,η,ζ	space coordinates
ψ	two-dimensional stream function
ψ_i	three-dimensional stream function

SCALES FOR PHYSICAL VARIABLES

Physical scales for the long scale analysis are denoted by upper case letters, *e.g.* H for a scale for the ice thickness. Scales for the short scale analysis are denoted by lower case letters with the subscript "0", *e.g.* t_0 for a time-scale.

H vertical length-scale, scale for the ice thickness

$\tilde{h}_0$ length-scale

L horizontal length-scale

T time scale (long scale analysis)

$\tilde{t}_0$ time scale (short scale analysis)

U scale for horizontal ice velocity

PHYSICAL PARAMETERS AND CONSTANTS

Physical constants are denoted by either upper case or lower case letters, *e.g.* A for the constant in Glen's flow law and g for the acceleration of gravity.

A constant in Glen's flow law, $bar^{-n}\ a^{-1}$, typical value for temperate ice and $n=3$ is 0.17 $bar^{-3}\ a^{-1}$

B constant in Glen's flow law, $bar\ a^{1/n}$, typical value for temperate ice and $n=3$ is 1.8 $bar\ a^{1/3}$

C constant in Weertman's sliding law, $bar^{-m}\ m\ a^{-1}$

g acceleration of gravity, 9.82 m/s^2

m power in Weertman's sliding law, dimensionless, typical value is 2

n power in Glen's flow law, dimensionless, typical value is 3

ρ ice density, 900 kg/m^3

MATHEMATICAL SYMBOLS AND DIMENSIONLESS PARAMETERS

Fourier transforms are indicated by the "^" sign, such that $\hat{f}$ is the Fourier transform of the function f. Terms in asymptotic expansions are indicated with superscripted numbers in parentheses, *e.g.* $f = f^{(0)} + \delta f^{(1)} + \delta^2 f^{(2)} + \cdots$.

A,B,C,D constants in a general expression for the stream function for linear Newtonian rheology for two-dimensional flow

A_i,B_i,C_i,D_i constants in a general expression for the stream function for linear Newtonian rheology for three-dimensional flow

$\vec{a}_i$ basis vectors of a coordinate system

$b(x)$ boxcar filter

b_1,b_2,b_3,b_4 constants used in the numerical formulation of two-dimensional ice flow

C_0 kinematic wave velocity

$C_0(k)$ wave number or wavelength dependent kinematic wave velocity

c dimensionless parameter describing the relative importance of basal sliding

D_0 diffusion coefficient

$D_0(k)$ wave number or wavelength dependent diffusion coefficient

$d(x)$ general function, string of δ-functions

d^* an independent variable which is used in the computation of the datum longitudinal deviatoric stress τ_{xx}

e a small dimensionless parameter that represents the ratio of the long scale longitudinal strain rate at the ice surface to the long scale shear strain rate at the bed

$f(x)$ general function, forcing function, filter in Kamb and Echelmeyer's filter theory

f_1,f_2,f_3,f_4 functions used in the numerical formulation of two-dimensional ice flow

$f_{i,j}_b, f_{i,j}_s$ functions used in the numerical formulation of two-dimensional ice flow

$\vec{f}$ general vector

G a stress gradient term involving $(\partial\tau_{xx}/\partial x)$ in the vertically integrated force equilibrium equations

G_e,G_n,G_b constants in a simplified derivation of flux filters

$g(x)$ general function, Green's function, filter function

$g^*(x)$ scaled Green's function

$g_e(x),g_n(x),g_b(x)$ flux filters; $g_e(x)$ is called the shear stress filter, $g_n(x)$ the normal stress filter, and $g_b(x)$ the basal filter

$g_\alpha(x)$ slope filter

$g_g(x)$,$g_t(x)$ filters which are used in a simplified derivation of flux filters

H_c,H_s functions related to the hyperbolic cosine and sine functions, $H_c(k) = \cosh k + ck\sinh k$, $H_s(k) = \sinh k + ck\cosh k$, where c is a dimensionless sliding parameter

$h(x)$ general function, solution corresponding to a forcing function $f(x)$

I_1,I_2,I_3,I_4,I_5 vertical integrals of the viscosity component η_2

$Im()$ imaginary part of a complex number

i complex imaginary unity, $i = \sqrt{-1}$

i,j subscripted indexes are used to denote vectors and tensors, *e.g.* u_i for a velocity vector and σ_{ij} for a stress tensor; the notation x_i and f_i is also used for a discrete sequence function values on a grid of equally spaced points in space, *e.g.* $f_i = f(x_i) = f(i\Delta x)$

K function related to the hyperbolic cosine and sine functions, $K = \cosh^2 k + k^2 + ck(\cosh k\sinh k + k)$, where c is a dimensionless sliding parameter

k wave number, $k = 2\pi/\lambda$

k_x,k_y wave number components along the x and y directions

L function related to the hyperbolic cosine and sine functions, $L = (2k + \cosh k\sinh k - k^2\tanh k)/(H_c + \cosh k)$

l filter length, length-scale for longitudinal stress gradients

l_1 length-scale for ice surface undulations for laminar flow

l_2 transverse length-scale for ice surface undulations for laminar flow in three dimensions

l_d decay length-scale for transient steady state flow

l_g length-scale for longitudinal stress gradients involving $(\partial\tau_{xx}/\partial x)$

l_t length-scale for longitudinal shear stress gradients involving $(\partial^2\tau_{xz}/\partial x^2)$

M function related to the hyperbolic cosine and sine functions, $M = (\cosh^2 k - (1+c)k^2)/(H_c + \cosh k)$

m_i unit vector normal to the ice surface

n_i unit vector normal to the bedrock

p_0,p_1,p_2, ... powers in an asymptotic expansion

$Q(k)$ wave number or wavelength dependent "quality factor" which describes the relative importance of propagation and diffusion of kinematic waves

$Re()$ real part of a complex number

$s(d^*)$ a function which is used in the computation of the datum longitudinal deviatoric stress τ_{xx}

s_1,s_2,s_3,s_4 constants used in the numerical formulation of two-dimensional ice flow

T a stress gradient term involving $(\partial^2\tau_{xz}/\partial x^2)$ in the vertically integrated force equilibrium equations

T_n,T_b constants in a simplified derivation of flux filters

$t(x)$ triangular filter

$t(k)$ complex transfer function (sometimes also transfer amplitude)

$w(x)$ weight function

$|t(k)|$ transfer amplitude

x,y,z independent variables

$x*$ scaled x coordinate

$<.>$ longitudinal weighted average

$*$ convolution operator, $g(x)*f(x) = \int g(x-\xi)f(\xi)d\xi$

∂ partial differentiation operator

$\vec{\nabla}$ gradient operator

$\vec{\nabla}.$ divergence operator

$\vec{\nabla}\times$ curl operator

∇^4 biharmonic operator, $\nabla^4 = \frac{\partial^4}{\partial x^4} + 2\frac{\partial^4}{\partial x^2\partial z^2} + \frac{\partial^4}{\partial z^4}$

$\Delta x, \Delta y, \Delta z$ grid spacing or step size in x,y,z

δ a small dimensionless parameter that represents the ratio of the vertical to the horizontal dimensions of an ice cap

δ_{ij}	Kroenecker delta, $\delta_{ij} = 1$ when $i = j$ and $\delta_{ij} = 0$ when $i \neq j$.
$\delta(x),\delta(x,y)$	δ-function
λ	wavelength, $\lambda = 2\pi/k$
ϕ	complex phase angle, transfer phase shift, general potential
$\phi(k)$	transfer phase shift
ξ,η,ζ	independent variables
τ_M	memory length or adjustment time of an ice cap or glacier
τ_C	time-scale related to propagation of kinematic waves
τ_D	time-scale related to diffusion of kinematic waves
$\tau_D(k)$	wave number or wave length dependent diffusion time-scale
ω	angular frequency

SYMBOLS IN CHAPTER 2

Symbols used in Chapter 2 describing previous work are different from the symbols which are used in the rest of the dissertation. This is so that the results of previous work can be expressed and discussed in traditional notation. Variables with the subscript "0" refer to long scale average flow. Perturbations are indicated by the "Δ" symbol, *e.g.* $\Delta\alpha$ for surface slope perturbations. Depth averages are indicated by a diacritical "-" sign on top of the corresponding variable, *e.g.* $\bar{u}$ for the depth average of the longitudinal velocity.

A	constant in Glen's flow law
b	mass balance
C_I	constant derived from Glen's flow law
C_{II}	constant derived from Weertman's sliding law
G	a stress gradient term involving $(\partial\tau_{xx}/\partial x)$ in the vertically integrated force equilibrium equations
g	acceleration of gravity
$f(x)$	filter in Kamb and Echelmeyer's filter theory
h	ice thickness

l	filter length in Kamb and Echelmeyer's filter theory
m	power in Weertman's sliding law
n	power in Glen's flow law
T	a stress gradient term involving $(\partial^2\tau_{xz}/\partial x^2)$ in the vertically integrated force equilibrium equations
u	longitudinal velocity
x,z	Cartesian coordinates, x-axis along flow, z-axis normal to the long scale average ice surface
z_b	z coordinate of the bedrock
z_s	z coordinate of the ice surface
α	surface slope
$\dot{\varepsilon}_{ij}$	strain rate tensor
ζ	integration variable for the z coordinate
η	viscosity
$\bar{\eta}$	effective longitudinal viscosity
$\tilde{\eta}$	effective shear viscosity
ξ	integration variable for the x coordinate
ρ	ice density
σ_{ij}	stress tensor
τ_{ij}	deviatoric stress tensor
τ_b	basal shear stress
τ_0	long scale average of the basal shear stress

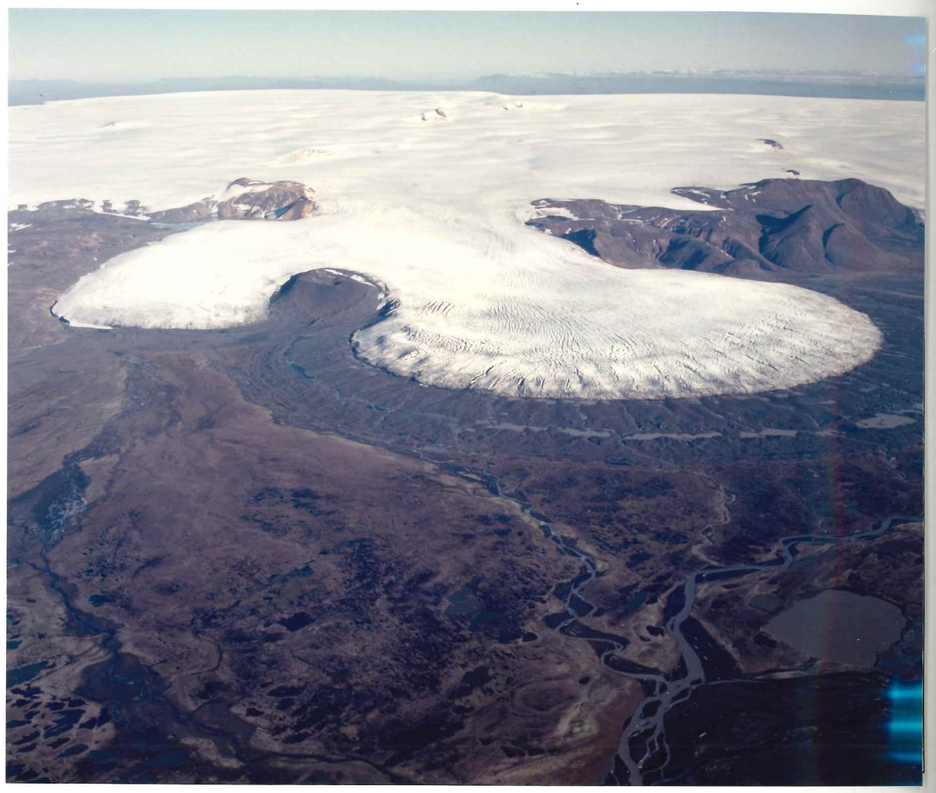

The Hofsjökull ice cap, Central Iceland, viewed from the south. The ice surface undulations which are the subject of this dissertation are clearly visible because of the low sun angle. Photograph by Björn Rúriksson, September 10, 1986.

ACKNOWLEDGEMENTS

I would like to thank Professor Charles F. Raymond for his continuing support during the course of this work. Discussions with him and Edwin D. Waddington have solved many problems that I have encountered. I would also like to thank my supervisory committee for their assistance, especially the reading committee: Charles F. Raymond, Christopher S. Bretherton and Edwin D. Waddington, who read the dissertation in draft form and suggested many improvements.

The data set on the geometry of Hofsjökull was made available for this analysis by Helgi Björnsson at the Science Institute, University of Iceland.

Many field trips to Hofsjökull with my colleague Oddur Sigurðsson at Orkustofnun (National Energy Authority) have given me the opportunity to observe the landscape of the ice cap at close quarters. Helgi Björnsson, Kristinn Einarsson and Magnús Már Magnússon read parts of the dissertation and gave useful advice. Professor Stephen Malone and John Firestone were often helpful when I ran into problems with the computers at the Geophysics Program. Fellow students in the Geophysics Program have been pleasant to work with and they helped make my stay in Seattle enjoyable. The Icelandic consul in Seattle Jon Marvin Jonsson and his wife Joanne Jonsson have been of great help and their hospitality made me and my family feel at home in Seattle. The photograph of Hofsjökull on the previous page was provided by the photographer Björn Rúriksson. His assistance in preparing the copies needed for its inclusion in this dissertation is acknowledged.

During the spring of 1991 I had the opportunity to spend a study leave from my work at Orkustofnun at the University of Washington and work on this dissertation. During that time I received support from Orkustofnun (National Energy Authority) and Minningarsjóður (Memorial Fund of) Helgu Jónsdóttur og Sigurliða Kristjánssonar which is gratefully acknowledged.

CHAPTER 1: INTRODUCTION

1.1 GLACIER LANDSCAPE

The shape of glaciers and ice sheets has been the subject of theoretical investigation for more than a century. One of the first efforts was Thomson's (Lord Kelvin's) (1888) derivation of the expression that describes the steady state shape of a linear Newtonian viscous ice sheet resting on a flat bed.

Around 1950 it was realized that the relation between stress and strain rate for glacier ice is non-linear. This meant that glacier ice could not realistically be treated as a Newtonian viscous material, not even as a first approximation. Since the discovery of the non-linear nature of the flow of ice, a number of studies of the long scale shape of glaciers and ice sheets have been published. Some treat ice as a perfectly plastic material (Orowan, 1949; Nye, 1951, 1952a,b; Reeh, 1982). Other studies (Vialov, 1958; Nye, 1959b; Weertman, 1961; Paterson, 1972, 1980; Halfar, 1981; Hindmarsh, 1990) are based on a more realistic power law representation of the rheology of ice (Glen, 1955) or assumptions about sliding of the ice along the bedrock. These studies successfully explain many long scale features of the shape of glaciers and ice sheets in terms of bedrock slope, glacier mass balance distribution and rheological properties and basal sliding of glacier ice. Among the features explained are the average and maximum ice thickness, the generally convex shape of the ice surface and the observed fact, which is related to the convex shape of the surface, that ice thickness is to a good approximation inversely proportional to long scale surface slope.

Figure 1.1.1 illustrates some of the features discussed above. It shows the surface and bedrock profiles along a 15.6 *km* long (approximate) flow line from the Þjórsárjökull outlet glacier of the Hofsjökull ice cap, Central Iceland (solid curves). These profiles and others from the same area of the ice cap will be described in more detail later in this dissertation. The figure also shows a linear least squares approximation to the bedrock profile (lower dashed curve) and a theoretical surface profile (upper dashed curve) predicted by perfect plasticity theory for yield stress equal to 1 *bar* for a glacier flowing down an inclined plane (Nye, 1951, Eq. 17). The inclined plane is taken to be the linear

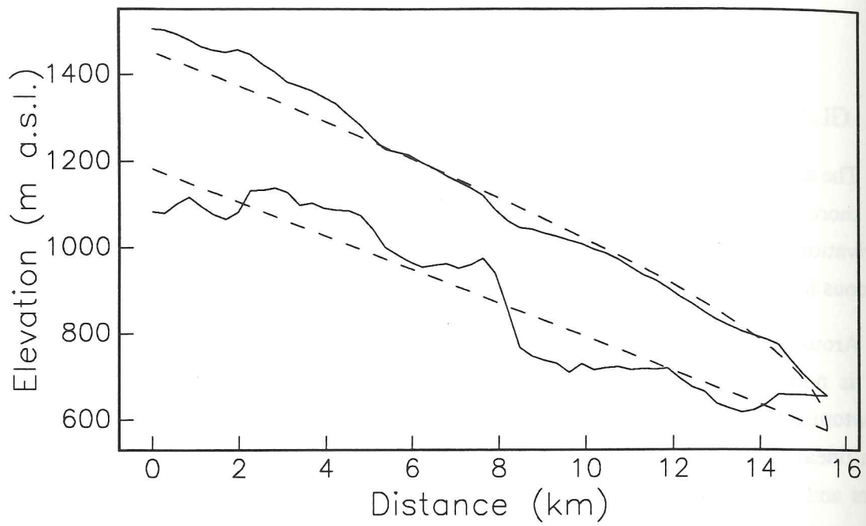

FIGURE 1.1.1: Surface and bedrock profiles along a 15.6 km long (approximate) flow line from the Þjórsárjökull outlet glacier of the Hofsjökull ice cap, Central Iceland (solid curves, data from Science Institute, University of Iceland, cf. Björnsson, 1988). Also shown are a linear least squares approximation to the bedrock profile (lower dashed curve) and a theoretical surface profile (upper dashed curve) predicted by perfect plasticity theory for a glacier flowing down an inclined plane (see text).

least squares approximation to the bedrock profile shown in the figure. The figure shows that perfect plasticity theory, despite its simplicity, does quite well in explaining the overall shape of the surface profile. Both the slow increase in the ice thickness in the interior of the glacier and the increasing steepness of the surface profile near the terminus are predicted. Theoretical profiles based on more realistic treatment of the mass balance of the glacier and the rheology of ice lead to similar predictions.

In addition to illustrating how the overall or long scale shape of glaciers can be theoretically explained, Figure 1.1.1 also demonstrates that there is more to glacier

landscape than the smooth overall shape. There are low amplitude short and intermediate scale undulations in the surface profile which seem to be related to bedrock undulations of much higher amplitude. Such undulations are familiar to every traveler of ice caps and ice sheets and they are the subject of this dissertation.

Short and intermediate scale glacier landscape has been investigated by a number of scientists since about 1960 and an account of previous work on this subject will be given in the following chapter. The surface profile shown in Figure 1.1.1 displays several of the better known properties of the transfer of bedrock undulations to the surface of an ice cap. First, the bedrock undulations are severely *damped* as they are transferred to the surface. The damping is approximately by a factor of 5-10 for the most pronounced features of the profiles shown in Figure 1.1.1. This is a similar order of magnitude of damping as has been observed for features with a length-scale of several ice thicknesses along a flow line to the south of Camp Century on the Greenland ice sheet (Robin, 1967) and on Dronning Maud Land in Antarctica (Beitzel, 1970). Second, the surface undulations are *shifted* with respect to the bedrock undulations such that maximum surface slopes occur above bedrock peaks and minimum surface slopes occur above bedrock troughs. Third, in spite of the damping, surface slope fluctuations are on the same order of magnitude as the long scale average surface slope. The ice may even flow uphill for short distances. Although this does not happen in the profile in Figure 1.1.1, it does happen at some other locations on the Hofsjökull ice cap. For lower values of the average slope the slope fluctuations may even be an order of magnitude greater than the average slope (Robin, 1967).

Figure 1.1.1 indicates that at least a part of the surface undulations on Hofsjökull is related to bedrock landscape. An effect of climate variations, variable basal sliding in space or time, or even glacier surges on the surface undulations, can of course not be excluded. The effect of climate variations on glacier landscape will be estimated in the dissertation. The effect of variable basal sliding or surges will, however, not be considered. The analysis is almost all based on the notion of steady state flow over a bedrock with relatively uniform sliding properties. The possible effect of non-uniform sliding or surges can therefore only be indirectly addressed by the success or failure of the theory.

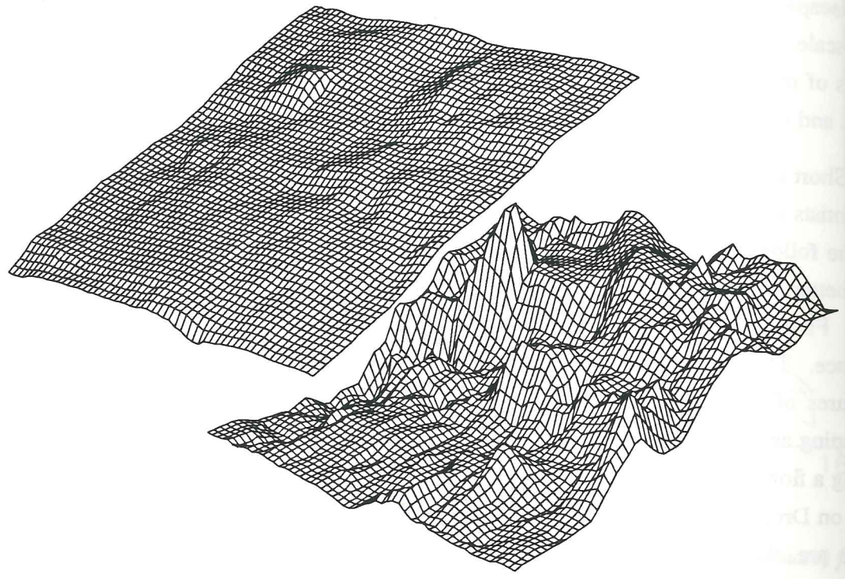

FIGURE 1.1.2: Perspective views of the bedrock (right) and surface (left) of a part of the Þjórsárjökull glacier viewed from the NE (data from Science Institute, University of Iceland, cf. Björnsson, 1988). The area shown is 11x11 km and the grid spacing is 200 m. The ice flow is to the SE and the ice thickness is between 200 and 300 m over most of the area shown. The flow line shown in Figure 1.1.1 runs from right to left along the diagonal from the top right corner to the bottom left corner of the surface.

Figure 1.1.2 shows perspective views of the bedrock and surface of a part of the Þjórsárjökull glacier viewed from the NE. The bedrock landscape is very complex and its relation to the surface landscape is not obvious from a first look at the figure. Upon closer examination the following pattern emerges. The surface has bulges upstream from bedrock peaks and transverse bedrock ridges, and troughs on the downstream side. Longitudinal bedrock ridges, *i.e.* ridges along the flow of the ice, do not seem to have much effect on the surface shape. This feature is more clearly seen in perspective views

from the Blautukvíslarjökull glacier which are shown in Chapter 7.

Figures 1.1.1 and 1.1.2 show examples of interesting glacier landscape which seems to be generated by flow of ice over and around bedrock undulations. This landscape must therefore be a consequence of ice dynamics in a general sense. Explaining this landscape in terms of continuum mechanics and rheological properties and basal sliding of glacier ice is a major and partly unsolved problem of dynamical glaciology. Conversely, observed landscape of glaciers and ice caps may throw some light on the nature of glacier flow in general and thus be of importance for other glaciological problems such as the response of glaciers to climatic fluctuations and the interpretation of deep ice cores.

Theoretical analysis of short and intermediate scale glacier landscape is in many ways different from analysis of the overall long scale shape (the meaning of "short", "intermediate" and "long" scale will be discussed later in the dissertation). The long scale shape is often analyzed on the basis of greatly simplified expressions for the flux of ice as a function of local ice thickness and surface slope. These expressions are *non-linear* and they involve empirically determined and very uncertain values of constants in the flow law of ice and sliding laws for basal sliding (*cf.* Paterson, 1981). The derived shapes depend to some extent on the distribution of mass balance over the area of the glacier.

Analysis of the short and intermediate scale landscape, on the other hand, is traditionally done in terms of perturbations from a datum (steady) state. This analysis is *linear* because the non-linear nature of glacier flow is taken care of by the datum solution. An important feature of this analysis is that it can to a large extent be done in terms of *relative* changes with respect to the datum solution. This means that absolute values of rheological and sliding parameters and the mass balance distribution will have much less influence on the short and intermediate scale landscape than on the long scale shape of the glacier. Uncertainty in the values of rheological and sliding parameters and limited knowledge of the mass balance distribution are thus somewhat less of a problem for the analysis of short and intermediate scale landscape than would perhaps be expected. However, the analysis is mathematically complex because the governing equations cannot be simplified as much as in the analysis of long scale glacier shape.

The last chapter of this dissertation is devoted to an analysis of digital maps of the Hofsjökull ice cap, Central Iceland, which were made available for this analysis by Helgi Björnsson at the Science Institute, University of Iceland. Long term measurements of the mass balance or ice flow velocity of the Hofsjökull ice cap are not available as mass balance measurements have only taken place since 1987 and velocity measurements have just recently been initiated. In spite of the limited knowledge of the mass balance of Hofsjökull, the data on the geometry of the ice cap contain a wealth of information on the relation between glacier surface and bedrock landscapes (*cf.* Figs. 1.1.1 and 1.1.2) which, in view of the above discussion, could be especially valuable for the analysis of the formation of short and intermediate scale glacier landscape.

1.2 GOALS OF DISSERTATION

The goal of the dissertation is to develop and test a theory of the relation between the steady state surface and bedrock topographies of temperate ice caps and glaciers. The main reasons for developing this theory are the following.

First, there is the desire to explain the observed landscape of ice caps and glaciers in terms of continuum mechanics and as a consequence of the rheological properties and basal sliding of glacier ice. How much of the surface landscape is a result of bedrock landscape and how much, if any, is a result of time-dependent evolution of the ice surface? As discussed in the next chapter there is a gap between current theoretical analyses and available field observations of glacier landscapes. Closing this gap is a major unsolved problem in dynamical glaciology.

Second, significant advances in dynamical glaciology have taken place during the last decade. Nevertheless, it is not clear how the theoretical treatments of several different authors on this subject should be reconciled. The theories of Hutter (1983), Johnson and McMeeking (1984), Dahl-Jensen (1985), and Echelmeyer and Kamb (1986) will be reviewed in the next chapter. An important goal of this dissertation is to outline the differences and the common points of these theories and to derive a theory that combines them in one consistent theory.

Third, there are relatively few current observations of the landscape of temperate glaciers and ice caps. The recent maps of the topography of the Hofsjökull ice cap, Central

Iceland (Björnsson, 1988) provide an opportunity to investigate whether the formation of surface undulations on temperate ice caps is similar to the formation of such undulations on the cold ice sheets of Greenland and Antarctica.

The theory which is developed in the dissertation is a synthesis of current theories of glacier flow. It is formulated in terms of filters which describe how the flow of an ice cap or a glacier depends on the geometry of the bedrock and the ice surface. The filters describe the influence of localized disturbances in the surface and bedrock topographies on the ice flow. They indicate the size of the area that needs to be measured in order to understand the ice flow at a particular point on an ice cap. Although the filters will primarily be used to study the formation of glacier landscape, they are potentially useful in many other glaciological problems, including studies of velocity and strain rate variations at the surface of an ice cap or a glacier, analyses of the adjustment of ice caps and glaciers to changes in climate, and formulation of ice flow in glaciological models.

Apart from being an interesting problem in its own right, the formation of glacier landscape is important in other glaciological problems. Improved understanding of the flow of ice caps and glaciers over bedrock topography will add to our understanding of the stratigraphy of ice sheets, and it is therefore of importance for the interpretation and dating of ice cores for paleoclimatic research.

Another related problem is the study of the rheology of glacier ice. Ice rheology can be investigated by observing how it manifests itself in the flow imposed by bedrock topography. Of special interest in this regard is the non-linear coupling of stress and strain components in the flow of glacier ice. The flow law of ice is normally taken to be isotropic. Nevertheless non-linear coupling makes glacier ice significantly softer when shearing in the downstream direction of the main flow is increased, than when shearing is introduced in the transverse direction. The resulting anisotropy in the viscosity of ice, for perturbations in the flow, may have significant effects on the flow around bedrock peaks. An observation of such effects will add to the understanding of the flow properties of glacier ice.

The last chapter of this dissertation is devoted to an analysis of digital maps of the Hofsjökull ice cap, Central Iceland, which were made available for this analysis by Helgi Björnsson at the Science Institute, University of Iceland. Long term measurements of the mass balance or ice flow velocity of the Hofsjökull ice cap are not available as mass balance measurements have only taken place since 1987 and velocity measurements have just recently been initiated. In spite of the limited knowledge of the mass balance of Hofsjökull, the data on the geometry of the ice cap contain a wealth of information on the relation between glacier surface and bedrock landscapes (*cf.* Figs. 1.1.1 and 1.1.2) which, in view of the above discussion, could be especially valuable for the analysis of the formation of short and intermediate scale glacier landscape.

1.2 GOALS OF DISSERTATION

The goal of the dissertation is to develop and test a theory of the relation between the steady state surface and bedrock topographies of temperate ice caps and glaciers. The main reasons for developing this theory are the following.

First, there is the desire to explain the observed landscape of ice caps and glaciers in terms of continuum mechanics and as a consequence of the rheological properties and basal sliding of glacier ice. How much of the surface landscape is a result of bedrock landscape and how much, if any, is a result of time-dependent evolution of the ice surface? As discussed in the next chapter there is a gap between current theoretical analyses and available field observations of glacier landscapes. Closing this gap is a major unsolved problem in dynamical glaciology.

Second, significant advances in dynamical glaciology have taken place during the last decade. Nevertheless, it is not clear how the theoretical treatments of several different authors on this subject should be reconciled. The theories of Hutter (1983), Johnson and McMeeking (1984), Dahl-Jensen (1985), and Echelmeyer and Kamb (1986) will be reviewed in the next chapter. An important goal of this dissertation is to outline the differences and the common points of these theories and to derive a theory that combines them in one consistent theory.

Third, there are relatively few current observations of the landscape of temperate glaciers and ice caps. The recent maps of the topography of the Hofsjökull ice cap, Central

Iceland (Björnsson, 1988) provide an opportunity to investigate whether the formation of surface undulations on temperate ice caps is similar to the formation of such undulations on the cold ice sheets of Greenland and Antarctica.

The theory which is developed in the dissertation is a synthesis of current theories of glacier flow. It is formulated in terms of filters which describe how the flow of an ice cap or a glacier depends on the geometry of the bedrock and the ice surface. The filters describe the influence of localized disturbances in the surface and bedrock topographies on the ice flow. They indicate the size of the area that needs to be measured in order to understand the ice flow at a particular point on an ice cap. Although the filters will primarily be used to study the formation of glacier landscape, they are potentially useful in many other glaciological problems, including studies of velocity and strain rate variations at the surface of an ice cap or a glacier, analyses of the adjustment of ice caps and glaciers to changes in climate, and formulation of ice flow in glaciological models.

Apart from being an interesting problem in its own right, the formation of glacier landscape is important in other glaciological problems. Improved understanding of the flow of ice caps and glaciers over bedrock topography will add to our understanding of the stratigraphy of ice sheets, and it is therefore of importance for the interpretation and dating of ice cores for paleoclimatic research.

Another related problem is the study of the rheology of glacier ice. Ice rheology can be investigated by observing how it manifests itself in the flow imposed by bedrock topography. Of special interest in this regard is the non-linear coupling of stress and strain components in the flow of glacier ice. The flow law of ice is normally taken to be isotropic. Nevertheless non-linear coupling makes glacier ice significantly softer when shearing in the downstream direction of the main flow is increased, than when shearing is introduced in the transverse direction. The resulting anisotropy in the viscosity of ice, for perturbations in the flow, may have significant effects on the flow around bedrock peaks. An observation of such effects will add to the understanding of the flow properties of glacier ice.

1.3 ORGANIZATION OF DISSERTATION

Some general remarks concerning the organization and style of the dissertation are presented here to aid the reader in the following chapters.

Equation numbers are enclosed in parentheses, *e.g.* (4.3.5) or (A1.2.3). The first number is the chapter or appendix number. The middle number (if present) is the chapter subsection where the equation is given. The final number is a consecutive number of the equation within that subsection. Only equations that need to be referenced by number in the text of the dissertation are numbered.

Figures and tables are numbered in the same way as equations except that figure and table numbers are not enclosed in parentheses.

References are cited in the style adopted by the *Journal of Glaciology* in 1988 (Vol. 34, No. 118).

A list of the symbols used together with a list of figures and a list of tables can be found in the preliminary pages at the beginning of the dissertation.

The dissertation consists of 8 chapters. Following this introductory chapter, Chapter 2 reviews previous glaciological research with particular relevance to the formation of glacier landscape. It starts with a section on past observations of surface undulations on ice sheets.

Chapter 3 defines the notation used in the remainder of the dissertation, introduces some mathematical preliminaries and describes the fundamental differential equations and boundary conditions of glacier flow. Readers familiar with glacier dynamics can skip the introductory material in Chapters 1-3 and refer to it as needed during the reading of the later chapters.

Chapter 4 develops a theory of two-dimensional flow along a flow line. The starting point of the theory is the expression of ice flux perturbations in terms of filtered perturbations of the surface and bedrock topographies. This theory is used to derive filters that describe the effect of bedrock undulations on the steady state geometry of the ice surface.

Chapter 5 is devoted to a generalization of some of the two-dimensional theory of Chapter 4 to three-dimensional glacier flow.

Chapter 6 addresses the question whether some of the landscape of the glacier surface could be a consequence of time-dependent adjustment of the ice flow rather than a result of the bedrock topography. This chapter also contains an analysis of the propagation and diffusion of kinematic waves.

In Chapter 7 the theory developed in Chapters 4 and 5 is tested using digital maps of the surface and basal topographies of the Hofsjökull ice cap, Central Iceland and the implications of the tests are discussed.

Chapter 8 is a synopsis of the results of the dissertation, providing a comparison with previous work and a perspective on future research.

CHAPTER 2: PREVIOUS WORK

2.1 OBSERVATIONS OF SURFACE UNDULATIONS

Surface undulations on a length-scale of several ice thicknesses have been reported on many ice sheets by a number of authors. Some of these authors have noted that undulations with a wavelength of approximately 3 to 4 ice thicknesses seem to be more pronounced than undulations of other wavelengths. As this issue will be analyzed and discussed in considerable detail in the following chapters it is worthwhile to examine these reports closely.

While discussing the significance and history of large scale surface undulations observed on the polar plateau in Antarctica, Lister (1959) remarked "... This [frequency of large migrating sastrugi] was comparable with the surface undulations which have a wavelength of about 12 *km* and a mean amplitude of 20 to 25 *m*." As the ice thickness in this area is on the order of 3 *km* the quoted wavelength is approximately 4 ice thicknesses.

Robinson (1966) presented data on the geometry of the south polar plateau along several profiles. Surface undulations on length-scales from approximately 5 to 20 *km* with amplitudes on the order of 20 *m* are evident from the data. This is equivalent to a length-scale of approximately 2 to 6 ice thicknesses if a thickness scale of 3 *km* is used.

Brockamp and Thyssen (1968) reported measurements of ice speed on the Greenland ice sheet. The measurements were made by estimating "The shifting of marked points relative to the fixed valleys and highlands of the ice surface ..." Their Figure 1 shows two measurements separated by a time period of 8 years of an undulation with an amplitude of tens of meters and a length-scale of several kilometers. The figure indicates that the ice sheet flows uphill for a distance of approximately 4 *km*.

Robin (1967) analyzed surface undulations along a flow line to the south of Camp Century on the Greenland ice sheet. The surface has many features with length-scales of several ice thicknesses which seem to be related to bedrock landscape. Maximum surface slopes clearly have a tendency to occur above bedrock peaks. The ice flows uphill

at several locations along this flow line.

Beitzel (1970) analyzed a profile from Dronning Maud Land in Antarctica in detail. Undulations on a length-scale of approximately 6 to 10 *km* or 2 to 4 ice thicknesses are very pronounced in his Figure 5.

Budd and Carter (1971) analyzed a profile from the Wilkes ice cap in Antarctica and the E.G.I.G. line from the Greenland ice sheet and reported minimum damping of bedrock undulations with wavelengths of 3 to 4 ice thicknesses.

Describing the surface geometry of the southern part of the Greenland ice sheet as measured by satellite radar altimetry Zwally and others (1979) said "Surface undulations or waves of various amplitudes and wavelengths are observed on the ice sheet. Over much of the surface, waves on the order of 10 *m* amplitude and 10 *km* in wavelength appear to be predominant. ..." Discussing the surface geometry of a part of this area a few years later Zwally and others (1983) observe "... the [surface] undulations appear to be dome-shaped with horizontal dimensions of the order of 10 *km* and a vertical dimension rarely exceeding 2 *m*. The horizontal spacing of the undulations is non-uniform, being anywhere from 10 *km* to many tens of kilometers. ..." Using 2 to 3 *km* as an order of magnitude estimate of the ice thickness, this length-scale of the surface undulations is approximately 3 to 5 ice thicknesses. The above observation, that the separation of the surface features is variable while their dimensions seem to be similar, is interesting and indicates that the dome-shaped features are in response to localized bed disturbances. This will be discussed more thoroughly later.

Overgaard and Gundestrup (1985) show surface undulations and ice thickness data along a profile near Dye 3, South Greenland. The profile is close to the estimated direction of flow for approximately 33 *km* (Dahl-Jensen, 1985). The amplitudes of the bedrock landscape (variations in the ice thickness) are 200 to 400 *m*, which amounts to approximately 15% of the ice thickness. The surface undulations, which have amplitudes of 10 to 20 *m*, have a clear relationship to the bedrock landscape, such that in many places the maxima and minima in the surface slope are found directly above bedrock peaks and troughs. The ice flows uphill at several locations along this profile. Whillans and others (1984) analyzed the surface and bedrock landscape of this area together with

measurements of velocities and strain rates at the surface. They note that "... the wavelength of the variation at the surface is 5 to 8 *km*, or 2.5 to 4 times the ice thickness ...". They found that variations in ice flow at the surface are mostly along the flow line and much less in the transverse direction. This indicates that three-dimensional flow around bedrock obstacles is not very important in this area compared to flow directly over the obstacles. They also concluded that the main thickness of the ice moves almost as a block with most of the shear associated with flow over the bedrock landscape taking place near the bed.

Robin and Millar (1982) analyzed three-dimensional ice flow around bedrock obstacles using radio echo sounding data from Antarctica. They concluded that, contrary to what seem to be the situation near Dye 3, such flow might be important over large areas of East Antarctica and probably also in West Antarctica.

Some general statements about observations of the landscape of ice sheets can also be found in the glaciological literature. Discussing transfer of bedrock undulations to the surface of ice sheets Budd (1970b) says "The occurrence of surface waves of about this scale [*i.e.* about 3.3 ice thicknesses] is well known on ice sheets, ..." and Paterson (1981, p. 166) reviewing the same subject remarks "Undulations with a dominant wavelength of several times the ice thickness appear to be widespread features of the surfaces of polar ice sheets. ..."

All of the above observations are from cold ice sheets. Similar observations from temperate ice caps and glaciers are much rarer. One early example is Paterson and Savage's (1963) observations from the Athabasca glacier which show ice surface undulations some of which may be related to bedrock relief. Another example is Björnsson's (1988) radio echo sounding profiles from temperate ice caps in Iceland. Björnsson's Figure 3.11 shows ice surface undulations which have a similar relation to bedrock landscape as has been observed on cold ice sheets.

Although the analysis in the following chapters is devoted to temperate ice caps, flow of temperate and cold ice caps and ice sheets over bedrock undulations is so similar that many of the conclusions of the analysis also apply to cold ice sheets. Conversely, observations on cold ice sheets provide insight into the problem of formation of glacier

landscape on temperate ice caps.

There have been a number of attempts to find theoretical explanations for the above observations in terms of glacier dynamics, the most important of which will be reviewed in the following subsections.

2.2 ANALYSIS BASED ON LOCAL ICE THICKNESS AND SURFACE SLOPE

Analyses based on greatly simplified expressions for the flow of glacier ice can provide intuitive understanding of the flow of ice over bedrock undulations, which is not easily acquired from more complex treatments of the problem.

The first attempt in this direction was not primarily aimed at explaining the shape of the ice surface. This was Nye's (1959a) use of a theory of plastic bending to explain variations in the longitudinal strain rate below an ice fall on the basis of the curvature of the streamlines at the surface. Although perfect plasticity theory is remarkably successful in predicting the long scale shape of ice sheets and glaciers, it is not particularly suitable for theoretical treatment of short scale flow. Therefore, Nye's theory of plastic bending has not been much used for analysis of surface undulations.

The first theoretical treatment dealing explicitly with the transfer of bedrock undulations to the surface is due to Nye (1959b,c). He based his analysis on an expression for the velocity of sliding (Weertman, 1957) and the assumption that the flow of ice can locally be approximated by a solution derived for the motion of a parallel sided slab of ice sliding over the bedrock. Nye (1959c) first considered the possible influence of non-steady flow on the geometry of an ice sheet. He estimated that non-steady surface features of the Antarctic ice sheet with length-scales on the order of several ice thicknesses would decay away by diffusion on a time-scale on the order of months. From this he concluded that observed surface undulations must be a result of bed topography. This question will be analyzed in Chapter 6 of the dissertation using recent theories of ice flow.

Having established that steady flow over bedrock undulations produces the landscape of the surface, Nye carried out a steady state analysis of two-dimensional ice flow along

a flow line of an ice sheet based on the abovementioned simplifying assumptions. Nye's main result is the following equation (in a slightly different notation from the one used by Nye)

$$(m+1)\frac{\Delta h}{h_0} + m\frac{\Delta \alpha}{\alpha_0} = 0\,, \qquad (2.2.1)$$

where α_0 and h_0 are long scale averages of the surface slope and the ice thickness, respectively, $\Delta\alpha$ and Δh are slope and thickness perturbations and $m \approx 2.5$ is a power in Weertman's sliding law. Since thickness perturbations are primarily caused by bedrock undulations, this equation predicts that perturbations in *surface slopes* should approximately be in phase with *bedrock relief*.

Robinson (1966) analyzed an extensive data set on the topography of the south polar plateau in order to test the predictions of Nye's theory. One of the profiles was measured on two different occasions with an interval of two years. The measurements showed essentially identical surface undulations, confirming Nye's prediction that the surface landscape should be fixed with respect to bedrock. However, the predicted relation between bedrock relief and surface slopes from (2.2.1) was in large disagreement with the data. Robinson concluded that surface landscape with wavelengths between 5 and 40 *km* was not adequately explained by the theory.

Equation (2.2.1) applies to profiles along flow lines. Robinson's profiles, however, were not along flow lines and no attempt seems to have been made to take this into account in his analysis. Therefore, Robinson's strong rejection of Nye's theory is probably not justified.

Robin (1967) compared Nye's theory to observations along a flow line to the south of Camp Century on the Greenland ice sheet. The phasing of the surface undulations along the profile is in accordance with the predictions of (2.2.1), but the predicted fluctuations in surface slope are far lower than the observed slope changes. This quantitative disagreement led Robin to an analysis of longitudinal coupling of the ice flow in order to account for the discrepancy.

In spite of these problems we will nevertheless see that (2.2.1) is useful for understanding of ice flow over bedrock undulations. A modified version of this equation will

be used in Chapter 4 to derive a simplified theory of the transfer of bedrock undulations to the surface of ice caps and data from the Hofsjökull ice cap agrees reasonably with this theory.

2.3 ANALYTICAL ANALYSIS FOR LINEAR NEWTONIAN RHEOLOGY

The rheology of glacier ice is non-linear. Nevertheless, considerable effort by several researchers has been made to understand steady flow of a hypothetical linear Newtonian glacier over bedrock undulations. The reason for the interest in linear Newtonian flow is twofold. First, linear flow can be analyzed by analytical methods and this yields an understanding that is difficult to obtain from the numerical solutions required by the considerably more complex non-linear problem. Second, the analytical solutions for linear material provide a valuable check of numerical results for more general rheologies.

Yosida (1964) considered two-dimensional steady flow of a snow cover without sliding down an inclined plane with small superimposed undulations. He derived analytical expressions for the surface geometry corresponding to sinusoidal bed undulations in the case of linear Newtonian rheology. It was soon realized that Yosida's results could be made useful in glaciological problems and Budd (1970b) made an attempt to extend Yosida's analysis to non-linear flow. Budd did not, however, derive any new expressions for the case of a linear Newtonian fluid. Yosida's treatment of the kinematic boundary condition at the ice surface is not entirely correct and therefore his results do not agree with solutions that have later been derived for the same problem.

Hutter and others (1981) attacked the problem of two-dimensional steady flow of a linear Newtonian fluid down an inclined plane using stream and stress functions to simplify the analysis. They generalized Yosida's original problem by allowing the fluid to slide along the bed. The sliding speed was assumed to be proportional to the shear stress along the bed. An error in the results was corrected by Hutter (1983) and this latter result was later rederived for the case of no sliding by Reeh (1987). Nevertheless, Hutter's results for non-zero sliding still seem to be in error as the sliding boundary condition at the bed is not satisfied by his solution except in the absence of basal sliding (*cf.* Chapter 4). For no sliding, Hutter's results show that the transfer function from the bed to the surface (*i.e.* the ratio of the surface to the bedrock undulations) increases monotonically

with the wavelength of the undulations for any slope of the inclined plane. In fact, the transfer function always approaches 1 as the wavelength goes to infinity. This property of the transfer function will be discussed more thoroughly in Chapter 4. The phase shift of the surface undulations is close to $\pi/2$ for the low slopes of the inclined plane that correspond to the surface slopes of glaciers and ice sheets. This result is equivalent to the statement that surface slopes and bedrock relief should be approximately in phase with each other, a result which was previously derived by Nye (1959b,c) from a very different analysis.

Whillans and Johnsen (1983) analyzed observed ice deformation at the surface near Byrd station, Antarctica using linear Newtonian rheology. They generalized the theory by allowing the viscosity to depend exponentially on ice depth. Assuming steady state flow, they deduced expressions for a number of derived quantities from given variations in the surface and basal topographies. They stressed the importance of variable basal sliding in determining the observed ice flow variations at the surface in the Byrd station strain network. This is not in agreement with other theoretical work on the formation of steady state surface undulations, that has focused on the effect from subglacial landscape rather than basal sliding. The important effect of bedrock landscape on the shape of the surface has been demonstrated by a number of observations on ice sheets as discussed in a previous subsection. It is possible that the flow along the Byrd station flow line is unusually insensitive to bedrock relief because of the close proximity of an ice divide. Theoretical analyses of glacier landscape (including the theory developed in this dissertation) usually do not apply close to ice divides or in the neighbourhood of the ice margin. Whillans and Johnsen furthermore computed theoretical transfer functions which show how the surface geometry depends on variations in basal sliding and basal relief. The transfer functions do not show an absolute maximum at wavelengths close to 3 ice thicknesses, which is in agreement with Hutter's (1983) results.

Balise and Raymond (1985) and Balise (unpublished) analyzed the transfer of velocity variations at the base to the surface of a glacier assuming linear Newtonian rheology. They did not consider the formation of steady state surface landscape, but many of their results are nevertheless relevant to the problem of steady state flow. Their analysis confirms some aspects of Hutter's (1983) results for linear Newtonian rheology in the

absence of basal sliding.

Reeh (1987) extended Hutter's (1983) two-dimensional theory to linear Newtonian flow in three dimensions without basal sliding. His transfer function is formally similar to Hutter's and it predicts that longitudinal (*i.e.* along the flow) bedrock ridges are not transferred to the surface at all. His analysis further predicts that if the transverse width of basal undulations is larger than about 2-3 times their length, then the finite width of the undulations has only minor influence on the flow, which can be considered two-dimensional to a good approximation.

2.4 LONGITUDINAL STRESS GRADIENTS

Nye's (1959b,c) analysis of surface undulations, which led to (2.2.1), was based on the assumption that ice flow is determined by local ice thickness and surface slope. Observed surface slope fluctuations on the ice sheets of Antarctica and Greenland, however, turned out to be significantly larger than predicted by Nye's theory. This problem was addressed by Robin (1967). He used a theory derived by Collins (1968) to analyze surface undulations along a flow line to the south of Camp Century on the Greenland ice sheet, as described above. Collins had used the two-dimensional force equilibrium equations, integrated over depth, to estimate the effect of longitudinal stress gradients on the shear stress at the base of an ice sheet. Nye (1969a) improved and simplified Collins' treatment and derived the following expression for the basal shear stress τ_b (slightly simplified and different notation from Nye's)

$$\tau_b = \rho g h \sin\alpha + 2G + T \,, \tag{2.4.1}$$

where

$$G = \int_{z_b}^{z_s} \frac{\partial \tau_{xx}}{\partial x} dz \,, \tag{2.4.2a}$$

and

$$T = \int_{z_b}^{z_s}\int_{z}^{z_s} \frac{\partial^2 \tau_{xz}}{\partial x^2} d\zeta dz \,. \tag{2.4.2b}$$

In these equations h is ice thickness, α is surface slope, τ_{xz} is shear stress and $\tau_{xx} = \frac{1}{2}(\sigma_{xx} - \sigma_{zz})$ is longitudinal deviatoric stress. In the absence of the longitudinal

gradient terms G and T, (2.4.1) reduces to $\tau_b = \rho g h \sin\alpha$, which is the basis for Nye's (1959b,c) theory as expressed by (2.2.1).

The G and T notation in the formulation (2.4.1) of the basal shear stress is actually due to Budd (1968, 1969, 1970a and 1971) although his derivations lead to slightly different equations for G and T compared to (2.4.2). Budd's analysis has been reviewed by Paterson (1981) and Hutter (1983). Recently, Kamb (1986) and Kamb and Echelmeyer (1986b) reconsidered the assumptions and approximations that have traditionally been used in derivations of (2.4.1) and deduced a new slightly more complex version of it.

Robin (1967) did not develop a complete theory of the formation of surface undulations. Rather, he evaluated the G term in (2.4.1) on the basis of a number of simplifying assumptions (*cf.* Paterson, 1981) and compared the variations in G to observed surface slope variations. Ignoring depth variations in the longitudinal deviatoric stress, velocity and strain rate, he estimated

$$G = h\frac{d\tau_{xx}}{dx}\,, \tag{2.4.3a}$$

$$\tau_{xx} = A^{-1/n}\,|\dot{\varepsilon}_{xx}|^{1/n}\,\mathrm{sign}(\dot{\varepsilon}_{xx})\,, \tag{2.4.3b}$$

$$\dot{\varepsilon}_{xx} = (b - u\,(dh/dx))/h\,, \tag{2.4.3c}$$

where $\dot{\varepsilon}_{xx}$ is the longitudinal strain rate, b is the surface mass balance, u is the longitudinal velocity and A, n are constants in the flow law of ice. For the Camp Century flow line, the predicted variations in G are similar to observed surface slope fluctuations, although Robin had to reduce his calculated strain rates by half and introduce longitudinal smoothing in the computed G values in order to get a good quantitative agreement. Predicted surface slope fluctuations from (2.2.1), on the other hand, were much to low. It therefore appears that longitudinal stress gradients play an important role in the formation of ice surface undulations.

Robin put heavy emphasis on the fact that strain rates estimated from (2.4.3c) change sign in the places where the most pronounced surface undulations are observed. This is because the viscosity of ice increases dramatically when strain rates approach zero. The

longitudinal strain rate is the only non-zero component of the strain rate tensor at the ice surface, since the shear strain rate parallel to the surface is zero at the surface. Therefore, longitudinal stress gradients near the ice surface may be expected to become very high in places where the longitudinal strain rate goes through zero. If this effect is in fact important, then ice flow perturbations caused by bedrock undulations will be non-linear in their very nature and this leads to great complications in their mathematical treatment. This question will be discussed in subsection 4.7.3 and in section 7.6 of the dissertation.

Budd (1968, 1969, 1970a) argued that the T term in (2.4.1) is important for undulations with wavelengths shorter than 3 to 4 ice thicknesses and that the G term is important for undulations with wavelengths up to 10 to 20 ice thicknesses. It is interesting that some of the largest surface undulations along the Camp Century flow line have wavelengths not far from 3 to 4 ice thicknesses. Therefore, one might expect the T term to be important for the undulations analyzed by Robin although he only considered the G term. The significance of the T term for the formation of surface undulations is discussed in subsection 4.7.9 of the dissertation.

Budd (1969, 1970a,b, 1971) developed theories of transfer of bedrock undulations to the surface, some of which are based on expressions similar to (2.4.1). Budd's theories predict minimum damping of wavelengths between 3 and 4 ice thicknesses, and observations (Beitzel, 1970; Budd and Carter, 1971) from Antarctica and Greenland have been interpreted to support Budd's predictions. As pointed out by Hutter and others (1981), Budd's (1970b) analysis is based on invalid assumptions. Budd's earlier theories, on the other hand, are based on *ad hoc* evaluations of the T term in equation (2.4.1). These theories will, therefore, not be further discussed here.

2.5 NUMERICAL SOLUTION OF THE FULL PROBLEM

It appears that it is difficult to formulate simplified theories of ice surface undulations for non-linear rheology, based on integrated forms of the equilibrium equations (*e.g.* (2.4.1)). Although Robin (1967) was partly successful in explaining observed surface slope fluctuations, his theory is not capable of predicting the undulations. Rather, he used the observed undulations to demonstrate that a previously neglected term in (2.4.1) is important. For this reason, recent work on the formation of surface undulations has

turned to numerical solution of the governing field equations and boundary conditions. A realistic formulation of the viscosity of the ice near the surface has been a principal source of difficulty in this work. This is because the standard solutions for glacier flow in the absence of flow perturbations caused by bedrock landscape, predict infinite viscosity at the surface of the ice (*cf.* Hutter, 1983).

Hutter and others (1981) used a modified form of Glen's flow law to circumvent the problem of infinite viscosity near the ice surface. Their analysis is related to Hutter's (1980, 1981) treatment of time-dependent glacier flow and longitudinal strain and it is summarized by Hutter (1983). The modification of Glen's flow law simply consists of an additional constant term so that for low strain rates the viscosity approaches a finite constant value. For low strain rates the rheology, therefore, approaches linear Newtonian rheology. The transfer functions predicted by this analysis are in most, but not all, cases uniformly increasing with wavelength, just as for linear Newtonian rheology. The transfer functions depend in a complicated way on the long scale average of the surface slope and on the amount of sliding at the base. Somewhat surprisingly, the transfer functions are quite sensitive to the value of the constant added to Glen's flow law. Close examination of Hutter's non-dimensionalization of this constant reveals that the level of stress, below which linear Newtonian rheology takes over, is highly dependent on the thickness of the ice, or equivalently on the long scale surface slope. Hutter argues that the value of the non-dimensional constant may be expected to be approximately equal to 10^{-n}, where n is the power in Glen's flow law. For $n = 3$ this implies that the transition stress, below which the rheology becomes essentially Newtonian, is 0.03 *bar* for an ice thickness of 10 *m*, 0.3 *bar* for an ice thickness of 100 *m*, and 3 *bar* for an ice thickness of 1000 *m*. However, Hutter states that this transition stress should be approximately equal to 0.1 *bar*. This discrepancy is caused by Hutter's choice of bedrock pressure instead of basal shear stress as a stress scale for the non-dimensionalization of stresses. For thick ice (low surface slope) the high and unrealistic value of the transition stress leads to transfer functions that closely correspond to linear Newtonian rheology. Furthermore, families of curves of transfer functions for a range of values of the long scale surface slope are likely to show, more than anything else, the varying relative importance of this non-dimensional constant. Therefore, an improved representation of the viscosity near the surface is necessary.

Dahl-Jensen (1985) used numerical modelling to analyze data along a flow line near Dye 3 on the Greenland ice sheet. She modelled the ice sheet as a number of essentially linear Newtonian layers of different viscosities. The viscosity of the layers was determined in part from longitudinal strain rates estimated from mass balance considerations. This approach avoided the abovementioned problems with an infinite viscosity at the surface, since strain rates at the surface do not go to zero in this case. The predicted transfer function was uniformly increasing with wavelength. Dahl-Jensen was able to predict the observed surface geometry and strain rate pattern fairly well. She found that the vertical inhomogeneity in the rheology of the cold ice played an important role in determining the deformation of the ice and the undulations of the surface.

2.6 LONGITUDINAL AVERAGING

A new approach to the problem of longitudinal stress gradients was developed by Echelmeyer (unpublished), Echelmeyer and Kamb (1986), Kamb (1986) and Kamb and Echelmeyer (1986a,b). They start from a version of (2.4.1) with the T term omitted. They furthermore make the assumptions that the depth average of the longitudinal velocity $\bar{u}$ may be expressed as

$$\bar{u} = C_I h \tau_b^n \,, \tag{2.6.1a}$$

or

$$\bar{u} = C_{II} \tau_b^m \,, \tag{2.6.1b}$$

and that the depth average of the longitudinal deviatoric stress $\bar{\tau}_{xx}$, may be approximated by

$$\bar{\tau}_{xx} = \frac{1}{h} \int_{z_b}^{z_s} \tau_{xx} dz = \bar{\eta} \frac{d\bar{u}}{dx} \,. \tag{2.6.2}$$

C_I, C_{II} are constants, n, m are the powers in Glen's flow law and Weertman's sliding law, respectively, and $\bar{\eta}$ is a weighted depth average of the viscosity which is called the effective longitudinal viscosity. On this basis, they are able to express relative perturbations in average flow velocity as weighted longitudinal averages of relative ice thickness and surface slope perturbations. In the case of (2.6.1a) the simplest expression for the relative velocity perturbation is

$$\frac{\Delta\bar{u}}{\bar{u}_0} = \int f(x-\xi)((n+1)\frac{\Delta h}{h_0} + n\frac{\Delta\alpha}{\alpha_0})d\xi\,, \tag{2.6.3}$$

where variables denoted by the subscript "0" refer to the long scale average flow. The filter

$$f(x) = \frac{1}{2l}e^{-|x|/l} \tag{2.6.4}$$

is an exponentially decaying function which describes the longitudinal velocity profile predicted for localized changes in ice thickness and surface slope. Similar expressions are found for (2.6.1b).

Neglecting a channel shape factor, the filter length l, which is called the longitudinal coupling length, is given by

$$l = \sqrt{4n\bar{u}_0 h\bar{\eta}/\tau_0} = \sqrt{(4/3)n\bar{\eta}/\tilde{\eta}}\,, \tag{2.6.5}$$

where $\tau_0 = \rho g h_0 \alpha_0$ is the long scale average of the basal shear stress τ_b and $\tilde{\eta} < \bar{\eta}$ is a weighted depth average of the viscosity which is called the effective shear viscosity. Predicted filter lengths depend on the longitudinal strain rate and turn out to be in the range 2 to 10 ice thicknesses.

Longitudinal variation in the long scale average flow, which is the datum for the perturbations, can be accounted for by introducing asymmetry in the filter $f(x)$. However, this is not required unless the long scale longitudinal variation is significant over the span of the filter.

This theory provides simple and intuitive understanding of the effect of longitudinal stress gradients. The explicit role of the longitudinal strain rate calls into question Hutter's (1983) treatment of the viscosity near the ice surface, which takes no account of longitudinal strain rates.

The question arises whether Kamb and Echelmeyer's filter theory can be used to analyze the formation of surface undulations, although Kamb and Echelmeyer did not develop the theory in that direction. We will see that this is not the case and that this is related to the omission of the T term of (2.4.1) in the filter theory. However, a modified

version of their theory can be used to simplify the analysis of surface undulations as will be seen in Chapter 4.

2.7 BOUNDARY LAYER AT THE SURFACE

Another new approach to longitudinal stress gradients was introduced by Johnson and McMeeking (1984). They used matched asymptotic expansions to combine the shear dominated flow away from the ice surface with a boundary layer near the surface where the flow is dominated by longitudinal compression or extension. The thickness of this boundary layer and the magnitude of the longitudinal deviatoric stress within it are directly related to the long scale longitudinal strain rate.

This approach turns out to be closely related to the filter theory of Kamb and Echelmeyer discussed in the previous subsection. In fact, the equation which determines the longitudinal deviatoric stress in the boundary layer in Johnson and McMeeking's analysis, turns out to be equivalent to an equation which is used in Kamb and Echelmeyer (1986a) to estimate the depth averaged viscosity $\bar{\eta}$. This same equation was used by Nye (1957) in his analysis of the distribution of stress in glaciers, as noted by Kamb and Echelmeyer. An almost equivalent equation was used by Dahl-Jensen (1985) to estimate the longitudinal deviatoric stress in her Dye 3 computations.

Hutter (1983) assumed linear Newtonian rheology at low stresses in order to eliminate problems associated with infinite viscosity at the surface. Johnson and McMeeking argue that even if ice rheology is linear at low stresses, the boundary layer, which follows from their theory, will be much thicker than the layer where Newtonian rheology dominates. Since Hutter found that the Newtonian layer did have an effect on the formation of ice surface undulations in his computations, this implies that the much thicker boundary layer near the surface must be important and cannot be ignored in a valid analysis of ice surface undulations.

2.8 SUMMARY AND DISCUSSION

From the preceding discussion it appears that valid theoretical analyses do not predict maximum transfer to the surface of bedrock undulations with a wavelength equal to several times the ice thickness. Nevertheless, as reviewed in the first subsection of this

chapter, there are many reports which indicate that precisely these wavelengths are often observed as pronounced surface features on ice sheets. Therefore, in spite of many research efforts since about 1960, a satisfactory theoretical explanation of these observations has still not been discovered.

After noting that Budd's (1970b) prediction of a maximum transfer from the bed to the surface for wavelengths about 3.3 times the ice thickness is based on unjustifiable assumptions Paterson (1981, p. 167) remarks that "Although these analyses do not make clear why the ice sheet behaves in this way, observations have confirmed the predictions [of the seemingly invalid theory]. ..."

If, as the current theoretical knowledge seems to indicate, there is no maximum in the transfer to the surface, then either the traditional interpretation of the observations or of the theory or both must be in error.

Some of the observations mentioned above have led to the conclusion that the transfer to the surface decays for wavelengths longer than 3 to 4 ice thicknesses (Beitzel, 1970; Budd and Carter, 1971). This conclusion, however, is based on power spectrum analyses of data series which are relatively short compared to the wavelengths in question. The power spectra are therefore quite sensitive to detrending and windowing of the data. The spectra contain large, seemingly random fluctuations and it is difficult to use them to determine the long wavelength behavior of the transfer of undulations to the surface. In fact Figure 3 in Budd and Carter (1971) shows that the ratio of the surface to the bedrock power spectra from the Wilkes ice cap starts to increase again for wavelengths longer than about 6 ice thicknesses. These wavelengths are not included in their Figure 4 which only shows data points that indicate decreasing transfer (increasing damping) for wavelengths above about 3 to 4 ice thicknesses. The observational basis for the conclusion that the transfer to the surface decreases for long wavelengths, therefore, does not appear convincing. This conclusion is also difficult to reconcile with a theoretical analysis of the problem as will be discussed in Chapter 4.

On the other hand there seems to be valid observational evidence for the conclusion that surface features with a length-scale of 3 to 4 ice thicknesses are more pronounced on ice sheets than features of other length-scales. Although this could perhaps in some

cases be explained by similar dominance of these wavelengths in the bedrock topography as suggested by Whillans and Johnsen (1983), that does not appear to be true in general. A sharp basal spike, for example, has spectral power which does not decay as the wavelength increases. Nevertheless, sharp spikes seem to produce distinct undulations in the surface with a wavelength close to 3 to 4 ice thicknesses as can be clearly seen in Robin's (1967) profile from the Greenland ice sheet (at distances approximately equal to 27 *km* and 35 *km*). Whillans and Johnsen discuss the dominance of surface features of wavelengths approximately equal to 3 ice thicknesses, after having demonstrated that transfer functions that they derive, do not exhibit an absolute maximum for these wavelengths. They seem to conclude that some physical processes, not included in the computation of the transfer functions, must be responsible for the dominance of such surface features. The question now becomes whether some other process is necessary or whether the observations can be reconciled with correct analysis of the ice flow. In the following chapters we will see that the flow analysis does explain the observations. In fact the model computations of Dahl-Jensen (1985) showed that a uniformly increasing transfer function can explain the observed surface undulations along flow lines in the neighbourhood of Dye 3 on the Greenland ice sheet.

Thus, in order to remove the apparent inconsistency between present observations and theories one first has to abandon the conclusion drawn from the observations that long waves are preferentially damped and second, one must reconsider the conclusion implicitly drawn from theory that a uniformly increasing transfer function contradicts the observation of dominant surface features with length-scales of 3 to 4 ice thicknesses.

Theoretical analyses of longitudinal stress gradients by Johnson and McMeeking (1984), Dahl-Jensen (1985), and Kamb and Echelmeyer (1986a) turn out to be related through the application of an equation that dates back to Nye (1957). This approach to longitudinal stress gradients avoids difficulties associated with an infinite viscosity at the ice surface in a way which is consistent with Glen's flow law, without introducing any new parameters or material constants into the problem. In Chapter 4 this approach will be merged with Hutter's (1983) methods for analyzing the formation of surface undulations. The resulting theory combines the theories of the abovementioned authors and makes it possible to compare them in a systematic way from a common viewpoint.

CHAPTER 3: ICE DYNAMICS

3.1 INTRODUCTION

This chapter introduces the notation used in the rest of the dissertation, defines some mathematical concepts and describes the fundamental differential equations and boundary conditions of glacier flow. The formulation draws on Paterson (1981), Hutter (1983) and Johnson and McMeeking (1984) in many ways.

The so-called laminar flow approximation to the glacier flow equations is described in the last subsection of the chapter. This approximation is valuable for the understanding of more elaborate ice flow solutions which are developed in the next two chapters.

The Cartesian coordinate system $\tilde{x},\tilde{y},\tilde{z}$, which is used for the formulation of field equations and boundary conditions for ice flow, has a vertical or a near vertical $\tilde{z}$-axis and horizontal or near horizontal $\tilde{x}$- and $\tilde{y}$-axes.

3.2 NOTATION

3.2.1 Vector notation

The Einstein notation for vectors and tensors is used throughout except in a few cases where expressions can be stated more simply in conventional vector notation. Thus, if $\vec{a}_i$ are basis vectors of a coordinate system, a vector

$$\vec{u} = u_i\vec{a}_i = \sum_i u_i\vec{a}_i$$

will be denoted by its components alone as u_i. A repeated index in a term indicates summation over the range of that index so an explicit summation sign can usually be avoided. Similarly, a tensor of rank 2

$$\vec{\vec{\tau}} = \tau_{ij}\vec{a}_i\vec{a}_j$$

(remember the summation convention) is denoted by τ_{ij} only. The indexes i and j take on the values 1,2 (or x,z) in two-dimensional analysis and 1,2,3 (or x,y,z) in three-dimensional analysis. The components of position and velocity vectors are sometimes

written as x,y,z and u,v,w instead of x_i and u_i when this is more natural.

Partial differentiation with respect to spatial coordinates is indicated by $\partial/\partial x_i$. Thus, the gradient of a vector field u_i is written as

$$\vec{\nabla}\vec{u} = \partial u_i/\partial x_i \ .$$

Sometimes, the notation x_i and f_i will be used for a discrete sequence of function values on a grid of equally spaced points in space, $f_i = f(x_i) = f(i\Delta x)$. When used, this meaning of the subscripted variables, as different from vectors and tensors, will be clear from the context.

3.2.2 Dimensional and non-dimensional variables

Expressing problems in non-dimensional form frequently simplifies analysis and distinguishes important terms from insignificant ones. Therefore, most of the following analysis is expressed in non-dimensional variables. Dimensional variables (but not physical constants) are indicated by the "~" sign, such that $\tilde{u}_i$ is a velocity vector in units of m/s or m/a. Variables without the "~" sign are non-dimensional, so that u_i is a non-dimensional velocity vector, implicitly referring to appropriate scales that have been chosen for the components of the velocity.

Scales used for defining non-dimensional variables are usually denoted by upper case letters, but sometimes by lower case letters with the subscript "0". Thus, a non-dimensional ice thickness h is defined as

$$h = \tilde{h}/H \ ,$$

where H is an appropriate thickness scale.

Physical constants, like the acceleration of gravity g, and the constants A and n in Glen's flow law of ice, are denoted by either upper case or lower case letters. Physical constants are most often dimensional quantities. They are, nevertheless, not expressed with a "~" sign, since the constants do not have non-dimensional counterparts, which they need to be differentiated from.

3.2.3 List of symbols

All symbols are defined in the list of symbols in the preliminary pages. The scalings between non-dimensional and dimensional variables are also listed there.

3.3 MATHEMATICAL PRELIMINARIES

3.3.1 Perturbation expansions

Perturbation or asymptotic expansions are used to break a complex problem, which involves a small parameter δ, into a sequence of more tractable problems. Typically, an unknown solution f, of the full problem, is written as

$$f = \delta^{p_0} f^{(0)} + \delta^{p_1} f^{(1)} + \delta^{p_2} f^{(2)} + \cdots . \tag{3.3.1}$$

The sequence of powers $p_0, p_1, p_2, \ldots$ depends on the nature of the problem. Each term $f^{(0)}, f^{(1)}, f^{(2)}, \ldots$ is found as the solution of a (we would hope simpler) problem which is derived from the full problem. Ordinarily, the terms $f^{(i)}$ are independent of δ. In general asymptotic expansions, however, the terms are allowed to depend on δ in addition to being multiplied by δ^{p_i} in (3.3.1).

A novel feature of asymptotic expansions is that they are usually *divergent*. Instead of satisfying a requirement of convergence, the expansion (3.3.1) must satisfy

$$\lim_{\delta \to 0} \frac{f - \sum_{i=0}^{n} \delta^{p_i} f^{(i)}}{\delta^{p_n}} = 0$$

in order to qualify as an asymptotic expansion. This requirement is usually written

$$f - \sum_{i=0}^{n} \delta^{p_i} f^{(i)} = o(\delta^{p_n}) , \tag{3.3.2a}$$

using the so-called *small o* notation. An equivalent expression using the *large O* notation is

$$f - \sum_{i=0}^{n-1} \delta^{p_i} f^{(i)} = O(\delta^{p_n}) , \tag{3.3.2b}$$

Detailed treatment of asymptotic expansions and perturbation methods can be found in Kevorkian and Cole (1981).

In glaciological problems the small parameter δ, is usually the ratio of the vertical to the horizontal dimensions of the glacier. Sometimes, the small parameter is a measure of the relative size of small flow perturbations which may for instance be caused by small amplitude bedrock undulations.

3.3.2 Fourier transforms

Analysis of linear problems is often greatly facilitated by the use of Fourier transforms. Continuous Fourier transforms are denoted by the "^" sign and defined by

$$\hat{f}(k) = \int_{-\infty}^{\infty} f(x) e^{-ikx} dx \tag{3.3.3a}$$

in one dimension and

$$\hat{f}(k_x, k_y) = \int_{-\infty}^{\infty} \int_{-\infty}^{\infty} f(x,y) e^{-ik_x x} e^{-ik_y y} dx dy \tag{3.3.3b}$$

in two dimensions, where k, k_x and k_y are wave numbers. The wave number k, satisfies $k = 2\pi/\lambda$ where λ is the wavelength of a harmonic function.

According to the Fourier integral theorem (Butkov, 1968), Fourier transforms can be inverted by the formulas

$$f(x) = \frac{1}{2\pi} \int_{-\infty}^{\infty} \hat{f}(k) e^{ikx} dk \tag{3.3.4a}$$

and

$$f(x,y) = \frac{1}{4\pi^2} \int_{-\infty}^{\infty} \int_{-\infty}^{\infty} \hat{f}(k_x, k_y) e^{ik_x x} e^{ik_y y} dk_x dk_y . \tag{3.3.4b}$$

The function $f(x)$ and its transform $\hat{f}(k)$ may have discontinuities and integrable singularities in which case they are considered distributions (*cf.* Butkov, 1968). The most important such function or distribution is the δ-function which is defined by $\delta(x) \equiv 0$ for all $x \neq 0$ and $\int_{-\infty}^{\infty} \delta(x) dx = 1$. For a continuous function $f(x)$ the δ-function has the property

$$\delta(x)*f(x) = \int_{-\infty}^{\infty} \delta(x-\xi)f(\xi)d\xi = f(x)\,,$$

where continuous convolution is indicated by the "*" sign.

3.3.3 Transfer functions

The problems, which are considered in the following chapters, typically have a solution, $h(x)$ say, which depends on a *forcing function* $f(x)$. When the problems are expressed in the wave number domain, the Fourier transform of the solution can as a rule be expressed in terms of the Fourier transform of the forcing function as

$$\hat{h}(k) = t(k)\hat{f}(k)\,. \tag{3.3.5}$$

The complex valued function $t(k)$, which relates the Fourier transforms of the solution and the forcing function to each other, is called the *transfer function*.

The transfer function may be written

$$t(k) = |t(k)|e^{i\phi(k)}\,, \tag{3.3.6}$$

where $|t(k)|$ is termed the *transfer amplitude* and $\phi(k)$ is called the *transfer phase shift*. When the meaning is clear from the context, the term *transfer function* will sometimes be used for the *transfer amplitude*.

The transfer amplitude is sometimes called the *filter function* by authors on glacier dynamics. The negative of the phase shift is called the *phase lag* and is sometimes used in the glaciological literature instead of the phase shift. To complicate things, there are examples of the phase lag being called phase shift in the literature and this has to be kept in mind when results of different authors are compared.

3.3.4 Green's functions

An alternative way to analyze the effect of the forcing function on the solution is to consider fundamental solutions corresponding to concentrated spikes or δ-functions in the forcing function. A general solution corresponding to an arbitrary forcing function may then be expressed as

$$h(x) = g(x)*f(x) = \int_{-\infty}^{\infty} g(x-\xi)f(\xi)d\xi\,, \tag{3.3.7}$$

where $g(x)$ is the Green's function of the problem and the "*" sign denotes continuous convolution. The Green's function is defined as the solution that corresponds to a forcing function equal to the δ-function, *i.e.* $f(x) = \delta(x)$.

By the convolution theorem (*cf.* Butkov, 1968), (3.3.7) may be expressed in the wave number domain as

$$\hat{h}(k) = \hat{g}(k)\hat{f}(k)\,. \tag{3.3.8}$$

Comparison with (3.3.5) shows that the Fourier transform of the Green's function is equal to the transfer function of the problem. In fact, the easiest way to derive the Green's function is usually to invert a transfer function which has been found from an analysis in the wave number domain.

Working with Green's functions has the advantage that the Green's function itself may have an obvious and intuitive physical meaning and may thus be easier to interpret and understand than transfer amplitudes and phase shifts. Most often the transfer function and the Green's function approaches aid and complement each other.

3.3.5 Continuous analysis — discrete data

When it comes to applying Green's functions and transfer functions in an analysis of real data, one must take into account the fundamental difference between the continuous nature of the Green's functions and the transfer functions on one hand and the discrete nature of the data on the other. The Green's functions may contain (absolutely) integrable singularities which make their direct application to data difficult, if not impossible. Such a singularity does not need to be physically unrealistic since a solution corresponding to a physically acceptable forcing function can be well behaved. This problem is treated in detail in Appendix 1 which describes the necessary adjustments that need to be made to continuous Green's functions before they are applied to real discrete data. Thus, the appearance of a discontinuity or even a singularity in a Green's function, which for example describes the surface of an ice cap, does not need to imply that the Green's function is invalid or unrealistic.

3.4 FIELD EQUATIONS

3.4.1 Conservation of mass

It is common to assume that the density of ice is constant in glacier flow. Then, the principle of mass conservation may be written in differential form as

$$\frac{\partial \tilde{u}_i}{\partial \tilde{x}_i} = 0 \,, \tag{3.4.1}$$

where $\tilde{u}_i$ is the ice flow vector. This equation is often called the equation of continuity.

3.4.2 Conservation of momentum

Accelerations in glacier flow are so small that one may to a very good approximation assume that all forces, acting on a hypothetical particle of moving ice, must balance. Then, the principle of momentum conservation may be stated as

$$\frac{\partial \tilde{\sigma}_{ij}}{\partial \tilde{x}_i} + \rho \tilde{g}_j = 0 \,, \tag{3.4.2}$$

where $\tilde{\sigma}_{ij}$ is the stress tensor, ρ is the (constant) density of ice and $\tilde{g}_j$ are the components of the acceleration of gravity.

3.4.3 Constitutive relations for ice

Constitutive relations for ice deformation relate the strain rate tensor $\tilde{\dot{\varepsilon}}_{ij} = \frac{1}{2}(\partial \tilde{u}_i/\partial \tilde{x}_j + \partial \tilde{u}_j/\partial \tilde{x}_i)$ to the stress tensor $\tilde{\sigma}_{ij}$. The constitutive relations for glacier ice are often called the *flow law of ice*. With the measurements of Glen (1952, 1955) it became clear that the flow law of ice is non-linear, such that the effective viscosity of the ice decreases sharply with an increase in the applied stress. Nye (1953, 1957) generalized the experimental results, found by Glen for a stress state of uniaxial compression, to an arbitrary state of stress. Nye assumed that the flow properties are isotropic and thus expressible in terms of the invariants of the stress and strain rate tensors. Assuming that the magnitude of the hydrostatic pressure $\tilde{p} = -\tilde{\sigma}_{ii}/3$, does not affect the creep rate, an expression of the flow law must involve the deviatoric stress tensor $\tilde{\tau}_{ij} = \tilde{\sigma}_{ij} + \tilde{p}$, rather than the stress tensor itself. Nye's generalization of Glen's experimental results is

$$\tilde{\dot{\varepsilon}}_{ij} = A\tilde{\tau}^{n-1}\tilde{\tau}_{ij} \,, \qquad \tilde{\tau}_{ij} = A^{-1/n}\tilde{\dot{\varepsilon}}^{-1+1/n}\tilde{\dot{\varepsilon}}_{ij} \,, \tag{3.4.3a}$$

or equivalently

$$\tilde{\dot{\varepsilon}}_{ij} = (\tilde{\tau}/B)^{n-1}(\tilde{\tau}_{ij}/B) \,, \qquad \tilde{\tau}_{ij} = B\tilde{\dot{\varepsilon}}^{-1+1/n}\tilde{\dot{\varepsilon}}_{ij} \,, \tag{3.4.3b}$$

where A, n and $B = A^{-1/n}$ are constants, and the *effective strain rate* $\tilde{\dot{\varepsilon}}$, and *effective shear stress* $\tilde{\tau}$, are defined by

$$2\tilde{\dot{\varepsilon}}^2 = \tilde{\dot{\varepsilon}}_{ij}\tilde{\dot{\varepsilon}}_{ij} \,, \qquad 2\tilde{\tau}^2 = \tilde{\tau}_{ij}\tilde{\tau}_{ij} \tag{3.4.4}$$

(*cf.* Paterson, 1981; Hutter, 1983). This formulation of the constitutive relations for glacier ice is called *Glen's flow law*.

The value of the flow law exponent n was found by Glen (1955) to be approximately equal to $n = 4.2$, but the value most frequently used in recent work is $n = 3$ (Paterson, 1981; Hooke, 1981). The value of A (or B) depends on the temperature of the ice and is highly variable and uncertain (*cf.* Paterson, 1981; Hooke, 1981). The numerical value recommended by Paterson (1981) for temperate ice and $n = 3$ is $A = 0.17\ bar^{-3}\ a^{-1}$, which is equivalent to $B = 1.8\ bar\ a^{1/3}$.

The determination of realistic constitutive relations for ice is a complex issue (*cf.* Hooke and others, 1980; Hooke, 1981; Paterson, 1981; Hutter, 1983), in part because of the dependency of the creep on ice fabric and texture. Other formulations than (3.4.3) of isotropic flow laws are possible and in many cases in nature the flow properties might well be non-isotropic. There is considerable scatter in the available data, from laboratory measurements and field work, which are the basis for the abovementioned values of the flow law constants A and n. Nevertheless, Glen's flow law is by far the most frequently used expression of the constitutive relations for glacier ice.

The formation of surface undulations on ice caps is primarily sensitive to the value of n rather than A (or B). The uncertainty in the value of A is therefore not critically important for the analysis of surface undulations. The value of n, on the other hand, is very important for the formation of glacier landscape.

3.5 BOUNDARY CONDITIONS

3.5.1 Kinematic boundary condition at the upper surface

The kinematic boundary condition at the ice surface describes the time evolution of the surface as a result of movement of the ice and addition or removal of ice by accumulation or ablation. Denoting the ice surface by $\tilde{z} = \tilde{z}_s(\tilde{x},\tilde{y},\tilde{t})$ the time evolution of $\tilde{z}_s$ is determined by the equation

$$\frac{\partial \tilde{z}_s}{\partial \tilde{t}} + \tilde{u}_i \frac{\partial \tilde{z}_s}{\partial \tilde{x}_i} = \tilde{w} + \tilde{b} \ , \ i=\tilde{x},\tilde{y} \ , \ \text{ at } \tilde{z} = \tilde{z}_s \ , \tag{3.5.1}$$

where $\tilde{u},\tilde{v},\tilde{w}$ are the ice velocity components in the $\tilde{x},\tilde{y},\tilde{z}$ directions and $\tilde{b}$ is mass balance measured along the $\tilde{z}$-axis. In the absence of mass balance this equation describes the evolution of what may be called a kinematic or a material surface.

3.5.2 Stress boundary condition at the upper surface

The stress boundary condition at the ice surface expresses the requirement of force balance for forces acting on the top and bottom of an infinitesimal surface element. Neglecting atmospheric pressure this requirement is written

$$\tilde{\sigma}_{ij} m_j = 0 \ , \ \text{ at } \tilde{z} = \tilde{z}_s \ , \tag{3.5.2}$$

where m_j is a unit vector normal to the ice surface.

3.5.3 Kinematic boundary condition at the base

In the absence of cavitation and basal melting/refreezing, the kinematic boundary condition at the bed states that the ice velocity must be parallel to the bed. Denoting the bed by $\tilde{z} = \tilde{z}_b(\tilde{x},\tilde{y})$ this means that

$$\tilde{u}_i n_i = 0 \ , \ \text{ at } \tilde{z} = \tilde{z}_b \ , \tag{3.5.3a}$$

where n_i is a unit vector normal to the bed. Since the vector $(-\partial\tilde{z}_b/\partial\tilde{x},-\partial\tilde{z}_b/\partial\tilde{y},1)$ is parallel to n_i, this equation may be rewritten

$$\tilde{u}_i \frac{\partial \tilde{z}_b}{\partial \tilde{x}_i} = \tilde{w} \ , \ i=\tilde{x},\tilde{y} \ , \ \text{ at } \tilde{z} = \tilde{z}_b \ . \tag{3.5.3b}$$

The effect of cavitation and basal melting/refreezing on the formation of surface undulations is normally not important outside of geothermal areas and is not considered in the following analysis. Basal melting associated with subglacial geothermal areas can lead to the formation of depressions in the ice surface, *e.g.* Grímsvötn and Skaftárkatlar in Vatnajökull (*cf.* Björnsson, 1974, 1977, 1988).

3.5.4 Basal sliding

The status of current knowledge of basal sliding leaves much to be desired. Although theoretical understanding of the sliding process was advanced with the work of Weertman (1957, 1964), Lliboutry (1968), Nye (1969b, 1970) and Kamb (1970), it is not possible to make quantitative predictions of sliding speeds on the basis of current theories. The theories do, however, seem to predict the correct order of magnitude of basal sliding of temperate glaciers, although the range of predicted sliding is very large, partly because of uncertain estimates of bed roughness (*cf.* Schweizer, 1989).

In general, it is found that the contribution of sliding to the flow of temperate glaciers is on the same order of magnitude as the contribution of internal ice deformation, although in some cases sliding speeds may far exceed the contribution from internal deformation (*cf.* Paterson, 1981; Raymond, 1980). Sliding speeds, measured on a number of temperate glaciers and reported by Paterson (1981), range from 3% to 90% of the total surface velocity.

The sliding relation adopted here is

$$\tilde{u}_b = C \tilde{\tau}_b^m \ , \tag{3.5.4}$$

where $\tilde{u}_b$ is sliding velocity parallel to the bed and $\tilde{\tau}_b$ is the bed parallel shear stress. We may further assume that the direction of the sliding velocity is parallel to the direction of the bed parallel shear stress.

The above formulation of basal sliding is due to Weertman (1957), and applies to sliding without cavitation. It is reviewed by Paterson (1981), Hutter (1983) and Schweizer (1989). The value of the power m is thought to be between 2 and 2.5 (Weertman, 1957, 1964; *cf.* Paterson, 1981). The value of the constant C is extremely uncertain and likely to be highly variable in nature both in space and time. We will not need an

explicit value of C. Rather, the importance of sliding will be quantified by its relative contribution to the flow of ice, compared to flow brought about by internal deformation.

Sliding speeds of most temperate glaciers are observed to vary between summer and winter, presumably because of varying basal water pressure. This variation is ignored in the following analysis of the formation of surface undulations. Sliding velocities predicted by (3.5.4) are best interpreted as annual averages in the following.

Glacier surges are extreme cases of varying basal sliding, both in space and time. Their effect on the landscape of temperate glaciers can be large, but will not be considered here.

3.6 ICE FLUX

3.6.1 General

Introducing the ice volume flux vector $\tilde{q}_i$, $i = \tilde{x},\tilde{y}$, leads to considerable simplification in many ice flow problems. The flux vector is defined as

$$\tilde{q}_i = \int_{\tilde{z}_b}^{\tilde{z}_s} \tilde{u}_i d\tilde{z} \ , \quad i = \tilde{x},\tilde{y} \ . \tag{3.6.1}$$

$\tilde{q}_i$ has only $\tilde{x}$ and $\tilde{y}$ components and this is implicit in the use of the index i.

The importance of the flux vector lies in the fact that evolution of the surface geometry and the steady state shape of ice caps and glaciers depend on the total flux integrated over depth, but not on velocity variations with depth that leave the flux unaltered.

3.6.2 Time-dependent evolution of surface geometry

The relevant property of the ice flow field for the evolution of the surface geometry is the gradient of the flux vector $\partial\tilde{q}_i/\partial\tilde{x}_i$. This can be seen by using (3.6.1) to expand the flux gradient as

$$\frac{\partial\tilde{q}_i}{\partial\tilde{x}_i} = \tilde{u}_i(\tilde{z}=\tilde{z}_s)\frac{\partial\tilde{z}_s}{\partial\tilde{x}_i} - \tilde{u}_i(\tilde{z}=\tilde{z}_b)\frac{\partial\tilde{z}_b}{\partial\tilde{x}_i} + \int_{\tilde{z}_b}^{\tilde{z}_s}\frac{\partial\tilde{u}_i}{\partial\tilde{x}_i}d\tilde{z} \ , \quad i=\tilde{x},\tilde{y} \ .$$

By the equation of continuity (3.4.1)

$$\int_{\tilde{z}_b}^{\tilde{z}_s}\left(\frac{\partial\tilde{u}_i}{\partial\tilde{x}_i}\right)_{i=\tilde{x},\tilde{y}}d\tilde{z} = -\int_{\tilde{z}_b}^{\tilde{z}_s}\frac{\partial\tilde{w}}{\partial\tilde{z}}d\tilde{z} = -\tilde{w}_{z=z_s} + \tilde{w}_{z=z_b} \ .$$

The two preceding equations together with the kinematic boundary conditions at the surface and at the bed, (3.5.1) and (3.5.3b), lead to

$$\frac{\partial\tilde{z}_s}{\partial\tilde{t}} + \frac{\partial\tilde{q}_i}{\partial\tilde{x}_i} = \tilde{b} \ . \tag{3.6.2}$$

This equation is the fundamental equation for analysis of time-dependent changes in the geometry of glaciers and ice caps. It has the intuitive meaning that changes in the surface elevation are caused by the combined effect of flow convergence/divergence and mass balance. In order for (3.6.2) to be useful one must have an expression for the flux vector $\tilde{q}_i$ in terms of the current geometry of the glacier. When used, (3.6.2) replaces the kinematic boundary condition at the ice surface (3.5.1).

3.6.3 Steady state

In a steady state there must be no time-dependent changes in the flow or in the geometry of the glacier. Assuming that the flux distribution can be computed for any geometry, a steady state geometry corresponding to a given mass balance distribution, must by (3.6.2) satisfy

$$\frac{\partial\tilde{q}_i}{\partial\tilde{x}_i} = \tilde{b} \ . \tag{3.6.3}$$

This equation is the fundamental equation for analysis of steady state glacier landscape. It is the basis for the analysis of surface undulations in the following two chapters.

3.7 LAMINAR FLOW APPROXIMATION

3.7.1 General

The laminar flow approximation is based on an idealized solution of the glacier flow equations corresponding to an ice slab of uniform thickness resting on an inclined plane. This solution is most simply expressed in a coordinate system with the $\tilde{x}$- and $\tilde{y}$-axes

parallel to the inclined plane and the x-axis pointing in the downslope direction. The $\tilde{z}$-axis points upward and makes an angle α with the vertical, where α is equal to the slope of the inclined plane (the angle α is written without the "~" sign since it is dimensionless). Then, the solution of the field equations (3.4.1), (3.4.2) and (3.4.3), and the boundary conditions (3.5.2), (3.5.3) and (3.5.4), is given by (for explanation of notation see the list of symbols in the preliminary pages)

$$\tilde{\sigma}_{xx} = \tilde{\sigma}_{yy} = \tilde{\sigma}_{zz} = -\tilde{p} = -\rho g \cos\alpha\,(\tilde{z}_s - \tilde{z})\,, \quad \tilde{\sigma}_{xz} = \rho g \sin\alpha\,(\tilde{z}_s - \tilde{z})\,, \quad \tilde{\sigma}_{xy} = \tilde{\sigma}_{yz} = 0\,, \tag{3.7.1}$$

$$\tilde{u} = C\,(\rho g \sin\alpha\,\tilde{h})^m + \frac{2A}{(n+1)}(\rho g \sin\alpha)^n(\tilde{h}^{n+1} - (\tilde{z}_s - \tilde{z})^{n+1})\,, \quad \tilde{v} = \tilde{w} = 0\,, \tag{3.7.2}$$

$$\tilde{q}_x = C\,(\rho g \sin\alpha)^m \tilde{h}^{m+1} + \frac{2A}{(n+2)}(\rho g \sin\alpha)^n \tilde{h}^{n+2}\,, \quad \tilde{q}_y = 0\,. \tag{3.7.3}$$

This solution is exact for the idealized case of an infinite slab of ice of uniform thickness and surface slope. Its importance lies in the fact that solutions of the glacier flow equations under more general circumstances will be close to this solution if longitudinal and transverse flow gradients are small. This will be the case when deviations from the parallel slab geometry have long wavelengths and therefore other more detailed solutions of the glacier flow equations will approach the laminar flow approximation in the so-called limit of asymptotically long wavelengths. In the next chapter the laminar flow approximation will appear as the zeroth order term in a perturbation expansion of glacier flow.

The ice flux expression (3.7.3) is suitable for use together with equations (3.6.3) and (3.6.2) in studies of long scale steady state shape and time-dependent evolution of glaciers and ice caps.

The stress solution which is the basis for the laminar flow approximation is in essence the same as stress solutions which were derived for a perfectly plastic glacier by Orowan (1949) and Nye (1951). Laminar flow solutions corresponding to Glen's flow law were derived soon after Glen's first experimental results were published. Early examples are Nye (1952b, 1957) and Bodvarson (1955) who derived expressions for the ice flux due to internal deformation identical to the deformation term (i.e. the latter term in the expression for $\tilde{q}_x$) in (3.7.3). Since then, numerous glaciological studies have been based on ice

flux formulations similar to (3.7.3). As an example Nye's (1959b,c) theory of surface undulations on ice sheets (*cf.* (2.2.1)) is based on the laminar flow approximation, in the special case that all the ice flux is modelled to come from sliding along the base so that the first term in (3.7.3) dominates.

3.7.2 Linearization of ice flux for laminar flow

Analysis of ice surface undulations is as a rule done in terms of small perturbations to the long scale average flow, which is called the *datum* flow. Therefore, it is of interest to consider flow perturbations predicted by the laminar flow approximation. Let perturbations be denoted by the Δ symbol and the datum flow be indicated by the subscript "0". Further, let $\tilde{q}_s = C\,(\rho g \sin\alpha)^m \tilde{h}^{m+1}$ and $\tilde{q}_d = (2A/(n+2))(\rho g \sin\alpha)^n \tilde{h}^{n+2}$ be the ice flux contributions from sliding and from internal deformation, respectively, and define $r = \tilde{q}_s/\tilde{q}_d$. Then, flux perturbations caused by small ice thickness changes and slope changes along the direction of flow are given by a linearization of (3.7.3) as

$$\frac{\Delta\tilde{q}_x}{\tilde{q}_{d_0}} = ((n+2) + r_0(m+1))\frac{\Delta\tilde{h}}{\tilde{h}_0} - (n + r_0 m)\frac{(\partial\Delta\tilde{z}_s/\partial\tilde{x})}{\tan\alpha_0} \tag{3.7.4a}$$

to first order in the perturbations. Thickness changes have by themselves no effect on the transverse flux $\tilde{q}_y$ to first order. Transverse slope changes, on the other hand, do affect the ice flux in the transverse direction. In part because of non-linearities in the flow law (3.4.3) and the sliding law (3.5.4), the effect of transverse slope changes on the ice flux is not as large as the effect of longitudinal slope changes. First order transverse flux perturbations are given by

$$\frac{\Delta\tilde{q}_y}{\tilde{q}_{d_0}} = -(1 + r_0)\frac{(\partial\Delta\tilde{z}_s/\partial\tilde{y})}{\tan\alpha_0} \tag{3.7.4b}$$

In order to find the expression (3.7.4b) for the transverse flux perturbation, one must express $\tilde{q}_x$ and $\tilde{q}_y$ given by (3.7.3) in a general coordinate system where the $\tilde{x}$-axis does not necessarily point in the downslope direction. A linearization of the resulting expressions for the ice flux vector leads to (3.7.4b).

The ice flux perturbation expressions (3.7.4a) and (3.7.4b) are suitable for use together with equations (3.6.3) and (3.6.2) in studies of small amplitude long scale ice surface undulations. Only (3.7.4a) is needed for two-dimensional planar flow studies. Both (3.7.4a) and (3.7.4b) are needed in the case of three-dimensional flow.

CHAPTER 4: TWO-DIMENSIONAL THEORY

4.1 INTRODUCTION

This chapter develops a theory of steady state two-dimensional glacier flow over bedrock undulations for non-linear rheology described by Glen's flow law and basal sliding according to Weertman's sliding law. The theory is first derived for two special cases; for the laminar flow approximation and for a linear Newtonian fluid with basal sliding. In all cases the approach is the same. First, an expression for the ice flux is derived for a general geometry. Then, the ice flux expression is used together with the steady state equation (3.6.3) to compute the transfer of bedrock undulations to the surface. The results are presented primarily as Green's functions that describe the steady state ice surface geometry corresponding to a sharp bedrock spike. Transfer functions in the wave number domain are also discussed.

4.2 LONG SCALE DATUM FLOW

4.2.1 General

It is helpful to view ice flow perturbations caused by bedrock undulations as superimposed on a long scale datum ice flow which would be realized in the absence of the basal undulations. Some properties of the datum flow are required for an analysis of ice flow over bedrock undulations. The most important such property is the datum ice viscosity distribution which is in part determined by longitudinal extension/compression in the datum flow. The datum longitudinal velocity at the base and at the ice surface is also important for correct formulation of boundary conditions that enter into the calculation of the ice flow perturbations. Therefore, an analysis of ice surface undulations must start with an analysis of the long scale datum flow in the absence of such undulations.

The coordinate system which is used for the long scale analysis has a horizontal $\tilde{x}$-axis and a vertical $\tilde{z}$-axis (Fig. 4.2.1). The development is built on Johnson and McMeeking's (1984) treatment of long scale glacier flow, with some modifications.

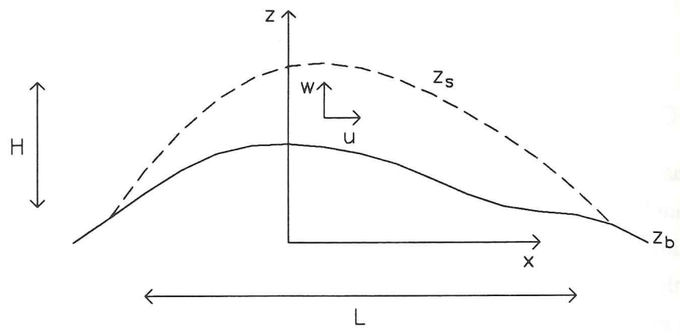

FIGURE 4.2.1: Definition of coordinate system and length-scales for long scale analysis.

4.2.2 Non-dimensional formulation

Non-dimensional formulation has been used in a number of recent glaciological studies in order to justify various approximations in a systematic way and to determine the independent combinations of physical parameters which affect the derived solutions. Examples of such studies are Fowler and Larson (1978, 1980), Hutter (1980, 1981, 1983), Hutter and others (1981), Morland and Johnson (1980), Johnson and McMeeking (1984) and more recently Hindmarsh (1990). Non-dimensional formulation has also been used in numerical studies of glacier flow (*e.g.* Huybrechts and Oerlemans, 1988; Jóhannesson and others, 1989) in order to simplify numerical computations and for identifying independent dimensionless parameters which determine the nature of the numerical solution. Typically, the non-dimensionalization involves a stretching of the original dimensional coordinate system such that different scales are used for the horizontal and vertical coordinates. A small ratio of the vertical to the horizontal dimensions of the glacier under consideration, may then be used as the small parameter in a perturbation expansion of the ice flow (*cf.* (3.3.1)).

Let a horizontal scale L and a vertical scale H be representative of the horizontal and vertical dimensions of the glacier, respectively (*cf.* Fig. 4.2.1). Denoting a time-scale, to be defined later, by T and defining $\delta = H/L$, the following system of dimensionless variables will be used for the long scale analysis.

$$\begin{aligned} &x = \tilde{x}/L\ ,\ z = \tilde{z}/H\ ,\ t = \tilde{t}/T\ ,\\ &u = \tilde{u}/(L/T)\ ,\ w = \tilde{w}/(H/T)\ ,\ b = \tilde{b}/(H/T)\ ,\\ &\sigma_{ij} = \tilde{\sigma}_{ij}/(\rho g H \delta)\ . \end{aligned} \tag{4.2.1}$$

This scaling of u and w allows the equation of continuity (3.4.1) to be expressed with terms $\partial u/\partial x$ and $\partial w/\partial z$ that are on the same order in δ (see below). The stresses are scaled to the driving shear stress rather than to pressure at the base as has been done by some authors (*e.g.* Hutter, 1983).

With the time-scale T defined as $T = \delta^{-1}A^{-1}(\rho g H \delta)^{-n}$, the dimensionless form of the field equations (3.4.1), (3.4.2) and (3.4.3) for two-dimensional flow is

Continuity: $$\frac{\partial u}{\partial x} + \frac{\partial w}{\partial z} = 0\ , \tag{4.2.2}$$

x–forces: $$\delta\frac{\partial \sigma_{xx}}{\partial x} + \frac{\partial \sigma_{xz}}{\partial z} = 0 \tag{4.2.3a}$$

z–forces: $$\delta\frac{\partial \sigma_{xz}}{\partial x} + \frac{\partial \sigma_{zz}}{\partial z} = \delta^{-1}\ , \tag{4.2.3b}$$

Glen's law: $$\begin{cases} \delta\dfrac{\partial u}{\partial x} = \tau^{n-1}\tau_{xx} & (4.2.4a)\\[2ex] \dfrac{\partial u}{\partial z} + \delta^2\dfrac{\partial w}{\partial x} = 2\tau^{n-1}\tau_{xz}\ , & (4.2.4b) \end{cases}$$

where $\tau_{ij} = \sigma_{ij} - (\sigma_{xx} + \sigma_{zz})/2$ and $\tau^2 = \tau_{xx}^2 + \tau_{xz}^2$.

The dimensionless form of the boundary conditions (3.6.2), (3.5.2), (3.5.3) and (3.5.4) is as follows.

At the surface $z = z_s(x,t)$:

Mass balance: $$\frac{\partial z_s}{\partial t} + \frac{\partial q}{\partial x} = b\ , \tag{4.2.5}$$

x–force at surface = 0: $$-\delta\frac{\partial z_s}{\partial x}\sigma_{xx} + \sigma_{xz} = 0 \tag{4.2.6a}$$

z–force at surface = 0: $$-\delta\frac{\partial z_s}{\partial x}\sigma_{xz} + \sigma_{zz} = 0\ . \tag{4.2.6b}$$

At the base $z = z_b(x)$:

Kinematic boundary condition: $$-u\frac{dz_b}{dx} + w = 0\,, \tag{4.2.7}$$

Sliding law: $$u_b = c\,|\tau_b|^{m-1}\tau_b\,, \tag{4.2.8}$$

where the basal velocity u_b, and the basal shear stress τ_b, are given by

$$u_b = (1 - \tfrac{1}{2}\delta^2(dz_b/dx)^2)u + \delta^2(dz_b/dx)w + O(\delta^4) \tag{4.2.9}$$

and

$$\tau_b = (1 - 2\delta^2(dz_b/dx)^2)\tau_{xz} - 2\delta(dz_b/dx)\tau_{xx} + O(\delta^4)\,, \tag{4.2.10}$$

and

$$c = C(\rho g H\delta)^m/(L/T) = (C/(AH))(\rho g H\delta)^{m-n} \tag{4.2.11}$$

is a dimensionless parameter that describes the relative importance of basal sliding compared to internal deformation. u_b and τ_b are velocity and shear stress components in a coordinate system which is tilted by a small angle $\tan\beta = -\delta(dz_b/dx)$ in the clockwise direction with respect to the original coordinate system. The expressions (4.2.9) and (4.2.10) for u_b and τ_b follow from the coordinate transformation rules for vectors and tensors when $\cos\beta$ and $\sin\beta$ are expanded in δ.

This formulation has two independent combinations of physical parameters, δ and c, which together with the flow law and sliding law powers n and m determine the nature of the problem. The dimensional physical parameters H, L, A, C, ρ and g only affect the ice flow solution through their influence on the dimensionless parameters δ and c.

The above dimensionless formulation is similar to Johnson and McMeeking's (1984) formulation for the case of small surface and bed slopes (their gentle slope case). Johnson and McMeeking used a sloping coordinate system with an inclination on the same order of magnitude as the small ratio $\delta = H/L$. It turns out to be simpler to formulate the problem in a coordinate system with a horizontal $\tilde{x}$-axis and therefore such a coordinate system is used here.

4.2.3 Boundary layer at the surface

Johnson and McMeeking (1984) used matched asymptotic expansions to derive an approximate solution of the dimensionless ice flow equations described in the previous

subsection. They show that a boundary layer at the ice surface is required in order to get a consistent solution. The thickness of the boundary layer is proportional to $\delta^{1/n}$, where n is the power in Glen's flow law. The value of n was chosen to be $n = 3$ in Johnson and McMeeking's treatment of the problem. As δ is on the order of 10^{-2} for glaciers and ice caps and 10^{-3} for ice sheets, this means that the thickness of the boundary layer is typically a significant fraction (10 - 20%) of the ice thickness. Within the boundary layer the ice flow is dominated by longitudinal extension/compression, but away from it the flow is dominated by shear. A particularly appealing feature of Johnson and McMeeking's solution is that the viscosity near the ice surface does not go to infinity as in the traditional long scale ice flow solution predicted by the laminar flow approximation. This non-singular viscosity distribution is achieved within the framework of Glen's flow law; no *ad hoc* modifications of the rheology or additional rheological parameters are introduced.

A problem with this boundary layer approach arises at points where the longitudinal strain rate at the ice surface equals zero (*e.g.* at a transition from extensive to compressive flow). This problem is discussed in subsections 4.3.5 and 4.7.3.

Johnson and McMeeking's boundary layer analysis is somewhat complex because terms of many different fractional powers in δ have to be derived in order to perform matching between an outer and an inner expansion of the solution. Stresses in the boundary layer for example, need to be expanded as $\tau_{ij} = \delta^{1/3}\tau_{ij}^{(0)} + \delta^{4/3}\tau_{ij}^{(1)} + \delta^{5/3}\tau_{ij}^{(2)} + \cdots$. This is partly because the inner variable in the boundary layer introduces terms of fractional powers in δ into the field equations. The passive nature of the boundary layer makes it possible to derive a slightly modified, but essentially equivalent, version of Johnson and McMeeking's solution by a relatively simple derivation using general asymptotic expansions (*cf.* subsection 3.3.1). This derivation avoids an explicit treatment of the boundary layer and the complex expansions of the solution within the boundary layer are therefore not needed. This derivation is presented in the next subsection for an arbitrary value of the flow law power n.

4.2.4 Derivation of the long scale datum flow

The small term δ always appears with integer powers in the field equations (4.2.3) and (4.2.4) and in the boundary conditions (4.2.6) and (4.2.8). This makes it tempting to expand the solution as an asymptotic expansion in integer powers of δ (*cf.* (3.3.1)).

Johnson and McMeeking (1984) show that such an expansion breaks down near the ice surface because of the non-linear nature of Glen's flow law. Terms of fractional powers in δ have to be introduced near the surface. However, it is possible to prevent the breakdown of the expansion if its terms are allowed to depend on the small parameter δ. This implies that care has to be taken to prevent the breakdown of the asymptotic expansion when small terms in the field equations and the boundary conditions are neglected in comparison with other larger terms.

More specifically, assume that the stress solution can be expanded as

$$\sigma_{ij} = \delta^{-1}\sigma_{ij}^{(-1)} + \sigma_{ij}^{(0)} + \delta\sigma_{ij}^{(1)} + \delta^2\sigma_{ij}^{(2)} + \cdots , \tag{4.2.12}$$

where $\sigma_{ij}^{(n)} = O(1)$ may depend on δ. Similar expansions are assumed for the deviatoric stresses τ_{ij}, and the velocities u_i. The ice surface $z = z_s(x,t)$ is assumed to be known and is not expanded. The goal is to derive the instantaneous stress and velocity fields corresponding to a given geometry. Therefore the boundary condition (4.2.5), which describes the time evolution of the ice surface, will not be needed in the derivation. Substituting the expansions for σ_{ij}, τ_{ij} and u_i into the field equations (4.2.2), (4.2.3) and (4.2.4) and the boundary conditions (4.2.6), (4.2.7) and (4.2.8) and collecting terms as described below, a hierarchy of problems is obtained.

The derivation of the datum flow which is presented below is not mathematically rigorous and it is possible that the solution cannot be carried out to higher than the second order in this simple way. It has been checked that the solution derived here is consistent with the solution derived by Johnson and McMeeking (1984) using traditional matched asymptotic expansions.

Order δ^{-1}:

The solution to this order is so simple that the corresponding equations will not be shown. These equations are the same as (4.2.2), (4.2.3), (4.2.4), (4.2.6), (4.2.7) and (4.2.8) when all terms involving δ are omitted. Their solution is

$$\sigma_{xx}^{(-1)} = \sigma_{zz}^{(-1)} = -(z_s - z)\,,\ \sigma_{xz}^{(-1)} = 0\,,$$
$$\tau_{ij}^{(-1)} = 0\,,\ u_i^{(-1)} = 0\,.$$

This solution determines a hydrostatic pressure field which is the main driving force of the ice motion at the next order.

Since $\tau_{ij}^{(-1)} = 0$ the effective shear stress τ can be expanded as

$$\tau^2 = \tau_{xx}^2 + \tau_{xz}^2 = \tau_{xx}^{(0)^2} + \tau_{xz}^{(0)^2} + 2\delta(\tau_{xx}^{(0)}\tau_{xx}^{(1)} + \tau_{xz}^{(0)}\tau_{xz}^{(1)}) + O(\delta^2)\,. \tag{4.2.13}$$

Order $\delta^0 = 1$:

Field equations:

$$\frac{\partial u^{(0)}}{\partial x} + \frac{\partial w^{(0)}}{\partial z} = 0\,, \tag{4.2.14}$$

$$\frac{\partial \sigma_{xx}^{(-1)}}{\partial x} + \frac{\partial \sigma_{xz}^{(0)}}{\partial z} = 0 \tag{4.2.15a}$$

$$\frac{\partial \sigma_{xz}^{(-1)}}{\partial x} + \frac{\partial \sigma_{zz}^{(0)}}{\partial z} = 0\,, \tag{4.2.15b}$$

$$\delta\frac{\partial u^{(0)}}{\partial x} = \tau^{(0)^{n-1}}\tau_{xx}^{(0)} \tag{4.2.16a}$$

$$\frac{\partial u^{(0)}}{\partial z} = 2|\tau_{xz}^{(0)}|^{n-1}\tau_{xz}^{(0)}\,. \tag{4.2.16b}$$

Boundary conditions at $z = z_s(x,t)$:

$$(-\frac{\partial z_s}{\partial x})\sigma_{xx}^{(-1)} + \sigma_{xz}^{(0)} = 0 \tag{4.2.17a}$$

$$(-\frac{\partial z_s}{\partial x})\sigma_{xz}^{(-1)} + \sigma_{zz}^{(0)} = 0\,. \tag{4.2.17b}$$

Boundary conditions at $z = z_b(x)$:

$$-u^{(0)}\frac{dz_b}{dx} + w^{(0)} = 0\,, \tag{4.2.18}$$

$$u^{(0)} = c|\tau_{xz}^{(0)}|^{m-1}\tau_{xz}^{(0)}\,. \tag{4.2.19}$$

$\tau^{(0)}$ is defined as $\tau^{(0)^2} = \tau_{xx}^{(0)^2} + \tau_{xz}^{(0)^2}$. The reason for retaining the term $\delta(\partial u^{(0)}/\partial x)$ in (4.2.16a) will be explained below.

Using the previously derived solution to order δ^{-1}, the zeroth order stress components $\sigma_{xz}^{(0)}$ and $\sigma_{zz}^{(0)}$ are found to be

$$\sigma_{xz}^{(0)} = \tau_{xz}^{(0)} = (-\frac{\partial z_s}{\partial x})(z_s - z)\,, \quad \sigma_{zz}^{(0)} = 0\,.$$

Let the x-axis point in the downslope direction for convenience. Then, the velocity components $u^{(0)}$ and $w^{(0)}$ and the ice flux $q^{(0)}$ follow from the flow law, the equation of continuity and the basal boundary conditions.

$$u^{(0)} = u_{z=z_b}^{(0)} + \frac{2}{(n+1)}(-\frac{\partial z_s}{\partial x})^n (h^{n+1} - (z_s - z)^{n+1})\,,$$

$$w^{(0)} = -\frac{\partial}{\partial x}\int_{z_b}^{z} u^{(0)}\,d\zeta = -\frac{\partial}{\partial x}\left[u_{z=z_s}^{(0)}(z - z_b) - \frac{2}{(n+1)(n+2)}(-\frac{\partial z_s}{\partial x})^n (h^{n+2} - (z_s - z)^{n+2})\right],$$

$$q^{(0)} = \int_{z_b}^{z_s} u^{(0)}\,dz = u_{z=z_b}^{(0)} h + \frac{2}{(n+2)}(-\frac{\partial z_s}{\partial x})^n h^{n+2}\,,$$

where $u_{z=z_b}^{(0)} = c\,((-\partial z_s/\partial x)h)^m$ and $h = z_s - z_b$.

The computation of $u^{(0)}$ from (4.2.16b) ignores the effect of the unknown $\tau_{xx}^{(0)}$ on τ. The most obvious way to determine $\tau_{xx}^{(0)}$ would be to neglect the left hand side of (4.2.16a) and conclude that $\tau_{xx}^{(0)} = 0$. This choice leads to problems at the next order, since then it is not possible to determine $\tau_{xx}^{(1)}$ such that $\tau_{xx}^{(1)} = O(1)$. Near the ice surface where $\tau_{xz}^{(0)}$ goes to zero, $\tau_{xx}^{(1)}$ would be required to be $O(\delta^{(1-n)/n})$ which contradicts the assumed form of the asymptotic expansion for τ_{ij} if $n > 1$. Therefore, the left hand side of (4.2.16a) must be retained and the equation interpreted as an implicit equation for determining $\tau_{xx}^{(0)} = -\tau_{zz}^{(0)}$. Written out in full this equation is

$$\delta\frac{\partial u^{(0)}}{\partial x} = (\tau_{xx}^{(0)^2} + \tau_{xz}^{(0)^2})^{(n-1)/2}\tau_{xx}^{(0)}\,. \tag{4.2.20}$$

This equation predicts that $\tau_{xx}^{(0)} = O(\delta^{1/n})$ near the ice surface and $\tau_{xx}^{(0)} = O(\delta)$ away from the surface. The thickness of the layer where $\tau_{xx}^{(0)}$ is on the order of $\delta^{1/n}$ may be estimated as the depth d_b below the ice surface where the shear stress $\sigma_{xz}^{(0)} = \tau_{xz}^{(0)} = (-\partial z_s/\partial x)(z_s - z)$ reaches the value of the longitudinal deviatoric stress at the surface $|\tau_{xx}^{(0)}_{z=z_s}| = |\delta(\partial u^{(0)}/\partial x)|_{z=z_s}^{1/n}$. This gives

$$d_b = \frac{|\delta(\partial u^{(0)}/\partial x)|_{z=z_s}^{1/n}}{(-\partial z_s/\partial x)}\,. \tag{4.2.21}$$

The error caused by ignoring $\tau_{xx}^{(0)}$ in the derivation of (4.2.16b), which was used for computing $u^{(0)}$, may now be estimated from (4.2.20) and can be shown to be $O(\delta)$. This error can therefore be taken into account at the next order. Thus, the non-zero $\tau_{xx}^{(0)}$ first affects the velocity field at order δ. This conclusion that $\tau_{xx}^{(0)}$ has a small effect on the velocity is an accordance with Nye's (1957) analysis of the effect of longitudinal extension/compression on the velocity field of a glacier (*cf.* Raymond, 1980).

Finally, $\sigma_{xx}^{(0)} = \sigma_{zz}^{(0)} + 2\tau_{xx}^{(0)}$ is found from the already derived expressions for $\sigma_{zz}^{(0)}$ and $\tau_{xx}^{(0)}$.

By allowing $\tau_{xx}^{(0)}$ to depend on δ in this way the breakdown of the asymptotic expansion (4.2.12) near the ice surface can be prevented. The boundary layer at the surface does not need to be derived from a special statement of the problem in an inner variable as is customary in boundary layer analysis. Rather, the boundary layer is implicitly described by (4.2.20).

Equation (4.2.20) is essentially equivalent to Johnson and McMeeking's (1984) equations (48) and (73) which determine the longitudinal stress in the boundary layer in their analysis.

Equation, (4.2.20) is also essentially equivalent to equations (26) and (30) in Nye's (1957) analysis of the distribution of stress in glaciers. Nye based his derivation on the idealized geometry of a block of ice of infinite extent and uniform thickness resting on an inclined plane. Johnson and McMeeking's boundary layer analysis and the above derivation are in essence a justification based on perturbation methods, of Nye's solution as the zeroth order approximation of the stress field of a glacier in the more realistic case of a slowly varying geometry.

Order δ:

The first order solution will primarily be used for comparing the asymptotic expansion of the long scale stress field with the stress field predicted by the laminar flow approximation. It is also useful for showing that the solution expansion can be extended

Using the previously derived solution to order δ^{-1}, the zeroth order stress components $\sigma_{xz}^{(0)}$ and $\sigma_{zz}^{(0)}$ are found to be

$$\sigma_{xz}^{(0)} = \tau_{xz}^{(0)} = (-\frac{\partial z_s}{\partial x})(z_s - z)\,, \quad \sigma_{zz}^{(0)} = 0\,.$$

Let the x-axis point in the downslope direction for convenience. Then, the velocity components $u^{(0)}$ and $w^{(0)}$ and the ice flux $q^{(0)}$ follow from the flow law, the equation of continuity and the basal boundary conditions.

$$u^{(0)} = u_{z=z_b}^{(0)} + \frac{2}{(n+1)}(-\frac{\partial z_s}{\partial x})^n (h^{n+1} - (z_s - z)^{n+1})\,,$$

$$w^{(0)} = -\frac{\partial}{\partial x}\int_{z_b}^{z} u^{(0)}\,d\zeta = -\frac{\partial}{\partial x}\left[u_{z=z_s}^{(0)}(z - z_b) - \frac{2}{(n+1)(n+2)}(-\frac{\partial z_s}{\partial x})^n (h^{n+2} - (z_s - z)^{n+2})\right],$$

$$q^{(0)} = \int_{z_b}^{z_s} u^{(0)}\,dz = u_{z=z_b}^{(0)} h + \frac{2}{(n+2)}(-\frac{\partial z_s}{\partial x})^n h^{n+2}\,,$$

where $u_{z=z_b}^{(0)} = c\,((-\partial z_s/\partial x)h)^m$ and $h = z_s - z_b$.

The computation of $u^{(0)}$ from (4.2.16b) ignores the effect of the unknown $\tau_{xx}^{(0)}$ on τ. The most obvious way to determine $\tau_{xx}^{(0)}$ would be to neglect the left hand side of (4.2.16a) and conclude that $\tau_{xx}^{(0)} = 0$. This choice leads to problems at the next order, since then it is not possible to determine $\tau_{xx}^{(1)}$ such that $\tau_{xx}^{(1)} = O(1)$. Near the ice surface where $\tau_{xz}^{(0)}$ goes to zero, $\tau_{xx}^{(1)}$ would be required to be $O(\delta^{(1-n)/n})$ which contradicts the assumed form of the asymptotic expansion for τ_{ij} if $n > 1$. Therefore, the left hand side of (4.2.16a) must be retained and the equation interpreted as an implicit equation for determining $\tau_{xx}^{(0)} = -\tau_{zz}^{(0)}$. Written out in full this equation is

$$\delta\frac{\partial u^{(0)}}{\partial x} = (\tau_{xx}^{(0)^2} + \tau_{xz}^{(0)^2})^{(n-1)/2}\tau_{xx}^{(0)}\,. \tag{4.2.20}$$

This equation predicts that $\tau_{xx}^{(0)} = O(\delta^{1/n})$ near the ice surface and $\tau_{xx}^{(0)} = O(\delta)$ away from the surface. The thickness of the layer where $\tau_{xx}^{(0)}$ is on the order of $\delta^{1/n}$ may be estimated as the depth d_b below the ice surface where the shear stress $\sigma_{xz}^{(0)} = \tau_{xz}^{(0)} = (-\partial z_s/\partial x)(z_s - z)$ reaches the value of the longitudinal deviatoric stress at the surface $|\tau_{xx\,z=z_s}^{(0)}| = |\delta(\partial u^{(0)}/\partial x)|_{z=z_s}^{1/n}$. This gives

$$d_b = \frac{|\delta(\partial u^{(0)}/\partial x)|_{z=z_s}^{1/n}}{(-\partial z_s/\partial x)}\,. \tag{4.2.21}$$

The error caused by ignoring $\tau_{xx}^{(0)}$ in the derivation of (4.2.16b), which was used for computing $u^{(0)}$, may now be estimated from (4.2.20) and can be shown to be $O(\delta)$. This error can therefore be taken into account at the next order. Thus, the non-zero $\tau_{xx}^{(0)}$ first affects the velocity field at order δ. This conclusion that $\tau_{xx}^{(0)}$ has a small effect on the velocity is an accordance with Nye's (1957) analysis of the effect of longitudinal extension/compression on the velocity field of a glacier (*cf.* Raymond, 1980).

Finally, $\sigma_{xx}^{(0)} = \sigma_{zz}^{(0)} + 2\tau_{xx}^{(0)}$ is found from the already derived expressions for $\sigma_{zz}^{(0)}$ and $\tau_{xx}^{(0)}$.

By allowing $\tau_{xx}^{(0)}$ to depend on δ in this way the breakdown of the asymptotic expansion (4.2.12) near the ice surface can be prevented. The boundary layer at the surface does not need to be derived from a special statement of the problem in an inner variable as is customary in boundary layer analysis. Rather, the boundary layer is implicitly described by (4.2.20).

Equation (4.2.20) is essentially equivalent to Johnson and McMeeking's (1984) equations (48) and (73) which determine the longitudinal stress in the boundary layer in their analysis.

Equation, (4.2.20) is also essentially equivalent to equations (26) and (30) in Nye's (1957) analysis of the distribution of stress in glaciers. Nye based his derivation on the idealized geometry of a block of ice of infinite extent and uniform thickness resting on an inclined plane. Johnson and McMeeking's boundary layer analysis and the above derivation are in essence a justification based on perturbation methods, of Nye's solution as the zeroth order approximation of the stress field of a glacier in the more realistic case of a slowly varying geometry.

Order δ:

The first order solution will primarily be used for comparing the asymptotic expansion of the long scale stress field with the stress field predicted by the laminar flow approximation. It is also useful for showing that the solution expansion can be extended

beyond the zeroth order without problems. The first order velocity solution will not be explicitly derived, as the zeroth order solution is satisfactory as a long scale datum solution for the analysis of ice surface undulations (*cf.* subsections 4.3.4 and 4.3.5).

Field equations:

$$\frac{\partial u^{(1)}}{\partial x} + \frac{\partial w^{(1)}}{\partial z} = 0\,, \tag{4.2.22}$$

$$\frac{\partial \sigma_{xx}^{(0)}}{\partial x} + \frac{\partial \sigma_{xz}^{(1)}}{\partial z} = 0 \tag{4.2.23a}$$

$$\frac{\partial \sigma_{xz}^{(0)}}{\partial x} + \frac{\partial \sigma_{zz}^{(1)}}{\partial z} = 0\,, \tag{4.2.23b}$$

$$\delta\frac{\partial u^{(1)}}{\partial x} = \tau^{(0)^{n-3}}((n\tau_{xx}^{(0)^2} + \tau_{xz}^{(0)^2})\tau_{xx}^{(1)} + (n-1)\tau_{xx}^{(0)}\tau_{xz}^{(0)}\tau_{xz}^{(1)}) \tag{4.2.24a}$$

$$\frac{\partial u^{(1)}}{\partial z} = (2/\delta)(\tau^{(0)^{n-1}} - |\tau_{xz}^{(0)}|^{n-1})\tau_{xz}^{(0)} + 2\tau^{(0)^{n-3}}(\tau_{xx}^{(0)^2} + n\tau_{xz}^{(0)^2})\tau_{xz}^{(1)}\,, \tag{4.2.24b}$$

Boundary conditions at $z = z_s(x,t)$:

$$(-\frac{\partial z_s}{\partial x})\sigma_{xx}^{(0)} + \sigma_{xz}^{(1)} = 0 \tag{4.2.25a}$$

$$(-\frac{\partial z_s}{\partial x})\sigma_{xz}^{(0)} + \sigma_{zz}^{(1)} = 0\,. \tag{4.2.25b}$$

Boundary conditions at $z = z_b(x)$:

$$-u^{(1)}\frac{dz_b}{dx} + w^{(1)} = 0\,, \tag{4.2.26}$$

$$u^{(1)} = mc((-\partial z_s/\partial x)h)^{m-1}\tau_{xz}^{(1)}\,. \tag{4.2.27}$$

The field equations (4.2.24) follow from the expansion (4.2.13) of the effective shear stress τ. A term involving $\tau_{xx}^{(1)}$ was omitted in the derivation of (4.2.24b) and a term involving $\tau_{xx}^{(0)}$ in the derivation of (4.2.27) since they can be shown to be $O(\delta)$ and can therefore be taken into account at the next order. The first term on the right hand side of (4.2.24b) can be shown to be $O(1)$ in spite of the $(2/\delta)$ multiplying factor. The term $\delta(\partial u^{(1)}/\partial x)$ on the left hand side of (4.2.24a) must be retained for the same reason as a similar term was retained in (4.2.16a) at the zeroth order.

Using the field equations (4.2.23), the boundary conditions (4.2.25) and the previously derived zeroth order solution we find

$$\sigma_{xz}^{(1)} = \tau_{xz}^{(1)} = 2(\frac{\partial z_s}{\partial x})\tau_{xx\,z=z_s}^{(0)} + 2\int_z^{z_s}\frac{\partial \tau_{xx}^{(0)}}{\partial x}d\zeta = 2(\frac{\partial z_s}{\partial x})\tau_{xx}^{(0)} + 2\int_z^{z_s}\left[\frac{\partial \tau_{xx}^{(0)}}{\partial x}\right]_{\substack{\text{fixed}\\ z_s - z}} d\zeta\,,$$

$$\sigma_{zz}^{(1)} = -(-\frac{\partial z_s}{\partial x})^2(z_s - z) - \tfrac{1}{2}\frac{\partial^2 z_s}{\partial x^2}(z_s - z)^2\,.$$

The notation $(\partial\tau_{xx}^{(0)}/\partial x)_{\substack{\text{fixed}\\ z_s - z}}$ means that $\tau_{xx}^{(0)}$ is expressed as a function of x and the depth below the ice surface $d = z_s - z$, and that the differentiation with respect to x is performed keeping d fixed, *i.e.* along the direction parallel to the ice surface. Note that $\tau_{xx\,z=z_s}^{(0)}$ in the first expression for $\sigma_{xz}^{(1)}$ is $\tau_{xx}^{(0)}$ evaluated at the ice surface $z = z_s$, whereas in the latter expression $\tau_{xx}^{(0)}$ is evaluated at same z value as $\sigma_{xz}^{(1)}$.

$u^{(1)}$ (and therefore $q^{(1)}$) may now be now be found by integration of (4.2.24b) using the boundary condition (4.2.27) and the expression just derived for $\tau_{xz}^{(1)}$. $w^{(1)}$ is similarly determined by the equation of continuity (4.2.22) and the boundary condition (4.2.26). Finally, the longitudinal deviatoric stress $\tau_{xx}^{(1)} = -\tau_{zz}^{(1)}$ and the longitudinal stress $\sigma_{xx}^{(1)} = \sigma_{zz}^{(1)} + 2\tau_{xx}^{(1)}$ follow from (4.2.24a) and the above expression for $\sigma_{zz}^{(1)}$. The expressions for $u^{(1)}$, $q^{(1)}$, $w^{(1)}$, $\tau_{xx}^{(1)}$ and $\sigma_{xx}^{(1)}$ will not be explicitly given as they are not needed in the following. It can be shown that $\tau_{xx}^{(1)} = O(\delta^{1/n})$ in the boundary layer and $\tau_{xx}^{(1)} = O(\delta)$ away from the boundary layer, just as was the case for $\tau_{xx}^{(0)}$. This justifies the omission of the term involving $\tau_{xx}^{(1)}$ from (4.2.24b).

Combined expansion for stresses:

Taken together the following expansions have been derived for the long scale stresses.

$$\sigma_{xz} = \tau_{xz} = (-\frac{\partial z_s}{\partial x})(z_s - z) - 2(-\delta\frac{\partial z_s}{\partial x})\tau_{xx}^{(0)} + 2\delta\int_z^{z_s}\left[\frac{\partial \tau_{xx}^{(0)}}{\partial x}\right]_{\substack{\text{fixed}\\ z_s - z}} d\zeta + O(\delta^2)\,,$$

$$\sigma_{zz} = -\delta^{-1}(z_s - z)(1 + (-\delta\frac{\partial z_s}{\partial x})^2) - \tfrac{1}{2}\delta\frac{\partial^2 z_s}{\partial x^2}(z_s - z)^2 + O(\delta^2)\,,$$

$$\tau_{xx} = \tau_{xx}^{(0)} + \delta\tau_{xx}^{(1)} + O(\delta^2)\,.$$

$$\sigma_{xx} = \sigma_{zz} + 2\tau_{xx} = \sigma_{zz} + 2\tau_{xx}^{(0)} + 2\delta\tau_{xx}^{(1)} + O(\delta^2)\,.$$

These expansions are valid as long as the surface and bedrock profiles z_s and z_b are not rapidly varying in the x direction.

4.2.5 Datum long scale solution

The long scale stress solution, which was derived in the previous subsection, is very much simplified when it is expressed in a coordinate system which is parallel to the local (long scale) surface slope (*cf.* Nye, 1969a). In fact, many of the smaller terms in the long scale stress expansions may be interpreted a resulting from a rotation of simpler expressions corresponding to a surface parallel coordinate system. Such a coordinate system would not have been suitable for deriving the solution, since the solution has to be derived for a profile with variable surface slope. A surface parallel coordinate system is, however, preferable for the analysis of short scale surface undulations where it is convenient to assume that the surface slope is nearly constant in the neighbourhood of an undulation which is under consideration. Therefore, an expression of the datum solution in a surface parallel coordinate system is needed.

When transforming the solution to the surface parallel coordinate system it has to be kept in mind that the transformation is a rotation in the original dimensional coordinates but not in the dimensionless coordinates. This for example means that the surface slope α is defined as

$$\tan\alpha = -\delta\frac{\partial z_s}{\partial x}\,,$$

(not $\tan\alpha = (-\partial z_s/\partial x)$). Let quantities in the surface parallel coordinate system be indicated by a prime mark. Then

$$\sigma_{x'x'} = \cos^2\alpha\,\sigma_{xx} + \sin^2\alpha\,\sigma_{zz} - 2\sin\alpha\cos\alpha\,\sigma_{xz}$$
$$\sigma_{z'z'} = \sin^2\alpha\,\sigma_{xx} + \cos^2\alpha\,\sigma_{zz} + 2\sin\alpha\cos\alpha\,\sigma_{xz}$$
$$\sigma_{x'z'} = \tau_{x'z'} = (\cos^2\alpha - \sin^2\alpha)\tau_{xz} + 2\sin\alpha\cos\alpha\,\tau_{xx}$$
$$\tau_{x'x'} = -\tau_{z'z'} = (\cos^2\alpha - \sin^2\alpha)\tau_{xx} - 2\sin\alpha\cos\alpha\,\tau_{xz}$$

Furthermore the following approximations hold true for small δ.

$$\cos\alpha = 1 - \tfrac{1}{2}(-\delta(\partial z_s/\partial x))^2 + O(\delta^4)$$
$$\sin\alpha = (-\delta(\partial z_s/\partial x)) + O(\delta^3)$$
$$z_s - z = (z'_s - z')/\cos\alpha = (z'_s - z')(1 + \tfrac{1}{2}(-\delta(\partial z_s/\partial x))^2) + O(\delta^4)$$
$$(\partial^2 z_s/\partial x^2) = (\partial^2 z'_s/\partial x'^2) + O(\delta^2)$$
$$(\partial/\partial x)_{\substack{\text{fixed}\\ z_s - z}} = (\partial/\partial x') + O(\delta^2)$$
$$\int_z^{z_s} d\zeta = \int_{z'}^{z'_s} d\zeta' + O(\delta^2)$$
$$u = u' + O(\delta^2)\,.$$
$$q = q' + O(\delta^2)\,.$$

Using the above transformation rules and approximations the stress solution found in the previous subsection may be written as

$$\sigma_{x'z'} = \tau_{x'z'} = \delta^{-1}(z'_s - z')\sin\alpha + 2\delta\int_{z'}^{z'_s}\frac{\partial \tau_{x'x'}^{(0)}}{\partial x'}d\zeta + O(\delta^2) \qquad (4.2.28a)$$

$$\sigma_{z'z'} = -\delta^{-1}(z'_s - z')\cos\alpha - \tfrac{1}{2}\delta\frac{\partial^2 z'_s}{\partial x'^2}(z'_s - z')^2 + O(\delta^2) \qquad (4.2.28b)$$

$$\tau_{x'x'} = -\tau_{z'z'} = \tau_{x'x'}^{(0)} + O(\delta) \qquad (4.2.28c)$$

$$\sigma_{x'x'} = \sigma_{z'z'} + 2\tau_{x'x'} = \sigma_{z'z'} + 2\tau_{x'x'}^{(0)} + O(\delta)\,. \qquad (4.2.28d)$$

The velocities u' and w' are given by

$$u' = u'^{(0)}_{z'=z'_b} + \frac{2}{(n+1)}(\delta^{-1}\sin\alpha)^n(h'^{n+1} - (z'_s - z')^{n+1}) + O(\delta) \qquad (4.2.29)$$

$$w' = -\frac{\partial}{\partial x'}\int_{z'_b}^{z'} u' d\zeta' ,$$

and the ice flux q' by

$$q' = u'^{(0)}_{z'=z'_b} h' + \frac{2}{(n+2)}(\delta^{-1}\sin\alpha)^n h'^{n+2} + O(\delta) , \qquad (4.2.30)$$

where $u'^{(0)}_{z'=z'_b} = c(\delta^{-1}\sin\alpha h')^m$ and $h' = z'_s - z'_b$.

An equation determining $\tau^{(0)}_{x'x'}$ must be derived from (4.2.20). This derivation may be simplified by noting that $\tau^{(0)}_{xx}$ (and $\tau^{(0)}_{x'x'}$) are $O(\delta)$ except in the surface boundary layer of thickness $O(\delta^{1/n})$. The vertical variation of $\delta(\partial u^{(0)}/\partial x)$ on the left hand side of (4.2.20) is very slow near the surface because $u^{(0)} = u^{(0)}_{z=z_s} + O((z_s - z)^{n+1})$. In fact, $\delta(\partial u^{(0)}/\partial x) = \delta(\partial u^{(0)}/\partial x)_{z=z_s} + O(\delta^2)$ in the boundary layer. Therefore the left hand side of (4.2.20) may be replaced by its value at the surface $\delta(\partial u^{(0)}/\partial x)_{z=z_s}$, and the resulting error in $\tau^{(0)}_{xx}$ will be $O(\delta)$. With this modification the equation determining $\tau^{(0)}_{x'x'}$ is

$$\delta\left(\frac{\partial u'^{(0)}}{\partial x'}\right)_{z'=z'_s} = (\tau^{(0)2}_{x'x'} + \tau^{(0)2}_{x'z'})^{(n-1)/2}\tau^{(0)}_{x'x'} . \qquad (4.2.31)$$

It is common in glaciological studies to compute the longitudinal deviatoric stress by assuming that the longitudinal velocity gradient is constant with depth (*e.g.* Nye (1957)). This assumption is of course not realistic as such because of internal ice deformation, especially in the case of low basal sliding when the longitudinal velocity gradient near the base must be small. The above argument shows that the longitudinal deviatoric stress can in fact be computed to leading order by using a constant value for the longitudinal velocity gradient equal to the longitudinal velocity gradient at the ice surface. Vertical variation of the velocity only affects the longitudinal deviatoric stress below the surface boundary layer where its magnitude is insignificant compared to the magnitude of the shear stress.

Comparing the solution given by (4.2.28), (4.2.29) and (4.2.30) with the ice flow solution predicted by the laminar flow approximation (3.7.1), (3.7.2) and (3.7.3), it is seen that with the exception of w' and $\tau_{x'x'}$ these solutions are identical to leading order, apart from trivial differences arising from the dimensionless form of (4.2.28), (4.2.29) and (4.2.30). Differences in the stress solutions at the next order are caused by $\tau_{x'x'} \neq 0$ and by a surface curvature term in $\sigma_{z'z'}$. For computation of ice viscosity or effective shear stress to the leading order, the stress solution (4.2.28) may therefore be considered to be the laminar flow solution with the addition of a longitudinal deviatoric stress $\tau^{(0)}_{x'x'}$, which is determined from the longitudinal velocity gradient at the ice surface using (4.2.31). The velocity and ice flux solutions (4.2.29) and (4.2.30) show that to lowest order the longitudinal velocity and the ice flux are identical to the laminar flow solution.

At the next order (4.2.28a) shows that the surface parallel shear stress is modified by a vertical integral of the longitudinal deviatoric stress gradient. Below the boundary layer, this term in the expansion for $\sigma_{x'z'}$ is $O(\delta^{1+2/n})$. This criterion arises because $\tau^{(0)}_{x'x'} = O(\delta^{1/n})$ in the boundary layer which has a thickness $d_b = O(\delta^{1/n})$. Below the boundary layer $\tau^{(0)}_{x'x'} = O(\delta)$ and does not contribute to the integral to leading order. Therefore, the integral term in the shear stress expansion (4.2.28a) is nearly constant below the boundary layer. This estimate of the effect of the longitudinal deviatoric stress on the shear stress is in agreement with Johnson and McMeeking's (1984) results in the case $n = 3$.

The long scale datum solution, which will be needed in the following analysis, consists of the leading order terms in (4.2.28), (4.2.29) and (4.2.30), using (4.2.31) to compute $\tau^{(0)}_{x'x'}$. Figures of the ice viscosity associated with this datum solution will be shown in subsection 4.3.5.

4.2.6 Failure for short scales

The long scale dimensionless formulation, which was used to derive the datum solution, works fine as long as the flow is slowly varying in the horizontal direction. However, it does not work for glacier flow over bedrock undulations. It is not justified to assume that such undulations are slowly varying over the horizontal dimensions of the glacier or ice cap. In fact, observations indicate that undulations on a length-scale of 3 to 4 ice thicknesses are an especially interesting problem for investigation. Ice flow

variations, which have a fixed length-scale with respect to ice thickness, cannot be expanded in a perturbation expansion based on the small parameter $\delta = H/L$, because horizontal flow gradients in the non-dimensional representation blow up when $\delta \rightarrow 0$ and the perturbation expansion breaks down. This is easily seen from (4.2.29) which predicts wild fluctuations in the longitudinal velocity at the leading order if there are short scale variations in the surface slope α, greater than say 50% of the long scale average surface slope. This magnitude of surface slope variations is common on real glaciers and ice caps and a theory of ice surface undulations must therefore be able to handle such variations in the surface slope. Unrealistic flow fluctuations at the leading order have to be corrected by equally large and opposite fluctuations at the next order, where the longitudinal stress gradients come into play. Consequently, the first order corrections to the flow are just as large as the leading order solution itself, which implies that the perturbations expansion has broken down.

The above discussion shows that the dimensionless formulation (4.2.2), (4.2.3), (4.2.4), (4.2.6), (4.2.7) and (4.2.8) of the ice flow equations is not suitable for an analysis of short scale flow. Therefore, a different dimensionless form of the ice flow equations has to derived for the short scale analysis.

4.3 SHORT SCALE FLOW

4.3.1 General

The analysis of short scale surface undulations is most naturally carried out in a coordinate system with the $\tilde{x}$-axis parallel to the long scale average ice surface (Fig. 4.3.1. This coordinate system leads to the simplest form of the long scale datum solution and it also simplifies the formulation of the boundary conditions at the ice surface and at the base. The $\tilde{z}$-axis points upward, perpendicular to the long scale average ice surface.

The long scale average ice thickness and surface slope are slowly varying over the area of the ice cap. Therefore, the tilting of the short scale coordinate system with respect to the vertical will depend on the location of the area under consideration on the ice cap. It is assumed that variations in the long scale average ice thickness and surface slope over this area are so small that they can be ignored (*cf.* subsections 4.3.6 and 4.7.3).

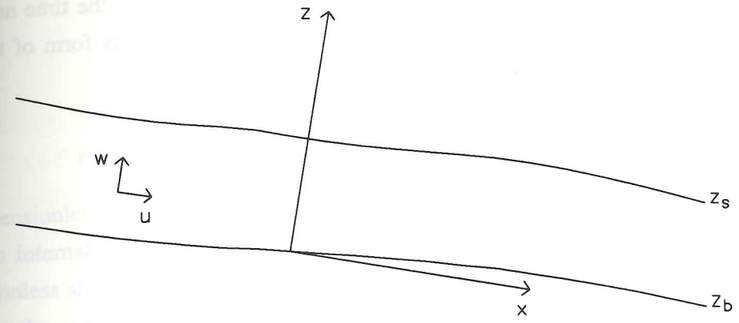

FIGURE 4.3.1: Definition of coordinate system for short scale analysis.

4.3.2 Non-dimensional formulation

The failure of the long scale dimensionless formulation at short scales means that the governing equations of ice flow must be non-dimensionalized in a different way when working with short scale flow variations. The failure at short scales arose because different scales L and H were used for the horizontal and vertical coordinates. Therefore, the $\tilde{x}$- and $\tilde{z}$-coordinates will be made dimensionless with the same length-scale in the short scale formulation. Let the origin of the $\tilde{x},\tilde{z}$-coordinate system be at the long scale average bedrock, approximately in the middle of the area under consideration. An obvious choice for the length-scale is the long scale average ice thickness at $\tilde{x} = 0$ which will be denoted by $\tilde{h}_0$. Denoting the long scale average surface slope at $\tilde{x} = 0$ by α_0 and a time-scale, to be defined later, with $\tilde{t}_0$, the following system of dimensionless variables may defined.

$$
\begin{aligned}
&x = \tilde{x}/\tilde{h}_0\ ,\ z = \tilde{z}/\tilde{h}_0\ ,\ t = \tilde{t}/\tilde{t}_0\ ,\\
&u = \tilde{u}/(\tilde{h}_0/\tilde{t}_0)\ ,\ w = \tilde{w}/(\tilde{h}_0/\tilde{t}_0)\ ,\ b = \tilde{b}/(\tilde{h}_0/\tilde{t}_0)\ ,\\
&\sigma_{ij} = \tilde{\sigma}_{ij}/(\rho g \tilde{h}_0 \sin\alpha_0)\ .
\end{aligned}
\tag{4.3.1}
$$

The stress scale $\rho g \tilde{h}_0 \sin\alpha_0$, is chosen to be equal to the long scale basal shear stress at $x = 0$. The same symbols are used for the dimensionless variables in both the long scale and the short scale formulations of the ice flow equations. This should not lead to problems as the meaning of the symbols is always clear from the context.

With the time-scale $\tilde{t}_0$ defined as $\tilde{t}_0 = A^{-1}(\rho g \tilde{h}_0 \sin\alpha_0)^{-n}$ (this is the time needed to achieve a strain of unity in basal shear at $x = 0$), the dimensionless form of the field equations (3.4.1), (3.4.2) and (3.4.3) for two-dimensional flow is

$$\frac{\partial u}{\partial x} + \frac{\partial w}{\partial z} = 0 \,, \tag{4.3.2}$$

$$\frac{\partial \sigma_{xx}}{\partial x} + \frac{\partial \sigma_{xz}}{\partial z} = -1 \tag{4.3.3a}$$

$$\frac{\partial \sigma_{xz}}{\partial x} + \frac{\partial \sigma_{zz}}{\partial z} = \cot\alpha_0 \,, \tag{4.3.3b}$$

$$\frac{\partial u}{\partial x} = \tau^{n-1}\tau_{xx} \tag{4.3.4a}$$

$$\frac{\partial u}{\partial z} + \frac{\partial w}{\partial x} = 2\tau^{n-1}\tau_{xz} \,, \tag{4.3.4b}$$

where $\tau_{ij} = \sigma_{ij} - (\sigma_{xx} + \sigma_{zz})/2$ and $\tau^2 = \tau_{xx}^2 + \tau_{xz}^2$.

The dimensionless form of the boundary conditions (3.6.2), (3.5.2), (3.5.3) and (3.5.4) is as follows.

At the surface $z = z_s(x,t)$:

$$\frac{\partial z_s}{\partial t} + \frac{\partial q}{\partial x} = b \,, \tag{4.3.5}$$

$$-\frac{\partial z_s}{\partial x}\sigma_{xx} + \sigma_{xz} = 0 \tag{4.3.6a}$$

$$-\frac{\partial z_s}{\partial x}\sigma_{xz} + \sigma_{zz} = 0 \,. \tag{4.3.6b}$$

At the base $z = z_b(x)$:

$$-u\frac{dz_b}{dx} + w = 0 \,, \tag{4.3.7}$$

$$u_b = c\,|\tau_b|^{m-1}\tau_b \,, \tag{4.3.8}$$

where the basal velocity u_b, and the basal shear stress τ_b, are given by

$$u_b = \cos\theta\, u - \sin\theta\, w \tag{4.3.9}$$

and

$$\tau_b = (\cos^2\theta - \sin^2\theta)\tau_{xz} + 2\sin\theta\cos\theta\,\tau_{xx} \,, \tag{4.3.10}$$

and

$$c = C(\rho g \tilde{h}_0 \sin\alpha_0)^m/(\tilde{h}_0/\tilde{t}_0) = (C/(A\tilde{h}_0))(\rho g \tilde{h}_0 \sin\alpha_0)^{m-n} \tag{4.3.11}$$

is a dimensionless parameter that describes the relative importance of basal sliding compared to internal deformation. c as defined by (4.3.11) is essentially the same as the dimensionless sliding parameter c defined by (4.2.11) in the long scale formulation and therefore the same symbol is used for both of them. u_b and τ_b are velocity and shear stress components in a coordinate system which is tilted by a small angle $\tan\theta = -(dz_b/dx)$ in the clockwise direction with respect to the original coordinate system.

It is interesting that the natural time-scale $\tilde{t}_0$, for short scale flow, is much shorter than the natural time-scale T, for long scale flow. In fact $\tilde{t}_0 \simeq \delta T$. In a dimensionless system of the ice flow equations, the decay time-scale of non-steady flow features may be expected to be on the order of 1. Thus, T is a rough estimate of the adjustment time in the long scale flow, whereas $\tilde{t}_0$ is a rough estimate of the adjustment time in the short scale flow. This means that the short scale flow will adjust much more quickly to changes than the long scale flow. This arises because comparable velocity variations lead to greater longitudinal velocity and flux gradients (*cf.* (3.6.2)) in the short scale flow than in the long scale flow. This difference in the time-scales is related to Nye's (1959c) theoretical prediction that non-steady short scale surface undulations on ice sheets should disappear on a time-scale much shorter than the time-scale of the overall flow of the ice sheet. In certain sense this prediction is built into the above short scale dimensionless formulation of the ice flow equations. Time-dependent glacier flow will be analyzed in Chapter 6 of the dissertation.

4.3.3 Linearized field equations for small perturbations

The analysis of ice surface undulations will be performed in terms of perturbations to a long scale datum flow. Indicating the datum solution by the subscript "0" and perturbation quantities by Δ, the ice flow solution is written as the sum of two terms

$$\sigma_{ij} = \underset{0}{\sigma_{ij}} + \Delta\sigma_{ij} \,, \quad \tau_{ij} = \underset{0}{\tau_{ij}} + \Delta\tau_{ij} \,, \quad \dot{\varepsilon}_{ij} = \underset{0}{\dot{\varepsilon}_{ij}} + \Delta\dot{\varepsilon}_{ij} \,,$$
$$u = u_0 + \Delta u \,, \quad w = w_0 + \Delta w \,, \quad q = q_0 + \Delta q \,.$$

It is assumed that the datum solution is slowly varying in the x-direction and can therefore be found from the long scale formulation of the ice flow equations. This means that all derivatives of the datum solution with respect to the short scale x-coordinate may be assumed to be $O(\delta)$, where $\delta = H/L$ is the small ratio of the vertical to the horizontal dimensions of the glacier.

The field equations determining the ice flow perturbations now follow directly from (4.3.2), (4.3.3) and (4.3.4), noting that the datum solution must solve the ice flow equations in the absence of perturbations. The equation of continuity (4.3.2) and the force balance equations (4.3.3) lead to

$$\frac{\partial \Delta u}{\partial x} + \frac{\partial \Delta w}{\partial z} = 0 \,, \tag{4.3.12}$$

$$\frac{\partial \Delta\sigma_{xx}}{\partial x} + \frac{\partial \Delta\sigma_{xz}}{\partial z} = 0 \tag{4.3.13a}$$

$$\frac{\partial \Delta\sigma_{xz}}{\partial x} + \frac{\partial \Delta\sigma_{zz}}{\partial z} = 0 \,. \tag{4.3.13b}$$

There are no gravitational or body force terms in the force balance equations for the stress perturbations since the datum stress field already balances the gravitational force.

It turns out to be slightly more convenient to write the linearization of the field equations (4.3.4), which arise from the flow law, as expressions for the deviatoric stresses perturbations $\Delta\tau_{ij}$, in terms of the strain rate perturbations $\Delta\dot{\varepsilon}_{ij}$. This is easily done using the latter form of Glen's flow law in (3.4.3a) and by noting that $\dot{\varepsilon} = \tau^n$. From the definition $\tau^2 = \tau_{xx}^2 + \tau_{xz}^2$, the perturbation $\Delta\tau$, in the effective shear stress τ, is found to be

$$\tau_0 \Delta\tau = \underset{0}{\tau_{xx}} \Delta\tau_{xx} + \underset{0}{\tau_{xz}} \Delta\tau_{xz} \,, \tag{4.3.14}$$

to first order in the perturbations. The field equations (4.3.4) then lead to the following expressions for the deviatoric stress perturbations $\Delta\tau_{xx}$ and $\Delta\tau_{xz}$.

$$\Delta\tau_{xx} = 2\eta_1 \Delta\dot{\varepsilon}_{xx} - 2\eta_3 \Delta\dot{\varepsilon}_{xz} \tag{4.3.15a}$$
$$\Delta\tau_{xz} = 2\eta_2 \Delta\dot{\varepsilon}_{xz} - 2\eta_3 \Delta\dot{\varepsilon}_{xx} \,, \tag{4.3.15b}$$

where

$$\eta_1 = \frac{1}{2n} \tau_0^{-(n+1)} (\underset{0}{\tau_{xx}^2} + n \underset{0}{\tau_{xz}^2})$$
$$\eta_2 = \frac{1}{2n} \tau_0^{-(n+1)} (n \underset{0}{\tau_{xx}^2} + \underset{0}{\tau_{xz}^2}) \tag{4.3.16}$$
$$\eta_3 = \frac{n-1}{2n} \tau_0^{-(n+1)} \underset{0}{\tau_{xx}} \underset{0}{\tau_{xz}} \,,$$

are three different definitions of viscosities which arise from a linearization of the nonlinear Glen's flow law. The viscosities η_1, η_2 and η_3 are all different from a standard definition of viscosity $\eta = \frac{1}{2}\tau/\dot{\varepsilon}$, which for Glen's flow law leads to

$$\eta = \tfrac{1}{2} \tau_0^{-(n-1)} \,. \tag{4.3.17}$$

It follows from (4.3.16) that $\eta = (n/(n+1))(\eta_1 + \eta_2)$. For linear Newtonian rheology, *i.e.* for $n = 1$, it is found that $\eta = \eta_1 = \eta_2 = \frac{1}{2}$ and $\eta_3 = 0$.

Equation (4.3.16) shows that the viscosity distribution which determines the ice flow perturbations is not isotropic, whereas Glen's flow law as such is isotropic. Interestingly, the linearization of Glen's flow law predicts that there is a direct interaction between the deviatoric stress component $\Delta\tau_{xx}$ and the strain rate component $\dot{\varepsilon}_{xz}$ and between $\Delta\tau_{xz}$ and $\dot{\varepsilon}_{xx}$ through η_3. The viscosity expressions (4.3.16) will be discussed more thoroughly when the datum solution, which determines $\underset{0}{\tau_{xx}}$ and $\underset{0}{\tau_{xz}}$, has been described.

The boundary conditions for the perturbations will be described in a later subsection as their derivation requires some properties of the datum flow.

An alternative to the above linearization would be to develop the short scale ice flow solution as an explicit perturbation expansion. Then, a small parameter describing the relative size of the bedrock undulations would be used as a small parameter in a perturbation expansion of the solution. This approach was used by Hutter (1983) in his analysis of ice surface undulations. Since the following analysis will only be carried out

to first order, the perturbation approach is equivalent to the linearization, but it is notationally more cumbersome.

4.3.4 Datum ice flow

The long scale solution given by (4.2.28), (4.2.29), (4.2.30) and (4.2.31) has a simple representation in the dimensionless coordinates x,z at $x = 0$. Since the datum flow is slowly varying in x it will be assumed that it is adequately described by the leading order terms of the long scale solution. Noting that at $x = 0$, the z-coordinate of long scale bedrock profile is equal to 0 and the z-coordinate of long scale ice surface is equal to 1, the datum stress solution (4.2.28) at $x = 0$ is given by

$$\underset{0}{\sigma_{xz}} = \underset{0}{\tau_{xz}} = (1-z)\,, \quad \underset{0}{\sigma_{zz}} = -(1-z)\cot\alpha_0\,, \quad \underset{0}{\sigma_{xx}} = \underset{0}{\sigma_{zz}} + 2\underset{0}{\tau_{xx}}\,. \tag{4.3.18}$$

The datum deviatoric stress $\underset{0}{\tau_{xx}} = -\underset{0}{\tau_{zz}}$ is determined as the solution of (4.2.31), which expressed in the short scale variables becomes

$$e = (\underset{0}{\tau_{xx}^2} + \underset{0}{\tau_{xz}^2})^{(n-1)/2}\underset{0}{\tau_{xx}} = (\underset{0}{\tau_{xx}^2} + (1-z)^2)^{(n-1)/2}\underset{0}{\tau_{xx}}\,, \tag{4.3.19}$$

where $e = \underset{0}{\dot\varepsilon_{xx}}(z=1) = (\partial u_0/\partial x)_{z=1}$ is the datum longitudinal strain rate at the surface. $e = O(\delta)$ is small because it is the longitudinal derivative of the datum velocity which is assumed to be slowly varying in the short scale x-coordinate. In dimensional variables e is the ratio of the long scale longitudinal strain rate at the ice surface to the long scale shear strain rate at the bed.

The velocities u_0 and w_0 and the ice flux q_0 derived from (4.2.29) and (4.2.30) are

$$u_0 = c + \frac{2}{(n+1)}(1-(1-z)^{n+1})\,, \quad w_0 = 0\,, \quad q_0 = c + \frac{2}{(n+2)}\,, \tag{4.3.20}$$

because $\underset{z=0}{u_0} = c$ and $h_0 = 1$ in the short scale coordinates. The datum vertical velocity w_0 is zero because the long scale vertical velocity is by (4.2.29) computed from a longitudinal derivative of the horizontal velocity and such longitudinal derivatives are $O(\delta)$ in the x,z-coordinates.

The following properties of the datum solution are needed for the derivation of boundary conditions for the ice flow perturbations.

$$(\partial\underset{0}{\sigma_{xz}}/\partial z) = (\partial\underset{0}{\tau_{xz}}/\partial z) = -1\,, \quad (\partial\underset{0}{\sigma_{zz}}/\partial z) = \cot\alpha_0\,,$$

$$\text{At } z=1\text{:}\quad \underset{0}{\sigma_{xz}} = \underset{0}{\tau_{xz}} = 0\,, \quad \underset{0}{\sigma_{zz}} = 0\,, \quad \underset{0}{\sigma_{xx}} = 2\underset{0}{\tau_{xx}} = 2|e|^{1/n}\mathrm{sign}(e)\,, \quad u_0 = c + 2/(n+1)\,,$$

$$\text{At } z=0\text{:}\quad \underset{0}{\sigma_{xz}} = \underset{0}{\tau_{xz}} = 1\,, \quad \underset{0}{\tau_{xx}} = O(\delta) \approx 0\,, \quad u_0 = c\,, \quad (\partial u_0/\partial z) = 2\,.$$

The datum velocity solution (4.3.20) needs to be slightly modified for the analysis of ice flow with non-linear rheology. This modification is described in section 4.6. Equation (4.3.20) provides a good approximation of this modified datum velocity solution.

4.3.5 Datum viscosity

The flow law field equations (4.3.15) may be interpreted as describing a fluid obeying a linear, anisotropic, incompressible rheology. In general, such rheology is described by a viscosity tensor η_{ijkl}, of rank 4 so that $\Delta\tau_{ij} = 2\eta_{ijkl}\Delta\dot\varepsilon_{kl}$. For incompressible flow in two dimensions, a viscosity tensor η_{ijkl}, has only 4 independent components because of the symmetry of the deviatoric stress and strain rate tensors $\Delta\tau_{ij}$ and $\Delta\dot\varepsilon_{ij}$. For small perturbations in glacier flow obeying Glen's flow law $\tau_{ij} = \tau_{ij}(\dot\varepsilon_{kl}) = \dot\varepsilon^{-(1-1/n)}\dot\varepsilon_{ij} = 2\eta(\dot\varepsilon)\dot\varepsilon_{ij}$, the viscosity tensor for the perturbation flow is $\eta_{ijkl} = \frac{1}{2}(\partial\tau_{ij}/\partial\dot\varepsilon_{kl})$. The non-linear viscosity $\eta = \frac{1}{2}\dot\varepsilon^{-(1-1/n)}$, only depends on the effective shear strain rate $\dot\varepsilon$ (*i.e.* the second invariant of the strain rate tensor). In that case, the viscosity η_{ijkl}, has only 3 independent components, which may be shown to be equal to one half of η_1, η_2 and η_3 defined by (4.3.16). Since the following analysis is carried out in a fixed coordinate system, the rheology as described by (4.3.15) using η_1, η_2 and η_3, is simpler to work with than the tensor form $\Delta\tau_{ij} = 2\eta_{ijkl}\Delta\dot\varepsilon_{kl}$.

The viscosities η_1, η_2 and η_3 defined by (4.3.16) may now be computed using the datum stress field given by (4.3.18) and (4.3.19). For this purpose, it is convenient to define the function $s(d^*)$ as the solution of the equation

$$1 = (s^2 + d^{*2})^{(n-1)/2}s\,. \tag{4.3.21}$$

This equation must be solved by numerical methods, except in the case $n = 3$, where a

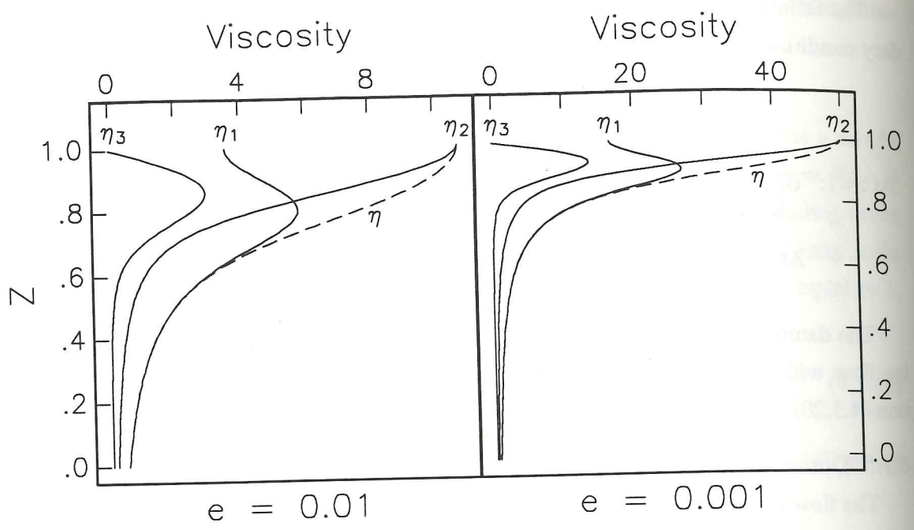

FIGURE 4.3.2: Dimensionless viscosity distribution predicted by a linearization of Glen's flow law for temperate ice for $n = 3$ and $e = 0.01$ (left) and $e = 0.001$ (right). e is the ratio of longitudinal strain rate at the ice surface to shear strain rate at the bed. The viscosity components η_1, η_2 and η_3 are defined by (4.3.16) (solid curves). The viscosity η defined by (4.3.17) is shown for comparison (dashed curves).

closed form solution can be given. Then, the datum longitudinal deviatoric stress τ_{xx}, given as the solution of (4.3.19), can be written as

$$\underset{0}{\tau_{xx}} = |e|^{1/n} s(|e|^{-1/n}(1-z))\text{sign}(e)\,. \tag{4.3.22}$$

Figure 4.3.2 shows the viscosity components η_1, η_2 and η_3 defined by (4.3.16) and the viscosity η defined by (4.3.17) for $e = 0.01$ and $e = 0.001$ in the case $n = 3$. $e = 0.01$ corresponds to the lower range of longitudinal strain rates which are observed on glaciers and ice caps, whereas $e = 0.001$ corresponds to the much lower strain rates which are found on larger ice sheets. The curves for $e = 0.001$ cannot be viewed as realistic for

cold ice sheets because changes in ice viscosity caused by variation of temperature with depth are not taken into account. The effect of the boundary layer on the viscosity is clearly seen. The thickness of the boundary layer $d_b = |e|^{1/3}$, is $d_b \approx 0.2$ for $e = 0.01$ and $d_b = 0.1$ for $e = 0.001$. The figure shows that the curves for η_1 and η_2 intersect and it follows from (4.3.16) that this should happen when $\underset{0}{\tau_{xz}} = \underset{0}{\tau_{xx}}$, which occurs at ice depth $d \approx d_b$.

From (4.3.16) and Figure 4.3.2 it is seen that the viscosity distribution predicted by a linearization of Glen's flow law has the following properties.

1. There is a pronounced variation of the viscosity with depth. The viscosity at the bed is given by $\eta_1 \approx \frac{1}{2}$, $\eta_2 \approx 1/(2n)$, $\eta_3 = O(e)$. The viscosity at the ice surface, on the other hand, is given by $\eta_1 = 1/(2n)|e|^{-(1-1/n)}$, $\eta_2 = \frac{1}{2}|e|^{-(1-1/n)}$, $\eta_3 = 0$. For $|e|$ in the range $0.001 - 0.01$ and $n = 3$, η_1, η_2 at the ice surface are in the range $3.5 - 50$ but the bedrock values are 1/2 and 1/6, respectively.
2. The linearized rheology is anisotropic although Glen's flow law is isotropic. The anisotropy is depth dependent. Near the base $\eta_1 > \eta_2$ which implies that the ice is stiffer in extension/compression than in shear. Near the ice surface $\eta_1 < \eta_2$ and the ice is softer in extension/compression than in shear. This may be understood from the fact that ice deformation, according to the non-linear Glen's flow law, takes advantage of an existing strain rate field. The datum deformation near the base is dominated by shear. Therefore, it is easiest to add more shear deformation there. Near the ice surface, the deformation is dominated by extension/compression in the datum flow. Therefore, it is easier to add more longitudinal deformation there than to initiate shear deformation.
3. There is cross-interaction between deviatoric stress components on one hand, and strain rate components on the other, which does not appear explicitly in the original non-linear form of Glen's flow law. The reason for this interaction is that changes in one strain rate component, for example $\dot{\varepsilon}_{xx}$, modify the effective shear strain rate $\dot{\varepsilon}$, which in turn influences all components of deviatoric stress tensor $\tau_{ij} = \dot{\varepsilon}^{-(1-1/n)}\dot{\varepsilon}_{ij}$, including τ_{xz}. This effect is described by the viscosity component η_3, which can be either positive or negative depending on the sign of e.

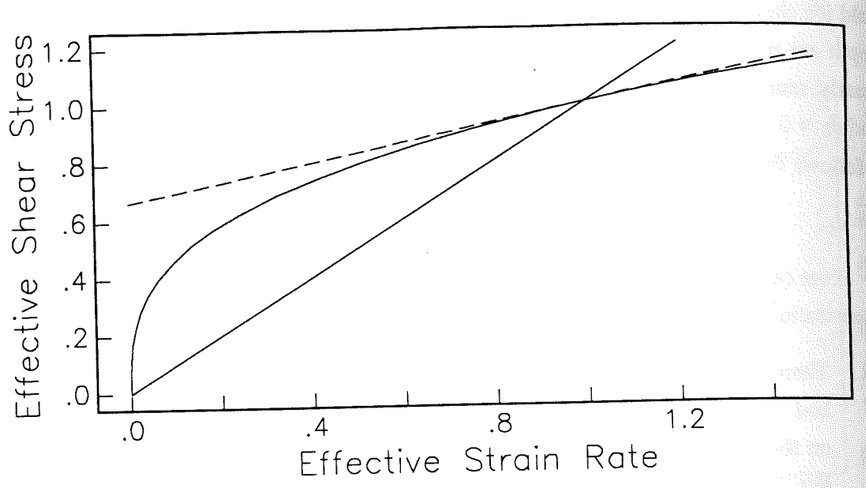

FIGURE 4.3.3: Graphical interpretation of the viscosity components η, η_1 *and* η_2 *(for explanation, see text).*

Figure 4.3.3 shows a graphical interpretation of the viscosity components η, η_1 and η_2. It shows the effective shear stress τ, as a function of the effective strain rate $\dot{\varepsilon}$ as given by Glen's flow law $\tau = \dot{\varepsilon}^{1/n}$ for $n = 3$ (solid concave curve). The standard definition of the viscosity η (*cf.* (4.3.17)) at some value of $\dot{\varepsilon}$ may be interpreted as (one half of) the slope of a line that goes through the origin and intersects the effective shear stress curve at the value of $\dot{\varepsilon}$ for which the viscosity is to be found (solid line, $\dot{\varepsilon}$ is chosen to be equal to 1). This value of the viscosity is the maximum possible value of the viscosity components η_1 and η_2 and corresponds to a perturbation strain rate component which is zero in the datum flow (for example η_2 at the ice surface). The minimum possible value of the viscosity components η_1 and η_2, on the other hand, is equal to (one half of) the slope of the tangent to the effective shear stress curve (dashed line) and corresponds to a change in a perturbation strain rate component when that component is the only non-zero strain rate component in the datum flow (for example η_1 at the ice surface). Other possible values of η_1 and η_2 correspond to (one half of) the slope of a line which intersects the effective shear stress curve at the value of $\dot{\varepsilon}$ and falls between the two lines shown in the figure.

Ice viscosity of cold ice sheets can, in principle, be treated in the same way as described above by allowing the ice flow parameter A to depend on the ice depth, or temperature which in turn depends on the ice depth. Then, the definition of the time-scale $\tilde{t}_0$ must use a scale for the variable A instead of A itself, and a dimensionless flow law parameter must be added to (4.3.4). As a rule the temperature of cold ice sheets increases with ice depth and the value of A, which is inversely proportional to ice viscosity, increases with temperature. Therefore, this leads to even larger vertical variation in the ice viscosity than shown in Figure 4.3.2.

Finally, it may be noted that for two-dimensional flow the problem of a singularity in the ice viscosity at the ice surface has not been completely solved by taking the effect of $\tau_{\underset{0}{xx}}$ on the viscosity into account as described above. The longitudinal velocity gradient in glacier flow ordinarily goes from positive values in the accumulation area to negative values in the ablation area. Therefore, there must be at least one point on each flow line, where the longitudinal velocity gradient at the ice surface is zero. At such a point, it is impossible to use (4.3.22) to find $\tau_{\underset{0}{xx}}$, since $e = 0$. This problem cannot be adequately solved for two-dimensional flow, which therefore cannot be linearized in this way at such points. However, all real glacier flow is to some extent three-dimensional. This means that there will in general be non-zero transverse deviatoric stress components $\tau_{\underset{0}{yy}}$ and $\tau_{\underset{0}{xy}}$, at the ice surface which will determine a finite ice viscosity at the surface, even when the longitudinal velocity gradient at the surface is zero. To deal with points where the longitudinal velocity gradient is zero in the following, rough estimates of e are assumed to incorporate the effect of non-zero $\tau_{\underset{0}{yy}}$ and $\tau_{\underset{0}{xy}}$ deviatoric stress components.

4.3.6 Linearization of boundary conditions

The boundary conditions (4.3.5), (4.3.6), (4.3.7) and (4.3.8) apply at the perturbed surface and bedrock profiles $z = z_{\underset{0}{s}} + \Delta z_s$ and $z = z_{\underset{0}{b}} + \Delta z_b$. This is inconvenient since the datum ice flow is only known for z between $z = z_{\underset{0}{s}}$ and $z = z_{\underset{0}{b}}$. At points where $\Delta z_s > 0$ or $\Delta z_b < 0$ the datum solution is undefined at the perturbed boundary. This problem is overcome by linearizing the boundary conditions about the datum geometry (*cf.*

Hutter, 1983). For this purpose the stress solution at $z = z_s$ is written as

$$\sigma_{ij}\Big|_{z=z_s} = \sigma_{ij}\Big|_{z=z_{s_0}} + \left[\frac{\partial\sigma_{ij}}{\partial z}\right]_{z=z_{s_0}} \Delta z_s = \sigma_{ij}\Big|_{z=z_{s_0}} + \Delta\sigma_{ij}\Big|_{z=z_{s_0}} + \left[\frac{\partial\sigma_{ij}}{\partial z}\right]_{z=z_{s_0}} \Delta z_s ,$$

to first order in the perturbations. The velocity components at the surface and the stresses and the velocity components at the base are expanded similarly. In this way the boundary conditions can be reformulated to apply at the datum ice surface and bedrock profiles.

The datum geometry is slowly varying in x. Also, the x-axis is parallel to the datum ice surface at $x = 0$ by definition, and $z_{s_0} = 1$ at $x = 0$. Thus, $z_{s_0} = 1 + \frac{1}{2}(\partial^2 z_{s_0}/\partial x^2)x^2 + \cdots = 1 + O(\delta^2)$. The datum bedrock geometry, on the other hand, satisfies $z_{b_0} = 0 + (dz_{b_0}/dx)x + \cdots = 0 + O(\delta)$, because $z_{b_0} = 0$ at $x = 0$. It will be assumed that this variation in the datum geometry can be ignored to a first approximation, so that the boundary conditions can be formulated at $z = 1$ and $z = 0$, independent of x. The validity of this approximation will, in the case of steady state surface undulations, depend on the length over which a localized bedrock disturbance influences the steady state surface geometry. This problem is further discussed in subsection 4.7.3.

The above approximations lead to the following boundary conditions for the ice flow perturbations to first order.

At the datum surface $z = 1$:

$$\frac{\partial\Delta z_s}{\partial t} + \frac{\partial\Delta q}{\partial x} = \Delta b \,, \quad \text{where} \quad \Delta q = \int_0^1 \Delta u dz + u_{0}\Big|_{z=1} \Delta z_s - u_{0}\Big|_{z=0} \Delta z_b \,, \tag{4.3.23}$$

$$-2\frac{\partial\Delta z_s}{\partial x}|e|^{1/n}\text{sign}(e) + \Delta\sigma_{xz} - \Delta z_s = 0 \,, \tag{4.3.24a}$$

$$\Delta\sigma_{zz} + \cot\alpha_0 \Delta z_s = 0 \,. \tag{4.3.24b}$$

At the datum base $z = 0$:

$$-u_0 \frac{d\Delta z_b}{dx} + \Delta w = 0 \,, \tag{4.3.25}$$

$$\Delta u + \frac{\partial u_0}{\partial z}\Delta z_b = mc(\Delta\tau_{xz} - \Delta z_b) \,. \tag{4.3.26}$$

The properties of the datum solution, which were derived in a previous subsection, were used in the derivation of the above boundary conditions, together with the fact that the original boundary conditions are satisfied by the datum solution in the absence of perturbations. In order to get (4.3.26) from (4.3.8) it was assumed that the angle $\tan\theta = -(d\Delta z_b/dx)$ is small so that $\cos\theta$ and $\sin\theta$ can be approximated by 1 and $-(d\Delta z_b/dx)$, respectively.

The above boundary conditions are correct to first order in the perturbations. The surface and basal slope perturbations $-\tan^{-1}(\partial\Delta z_s/\partial x)$ and $-\tan^{-1}(d\Delta z_b/dx)$ have to be small compared to 1 in order for the boundary conditions to be valid. The slope perturbations do *not*, however, have to be small compared to the long scale average slope $\tan\alpha_0$. This is important, since a theory of ice surface undulations must be able to handle surface slope fluctuations equal to or greater than the long scale average surface slope, as noted earlier.

The system of field equations (4.3.12), (4.3.13) and (4.3.15) together with the boundary conditions (4.3.23), (4.3.24), (4.3.25) and (4.3.26) has only two independent, dimensionless combinations of physical parameters, c and e. The values of c and e together with the long scale surface slope α_0 and the flow law and sliding law powers n and m fully determine the nature of the problem. The dimensional physical parameters $\tilde{h}_0$, A, C, ρ and g only affect the ice flow solution through their influence on the dimensionless parameters c and e.

4.3.7 Ice flux perturbations

It is convenient to start an analysis of steady state ice surface undulations by computing the ice flux perturbation Δq, for general surface and basal geometries, without assuming steady state flow, which means that the boundary condition (4.3.23) is not used. Apart from being a good starting point for the steady state analysis, expressions for flux

perturbations are useful for time-dependent analysis of glacier flow through (3.6.2) and (4.3.23). Time-dependent glacier flow is examined in Chapter 6.

The system of field equations (4.3.12), (4.3.13) and (4.3.15) is homogeneous, which means that all flow perturbations are brought about by perturbations in the surface and basal geometries through the boundary conditions (4.3.24), (4.3.25) and (4.3.26). Four different causes for flux variations may be identified from the boundary conditions.

1. Variations in the shear stress, $\Delta\sigma_{xz}$ at $z = 1$.
2. Variations in the normal stress, $\Delta\sigma_{zz}$ at $z = 1$.
3. Advection of surface undulations Δz_s, with the datum surface speed $u_{0\,z=1}$.
4. Variations in the bedrock geometry Δz_b.

Based on this list the flux perturbation Δq may be decomposed into four components

$$\Delta q = \Delta q_e + \Delta q_n + \Delta q_a + \Delta q_b \,. \tag{4.3.27}$$

By the linearity of the problem, each component may be found separately from a corresponding set of simplified boundary conditions, derived from (4.3.24), (4.3.25) and (4.3.26). It turns out to have certain advantages to split the effect of the ice surface undulations Δz_s into the three different components; (1) the shear stress component Δq_e, (2) the normal stress component Δq_n, and (3) the advection component Δq_a. In this way the full problem of determining Δq is split into four independent subproblems, each determining one of the components Δq_e, Δq_n, Δq_a and Δq_b.

The advection component is easily determined from the datum flow as

$$\Delta q_a = u_{0\,z=1}\,\Delta z_s = (2/(n+1) + c)\Delta z_s \,. \tag{4.3.28}$$

The other three flux perturbation components must be found by solving the system of field equations and boundary conditions for the perturbation ice flow. Each component corresponds to a different version of the boundary conditions (4.3.24), (4.3.25) and (4.3.26).

Δq_e:

$$\text{At } z=1:\ \Delta\sigma_{xz} = \Delta\sigma_{xz\,z=1} = \Delta z_s + 2(\partial\Delta z_s/\partial x)\,|e|^{1/n}\text{sign}(e)\,,\ \ \Delta\sigma_{zz} = 0\,, \tag{4.3.29a}$$

$$\text{At } z=0:\ \Delta w = 0\,,\ \ \Delta u = mc\Delta\tau_{xz}\,.$$

Δq_n:

$$\text{At } z=1:\ \Delta\sigma_{xz} = 0\,,\ \ \Delta\sigma_{zz} = \Delta\sigma_{zz\,z=1} = -\cot\alpha_0\Delta z_s\,, \tag{4.3.29b}$$

$$\text{At } z=0:\ \Delta w = 0\,,\ \ \Delta u = mc\Delta\tau_{xz}\,.$$

Δq_b:

$$\text{At } z=1:\ \Delta\sigma_{xz} = 0\,,\ \ \Delta\sigma_{zz} = 0\,, \tag{4.3.29c}$$

$$\text{At } z=0:\ -u_0\frac{d\Delta z_b}{dx} + \Delta w = 0\,,\ \ \Delta u + \frac{\partial u_0}{\partial z}\Delta z_b = mc(\Delta\tau_{xz} - \Delta z_b)\,.$$

The "forcing" functions $\Delta\sigma_{xz\,z=1} = \Delta z_s + 2(\partial\Delta z_s/\partial x)\,|e|^{1/n}\text{sign}(e)$, $\Delta\sigma_{zz\,z=1} = -\cot\alpha_0\Delta z_s$, Δz_s and Δz_b determine the flux perturbation components Δq_e, Δq_n, Δq_a and Δq_b, respectively. Although both $\Delta\sigma_{xz\,z=1}$ and $\Delta\sigma_{zz\,z=1}$ are uniquely determined by Δz_s, these functions may be considered independent of Δz_s during the computation of the flux perturbations.

Interestingly, the long scale surface slope α_0, only appears as a multiplying factor $\cot\alpha_0$, in the expression for $\Delta\sigma_{zz\,z=1}$. Furthermore, it does not influence the field equations since the viscosity distribution is independent of α_0. As a consequence the flux perturbation components can be computed without considering the effect of α_0, except for a $\cot\alpha_0$ multiplying factor in the expression for Δq_n. This decoupling makes the analysis simpler than it would otherwise be.

4.3.8 Steady state ice surface undulations

In the absence of mass balance variations, steady state two-dimensional flow must by (4.3.23) satisfy $(d\Delta q/dx) = 0$; thus, Δq = constant, equal to zero, independent of x. Steady state two-dimensional flow must therefore satisfy

$$\Delta q = \Delta q_e + \Delta q_n + \Delta q_a + \Delta q_b = 0 \,. \tag{4.3.30}$$

If Δq_e, Δq_n, Δq_a and Δq_b have been found for general variations in the surface and basal geometries Δz_s and Δz_b, (4.3.30) can be solved for Δz_s in terms of Δz_b. Therefore, (4.3.30) determines the transfer of bedrock undulations to the ice surface.

Ice surface undulations may lead to mass balance perturbations, which can for example be caused by snowdrift from high to low places on the ice surface. In that case the above steady state equation becomes

$$\Delta q = \Delta q_e + \Delta q_n + \Delta q_a + \Delta q_b = \int_{-\infty}^{x} \Delta b d\xi \,. \tag{4.3.31}$$

If Δb can be expressed as a function of Δz_s this equation may be viewed as an implicit equation determining Δz_s in terms of Δz_b.

The computation of the flux perturbation components Δq_e, Δq_n, Δq_a and Δq_b for non-linear rheology must be done by numerical methods. Before this is done, the flux analysis and the corresponding steady state analysis will be carried out analytically for two special cases; for the laminar flow approximation and for linear Newtonian rheology. The analytical results provide background for interpretation and understanding of the corresponding results for non-linear rheology.

4.4 LAMINAR FLOW APPROXIMATION

4.4.1 General

The laminar flow approximation should provide an accurate representation of glacier flow if all longitudinal flow gradients are small. Thus, ice surface undulations predicted by the laminar flow approximation may be expected to be reasonable when the bedrock undulations are slowly varying. In fact, a theory based on the laminar flow approximation should be valid as the long wavelength limit of any theory based on the full ice flow equations developed in the previous subsections, as these equations reduce to the laminar flow approximation in the limit of long wavelengths.

Flux perturbations predicted by the laminar flow approximation (3.7.4a), expressed in the short scale variables, are given by

$$\frac{\Delta q}{q_{d_0}} = ((n+2) + r_0(m+1))(\Delta z_s - \Delta z_b) - (n + r_0 m)\cot\alpha_0(\partial \Delta z_s/\partial x) \,, \tag{4.4.1}$$

where $q_{d_0} = 2/(n+2)$, $q_{s_0} = c$ and $r_0 = q_{s_0}/q_{d_0} = c\,(n+2)/2$. Since the datum longitudinal velocity at the ice surface is given by $u_{0\,z=1} = c + 2/(n+1)$, the flux perturbation components Δq_e, Δq_n, Δq_a and Δq_b, predicted by the laminar flow approximation are

$$\begin{aligned} \Delta q_e &= (2n/(n+1) + mc)\Delta z_s \\ \Delta q_n &= (2n/(n+2) + mc)\cot\alpha_0(-\partial \Delta z_s/\partial x) \\ \Delta q_a &= (2/(n+1) + c)\Delta z_s \\ \Delta q_b &= -(2 + (m+1)c)\Delta z_b \,. \end{aligned} \tag{4.4.2}$$

These expressions will be useful later on.

The steady state equation for the laminar flow approximation in the absence of mass balance perturbations, follows from (4.3.30) and (4.4.1)

$$((n+2) + r_0(m+1))(\Delta z_s - \Delta z_b) - (n + r_0 m)\cot\alpha_0(d\Delta z_s/dx) = 0 \,.$$

This equation may be rewritten as

$$-l_1 \frac{d\Delta z_s}{dx} + \Delta z_s = \Delta z_b \,, \tag{4.4.3}$$

where the length l_1, is defined by

$$l_1 = \frac{n + r_0 m}{(n+2) + r_0(m+1)}\cot\alpha_0 \,. \tag{4.4.4}$$

For long scale surface slopes $\tan\alpha_0$ between 0.1 and 0.01, $n = 3$ and $m = 2$, the length l_1 is in the range 6 - 70.

It is seen from (4.4.4) that the most important parameter determining the length scale l_1, is the long scale surface slope α_0. The relative importance of basal sliding as described by r_0, does not have a large effect on the problem. The effect of r_0 is equivalent to a relatively small change in the powers n and m or in the long scale surface slope $\tan\alpha_0$. The non-linear flow law ($n > 1$) and sliding law ($m > 1$) of ice lead to an increase in l_1 compared to linear behavior for which $n = m = 1$. For $n = 3$ and $m = 2$, l_1

is increased by a factor between 4/3 and 9/5 compared to $n = m = 1$, depending on the relative importance of basal sliding. In the limit n and $m \to \infty$, which corresponds to perfectly plastic rheology, the length-scale becomes $l_1 = \cot\alpha_0$. Equation (4.4.3) and the effect of the flow law and sliding law powers n and m on l_1 given by (4.4.4) provides a simple interpretation of the influence of the non-linear rheology and sliding of glaciers on (long wavelength) ice surface undulations.

Equations (4.4.3) and (4.4.4) are equivalent to Nye's (1959b,c) result as expressed by (2.2.1) in the case of pure sliding (*i.e.* in the limit $r_0 \to \infty$).

Equation (4.4.3) is an ordinary differential equation which can be solved for Δz_s in terms of the "forcing" function Δz_b. It is instructive to carry this solution out both in the frequence domain using a transfer function, and in the space domain using a Green's function.

4.4.2 Transfer functions

Taking the Fourier transform (*cf.* subsection 3.3.2) of (4.4.3) leads to

$$(-ikl_1 + 1)\Delta\hat{z}_s = \Delta\hat{z}_b \, .$$

Thus, the Fourier transform of the ice surface undulations can be written

$$\Delta\hat{z}_s = t(k)\Delta\hat{z}_b \, , \tag{4.4.5}$$

where the transfer function $t(k)$ (*cf.* subsection 3.3.3) from the base to the surface is given by

$$t(k) = \frac{1}{1 - ikl_1} \, . \tag{4.4.6}$$

The transfer amplitude and phase shift are then found to be

$$|t(k)| = \frac{1}{\sqrt{1 + (kl_1)^2}} \, , \quad \phi(k) = \tan^{-1}(kl_1) \, . \tag{4.4.7}$$

The wave number k is defined as $k = 2\pi/\lambda$ where λ is the wavelength of a harmonic undulation.

By (4.4.4), the length l_1 is inversely proportional to the long scale surface slope $\tan\alpha_0$. Thus, l_1 is a relatively large number for the low values of the surface slope found on glaciers and ice caps. As a consequence, the transfer amplitude given by (4.4.7) is small as long as $k = 2\pi/\lambda = O(1)$, which corresponds to undulation wavelengths on the order of a few to ten ice thicknesses. Furthermore, the transfer phase shift $\phi(k) \simeq \pi/2$ for such undulations. On the other hand, (4.4.7) also shows that as $k \to 0$, *i.e.* in the limit of asymptotically long wavelengths, $t(k) \to 1$ and consequently $|t(k)| \to 1$, $\phi(k) \to 0$. This means that very long bedrock undulations are perfectly transferred to the ice surface, independent of the value of the long scale surface slope or the relative importance of basal sliding.

Figure 4.4.1 shows the transfer amplitude $|t(k)|$, and phase shift $\phi(k)$, given by (4.4.7) plotted as functions of the wavelength $\lambda = 2\pi/k$ for no basal sliding and the flow law powers $n = 3$ (solid curves) and $n = 1$ (dashed curves). The picture is essentially the same independent of the relative importance of basal sliding. For $\lambda \gtrsim 4\pi$ or $k \lesssim ½$, $|t|$ and ϕ as predicted by the laminar flow approximation for $n = 1$ are close to the transfer amplitude and phase shift predicted by linear Newtonian rheology (*cf.* Hutter, 1983, Figs. 4.3 and 4.4; see also Figures 4.5.3 and 4.5.4 in section 4.5, on linear Newtonian flow, below). This indicates that for $\lambda \gtrsim 4\pi$ or $k \lesssim ½$, much of the variation of the transfer function with the wavelength $\lambda = 2\pi/k$, and the long scale surface slope $\tan\alpha_0$, can be adequately explained by the laminar flow approximation. Figure 4.4.1 does not extend to very long wavelengths and therefore the approach to the limit $|t| \to 1$ and $\phi \to 0$ as $\lambda \to \infty$ or $k \to 0$ is not fully illustrated. The predicted transfer amplitudes for $n = 3$ are lower than the corresponding curves for $n = 1$, which shows that the non-linear flow law of ice leads to more damping than would be the case for linear Newtonian rheology.

4.4.3 Green's functions

Using standard methods for the solution of first order ordinary differential equations, the space domain solution of (4.4.3) is found to be

$$\Delta z_s = \int_x^\infty \frac{1}{l_1} e^{(x-\xi)/l_1} \Delta z_b(\xi) d\xi = \int_{-\infty}^{\infty} g(x-\xi)\Delta z_b(\xi) d\xi = g(x) * \Delta z_b(x) \, . \tag{4.4.8}$$

The Green's function $g(x)$ (*cf.* subsection 3.3.4) for the transfer of bedrock undulations to

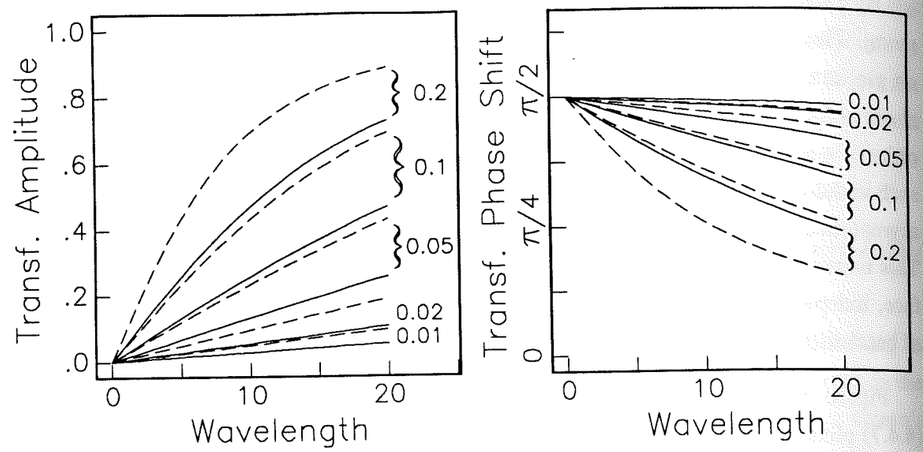

FIGURE 4.4.1: *The transfer amplitude $|t|$ (left) and phase shift ϕ (in radians) (right) for the transfer of bedrock undulations to the ice surface predicted by the laminar flow approximation for no basal sliding ($r_0 = 0$) and a range of long scale surface slopes $\tan\alpha_0$ (cf. (4.4.7)). $|t|$ and ϕ are plotted as functions of dimensionless wavelength $\lambda = 2\pi/k$. Solid curves are for $n = 3$. Dashed curves are for $n = 1$. The curves are labeled with $\tan\alpha_0$. The $n = 1$ amplitude curves are higher that the corresponding curves for $n = 3$, but the $n = 1$ phase shift curves are lower.*

the surface is therefore given by

$$g(x) = 0 \text{ for } x > 0\,, \quad g(x) = \frac{1}{l_1} e^{x/l_1} \text{ for } x < 0\,. \tag{4.4.9}$$

$g(x)$ can also by found by inverting $t(k)$ given by (4.4.6), since $\hat{g}(k) = t(k)$ (*cf.* subsection 3.3.4).

The Green's function $g(x)$, is the solution of (4.4.3) corresponding to a sharp spike or δ-function in the bedrock geometry Δz_b. A δ-function in the bedrock geometry cannot, of course, be considered to be slowly varying in x, which is a condition for the validity of

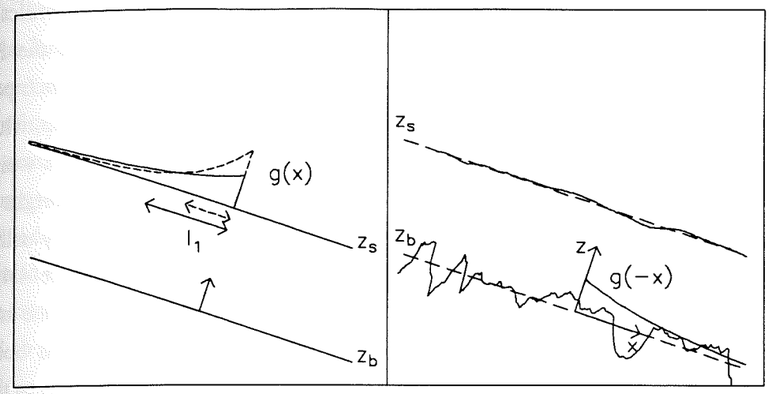

FIGURE 4.4.2: *The Green's function $g(x)$ predicted by the laminar flow approximation (left) (cf. (4.4.9)) and an illustration of its use as a filter (right) (see text). The figures show a parallel slab of ice resting on an inclined plane with perturbations in the basal and ice surface geometries z_b and z_s. The arrow in the left figure indicates a δ-function perturbation in the basal geometry. The x,z-coordinate system is indicated with arrows in the figure on the right. The dashed $g(x)$ curve in the left figure is computed for $n = 1$ for comparison with the solid curve which is computed for $n = 3$. The length-scales l_1 (cf. (4.4.4)) are indicated below the curves of $g(x)$.*

the laminar flow approximation as noted earlier. This does not, however, mean that $g(x)$ is invalid. It only means that when $g(x)$ is used to compute Δz_s from Δz_b using (4.4.8), then Δz_b, and consequently Δz_s, must be slowly varying in x.

Equation (4.4.9) shows that, according to the laminar flow approximation, a sharp basal peak leads to the creation of a surface bump on the upstream side of the peak as illustrated in Figure 4.4.2 (left). The bump decays exponentially on the length-scale l_1 away from the spike. The basal peak has no effect on the ice surface on the downstream side. The non-linear flow law and sliding law influence the Green's function $g(x)$, through their effect on the length-scale l_1, defined by (4.4.4).

Equations (4.4.8) and (4.4.9) show that the ice surface undulations Δz_s, predicted by the laminar flow approximation are an exponentially weighted average of the *downstream* bedrock undulations Δz_b. This is illustrated in Figure 4.4.2 (right). Each point ξ on the downstream side of a point x can be associated with an upstream bump, which is proportional to Δz_b at ξ. The predicted ice surface perturbation Δz_s, at x is a weighted sum of Δz_b at all points ξ, on the downstream side of x using $g(x-\xi)$ as a weight function. In this way, the ice surface geometry is obtained from the basal geometry using the Green's function as a filter. Note how areas of high bedrock relief in Figure 4.4.2 are associated with large ice surface slopes, whereas bedrock troughs lead to low ice surface slopes. Figure 4.4.2 shows that the Green's function or filter $g(x)$ explains both the *damping* and the *phase shift* associated with the transfer of bedrock undulations to the ice surface.

Since $\int_{-\infty}^{\infty} g(x)dx = 1$, (4.4.8) and (4.4.9) predict that the total volume of ice in the surface perturbations $\int_{-\infty}^{\infty} \Delta z_s dx$, is exactly equal to the total volume of the bedrock perturbations $\int_{-\infty}^{\infty} \Delta z_b dx$. This is related to the fact that the limit of the transfer function $t(k)$ as $k \rightarrow 0$ or $\lambda \rightarrow \infty$ is equal to 1, since $t(k=0) = \int_{-\infty}^{\infty} g(x)dx = 1$.

Figures 4.4.1 and 4.4.2 illustrate two equivalent ways of describing the transfer of bedrock undulations to the surface of an ice cap. The transfer function description ((4.4.5), (4.4.6) and (4.4.7), on one hand, and the Green's function description ((4.4.8) and (4.4.9), on the other, are both valuable for an understanding of the nature of the transfer. The Green's function $g(x)$, is a real function (Fig. 4.4.2), whereas the transfer function $t(k)$, is complex and therefore has to be represented as two real functions $|t(k)|$ and $\phi(k)$ (Fig. 4.4.1). The figures show that a simple form of the Green's function may not be easily recognized from a plot of the transfer amplitude and phase shift. Furthermore, the Green's function is often easier to understand in terms of the physics of the ice flow. More emphasis will, therefore, be placed on an interpretation of Green's functions in the following.

4.4.4 Transfer of long undulations

The laminar flow approximation is an exact solution of the ice flow equations in the absence of longitudinal flow gradients. As longitudinal gradients must become insignificant for very long undulations, the laminar flow approximation becomes increasingly accurate as the wavelength of flow undulations becomes longer. This means that in the long wavelength limit, conclusions drawn from the laminar flow approximation must be valid for any theory based on the full ice flow equations. In particular, this means that any valid theory of ice surface undulations must predict that asymptotically long waves in the bedrock geometry must be perfectly transferred to the ice surface, since this was found to be a consequence of the laminar flow approximation in the long wavelength limit.

It appears that many previous authors did not realize that bedrock undulations with infinite wavelength, *i.e.* a layer of uniform thickness, must be perfectly transferred to the surface. This is equivalent to saying that the transfer function must approach 1 as the wavelength of the undulations goes to infinity. Yosida's (1964) original analytical solution for a linear Newtonian fluid without basal sliding does not satisfy this requirement. Neither does the considerable improvement of Hutter and others (1981) over Yosida's solution. Budd's (1969, 1970b) conclusion that the transfer decays to zero as the wavelength goes to infinity is of course in direct contradiction to the above requirement. It is only with Hutter's (1983) and Reeh's (1987) improved analytical solutions for linear rheology that the requirement of perfect transfer at infinite wavelengths is satisfied. Even then, Hutter's (1983, Eq. (4.56)) expression for the limit of the transfer function for asymptotically long wavelengths, apparently incorrectly derived from the full expression, is not 1 for non-zero basal sliding, and this is explicitly mentioned in the text as a valid theoretical prediction.

In view of the above it is worthwhile to reiterate the physical basis for perfect transfer of bedrock undulations with asymptotically long wavelengths to the surface. The analyses of the problem of steady flow over bedrock undulations are perturbation analyses based on the assumption of a datum solution. The datum solution corresponds to uniform flow down an inclined plane. This solution would be realized in the complete absence of bedrock perturbations. A bedrock "undulation" of infinite wavelength

amounts to nothing more than a uniform vertical shifting of the inclined plane. Therefore, the datum solution itself, vertically shifted by the same distance as the inclined plane, solves the problem when the wavelength of the undulation is infinite. This clearly means that the steady state surface will be shifted by the same distance, *i.e.* that the undulation is perfectly transferred. Thus, the limit of the transfer function for infinite wavelengths is equal to 1. Assuming that the solution of the problem is unique, this statement is not restricted to linear Newtonian fluid nor to small perturbations. This is because the vertically shifted datum solution for uniform flow with a given flux of ice down an inclined plane with non-linear rheology and a particular basal sliding law, will be the only solution of the perturbed problem for any uniform vertical displacement of the plane. Thus, the requirement of perfect transfer at infinite wavelengths must be satisfied for any analytical or numerical model of steady flow over bedrock undulations. This requirement is essentially equivalent to the statement that the steady state flow and geometry of a glacier will not be altered by a uniform uplift of the underlying bedrock alone.

4.5 LINEAR NEWTONIAN FLOW

4.5.1 General

The system of field equations (4.3.12), (4.3.13) and (4.3.15) together with the boundary conditions (4.3.24), (4.3.25) and (4.3.26) for ice flow perturbations can be solved analytically in the wave number domain for linear Newtonian rheology, in which case $n = m = 1$. This analytical solution is important for comparison with the laminar flow approximation and with numerical solutions for non-linear rheology.

The viscosities η_1, η_2 and η_3 defined by (4.3.16) are given by $\eta_1 = \eta_2 = ½$ and $\eta_3 = 0$ for linear Newtonian rheology, as noted earlier. Viscosity computations based on (4.3.19) and (4.3.21) are therefore not needed in this case. Moreover, as $\underset{0}{\tau_{xx}} = \underset{0}{\dot{\varepsilon}_{xx}} = O(\delta)$, the term arising from $\underset{0}{\tau_{xx}}$ in the surface boundary condition (4.3.24a) is small and may be neglected to first approximation.

The long scale datum velocity solution for $n = 1$ is given by

$$u_0 = c + (1 - (1-z)^2)\,, \quad w_0 = 0\,,$$
$$\underset{z=0}{u_0} = c\,, \quad \underset{z=1}{u_0} = c + 1\,, \quad (\partial u_0/\partial z)_{z=0} = 2\,,$$
$$q_0 = c + 2/3\,.$$

4.5.2 The stream function

The easiest way to solve the ice flow equations for linear Newtonian rheology is to introduce a stream function ψ, for the perturbation velocity field, such that

$$\Delta u = \frac{\partial \psi}{\partial z}\,, \quad \Delta w = -\frac{\partial \psi}{\partial x}\,. \tag{4.5.1}$$

The equation of continuity (4.3.12), is automatically satisfied when the velocity field is expressed in this way.

The deviatoric stress perturbations $\Delta\tau_{ij}$, can then be written as

$$\Delta\tau_{xx} = \frac{\partial^2 \psi}{\partial x \partial z}\,, \quad \Delta\sigma_{xz} = \Delta\tau_{xz} = ½\left(\frac{\partial^2 \psi}{\partial z^2} - \frac{\partial^2 \psi}{\partial x^2}\right), \tag{4.5.2}$$

by substituting (4.5.1) into (4.3.15). Using (4.5.1) and (4.5.2), the field equations and boundary conditions for the ice flow perturbations can be written entirely in terms of the stream function ψ. This reduces the number of independent unknown functions that need to be found from 5 to 1.

The ice flux perturbation Δq, defined in (4.3.23), can also be written in terms of the stream function as

$$\Delta q = \psi_{z=1} - \psi_{z=0} + (1 + c)\Delta z_s - c\Delta z_b\,.$$

4.5.3 Field equations

The equation of continuity (4.3.12) is already satisfied by the stream function formulation. The flow law equations (4.3.15) are also automatically satisfied by expressing the deviatoric stresses $\Delta\tau_{ij}$, in terms of the stream function ψ, using (4.5.2). The only field equations left are the force balance equations (4.3.13). Subtracting the $(\partial/\partial x)$ derivative of (4.3.13b) from the $(\partial/\partial z)$ derivative of (4.3.13a) and using (4.5.2), leads to the so-called biharmonic equation for the stream function ψ

$$\frac{\partial^4\psi}{\partial x^4} + 2\frac{\partial^4\psi}{\partial x^2\partial z^2} + \frac{\partial^4\psi}{\partial z^4} = \nabla^4\psi = 0\,. \qquad (4.5.3)$$

If the stream function satisfies the biharmonic equation (4.5.3), then the velocity field given by (4.5.1) and the stress field given by (4.5.2) will satisfy the equation of continuity and the force balance equations. Thus, all the field equations (4.3.12), (4.3.13) and (4.3.15) may be replaced by the biharmonic equation (4.5.3).

4.5.4 Boundary conditions

The stress boundary condition (4.3.24b) involves $\Delta\sigma_{zz}$ at the ice surface. $\Delta\sigma_{zz}$ does not follow directly from the stream function and therefore (4.3.24b) must be reformulated slightly in order to express it in terms of ψ. This is done by writing the $(\partial/\partial x)$ derivative of $\Delta\sigma_{zz}$ as

$$\frac{\partial\Delta\sigma_{zz}}{\partial x} = \frac{\partial\Delta\sigma_{xx}}{\partial x} - 2\frac{\partial\Delta\tau_{xx}}{\partial x} = -\frac{\partial\Delta\tau_{xz}}{\partial z} - 2\frac{\partial\Delta\tau_{xx}}{\partial x} = -\tfrac{1}{2}\left(\frac{\partial^3\psi}{\partial z^3} + 3\frac{\partial^3\psi}{\partial x^2\partial z}\right),$$

using (4.3.13a) and (4.5.2), and replacing the boundary condition (4.3.24b) by its $(\partial/\partial x)$ derivative.

The boundary conditions (4.3.24), (4.3.25) and (4.3.26) then become as follows.

At the datum surface $z = 1$:

$$\tfrac{1}{2}\left(\frac{\partial^2\psi}{\partial z^2} - \frac{\partial^2\psi}{\partial x^2}\right) = \Delta\sigma_{\underset{z=1}{xz}} = \Delta z_s\,, \qquad (4.5.4)$$

$$-\tfrac{1}{2}\left(\frac{\partial^3\psi}{\partial z^3} + 3\frac{\partial^3\psi}{\partial x^2\partial z}\right) = \frac{\partial\Delta\sigma_{\underset{z=1}{zz}}}{\partial x} = -\cot\alpha_0\frac{\partial\Delta z_s}{\partial x}\,. \qquad (4.5.5)$$

At the datum base $z = 0$:

$$-c\frac{d\Delta z_b}{dx} - \frac{\partial\psi}{\partial x} = 0\,, \qquad (4.5.6)$$

$$\frac{\partial\psi}{\partial z} + 2\Delta z_b = c\left(\tfrac{1}{2}\left(\frac{\partial^2\psi}{\partial z^2} - \frac{\partial^2\psi}{\partial x^2}\right) - \Delta z_b\right). \qquad (4.5.7)$$

4.5.5 Transformation into the wave number domain

An analytical solution of equations (4.5.3), (4.5.4), (4.5.5), (4.5.6) and (4.5.7) can be derived by taking the Fourier transform in the x-direction. The transformed biharmonic equation is

$$k^4\hat{\psi} - 2k^2\frac{\partial^2\hat{\psi}}{\partial z^2} + \frac{\partial^4\hat{\psi}}{\partial z^4} = 0\,. \qquad (4.5.8)$$

Boundary conditions at the datum surface $z = 1$:

$$\tfrac{1}{2}\left(\frac{\partial^2\hat{\psi}}{\partial z^2} + k^2\hat{\psi}\right) = \Delta\hat{\sigma}_{\underset{z=1}{xz}} = \Delta\hat{z}_s\,, \qquad (4.5.9)$$

$$-\tfrac{1}{2}\left(\frac{\partial^3\hat{\psi}}{\partial z^3} - 3k^2\frac{\partial\hat{\psi}}{\partial z}\right) = ik\Delta\hat{\sigma}_{\underset{z=1}{zz}} = \cot\alpha_0(-ik\Delta\hat{z}_s)\,. \qquad (4.5.10)$$

Boundary conditions at the datum base $z = 0$:

$$-ikc\,\Delta\hat{z}_b - ik\hat{\psi} = 0\,, \qquad (4.5.11)$$

$$\frac{\partial\hat{\psi}}{\partial z} + 2\Delta\hat{z}_b = c\left(\tfrac{1}{2}\left(\frac{\partial^2\hat{\psi}}{\partial z^2} + k^2\hat{\psi}\right) - \Delta\hat{z}_b\right). \qquad (4.5.12)$$

The transformed biharmonic equation (4.5.8) is a linear ordinary differential equation in z and has the general solution

$$\hat{\psi} = (A + Cz)\sinh kz + (B + Dz)\cosh kz\,. \qquad (4.5.13)$$

The constants A, B, C and D must be determined so that the boundary conditions (4.5.9), (4.5.10), (4.5.11) and (4.5.12) are satisfied. The expression of the boundary conditions as equations for A, B, C and D and the solution of the resulting equations is carried out in Appendix 2.

The result of the derivation in Appendix 2 is an analytical expression (A2.4) for the Fourier transforms of the ice flux perturbation components Δq_e, Δq_n, Δq_a and Δq_b, (*cf.* subsection 4.3.7) predicted by linear Newtonian rheology for perturbations in $\Delta\sigma_{\underset{z=1}{xz}}$, $\Delta\sigma_{\underset{z=1}{zz}}$ and Δz_s and Δz_b, respectively. This expression is

$$\Delta\hat{q}_e = \frac{1+c}{K}\,\Delta\hat{\sigma}_{\substack{xz\\z=1}}\,, \quad \Delta\hat{q}_n = \frac{H_c\sinh k - k}{k^3 K}\,(ik\Delta\hat{\sigma}_{\substack{zz\\z=1}})\,, \tag{4.5.14}$$

$$\Delta\hat{q}_a = (1+c)\Delta\hat{z}_s\,, \quad \Delta\hat{q}_b = -\frac{(1+c)H_c + (1+c+c^2k^2)\cosh k}{K}\,\Delta\hat{z}_b\,,$$

where the functions $K(k), H_c(k)$ and $H_s(k)$ are defined by

$$\begin{aligned} K(k) &= \cosh^2 k + k^2 + ck(\cosh k\sinh k + k) = H_c\cosh k + (1+c)k^2 \\ H_c(k) &= \cosh k + ck\sinh k \\ H_s(k) &= \sinh k + ck\cosh k\,, \end{aligned} \tag{4.5.15}$$

and

$$\Delta\hat{\sigma}_{\substack{xz\\z=1}} = \Delta\hat{z}_s\,, \quad \Delta\hat{\sigma}_{\substack{zz\\z=1}} = \cot\alpha_0(-\Delta\hat{z}_s)\,. \tag{4.5.16}$$

The total ice flux perturbation Δq, caused by the perturbations in $\Delta\sigma_{\substack{xz\\z=1}}$, $\Delta\sigma_{\substack{zz\\z=1}}$, Δz_s and Δz_b, is by (4.3.27) given as $\Delta q = \Delta q_e + \Delta q_n + \Delta q_a + \Delta q_b$.

4.5.6 Ice flux filters

Since filtering or convolution in the space domain is equivalent to multiplication in the wave number domain, the flux perturbation expressions (4.5.14) of the previous subsection may be interpreted as convolutions of filters with the perturbations $\Delta\sigma_{\substack{xz\\z=1}}$, $\Delta\sigma_{\substack{zz\\z=1}}$ and Δz_b. More specifically, define the filters $g_e(x)$, $g_n(x)$ and $g_b(x)$ such that their Fourier transforms are given by

$$\hat{g}_e(k) = \frac{1+c}{K}\,,\ \hat{g}_n(k) = \frac{H_c\sinh k - k}{k^3 K}\,,\ \hat{g}_b(k) = \frac{(1+c)H_c + (1+c+c^2k^2)\cosh k}{K}\,. \tag{4.5.17}$$

Then the flux expressions (4.5.14) in the wave number domain can be written in the space domain in terms of the filters $g_e(x)$, $g_n(x)$ and $g_b(x)$ as

$$\Delta q_e = g_e * \Delta\sigma_{\substack{xz\\z=1}}\,,\ \Delta q_n = g_n * (\partial\Delta\sigma_{\substack{zz\\z=1}}/\partial x)\,,\ \Delta q_a = (1+c)\Delta z_s\,,\ \Delta q_b = -g_b * \Delta z_b\,. \tag{4.5.18}$$

The advection component Δq_a, does not have a corresponding filter, since it depends on the local value of the ice surface perturbation Δz_s. Alternatively, the filter corresponding

to Δq_a may be defined to be $(1+c)$ times the δ-function. The differentiation of $\Delta\sigma_{\substack{zz\\z=1}}$ in (4.5.18) is represented by the multiplication of $\Delta\hat{\sigma}_{\substack{zz\\z=1}}$ with ik in (4.5.14). Multiplication by ik in the wave number domain is equivalent to a differentiation in the space domain by the properties of Fourier transforms.

The flux filters $g_e(x)$, $g_n(x)$ and $g_b(x)$ have the direct physical interpretation that they describe the longitudinal ice flux perturbations caused by sharp (δ-function) spikes in the boundary conditions as described by $\Delta\sigma_{\substack{xz\\z=1}}$, $\Delta\sigma_{\substack{zz\\z=1}}$ and Δz_b. The filter $g_e(x)$ describes the flux perturbation resulting from a localized disturbance or *spike* in the shear stress $\Delta\sigma_{\substack{xz\\z=1}}$, applied at the datum ice surface. Since it is more convenient to work with the derivative of $\Delta\sigma_{\substack{zz\\z=1}}$ rather than $\Delta\sigma_{\substack{zz\\z=1}}$ itself, the filter $g_n(x)$ describes the flux perturbation resulting from a sharp *step* in the normal stress $\Delta\sigma_{\substack{zz\\z=1}}$, applied at the datum ice surface. The filter $g_b(x)$ describes the (negative of the) ice flux perturbation resulting from a sharp peak in the basal geometry Δz_b.

From (4.5.17) it is seen that the flux filters $g_e(x)$, $g_n(x)$ and $g_b(x)$ are completely determined by the sliding parameter c. They are independent of the long scale surface slope α_0, which only enters as the multiplying factor $\cot\alpha_0$, in the expression (4.5.16) for $\Delta\sigma_{\substack{zz\\z=1}}$.

The Fourier transforms $\hat{g}_e(k)$, $\hat{g}_n(k)$ and $\hat{g}_b(k)$ are real and symmetric in k. Therefore the corresponding filters $g_e(x)$, $g_n(x)$ and $g_b(x)$ are also symmetric in x by the properties of Fourier transforms.

Equation (4.5.18) states that the flux perturbations Δq_e, Δq_n and Δq_b can be computed as weighted averages of perturbations in $\Delta\sigma_{\substack{xz\\z=1}}$, $\Delta\sigma_{\substack{zz\\z=1}}$ and Δz_b, respectively. The advection component Δq_a, on the other hand, can be computed from the local value of Δz_s.

The areas under the flux filters $g_e(x)$, $g_n(x)$ and $g_b(x)$ are by the properties of Fourier transforms equal to the values of $\hat{g}_e(k)$, $\hat{g}_n(k)$ and $\hat{g}_b(k)$ at $k = 0$. Thus,

$$\int_{-\infty}^{\infty} g_e(x)dx = \hat{g}_e(k=0) = 1 + c\ ,$$
$$\int_{-\infty}^{\infty} g_n(x)dx = \hat{g}_n(k=0) = 2/3 + c\ , \qquad (4.5.19)$$
$$\int_{-\infty}^{\infty} g_b(x)dx = \hat{g}_b(k=0) = 2(1 + c)\ .$$

In order to derive the above expression for $\hat{g}_n(k=0)$, $\cosh k$, $\sinh k$, and $H_c(k)$ must be expanded as power series in k, for small k.

Equation (4.5.19) implies that for long undulations, *i.e.* when $k \to 0$, $\lambda = 2\pi/k \to \infty$, the ice flux perturbations predicted by (4.5.18) must satisfy

$$\Delta q_e \approx (1 + c)\Delta\sigma_{\underset{z=1}{xz}}\ ,\quad \Delta q_n \approx (2/3 + c)(\partial\Delta\sigma_{\underset{z=1}{zz}}/\partial x)\ , \qquad (4.5.20)$$
$$\Delta q_a = (1 + c)\Delta z_s\ ,\quad \Delta q_b \approx -2(1 + c)\Delta z_b\ .$$

Comparison with the corresponding expressions for the laminar flow approximation (4.4.2) for $n = m = 1$, shows that the above theory for linear Newtonian rheology agrees with the laminar flow approximation in the limit of long undulations. This is a condition that must be satisfied by any theory of glacier flow as discussed previously, and it is an important check of the analytical derivation in Appendix 2.

Figure 4.5.1 shows the Fourier transforms $\hat{g}_e(k)$, $\hat{g}_n(k)$ and $\hat{g}_b(k)$ (left) and the corresponding flux filters $g_e(x)$, $g_n(x)$ and $g_b(x)$ (right) for the case of no basal sliding ($c = 0$). The curves are normalized with the value of the Fourier transforms at $k = 0$. Thus, the Fourier transforms all start at the value 1 at $k = 0$, and the area below each of the normalized filters is equal to 1. Because of the symmetry of the transforms and the filters they are only shown for $k > 0$ and $x > 0$, respectively. It is seen that $\hat{g}_b(k)$ is higher than the other transforms $\hat{g}_e(k)$ and $\hat{g}_n(k)$. This is because perturbations in the bedrock geometry affect the velocity field in a more direct way than perturbations in the stress field at the ice surface. Perturbations in the basal geometry induce variations in the

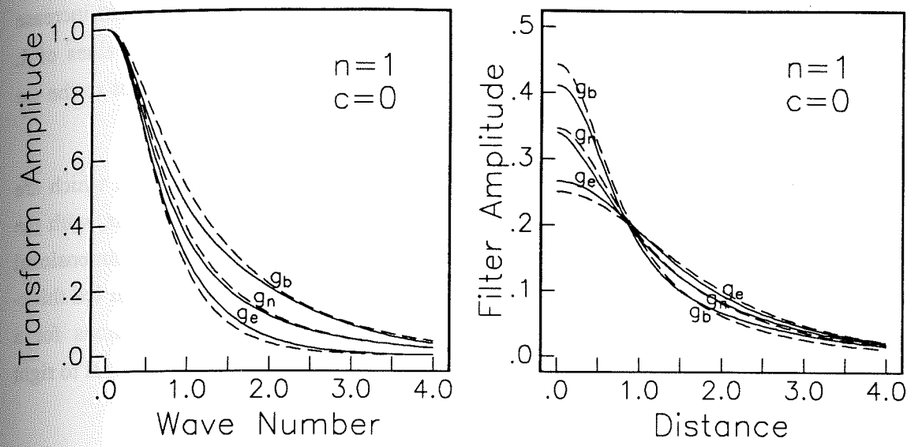

FIGURE 4.5.1: Normalized Fourier transforms $\hat{g}_e(k)$, $\hat{g}_n(k)$ and $\hat{g}_b(k)$ (solid curves) of flux filters for linear Newtonian rheology defined by (4.5.17) (left) and corresponding normalized flux filters $g_e(x)$, $g_n(x)$ and $g_b(x)$ (cf. (4.5.18)) (right) for no basal sliding ($c = 0$). The curves are normalized with the value of the Fourier transforms at $k = 0$. The wave number k is defined as $k = 2\pi/\lambda$ where λ is the wavelength of a harmonic undulation. Dashed curves show the results of a simplified analysis, which will be discussed in subsection 4.6.8.

perturbation velocity field itself by (4.3.25) and (4.3.26). This leads to first order derivatives in the stream function formulation of the boundary conditions (4.5.6) and (4.5.7), which determine $\hat{g}_b(k)$. Perturbations in the stress field at the datum ice surface, on the other hand, involve strain rate variations and this leads to second and third order derivatives in the boundary conditions (4.5.4) and (4.5.5), which determine $\hat{g}_e(k)$ and $\hat{g}_n(k)$. As a consequence the flow field corresponding to perturbations in the basal boundary conditions is not very restricted by the boundary conditions at the ice surface, whereas the flow fields corresponding to perturbations in the stress field at the ice surface are much more influenced by the basal boundary conditions. This reduces the magnitude of the flux filters $\hat{g}_e(k)$ and $\hat{g}_n(k)$ for moderate values of k in comparison with $\hat{g}_b(k)$. Perturbations in the basal geometry also lead to direct changes in the ice thickness, which is not the

case for perturbations in the stress field at the datum ice surface. This tends to increase the magnitude of $\hat{g}_b(k)$ in comparison with $\hat{g}_e(k)$ and $\hat{g}_n(k)$ for moderate values of k. This difference turns out to be crucial for the transfer of bedrock undulations to the ice surface.

The wave number $k = 2\pi/\lambda$, the wavelength $\lambda = 2\pi/k$, and the distance x which are used in Figure 4.5.1 and the following figures are all in dimensionless units, with the datum ice thickness as the unit of length. The figures can be interpreted in dimensional units by multiplying the λ- and x-values and dividing k-values by the datum ice thickness. Some of the following figures show predicted ice surface undulations for a prescribed basal geometry. The datum ice flow is always assumed to go from left to right in these figures.

The flux filters $g_e(x)$, $g_n(x)$ and $g_b(x)$ shown on the left of Figure 4.5.1 have a smooth bell shaped form. They decay to near-zero on a length-scale of 1 - 2 ice thicknesses. The normalized $g_b(x)$ is higher and narrower than the other filters as a consequence of its wider Fourier transform.

Figure 4.5.2 shows the normalized Fourier transforms (left) and flux filters (right) for non-zero basal sliding with $c = 2/3$. The datum ice flux for linear Newtonian rheology is $q_0 = 2/3 + c$. Thus, $c = 2/3$ corresponds to datum ice flow where the ice flux due to basal sliding is equal to the ice flux due to internal deformation. This value of c will be used to specify non-zero basal sliding in a number of figures in the following.

Figure 4.5.2 (left) shows that the relative height of $\hat{g}_e(k)$ and $\hat{g}_n(k)$ with respect to $\hat{g}_b(k)$ is lower than was the case for no basal sliding (Fig. 4.5.1). As a consequence the normalized $g_e(x)$ and $g_n(x)$ are wider for non-zero basal sliding than for no basal sliding. This has to do with increased relative importance of longitudinal stress gradients when basal sliding becomes significant. It is also possible to understand the increased importance for non-zero basal sliding of $\hat{g}_b(k)$ over $\hat{g}_e(k)$ and $\hat{g}_n(k)$ by the fact that the basal geometry must lead to more disturbance in the flow field when velocities in the vicinity of the base are high, *i.e.* when basal sliding is significant.

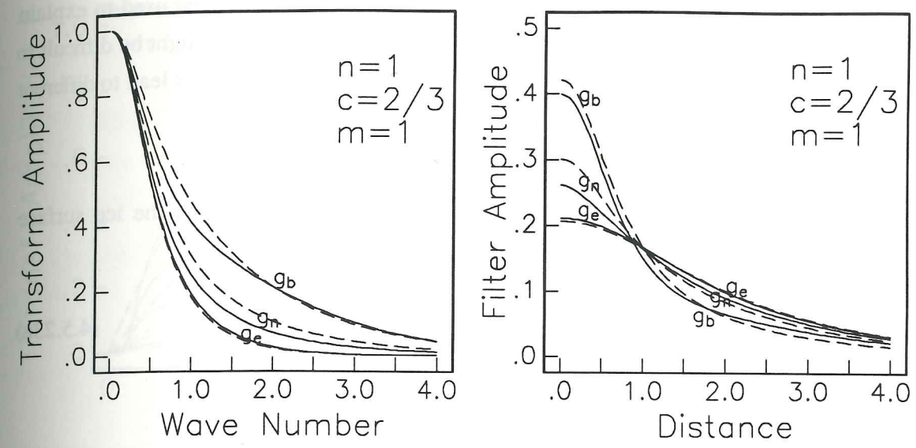

FIGURE 4.5.2: Same as Figure 4.5.1 except that the curves in this figure correspond to non-zero basal sliding with c = 2/3.

4.5.7 Steady state ice surface undulations

The steady state ice surface geometry Δz_s, corresponding to specified bedrock undulations Δz_b, is determined by the steady state equation (4.3.30) using the advective flux component Δq_a given by (4.5.14) and the flux filters $g_e(x)$, $g_n(x)$ and $g_b(x)$ defined by (4.5.16), (4.5.17) and (4.5.18). In the space domain the equation determining Δz_s is

$$g_e * \Delta z_s + g_n * (-\partial \Delta z_s/\partial x)\cot\alpha_0 + (1 + c)\Delta z_s - g_b * \Delta z_b = 0 \,. \qquad (4.5.21)$$

The wave number representation of this equation is

$$(\hat{g}_e(k) + (1 + c) - ik\hat{g}_n(k)\cot\alpha_0)\Delta z_s = \hat{g}_b(k)\Delta z_b \,. \qquad (4.5.22)$$

Equation (4.5.22) determines the transfer function $t(k)$ (*cf.* subsection 3.3.3) for the steady state transfer of bedrock undulations to the ice surface, *i.e.* $\Delta\hat{z}_s = t(k)\Delta\hat{z}_b$. The transfer function may be inverted using (3.3.4a) to yield the Green's function $g(x)$ (*cf.* subsection 3.3.4), such that $\Delta z_s = g(x) * \Delta z_b$. Δz_s determined in this way as the convolution of $g(x)$ and the specified bedrock geometry Δz_b, will then satisfy (4.5.21). Using (4.5.21) and the flux filters $g_e(x)$, $g_n(x)$ and $g_b(x)$, therefore, leads directly to transfer functions and Green's functions for the transfer of bedrock undulations to the ice surface.

This has the advantage that known properties of the flux filters may be used to explain certain features of the transfer functions and Green's functions which might be difficult to explain otherwise. In particular, (4.5.22) shows how the same flux filters lead to different transfer functions for different values of the long scale surface slope α_0.

4.5.8 Transfer functions

By (4.5.22) and (4.5.17), the transfer function from the bedrock to the ice surface predicted by linear Newtonian rheology is given by

$$t(k) = \frac{\hat{g}_b(k)}{\hat{g}_e(k) + (1+c) - ik\hat{g}_n(k)\cot\alpha_0} \qquad (4.5.23a)$$
$$= \frac{(1+c)H_c + (1 + c + c^2k^2)\cosh k}{(1+c)(1+K) - ik((H_c\sinh k - k)/k^3)\cot\alpha_0},$$

where $K(k)$, $H_c(k)$ and $H_s(k)$ are defined by (4.5.15). From this expression for $t(k)$ the transfer amplitude $|t(k)|$ and the phase shift $\phi(k)$ are predicted to be

$$|t(k)| = \frac{(1+c)H_c + (1 + c + c^2k^2)\cosh k}{((1+c)^2(1+K)^2 + ((H_c\sinh k - k)^2/k^4)\cot^2\alpha_0)^{1/2}} \qquad (4.5.23b)$$

$$\tan\phi(k) = \frac{(H_c\sinh k - k)}{(1+c)(1+K)k^2}\cot\alpha_0 . \qquad (4.5.23c)$$

In the case of no basal sliding the above expressions simplify to

$$t(k) = \frac{2\cosh k}{(\cosh^2 k + 1 + k^2) - ik((\cosh k\sinh k - k)/k^3)\cot\alpha_0}, \qquad (4.5.24a)$$

$$|t(k)| = \frac{2\cosh k}{((\cosh^2 k + 1 + k^2)^2 + ((\cosh k\sinh k - k)^2/k^4)\cot^2\alpha_0)^{1/2}} \qquad (4.5.24b)$$

$$\tan\phi(k) = \frac{(\cosh k\sinh k - k)}{(\cosh^2 k + 1 + k^2)k^2}\cot\alpha_0 . \qquad (4.5.24c)$$

Equations (4.5.24) are in agreement with Hutter's (1983) and Reeh's (1987) results for the transfer of bedrock undulations to the surface for linear Newtonian rheology in the absence of basal sliding. Equations (4.5.23), however, do not agree with Hutter's (1983) results when basal sliding is present. This discrepancy appears to be caused by an

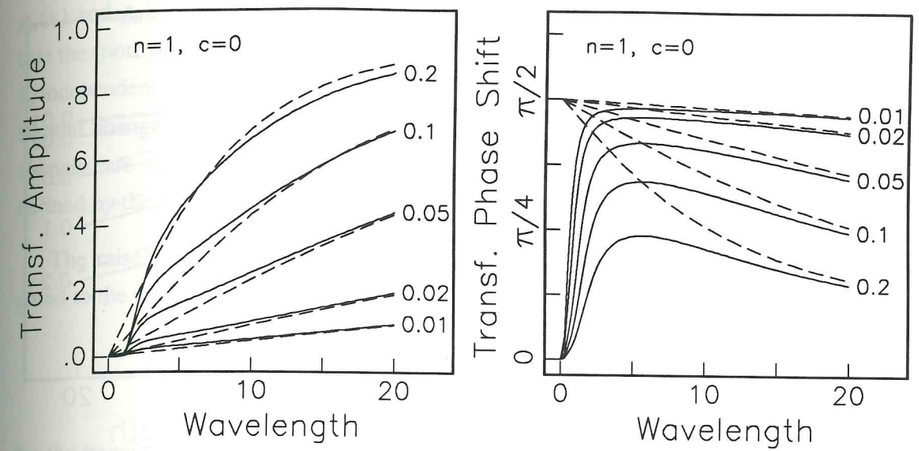

FIGURE 4.5.3: The transfer amplitude $|t|$ (left) and phase shift ϕ (right) for the transfer of bedrock undulations to the ice surface predicted by linear Newtonian rheology for no basal sliding and a range of long scale surface slopes $\tan\alpha_0$ (solid curves) (cf. (4.5.24)). $|t|$ and ϕ are plotted as functions of dimensionless wavelength $\lambda = 2\pi/k$. Dashed curves are the corresponding transfer amplitude and phase shift predicted by the laminar flow approximation (4.4.7). The curves are labeled with $\tan\alpha_0$.

error in Hutter's results. It may be shown by insertion of Hutter's solution into his formulation of the boundary conditions, that his sliding boundary condition at the base is not satisfied.

Equations (4.5.19) show that the limit of the transfer functions $t(k)$, given by (4.5.23a) and (4.5.24a) as $k \to 0$ is $\lim_{k\to 0} t(k) = 1$ as expected from the discussion in subsection 4.4.4 on the laminar flow approximation.

Figure 4.5.3 shows the transfer amplitude (left) and phase shift (right) for no basal sliding given by (4.5.24) for a range of long scale surface slopes $\tan\alpha_0$ (solid curves). The figure also shows the transfer amplitude and phase shift predicted by the laminar

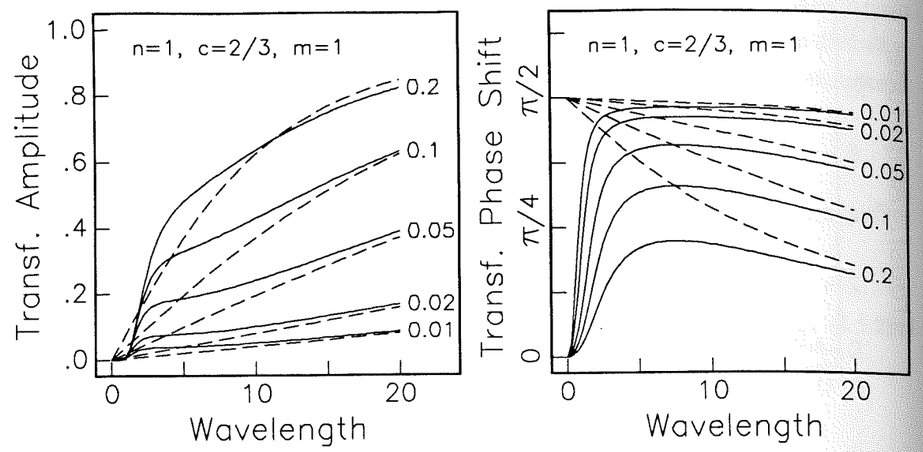

FIGURE 4.5.4: Same as Figure 4.5.3 except that the curves in this figure correspond to non-zero basal sliding with c = 2/3.

flow approximation (with $n = 1$) (4.4.7) (dashed curves) for comparison. The figure shows that the transfer function predicted by linear rheology is close to the laminar flow approximation for $\lambda \gtrsim 4\pi$ or $k \lesssim ½$ as discussed in subsection 4.4.2 on the laminar flow approximation. For wavelengths in the approximate range 2 - 10 ice thicknesses the predicted transfer amplitude is *higher* than predicted by the laminar flow approximation. Below a wavelength of approximately 2 ice thicknesses the transfer function decays abruptly to zero.

Figure 4.5.4 shows the transfer amplitude (left) and phase shift (right) for non-zero basal sliding given by (4.5.23) with $c = 2/3$. Figure 4.5.4 is similar to Figure 4.5.3, except that the transfer for wavelengths in the approximate range 2 - 10 ice thicknesses is higher than for no sliding.

Both Figures 4.5.3 and 4.5.4 show the transfer amplitude increasing monotonically with the wavelength of the bedrock undulations. The overall shape of the transfer function is well predicted by the laminar flow approximation for $\lambda \gtrsim 4\pi$ or $k \lesssim ½$, especially the effect of the long scale average slope on the transfer. This is perhaps surprising. The laminar flow approximation may be interpreted as predicting that the flux filters $g_e(x)$,

$g_n(x)$ and $g_b(x)$ are δ-functions. This means that laminar flow approximation predicts that the (normalized) Fourier transforms $\hat{g}_e(k)$, $\hat{g}_n(k)$ and $\hat{g}_b(k)$ are all uniformly equal to 1, independent of wavelength. Figures 4.5.1 and 4.5.2, however, show that there are substantial changes in the transforms $\hat{g}_e(k)$, $\hat{g}_n(k)$ and $\hat{g}_b(k)$ in the range $0 \le k \le ½$. These changes are so similar for all three flux filters that their combined effect on $t(k)$ as defined by the first expression in (4.5.23a) is small.

The raised transfer amplitude in the wavelength range 2 - 10 ice thicknesses compared to the laminar flow approximation may be explained by the expression (4.5.23a)

$$t(k) = \frac{\hat{g}_b(k)}{\hat{g}_e(k) + (1 + c) - ik\hat{g}_n(k)\cot\alpha_0} \tag{4.5.25}$$

for the transfer function in terms of the Fourier transforms of the flux filters $g_e(x)$, $g_n(x)$ and $g_b(x)$. If all the filters had the same shape then $t(k)$ would be much closer to the laminar flow approximation than is the case when the true expressions (4.5.17) for the flux filters are used. The reason for the higher values of $t(k)$ in the wavelength range 2 - 10 ice thicknesses is that $\hat{g}_b(k)$ is relatively high in this range of wavelengths compared to $\hat{g}_e(k)$ and $\hat{g}_n(k)$. This is caused by the different nature of the boundary conditions corresponding to $g_b(x)$, on one hand, and $g_e(x)$ and $g_n(x)$, on the other, as discussed in subsection 4.5.6. Bedrock undulations with wavelengths in the approximate range 2 - 10 ice thicknesses, therefore, lead to relatively large ice flux perturbations. Relatively large ice surface undulations are required in order to generate a steady state flow field corresponding to the ice flux perturbations, because of the relatively small effect of ice surface undulations on the ice flux at these wavelengths. In this way, the increased transfer of bedrock undulations to the ice surface in the wavelength range 2 - 10 ice thicknesses can be directly related to the difference in the shape of $\hat{g}_b(k)$, on one hand, and $\hat{g}_e(k)$ and $\hat{g}_n(k)$, on the other.

The sharp decline of the transfer amplitude below a wavelength of approximately 2 ice thicknesses can similarly be explained by the flux filters and (4.5.25). The wave number corresponding to $\lambda \approx 2$ is $k \approx 3$ and Figures 4.5.1 and 4.5.2 show that $\hat{g}_b(k)$ has become very small above this value of k. The advective ice flux perturbation component $\Delta q_a = (1 + c)\Delta z_s$, which occurs in the denominator of (4.5.25), is independent of k,

however. Therefore, $t(k)$ decays rapidly with increasing k or decreasing λ as a consequence of the rapid falloff in $\hat{g}_b(k)$. The physical meaning of this argument is that short wavelength bedrock undulations lead to very small ice flux perturbations because of recirculation in the perturbation ice flow (*cf.* Balise and Raymond, 1985). Short wavelength ice surface undulations, on the other hand, lead to relatively large ice flux perturbations through the advection term Δq_a. Therefore, small ice surface undulations are sufficient to balance the ice flux perturbations caused by short wavelength bedrock undulations.

4.5.9 Green's functions

The Green's function $g(x)$ found by inverting $\hat{g}(k) = t(k)$ given by (4.5.23a) or (4.5.24a) describes the ice surface geometry corresponding to a sharp spike in the bedrock geometry. As $t(k=0) = 1$, the area under the Green's function, $\int_{-\infty}^{\infty} g(x)dx = t(k=0) = 1$, independent of basal sliding or the long scale surface slope.

Therefore, the total volume of ice in the surface perturbations $\int_{-\infty}^{\infty} \Delta z_s dx$, is exactly equal to the total volume of the bedrock perturbations $\int_{-\infty}^{\infty} \Delta z_b dx$, as was found earlier in the case of the laminar flow approximation.

Figure 4.5.5 compares the Green's function predicted by linear Newtonian rheology for no basal sliding for a range of long scale surface slopes $\tan\alpha_0$ with the one-sided exponential Green's function predicted by the laminar flow approximation (4.4.9) and shown in Figure 4.4.2. In order to simplify the comparison, the figure shows a scaled Green's function $g^*(x^*) = l_1 g(x/l_1)$, as a function of scaled distance $x^* = x/l_1$, where l_1 is given by (4.4.4). The Green's function for laminar flow is then simply $g^*(x^*) = e^{x^*}$ for $x < 0$, independent of the long scale surface slope (shown as a barely visible dashed curve in the figure). Length-scales equal to $1/l_1$ in the x^* variable, which corresponds to one ice thickness in the unscaled x coordinate, are shown in the upper left corner of the figure for each value of $\tan\alpha_0$. The figure shows that the Green's functions predicted by linear Newtonian rheology are close to the one-sided exponential Green's function predicted by the laminar flow approximation, except for a "standing wave" near x=0. In

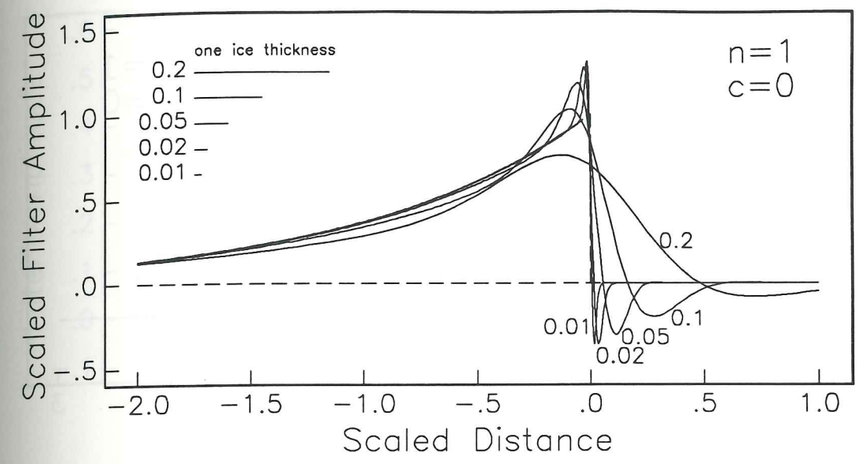

FIGURE 4.5.5: Green's functions predicted by linear Newtonian rheology for no basal sliding and a range of long scale surface slopes $\tan\alpha_0$ *(solid curves) compared to the one-sided exponential Green's function predicted by the laminar flow approximation (4.4.9) (barely visible dashed curve). The curves are scaled horizontally and vertically and labeled with* $\tan\alpha_0$. *Length-scales corresponding to one ice thickness for each value of* $\tan\alpha_0$ *are shown in the upper left corner (for explanation, see text).*

fact, the dashed curve corresponding to the laminar flow approximation can hardly be distinguished in the figure because the other curves are so close to it. For x values more than approximately 2 ice thicknesses away from $x = 0$, there is insignificant difference between the Green's function predicted by linear Newtonian rheology and the Green's function predicted by the laminar flow approximation.

Figures 4.5.6 and 4.5.7 provide a closer view of the central part of the Green's functions predicted by linear Newtonian rheology. The Green's functions predicted by the laminar flow approximation are indicated by diamond symbols which are plotted where the tops of the one-side exponentials (4.4.9) would be located. The exponentials themselves are not shown as the pictures would then become too crowded. The figures show

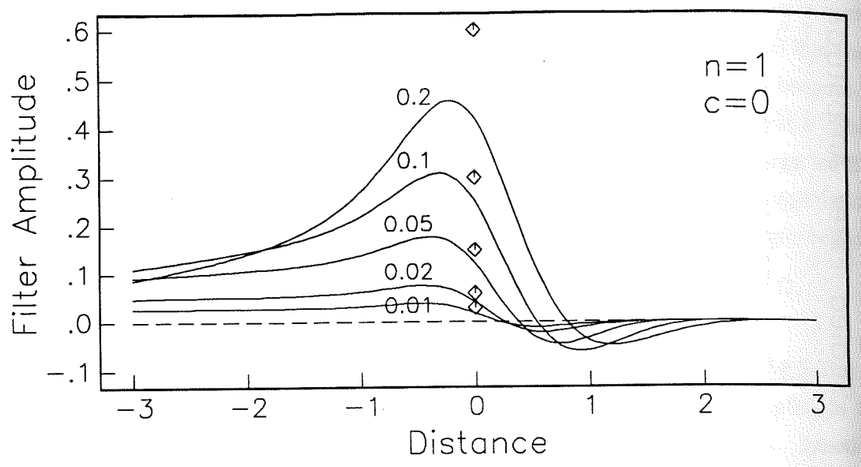

FIGURE 4.5.6: Green's functions predicted by linear Newtonian rheology for no basal sliding and a range of long scale surface slopes $\tan\alpha_0$. *The Green's functions predicted by the laminar flow approximation are indicated by diamond symbols which are plotted where the tops of the one-side exponentials would be located. The curves are labeled with* $\tan\alpha_0$.

that the standing wave, which was observed in Figure 4.5.5, consists of a peak on the upstream side of the basal spike and a trough on the downstream side. The distance between the peak and the trough of the standing wave is between 0.85 and 1.5 ice thicknesses for the entire range $0.01 \leq \tan\alpha_0 \leq 0.2$ of the long scale surface slope, both in the case of no sliding (Fig. 4.5.6) and for non-zero basal sliding (Fig. 4.5.7). This corresponds to approximate wavelengths in the range 2 - 3 ice thicknesses. The amplitude of the wave is slightly higher for non-zero basal sliding. The standing wave in the Green's function appears in spite of the fact that there is no maximum, neither absolute nor relative, in the transfer function $t(k) = \hat{g}(k)$, in the wavelength range 2 - 3 ice thicknesses (*cf.* Figs. 4.5.3 and 4.5.4).

The steady state ice surface geometry Δz_s, corresponding to a given basal topography Δz_b, can be found by convolution of Δz_b with the Green's function $g(x)$, *i.e.* $\Delta z_s = g * \Delta z_b$. Alternatively, the Fourier transform of Δz_s can be computed as $\Delta\hat{z}_s = t(k)\Delta\hat{z}_b$ and

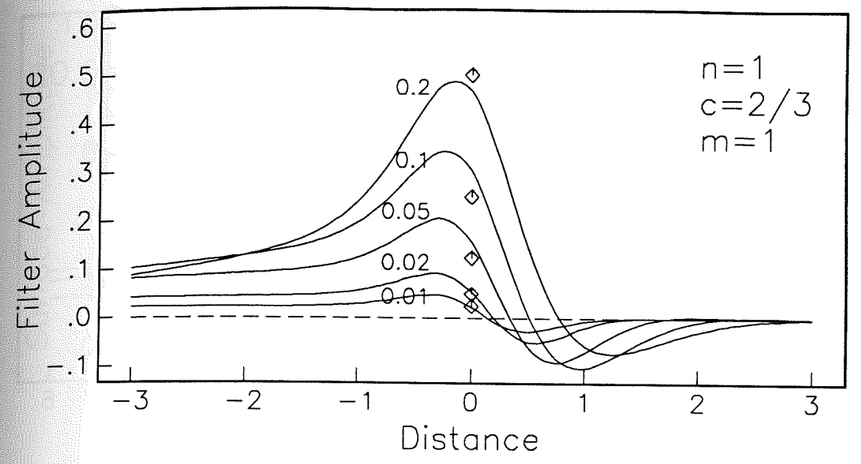

FIGURE 4.5.7: Same as Figure 4.5.6 except that the Green's functions in this figure correspond to non-zero basal sliding with $c = 2/3$.

inverted to yield Δz_s. Figure 4.5.8 shows the steady state ice surface geometry Δz_s corresponding to a smooth basal mountain described by a Gaussian bell function

$$\Delta z_b(x) = \frac{1}{\sqrt{2\pi}\,\sigma} e^{-x^2/(2\sigma^2)}\,, \quad \Delta\hat{z}_b(k) = e^{-\sigma^2 k^2/2}\,. \tag{4.5.26}$$

A basal mountain described by (4.5.26) has unit area and an approximate width equal to 2σ. The curves in Figure 4.5.8 are drawn for no basal sliding and $\tan\alpha_0 = 0.05$. The solid curves are computed from the Green's function predicted by linear Newtonian rheology. The dashed curves are computed from the Green's function predicted by the laminar flow approximation. The figure shows that the ice surface shapes predicted by linear Newtonian rheology, on one hand, and the laminar flow approximation, on the other, agree quite well for $\sigma \gtrsim 1$, *i.e.* as long as the width of the basal mountain is larger than approximately 2 ice thicknesses. For basal mountains wider than approximately 2 ice thicknesses there is almost no noticeable effect from the standing wave in the linear Newtonian Green's function (*cf.* Figs. 4.5.5, 4.5.6 and 4.5.7). The standing wave appears abruptly as a surface feature when the width of the basal mountain is reduced below approximately 2 ice thicknesses.

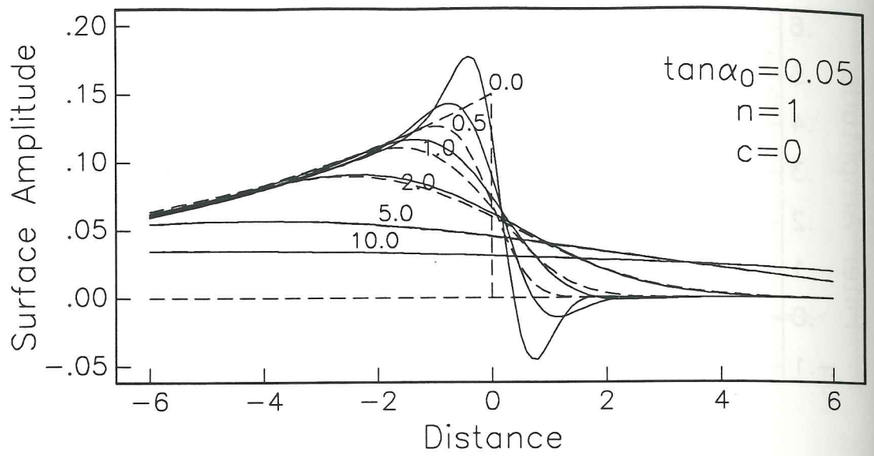

FIGURE 4.5.8: Steady state ice surface geometry predicted by linear Newtonian rheology and no basal sliding for a basal mountain given by (4.5.26) for a range of half widths σ (solid curves). The long scale surface slope is $\tan\alpha_0 = 0.05$. *The curves are labeled with the values of σ. The curve labeled with "0.0" is the Green's function corresponding to a basal spike. Unlabeled dashed curves show the steady state surface geometry predicted by the one-sided exponential Green's function corresponding to the laminar flow approximation (4.4.9).*

Figure 4.5.9 shows essentially the same curves as Figure 4.5.8. The Gaussian basal mountain has been multiplied by $\sqrt{2\pi}\ \sigma$, for $\sigma > 0.0$, so that the mountain height at $x = 0$ is equal to 1 independent of σ. The curves in Figure 4.5.9, therefore, show the ice surface as a basal mountain of constant amplitude becomes wider. The ice surface geometry is very smooth for the wider basal mountains. The standing wave appears abruptly as a surface feature when the width of the basal mountain is reduced below approximately 2 ice thicknesses.

4.5.10 Slope filters

Studies of ice surface undulations have often been carried out in terms of surface slope fluctuations $\Delta\alpha = -(\partial\Delta z_s/\partial x)$, rather than in terms of the surface undulations Δz_s,

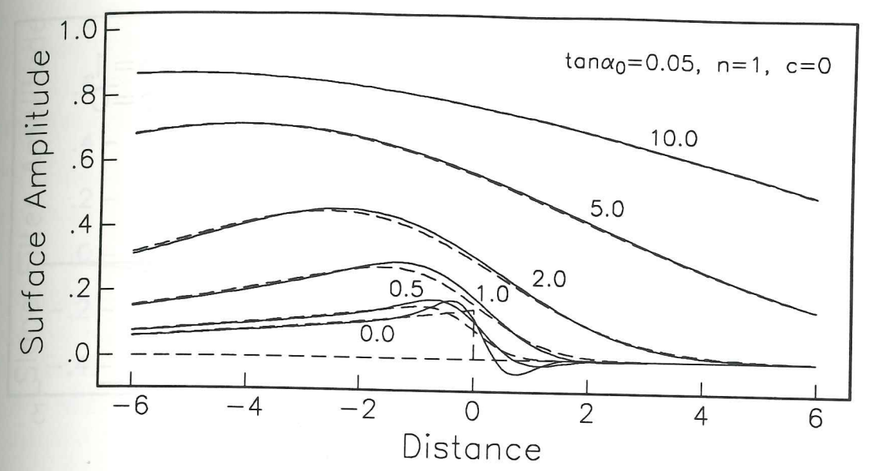

FIGURE 4.5.9: Same as Figure 4.5.8 except that the predicted Δz_s *curves in this figure correspond to a Gaussian basal mountain given by (4.5.26) multiplied by* $\sqrt{2\pi}\ \sigma$, *for* $\sigma > 0.0$, *so that the mountain height at* $x = 0$ *is equal to 1 independent of* σ. *The curve labeled with "0.0" is the Green's function corresponding to a sharp spike in the basal geometry.*

themselves (*e.g.* Robin, 1967). Therefore, it is of interest to compute a slope filter $g_\alpha(x)$, which is defined by the relation

$$\Delta\alpha = -(\partial\Delta z_s/\partial x) = g_\alpha(x) * \Delta z_b\ . \tag{4.5.27}$$

By the properties of convolutions and Fourier transforms, $g_\alpha(x)$ and its Fourier transform are given by

$$g_\alpha(x) = -(dg(x)/dx)\ ,\quad \hat{g}_\alpha(k) = -ikt(k)\ , \tag{4.5.28}$$

where the transfer function $t(k)$ is given by (4.5.23a) or (4.5.24a) in the case of linear Newtonian rheology and $g(x)$ is the corresponding Green's function. The filter $g_\alpha(x)$ describes the predicted surface slope perturbation in response to a sharp spike in the basal geometry.

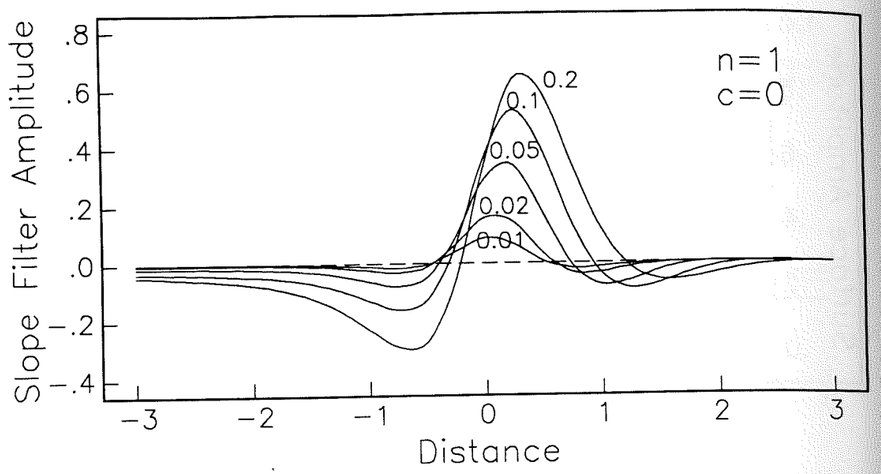

FIGURE 4.5.10: Surface slope filters predicted by linear Newtonian rheology for no basal sliding and a range of long scale surface slopes $\tan\alpha_0$. *The curves are labeled with* $\tan\alpha_0$.

Some previous studies have described surface slope variations $\Delta\alpha = -(\partial\Delta z_s/\partial x)$, in terms of basal slope variations $\Delta\beta = -(\partial\Delta z_b/\partial x)$ (*e.g.* Budd, 1969). By the properties of convolutions and Fourier transforms $\Delta\alpha$ and $\Delta\beta$ must be related in the same way as the perturbations Δz_s and Δz_b themselves, *i.e.* $\Delta\alpha = g(x)*\Delta\beta$ and $\Delta\hat{\alpha} = t(k)\Delta\hat{\beta}$.

The slope filter $g_\alpha(x)$, is shown for a range of long scale surface slopes $\tan\alpha_0$ in Figure 4.5.10 for no sliding and in Figure 4.5.11 for non-zero basal sliding with $c = 2/3$. The figures show an interval of positive slope perturbation, about 1 ice thickness wide, with the maximum slope occurring directly above or slightly downstream from the basal spike, with intervals of negative slope perturbation on each side. The amplitude of the slope perturbation is slightly higher in the case of non-zero basal sliding (Fig. 4.5.11). The effect of the long exponential upstream tail of $g(x)$ (*cf.* Figs. 4.5.5, 4.5.6 and 4.5.7), on the slope filter $g_\alpha(x)$, is small. Therefore, the effect of a sharp basal spike on the surface slope is more or less limited to an interval with a length approximately equal to 3 ice thicknesses centered about the basal spike.

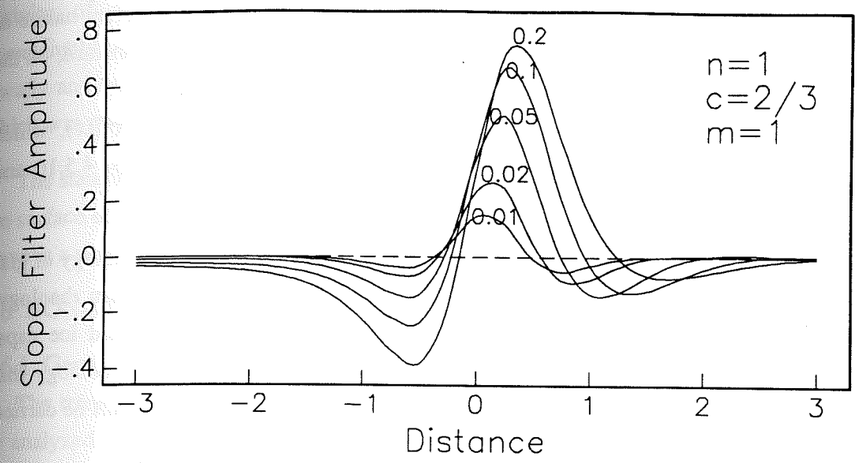

FIGURE 4.5.11: Same as Figure 4.5.10 except that the slope filters in this figure correspond to non-zero basal sliding with $c = 2/3$.

The slope filters in Figures 4.5.10 and 4.5.11 predict that relatively small basal obstructions can lead to substantial surface slope changes. A relatively narrow basal mountain with an area equal to 0.1, *e.g.* a Gaussian bump given by (4.5.26) multiplied by 0.1, with width between 0.5 and 1.0 ice thicknesses (*i.e.* $0.25 \le \sigma \le 0.5$) and height between 0.08 and 0.16 ice thicknesses, will be associated with slope changes between 20 and 100% of the long scale surface slope $\tan\alpha_0$ for the values of $\tan\alpha_0$ shown in Figures 4.5.10 and 4.5.11.

4.5.11 Discussion

Steady state transfer of bedrock undulations to the ice surface predicted by linear Newtonian rheology has the following main features.

1. For long undulations the transfer is well explained by the laminar flow approximation. The transfer is described by a Green's function which corresponds to a spike in the basal geometry and has the shape of a long one-sided exponential on the upstream side of the basal spike (*cf.* Fig. 4.5.5).
2. On shorter length-scales a "standing wave" in the linear Newtonian Green's function with wavelength between 2 and 3 ice thicknesses becomes important (*cf.* Figs.

4.5.6 and 4.5.7). The standing wave can be understood from the different nature of the boundary conditions at the bedrock, on one hand, and at the ice surface, on the other, using ice flux filters.

3. The standing wave is the most outstanding feature of the filter $g_\alpha(x)$, which describes the effect of a basal spike on the surface slope (*cf.* Figs. 4.5.10 and 4.5.11).

Linear Newtonian rheology is far from being a realistic model of the rheology of glacier ice. Therefore, the above analytical results derived for linear Newtonian rheology, must be treated with caution as predictions that apply to real glaciers and ice caps. Nevertheless, there are some features of the theory for linear Newtonian rheology that seem to be so fundamental to the flow over bedrock undulations that they must be carried over to the case of non-linear rheology in some form.

1. The laminar flow approximation may be expected to provide a reasonable approximation to the flow over long wavelength bedrock undulations for non-linear rheology.
2. The decomposition of the ice flux perturbation Δq, into flux perturbation components according to (4.3.27), applies to non-linear rheology as well as to linear Newtonian rheology. Therefore, flux filters can also be defined for non-linear rheology.
3. The standing wave may be expected to be an important feature in Green's functions derived for non-linear rheology, since the nature of the boundary conditions is essentially the same as for linear Newtonian rheology.
4. The Green's function for non-linear rheology may be expected to have the shape of the one-sided exponential predicted by the laminar flow approximation with a superimposed standing wave. The amplitude and the wavelength of the expected standing wave for non-linear rheology must be determined by numerical solution of the ice flow equations.

It is tempting to relate the standing wave in the linear Newtonian Green's function to observations of dominant ice surface features with wavelengths in the range 3 - 4 ice thicknesses, which were discussed in Chapter 2. The Green's functions shown in Figures 4.5.6 and 4.5.7 predict that the surface of ice caps is very smooth except in the immediate

vicinity of sharp bedrock peaks or troughs, where localized undulations with wavelengths approximately equal to 3 ice thicknesses are predicted. This is similar to Zwally and others (1983) description of the surface features of the Greenland ice sheet which was quoted in Chapter 2.

The standing wave of the linear Newtonian Green's function is similar to the shape of the surface of a river flowing over stones in the river bed. This indicates that the standing wave is a persistent feature of fluid flow over obstacles in general.

4.6 NON-LINEAR FLOW — FLUX PERTURBATIONS

4.6.1 General

The transfer of bedrock undulations to the ice surface for non-linear rheology must be analyzed by numerical methods. Nevertheless, many of the concepts that were used in the analysis of linear Newtonian rheology are also useful for non-linear rheology. In particular, the introduction of ice flux filters, (*cf.* subsection 4.5.6) leads to considerable simplification in the analysis and reduces the amount of numerical computations substantially. Both time-dependent evolution of the ice surface and steady state transfer of bedrock undulations to the surface depend on perturbations in the ice flux through (4.3.23). No other property of the perturbation flow field enters in (4.3.23). This makes ice flux perturbations and ice flux filters especially useful for expressing the results of the analysis for non-linear rheology. Therefore, the non-linear analysis will start with an analysis of ice flux perturbations caused by perturbations in $\Delta\sigma_{\underset{z=1}{xz}}$, $\Delta\sigma_{\underset{z=1}{zz}}$, Δz_s and Δz_b in the ice flow boundary conditions (4.3.24), (4.3.25) and (4.3.26).

The datum velocity solution, which is described in subsection 4.3.4, and the laminar flow approximation (3.7.4a), (4.4.1) and (4.4.2), need to be modified slightly in order to be consistent with the solutions for non-linear rheology for slowly varying flow. The viscosity components η_1, η_2 and η_3 in the perturbation equations for non-linear rheology incorporate the effect of longitudinal extension/compression in the datum flow. The solution of the perturbation equations will therefore not be entirely consistent with the datum velocity field unless the effect of extension/compression on the viscosity is also taken into account in the derivation of the datum velocity. Similarly, the effect of longitudinal extension/compression on the viscosity must be taken into account in the derivation of

the laminar flow approximation if it is to be fully consistent with the non-linear analysis. This effect is small (*cf.* subsection 4.2.4), but taking it into account by expressing the datum velocity in terms of η_1, η_2 and η_3 makes it easier to demonstrate the internal consistency of the results for non-linear rheology. The datum velocity field affects the perturbation problem through the terms $u_{0\,z=0}$, $u_{0\,z=1}$ and $(\partial u_0/\partial z)_{z=0}$ in the boundary conditions (4.3.23), (4.3.25) and (4.3.26) and in the expression (4.3.28) for the advection flux perturbation component Δq_a.

The datum velocity field may be related to the viscosity components η_1, η_2 and η_3 by writing the datum vertical shear stress gradient $(\partial \tau_{xz\,0}/\partial z)$ as

$$\frac{\partial \tau_{xz\,0}}{\partial z} = 2\eta_2 \frac{\partial \dot{\varepsilon}_{xz\,0}}{\partial z} - 2\eta_3 \frac{\partial \dot{\varepsilon}_{xx\,0}}{\partial z} \,. \tag{4.6.1}$$

This equation is essentially the same as (4.3.15b) and follows from the definition of η_2 and η_3 as $\eta_2 = \tfrac{1}{2}(\partial \tau_{xz\,0}/\partial \dot{\varepsilon}_{xz\,0})_{\dot{\varepsilon}_{xz\,0}}$ and $\eta_3 = \tfrac{1}{2}(\partial \tau_{xz\,0}/\partial \dot{\varepsilon}_{xx\,0})_{\dot{\varepsilon}_{xz\,0}}$. The datum shear stress solution (4.3.18) gives $(\partial \tau_{xz\,0}/\partial z) = -1$. The longitudinal strain rate component $\dot{\varepsilon}_{xx\,0} = (\partial u_0/\partial x)$ in the datum flow is $O(\delta)$ and will therefore be neglected. The term $(\partial w_0/\partial x)$ in the shear strain rate $\dot{\varepsilon}_{xz\,0} = \tfrac{1}{2}(\partial u_0/\partial z + \partial w_0/\partial x)$ may also be neglected for the same reason. Equation (4.6.1) may thus be rewritten as

$$\frac{\partial^2 u_0}{\partial z^2} = -\frac{1}{\eta_2} \,. \tag{4.6.2}$$

From the boundary conditions (4.3.6a) and (4.3.8), and the shear stress solution (4.3.18) it follows that

$$(\partial u_0/\partial z)_{z=1} = 0 \tag{4.6.3}$$

and

$$u_{0\,z=0} = c \,. \tag{4.6.4}$$

$(\partial u_0/\partial z)_{z=1}$ and $u_{0\,z=0}$ as given by (4.6.3) and (4.6.4) are consistent with the previously derived datum velocity solution (4.3.20).

Integration of (4.6.2) using (4.6.3) and (4.6.4) leads to

$$(\partial u_0/\partial z)_{z=0} = \int_0^1 \frac{1}{\eta_2} dz \approx 2 \,, \tag{4.6.5}$$

$$u_{0\,z=1} = u_{0\,z=0} + \int_0^1 \frac{z}{\eta_2} dz \approx 2/(n+1) + c \tag{4.6.6}$$

and

$$q_0 = u_{0\,z=0} + \int_0^1 \frac{z - \tfrac{1}{2}z^2}{\eta_2} dz \approx 2/(n+2) + c \,. \tag{4.6.7}$$

In order to derive (4.6.6) and (4.6.7), double and triple integrals of (4.6.2) must be reformulated using integration by parts.

The datum ice flow solution describes laminar flow which is parallel to the local surface slope. Longitudinal flow variations only affect the datum velocity field through the effect of the longitudinal extension/compression on the viscosity component η_2. The ice flux given by (4.6.7) may therefore be interpreted as the flux predicted by a modified laminar flow approximation where the effect of longitudinal extension/compression on the viscosity is taken into account. The flux perturbation components Δq_e, Δq_n, Δq_a and Δq_b, predicted by this modified laminar flow approximation (*cf.* (4.4.2)) must be determined from (4.6.2), taking the effect of perturbations in Δz_s and Δz_b at both boundaries and on η_2 into account. The result is

$$\begin{aligned}
\Delta q_e &= \left(\int_0^1 \frac{1-z}{\eta_2} dz + mc\right)\Delta z_s \approx (2n/(n+1) + mc)\Delta z_s \\
\Delta q_n &= \left(\int_0^1 \frac{(1-z)^2}{\eta_2} dz + mc\right)\cot\alpha_0(-\partial \Delta z_s/\partial x) \approx (2n/(n+2) + mc)\cot\alpha_0(-\partial \Delta z_s/\partial x) \\
\Delta q_a &= \left(\int_0^1 \frac{z}{\eta_2} dz + u_{0\,z=0}\right)\Delta z_s \approx (2/(n+1) + c)\Delta z_s \\
\Delta q_b &= -\left(\int_0^1 \frac{1}{\eta_2} dz + u_{0\,z=0} + mc\right)\Delta z_b \approx -(2 + (m+1)c)\Delta z_b \,.
\end{aligned} \tag{4.6.8}$$

The approximate expressions on the far right of (4.6.5), (4.6.6), (4.6.7) and (4.6.8) are found by neglecting the effect of the boundary layer at the surface so that $\eta_1 = \frac{1}{2}(1-z)^{-(n-1)}$, $\eta_2 = (1-z)^{-(n-1)}/(2n)$ and $\eta_3 = 0$. The approximations show that, in the absence of longitudinal extension/compression, (4.6.5), (4.6.6), (4.6.7) and (4.6.8) are reduced to the previously derived datum velocity and laminar flow solutions. The error in the approximations is caused by the datum longitudinal extension/compression e in the boundary layer and is on the order of $|e|^{1+2/n}$. For $|e| = 0.01$ this error is a few parts in 1000.

The expressions for $(\partial u_0/\partial z)_{z=0}$ and $\underset{z=1}{u_0}$ given by (4.6.5) and (4.6.6) are useful in the derivation of flux filters for non-linear rheology and the flux perturbation components given by (4.6.8) are useful for comparison with the flux perturbations predicted by the non-linear analysis.

The viscosity components η_1, η_2 and η_3 are derived from the datum flow. Changes in the datum flow as described above therefore require corrections in η_1, η_2 and η_3, which again result in a modification of the datum flow, *etc.* Since the changes in question are very small, this process converges rapidly to a datum velocity field which is consistent with η_1, η_2 and η_3. Furthermore, the only property of the datum velocity field, which is required for the determination of η_1, η_2 and η_3, is the datum longitudinal extension/compression. In practice the datum longitudinal extension/compression will only be known as a rough approximation and the analysis is not sensitive to its exact value. Therefore, the corrections of η_1, η_2 and η_3 required by the modifications (4.6.5) and (4.6.6) of the datum velocity are of little importance. The important point is that if η_1, η_2 and η_3 are consistent with the datum velocity field then (4.6.5), (4.6.6), (4.6.7) and (4.6.8) follow.

4.6.2 Stream and stress functions

The stream function ψ defined by (4.5.1) is not convenient when the viscosities η_1, η_2 and η_3 in the field equations (4.3.15) depend on the ice depth. Stress gradients cannot be represented in terms of the stream function without introducing viscosity gradients, which complicate the formulation of both field equations and boundary conditions. This problem is overcome by introducing a stress function ϕ, in addition to the stream function

ψ (*cf.* Hutter, 1983). The stress function ϕ, is defined by the relations

$$\Delta\sigma_{xx} = \frac{\partial^2\phi}{\partial z^2}\,, \quad \Delta\sigma_{xz} = \Delta\tau_{xz} = -\frac{\partial^2\phi}{\partial x\partial z}\,, \quad \Delta\sigma_{zz} = \frac{\partial^2\phi}{\partial x^2}\,. \tag{4.6.9}$$

The force balance equations (4.3.13), are automatically satisfied when the stress field is expressed in this way.

The deviatoric stress perturbation $\Delta\tau_{xx}$, can be expressed in terms of the stress function ϕ, as

$$\Delta\tau_{xx} = -\Delta\tau_{zz} = \tfrac{1}{2}(\Delta\sigma_{xx} - \Delta\sigma_{zz}) = \tfrac{1}{2}\left(\frac{\partial^2\phi}{\partial z^2} - \frac{\partial^2\phi}{\partial x^2}\right). \tag{4.6.10}$$

The strain rate components $\Delta\dot{\varepsilon}_{xx}$ and $\Delta\dot{\varepsilon}_{xz}$, can be expressed in terms of the stream function ψ, as

$$\Delta\dot{\varepsilon}_{xx} = -\Delta\dot{\varepsilon}_{zz} = \frac{\partial^2\psi}{\partial x\partial z}\,, \quad \Delta\dot{\varepsilon}_{xz} = \tfrac{1}{2}\left(\frac{\partial^2\psi}{\partial z^2} - \frac{\partial^2\psi}{\partial x^2}\right). \tag{4.6.11}$$

Using a stream function ψ defined by (4.5.1), and a stress function ϕ defined by (4.6.9), the field equations (4.3.12), (4.3.13) and (4.3.15), and the boundary conditions (4.3.24), (4.3.25) and (4.3.26), for the ice flow perturbations can be written entirely in terms of ψ and ϕ. This reduces the number of independent unknown functions that need to be found from 5 to 2.

The ice flux perturbation Δq, defined in (4.3.23), is given by

$$\Delta q = \psi_{z=1} - \psi_{z=0} + \underset{z=1}{u_0}\,\Delta z_s - \underset{z=0}{u_0}\,\Delta z_b \tag{4.6.12}$$

in terms of the stream function ψ.

4.6.3 Field equations

The equation of continuity (4.3.12) is already satisfied by the stream function formulation of the velocity field. The force balance equations (4.3.13) are similarly satisfied by stress function formulation of the stress field. The only remaining field equations are the flow law equations (4.3.15). Expressed in terms of ψ and ϕ equations (4.3.15) become

$$\Delta\tau_{xx} = \tfrac{1}{2}\left(\frac{\partial^2\phi}{\partial z^2} - \frac{\partial^2\phi}{\partial x^2}\right) = 2\eta_1\Delta\dot{\varepsilon}_{xx} - 2\eta_3\Delta\dot{\varepsilon}_{xz} = 2\eta_1\frac{\partial^2\psi}{\partial x\partial z} - \eta_3\left(\frac{\partial^2\psi}{\partial z^2} - \frac{\partial^2\psi}{\partial x^2}\right)$$

$$\Delta\tau_{xz} = -\frac{\partial^2\phi}{\partial x\partial z} = 2\eta_2\Delta\dot{\varepsilon}_{xz} - 2\eta_3\Delta\dot{\varepsilon}_{xx} = \eta_2\left(\frac{\partial^2\psi}{\partial z^2} - \frac{\partial^2\psi}{\partial x^2}\right) - 2\eta_3\frac{\partial^2\psi}{\partial x\partial z}\,.$$

For numerical computations it is convenient to rearrange the above equations so that they become

$$\frac{\partial^2\phi}{\partial z^2} = \frac{\partial^2\phi}{\partial x^2} + 2\frac{\eta_3}{\eta_2}\frac{\partial^2\phi}{\partial x\partial z} + 4\left(\eta_1 - \frac{\eta_3^2}{\eta_2}\right)\frac{\partial^2\psi}{\partial x\partial z} \qquad (4.6.13a)$$

$$\frac{\partial^2\psi}{\partial z^2} = \frac{\partial^2\psi}{\partial x^2} + 2\frac{\eta_3}{\eta_2}\frac{\partial^2\psi}{\partial x\partial z} - \frac{1}{\eta_2}\frac{\partial^2\phi}{\partial x\partial z}\,. \qquad (4.6.13b)$$

In order to derive (4.6.13a) ($\partial^2\psi/\partial z^2$) was eliminated using (4.6.13b).

Equations (4.6.13) are the field equations that will be solved numerically in the non-linear analysis.

The field equations (4.6.13) will be solved in the wave number domain. Assuming that longitudinal variation in the viscosity components η_1, η_2 and η_3 is negligible, the Fourier transforms of the field equations are

$$\frac{\partial^2\hat{\phi}}{\partial z^2} = -k^2\hat{\phi} + 2ik\frac{\eta_3}{\eta_2}\frac{\partial\hat{\phi}}{\partial z} + 4ik\left(\eta_1 - \frac{\eta_3^2}{\eta_2}\right)\frac{\partial\hat{\psi}}{\partial z} \qquad (4.6.14a)$$

$$\frac{\partial^2\hat{\psi}}{\partial z^2} = -k^2\hat{\psi} + 2ik\frac{\eta_3}{\eta_2}\frac{\partial\hat{\psi}}{\partial z} - ik\frac{1}{\eta_2}\frac{\partial\phi}{\partial z}\,. \qquad (4.6.14b)$$

4.6.4 Boundary conditions

The boundary conditions for the ice flow perturbations for non-linear rheology are derived from the boundary conditions (4.3.24), (4.3.25) and (4.3.26) in the same way as in subsection 4.5.4 for linear Newtonian rheology, except that the term arising from τ_{xx_0} in (4.3.24a), involving the datum longitudinal velocity gradient e, at the datum ice surface, is *not* neglected. Although this term is $O(e^{1/n})$ for non-linear rheology, it nevertheless does not turn out to be significant for the computation of ice flux. Therefore, it will sometimes be dropped for convenience in the following. Written in terms of the stream and stress functions ψ and ϕ, the boundary conditions are given by (remember that

(4.3.24b) is replaced by its $(\partial/\partial x)$ derivative)

At the datum surface $z = 1$:

$$-\frac{\partial^2\phi}{\partial x\partial z} = \Delta\sigma_{\underset{z=1}{xz}} = \Delta z_s + 2(\partial\Delta z_s/\partial x)\,|e|^{1/n}\mathrm{sign}(e)\,, \qquad (4.6.15)$$

$$\frac{\partial^3\phi}{\partial x^3} = (\partial\Delta\sigma_{\underset{z=1}{zz}}/\partial x) = -\cot\alpha_0(\partial\Delta z_s/\partial x)\,. \qquad (4.6.16)$$

At the datum base $z = 0$:

$$-u_0\frac{d\Delta z_b}{dx} - \frac{\partial\psi}{\partial x} = 0\,, \qquad (4.6.17)$$

$$\frac{\partial\psi}{\partial z} + \frac{\partial u_0}{\partial z}\Delta z_b = -mc\left(\frac{\partial^2\phi}{\partial x\partial z} + \Delta z_b\right). \qquad (4.6.18)$$

The terms $u_{\underset{z=0}{0}}$ and $(\partial u_0/\partial z)_{z=0}$ in (4.6.17) and (4.6.18) are given by (4.6.4) and (4.6.5).

It is not strictly necessary to replace (4.3.24b) by its $(\partial/\partial x)$ derivative in order to derive a boundary condition, since it is straightforward to write $\Delta\sigma_{zz}$ at the ice surface using the stress function ϕ. The differentiation form represented by (4.6.16) is chosen because it is convenient for the computation of flux filters.

Integrating (4.6.17) with respect to x, the ice flux perturbation Δq given by (4.6.12) may be written

$$\Delta q = \psi_{z=1} + u_{\underset{z=1}{0}}\,\Delta z_s\,. \qquad (4.6.19)$$

Ice flux perturbation components Δq_e, Δq_n, Δq_a and Δq_b (*cf.* subsection 4.3.7), and ice flux filters $g_e(x)$, $g_n(x)$ and $g_b(x)$ (*cf.* subsection 4.5.6) are derived from the boundary conditions (4.6.15), (4.6.16), (4.6.17) and (4.6.18) by defining subproblems for each of the "forcing" functions $\Delta\sigma_{\underset{z=1}{xz}} = \Delta z_s + 2(\partial\Delta z_s/\partial x)\,|e|^{1/n}\mathrm{sign}(e)$, $(\partial\Delta\sigma_{\underset{z=1}{zz}}/\partial x) = -\cot\alpha_0(\partial\Delta z_s/\partial x)$, Δz_s and Δz_b.

The advection component Δq_a, is directly determined from the datum flow by (4.3.28), *i.e.*

$$\Delta q_a = u_{0\,z=1}\,\Delta z_s \simeq (2/(n+1)+c)\Delta z_s\,, \tag{4.6.20}$$

where $u_{0\,z=1}$ is given by (4.6.6). The datum velocity solution needs to be slightly modified for non-linear rheology as was discussed in subsection 4.6.1. Therefore, $u_{0\,z=1}$ as given by (4.6.6), is only approximately equal to $(2/(n+1)+c)$, but not exactly equal as in (4.3.28).

The boundary conditions (4.3.29a), (4.3.29b) and (4.3.29c), which determine Δq_e, Δq_n and Δq_b, respectively, follow from (4.6.15), (4.6.16), (4.6.17) and (4.6.18) by specifying $\Delta\sigma_{xz\,z=1}$, $(\partial\Delta\sigma_{zz\,z=1}/\partial x)$ and Δz_b as follows

Δq_e:

$$\Delta\sigma_{xz\,z=1} \neq 0\,,\quad (\partial\Delta\sigma_{zz\,z=1}/\partial x) = 0\,,\quad \Delta z_b = 0\,. \tag{4.6.21a}$$

Δq_n:

$$\Delta\sigma_{xz\,z=1} = 0\,,\quad (\partial\Delta\sigma_{zz\,z=1}/\partial x) \neq 0\,,\quad \Delta z_b = 0\,. \tag{4.6.21b}$$

Δq_b:

$$\Delta\sigma_{xz\,z=1} = (\partial\Delta\sigma_{zz\,z=1}/\partial x) = 0\,,\quad \Delta z_b \neq 0\,. \tag{4.6.21c}$$

The ice flux filters $g_e(x)$, $g_n(x)$ and $g_b(x)$ are defined by the relations (4.5.18)

$$\Delta q_e = g_e * \Delta\sigma_{xz\,z=1}\,,\quad \Delta q_n = g_n * (\partial\Delta\sigma_{zz\,z=1}/\partial x)\,,\quad \Delta q_b = -g_b * \Delta z_b\,. \tag{4.6.22}$$

They correspond to δ-functions in the boundary conditions (4.6.21), *i.e.*

$g_e(x)$:

$$\Delta\sigma_{xz\,z=1} = \delta(x)\,,\quad (\partial\Delta\sigma_{zz\,z=1}/\partial x) = 0\,,\quad \Delta z_b = 0\,. \tag{4.6.23a}$$

$g_n(x)$:

$$\Delta\sigma_{xz\,z=1} = 0\,,\quad (\partial\Delta\sigma_{zz\,z=1}/\partial x) = \delta(x)\,,\quad \Delta z_b = 0\,. \tag{4.6.23b}$$

$g_b(x)$:

$$\Delta\sigma_{xz\,z=1} = (\partial\Delta\sigma_{zz\,z=1}/\partial x) = 0\,,\quad \Delta z_b = \delta(x)\,. \tag{4.6.23c}$$

By (4.6.19) and (4.6.20) each flux filter is given as the surface value of the stream function, *i.e.* $\hat{\psi}(z=1)$, corresponding to the appropriate version of (4.6.23).

The boundary conditions (4.6.15), (4.6.16), (4.6.17) and (4.6.18) in the wave number domain are found by taking Fourier transforms.

At the datum surface $z = 1$:

$$-ik\,\frac{\partial\hat{\phi}}{\partial z} = \Delta\hat{\sigma}_{xz\,z=1} = (1 + 2ik\,|e|^{1/n}\mathrm{sign}(e))\Delta\hat{z}_s\,, \tag{4.6.24}$$

$$-ik^3\hat{\phi} = ik\Delta\hat{\sigma}_{zz\,z=1} = \cot\alpha_0(-ik\Delta\hat{z}_s)\,. \tag{4.6.25}$$

At the datum base $z = 0$:

$$-iku_0\Delta\hat{z}_b - ik\hat{\psi} = 0\,, \tag{4.6.26}$$

$$\frac{\partial\hat{\psi}}{\partial z} + \frac{\partial u_0}{\partial z}\Delta\hat{z}_b = -mc\left(ik\frac{\partial\hat{\phi}}{\partial z} + \Delta\hat{z}_b\right). \tag{4.6.27}$$

Since the Fourier transform of a δ-function is equal to 1, independent of k, the Fourier transforms of the expressions (4.6.23), for $\Delta\sigma_{xz\,z=1}$, $(\partial\Delta\sigma_{zz\,z=1}/\partial x)$ and Δz_b, which determine the flux filters $g_e(x)$, $g_n(x)$ and $g_b(x)$, are as follows.

$\hat{g}_e(k)$:

$$\Delta\hat{\sigma}_{xz\,z=1} = 1\,,\quad ik\Delta\hat{\sigma}_{zz\,z=1} = 0\,,\quad \Delta\hat{z}_b = 0\,. \tag{4.6.28a}$$

$\hat{g}_n(k)$:

$$\Delta\hat{\sigma}_{\substack{xz\\z=1}} = 0\,,\quad ik\Delta\hat{\sigma}_{\substack{zz\\z=1}} = 1\,,\quad \Delta\hat{z}_b = 0\,. \tag{4.6.28b}$$

$\hat{g}_b(k)$:

$$\Delta\hat{\sigma}_{\substack{xz\\z=1}} = ik\Delta\hat{\sigma}_{\substack{zz\\z=1}} = 0\,,\quad \Delta\hat{z}_b = 1\,. \tag{4.6.28c}$$

4.6.5 Numerical formulation

The field equations (4.6.14) in the wave number domain are a system of two coupled second order ordinary differential equations for the complex Fourier transforms $\hat{\psi}$ and $\hat{\phi}$, of the stream and stress functions. Given the viscosity components η_1, η_2 and η_3, computed as functions of z as described in subsection 4.3.5, the equations can be solved by traditional numerical methods for such systems, *e.g.* Runge-Kutta methods (*cf.* Conte and de Boor, 1980, Chapter 8). Having found $\hat{\psi}$ and $\hat{\phi}$ on a grid of values of the wave number k, the functions may be numerically inverted to the space domain using (3.3.4a) in order to find their space domain representations.

The field equations (4.6.14) must be reformulated as a first order system for the numerical computations. This is done by defining the functions

$$f_1 = \hat{\psi}\,,\quad f_2 = ik^3\hat{\phi}\,,\quad f_3 = \frac{\partial\hat{\psi}}{\partial z}\,,\quad f_4 = ik\frac{\partial\hat{\phi}}{\partial z}\,. \tag{4.6.29}$$

The factors ik^3 and ik in the definitions of f_2 and f_4, simplify the formulation of the boundary conditions for ice flux filters.

Using (4.6.29) the field equations (4.6.14) may be written as the first order system

$$\frac{\partial}{\partial z}\begin{bmatrix} f_1\\ f_2\\ f_3\\ f_4\end{bmatrix} = \begin{bmatrix} f_3\\ k^2 f_4\\ -k^2 f_1 + 2ik(\eta_3/\eta_2)f_3 - (1/\eta_2)f_4\\ -f_2 + 2ik(\eta_3/\eta_2)f_4 - 4k^2(\eta_1 - \eta_3^2/\eta_2)f_3\end{bmatrix}. \tag{4.6.30}$$

In terms of f_1, f_2, f_3 and f_4 the boundary conditions (4.6.24), (4.6.25), (4.6.26) and (4.6.27) are given by

At the datum surface $z = 1$:

$$f_4 = -\Delta\hat{\sigma}_{\substack{xz\\z=1}}\,,\quad f_2 = -ik\Delta\hat{\sigma}_{\substack{zz\\z=1}}\,. \tag{4.6.31}$$

At the datum base $z = 0$:

$$f_1 = -u_0\Delta\hat{z}_b\,,\quad f_3 + mcf_4 = -((\partial u_0/\partial z) + mc)\Delta\hat{z}_b\,. \tag{4.6.32}$$

The Fourier transforms of the ice flux filters $g_e(x)$, $g_n(x)$ and $g_b(x)$, are found by repeated solutions of the system (4.6.30) subject to the boundary conditions (4.6.31) and (4.6.32), using (4.6.28) to specify the correct boundary values of $\Delta\hat{\sigma}_{\substack{xz\\z=1}}$, $(ik\Delta\hat{\sigma}_{\substack{zz\\z=1}})$ and $\Delta\hat{z}_b$, for each filter. The transforms of the flux filters are given as the surface values of the corresponding stream functions, *i.e.* $\hat{\psi}(z=1) = f_1(z=1)$.

The boundary conditions (4.6.31) and (4.6.32) are specified at *two* boundaries, whereas efficient differential equation solvers like Runge-Kutta, are designed for *initial value* problems, where all the boundary conditions are specified at *one* boundary. This problem can be overcome in a way described by Hutter (1983) by using a "shooting" method to solve the boundary value problem (*cf.* Conte and de Boor, 1980, Chapter 9). In this method, a set of 4 linearly independent solutions of (4.6.30) is computed numerically by solving 4 independent initial value problems, starting either at the base or at the surface. Let $f_{i,\substack{1\\b}}$, $i=1,2,3,4$, denote the solution of the system (4.6.30) computed by starting an integration of the system at the base $z = 0$ and specifying the initial condition $f_1 = 1$, $f_2 = f_3 = f_4 = 0$. Let $f_{i,\substack{2\\b}}$, $f_{i,\substack{3\\b}}$ and $f_{i,\substack{4\\b}}$ be defined similarly by specifying the other components of f_i to be equal to 1 at $z = 0$, one at a time. Because of the linearity of the problem, a general solution of (4.6.30) may be written

$$f_i = b_1 f_{i,\substack{1\\b}} + b_2 f_{i,\substack{2\\b}} + b_3 f_{i,\substack{3\\b}} + b_4 f_{i,\substack{4\\b}}\,, \tag{4.6.33}$$

where b_1, b_2, b_3 and b_4 are constants.

The constants b_1, b_2, b_3 and b_4 must be determined so that the boundary conditions (4.6.31) and (4.6.32) are satisfied. This leads to the equations

$$b_1 = -u_{0\,z=0}\,\Delta\hat{z}_b \tag{4.6.34}$$

$$b_3 + mcb_4 = -((\partial u_0/\partial x)_{z=0} + mc)\Delta\hat{z}_b$$

$$\begin{bmatrix} f_{4,2}_b & f_{4,4}_b - mcf_{4,3}_b \\ f_{2,2}_b & f_{2,4}_b - mcf_{2,3}_b \end{bmatrix}_{z=1} \begin{bmatrix} b_2 \\ b_4 \end{bmatrix} = \begin{bmatrix} -\Delta\hat{\sigma}_{xz\,z=1} + (u_{0\,z=0}\,f_{4,1}_b + ((\partial u_0/\partial x)_{z=0} + mc)f_{4,3}_b)\Delta\hat{z}_b \\ -ik\Delta\hat{\sigma}_{zz\,z=1} + (u_{0\,z=0}\,f_{2,1}_b + ((\partial u_0/\partial x)_{z=0} + mc)f_{2,3}_b)\Delta\hat{z}_b \end{bmatrix} \tag{4.6.35}$$

The $f_{i,j}_b$ values in (4.6.35) are evaluated at $z = 1$.

Equation (4.6.35) is a system of 2 linear equations for the 2 unknown constants b_2 and b_4. It can be solved by Gaussian elimination using complex arithmetic. The constants b_1 and b_3 are then given by (4.6.34). The linearly independent solutions $f_{i,1}_b$, $f_{i,2}_b$, $f_{i,3}_b$ and $f_{i,4}_b$ are found by repeated upward integration of (4.6.30) with the appropriate initial condition at $z = 0$. The same solutions may be used to determine all of $\hat{g}_e(k)$, $\hat{g}_n(k)$ and $\hat{g}_b(k)$ by using an appropriate version of (4.6.34) and (4.6.35).

An alternative way to satisfy the boundary conditions (4.6.31) and (4.6.32) is to start the numerical integration at the surface $z = 1$. Then a set of linearly independent solutions $f_{i,1}_s$, $f_{i,2}_s$, $f_{i,3}_s$ and $f_{i,4}_s$, of the system (4.6.30) is computed by specifying the components f_i to be equal to 1 at $z = 1$, one at a time, while the other components are put equal to 0. A general solution of (4.6.30) may be written

$$f_i = s_1 f_{i,1}_s + s_2 f_{i,2}_s + s_3 f_{i,3}_s + s_4 f_{i,4}_s\,, \tag{4.6.36}$$

where s_1, s_2, s_3 and s_4 are constants. The constants are chosen so that the boundary conditions (4.6.31) and (4.6.32) are satisfied. This leads to

$$s_4 = -\Delta\hat{\sigma}_{xz\,z=1} \tag{4.6.37}$$

$$s_2 = -ik\Delta\hat{\sigma}_{zz\,z=1}$$

$$\begin{bmatrix} f_{1,1}_s & f_{1,3}_s \\ f_{3,1}_s + mcf_{4,1}_s & f_{3,3}_s + mcf_{4,3}_s \end{bmatrix}_{z=0} \begin{bmatrix} s_1 \\ s_3 \end{bmatrix} = \begin{bmatrix} -u_{0\,z=0}\,\Delta\hat{z}_b + f_{1,2}_s ik\Delta\hat{\sigma}_{zz\,z=1} + f_{1,4}_s\Delta\hat{\sigma}_{xz\,z=1} \\ -((\partial u_0/\partial x)_{z=0} + mc)\Delta\hat{z}_b + (f_{3,2}_s + mcf_{4,2}_s)ik\Delta\hat{\sigma}_{zz\,z=1} + (f_{3,4}_s + mcf_{4,4}_s)\Delta\hat{\sigma}_{xz\,z=1} \end{bmatrix} \tag{4.6.38}$$

The $f_{i,j}_s$ values in (4.6.38) are evaluated at $z = 0$.

Equation (4.6.38) can be solved for s_1 and s_3 just as (4.6.35) was solved for b_2 and b_4. Then s_2 and s_4 are given by (4.6.37). The linearly independent solutions $f_{i,1}_s$, $f_{i,2}_s$, $f_{i,3}_s$ and $f_{i,4}_s$, are found by repeated downward integration of (4.6.30) with the appropriate initial condition at $z = 1$. The same solutions may be used to determine all of $\hat{g}_e(k)$, $\hat{g}_n(k)$ and $\hat{g}_b(k)$ by using an appropriate version of (4.6.37) and (4.6.38).

Equations (4.6.34) and (4.6.35), on one hand, and (4.6.37) and (4.6.38), on the other, are two equivalent ways of satisfying the boundary conditions (4.6.31) and (4.6.32). It is advantageous to use both these possibilities in order to check the validity of the numerical computations.

The matrixes on the left hand sides of (4.6.35) and (4.6.38) may be badly conditioned for high values of k, even though the matrixes are only 2x2 matrixes. This situation arises because solutions of (4.6.30) may be very rapidly rising or decaying in z for high values of k. Therefore, many significant digits may be lost when (4.6.35) and (4.6.38) are solved. Similarly, loss of significant digits may be encountered when (4.6.33) and (4.6.36) are used to compute a solution of (4.6.30), which satisfies the boundary conditions (4.6.31) and (4.6.32). Insignificant result may be prevented to some extent by using double precision arithmetic. Nevertheless, the accuracy of the computed results must be checked by computing the condition number of the matrixes in (4.6.35) and (4.6.38) (*cf.* Conte and de Boor, 1980, Chapter 4) and by checking for loss of significant digits when

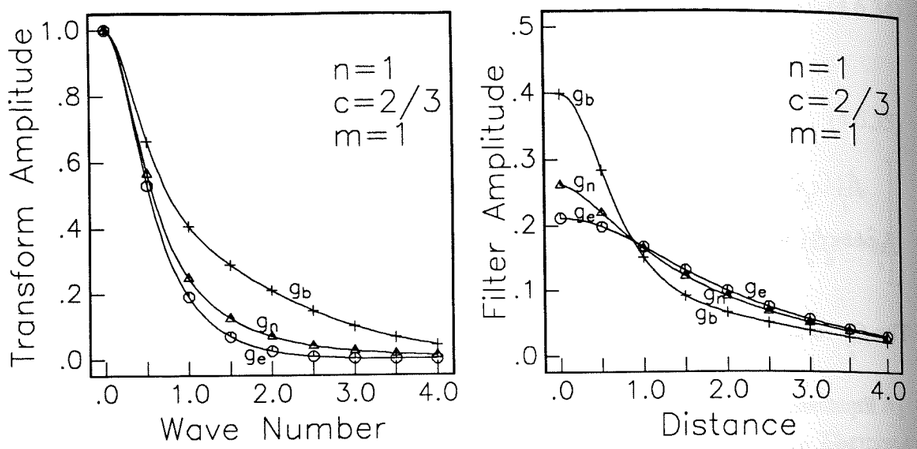

FIGURE 4.6.1: Normalized Fourier transforms $\hat{g}_e(k)$, $\hat{g}_n(k)$ and $\hat{g}_b(k)$ of flux filters for linear Newtonian rheology (left) and corresponding normalized flux filters $g_e(x)$, $g_n(x)$ and $g_b(x)$ (right) for basal sliding given by $c = 2/3$. The curves are normalized with the value of the Fourier transforms at $k = 0$. Solid curves are analytical results given by (4.5.17) (same as in shown Figure 4.5.2). Numerical results, computed with the fourth order Runge-Kutta method with a vertical step size equal to 0.02, are plotted as symbols.

(4.6.33) and (4.6.36) are used. When computing flux filters, numerically insignificant values of the stream function ψ, can always be replaced by 0 without introducing significant errors in the space domain representation of the filters.

4.6.6 Verification of numerical computations

The numerical formulation, which was developed in the previous subsection, was tested in two ways. First, numerical results for linear Newtonian rheology with basal sliding, *i.e.* for $n = m = 1$, were compared to the analytical solution given by (4.5.17) (Fig. 4.6.1). The numerical results, computed by integrating upward from the base (using (4.6.34) and (4.6.35)) and by integrating downward from the surface (using (4.6.37) and (4.6.38)), agreed with each other and with the analytical solution (4.5.17) to 7 or more

significant digits in the range $0 \le k \le 4$. The problems with loss of significant digits, which were discussed in the previous subsection, are only encountered for non-linear rheology and for higher values of k.

Second, numerical results for $k = 0$ were compared with the modified laminar flow approximation (4.6.8). The laminar flow approximation (4.4.2) must be modified slightly, as described in subsection 4.6.1 before accurate comparison with the numerical results can be made. When this is done the numerical results agree with the laminar flow approximation to more than 7 significant digits.

The numerical results that are described in the following are computed using the fourth order Runge-Kutta method with a fixed vertical step size of 0.02 or 0.01. By using a fixed step size it is possible to tabulate η_1, η_2 and η_3 on an equally spaced grid in z at the start of the computations. This leads to significant reduction in the amount of computer time needed for the computations.

4.6.7 Flux filters

The viscosity components η_1, η_2 and η_3, in the field equations (4.6.14) are determined by the flow law power n and the datum longitudinal extension/compression e (*cf.* subsection 4.3.5). From the field equations (4.6.14) and the boundary conditions (4.6.24), (4.6.25), (4.6.26) and (4.6.27) together with (4.6.28), it therefore follows that the flux filters $g_e(x)$, $g_n(x)$ and $g_b(x)$ are completely determined by the flow law and sliding law powers n and m, the datum longitudinal extension/compression e, and the sliding parameter c. They are independent of the long scale surface slope α_0, which only enters as the multiplying factor $\cot\alpha_0$, in the expression (4.6.25) for $\Delta\sigma_{zz}\big|_{z=1}$.

The flux filters $g_e(x)$, $g_n(x)$ and $g_b(x)$, for non-linear rheology are not necessarily symmetric as was the case for linear Newtonian rheology. This is caused by the viscosity component η_3 in the field equations (4.6.14), which leads to non-zero imaginary parts in the transforms of the stream and stress functions. A non-zero imaginary part in the wave number domain results in asymmetry in the corresponding function in space domain by the properties of Fourier transforms. The asymmetry of $g_e(x)$, $g_n(x)$ and $g_b(x)$, is, therefore, indicative of the importance of the viscosity component η_3 in the perturbation ice flow. This effect of η_3 leads to non-trivial variation in the phase of $\hat{g}_e(k)$ and $\hat{g}_b(k)$ with

k, but the resulting asymmetry in the filters in the space domain is not great and has little effect on the steady state transfer of undulations to the ice surface. The asymmetry in the flux filters depends on the sign of the datum longitudinal extension/compression e, such that if the sign of e is changed, then the filters are reflected about $x = 0$. It turns out that the flux filter $g_n(x)$ is, nevertheless, symmetric in x, but $g_e(x)$ and $g_b(x)$ are slightly asymmetric.

The field equations (4.6.14) can be solved analytically for $k = 0$ to find $\hat{g}_e(k=0)$, $\hat{g}_n(k=0)$ and $\hat{g}_b(k=0)$. The values of the Fourier transforms for $k = 0$ are equal to the integrals or areas of the corresponding filters by the properties of Fourier transforms.

$$\int_{-\infty}^{\infty} g_e(x)dx = \hat{g}_e(k=0) = \int_0^1\int_0^z \frac{1}{\eta_2}d\zeta dz + mc = \int_0^1 \frac{1-z}{\eta_2}dz + mc \simeq 2n/(n+1) + mc \,,$$
$$\int_{-\infty}^{\infty} g_n(x)dx = \hat{g}_n(k=0) = \int_0^1\int_0^z \frac{1-\zeta}{\eta_2}d\zeta dz + mc = \int_0^1 \frac{(1-z)^2}{\eta_2}dz + mc \simeq 2n/(n+2) + mc \,, \quad (4.6.39)$$
$$\int_{-\infty}^{\infty} g_b(x)dx = \hat{g}_b(k=0) = (\partial u_0/\partial z)_{z=0} + u_{0\,z=0} + mc \simeq 2 + (m+1)c \,.$$

Using (4.6.39) together with (4.6.5) and (4.6.6), the advective flux perturbation component given by (4.6.20) may be rewritten as

$$\Delta q_a = u_{0\,z=1}\Delta z_s = (u_{0\,z=0} + \int_0^1 \frac{z}{\eta_2}dz)\Delta z_s = (\hat{g}_b(k=0) - \hat{g}_e(k=0))\Delta z_s \simeq (2/(n+1)+c)\Delta z_s \,. \quad (4.6.40)$$

The approximate expressions on the far right of (4.6.39) and (4.6.40) are found by neglecting the effect of the boundary layer at the surface so that $\eta_2 = (1-z)^{-(n-1)}/(2n)$. The error in the approximations is caused by the datum longitudinal extension/compression e in the boundary layer and is on the order of $|e|^{1+2/n}$. For $|e| = 0.01$ this error is less than 1 part in 1000.

For slowly varying flow, *i.e.* when $k \to 0$, $\lambda = 2\pi/k \to \infty$, the ice flux perturbations predicted by (4.6.20) and (4.6.22) must satisfy

$$\Delta q_e \simeq \hat{g}_e(k=0)\Delta\sigma_{xz\,z=1} = \hat{g}_e(k=0)(\Delta z_s + 2(\partial\Delta z_s/\partial x)|e|^{1/n}\mathrm{sign}(e)) \,,$$
$$\Delta q_n \simeq \hat{g}_n(k=0)(\partial\Delta\sigma_{zz\,z=1}/\partial x) = \hat{g}_n(k=0)\cot\alpha_0(-\partial\Delta z_s/\partial x) \,, \quad (4.6.41)$$
$$\Delta q_a = u_{0\,z=0}\Delta z_s \,,$$
$$\Delta q_b \simeq -\hat{g}_b(k=0)\Delta z_b \,.$$

For slowly varying flow, the second term $2(\partial\Delta z_s/\partial x)|e|^{1/n}\mathrm{sign}(e)$ in the above expression for Δq_e becomes unimportant in comparison with the first term Δz_s. Thus, comparison of (4.6.39), (4.6.40) and (4.6.41) with the corresponding expressions for the modified laminar flow approximation (4.6.8) shows that ice flow predicted by the non-linear analysis agrees with the laminar flow approximation in the limit $k \to 0$, $\lambda = 2\pi/k \to \infty$. This is a condition that must be satisfied by any correct theory of glacier flow as discussed previously.

Figure 4.6.2 shows the normalized Fourier transforms $\hat{g}_e(k)$, $\hat{g}_n(k)$ and $\hat{g}_b(k)$, computed numerically for $n = 3$, $e = 0.01$ and no basal sliding. Figure 4.6.3 shows the corresponding normalized flux filters in the space domain. The complex transforms are displayed as transform amplitude (left) and phase (right). The transforms and the filters are normalized with the value of the Fourier transforms at $k = 0$ (*cf.* (4.6.39)) in order to make it easier to compare the shapes of the curves. The normalized amplitude curves start at the value 1 at $k = 0$, and the areas below each of the corresponding normalized flux filters are equal to 1. Comparing the amplitude curves with the corresponding curves for linear Newtonian rheology (Fig. 4.5.1 (left)) shows that the transforms $\hat{g}_e(k)$, $\hat{g}_n(k)$ and $\hat{g}_b(k)$, decay much faster to zero with increasing k for non-linear rheology than for linear rheology. As a consequence the normalized flux filters for non-linear rheology (Fig. 4.6.3) are lower and wider than the filters for linear rheology (Fig. 4.5.1 (right) (note the different scales of the x-axes)). This can be understood from the increased range of longitudinal stress gradients for non-linear rheology, resulting from relatively stiff ice in the boundary layer near the ice surface.

The decay of $\hat{g}_b(k)$ with k for non-linear rheology is significantly slower than the decay of $\hat{g}_n(k)$ and $\hat{g}_e(k)$. Furthermore, the decay of $\hat{g}_n(k)$ is somewhat slower than that of $\hat{g}_e(k)$. This was also the case for linear rheology and turns out to be true in general

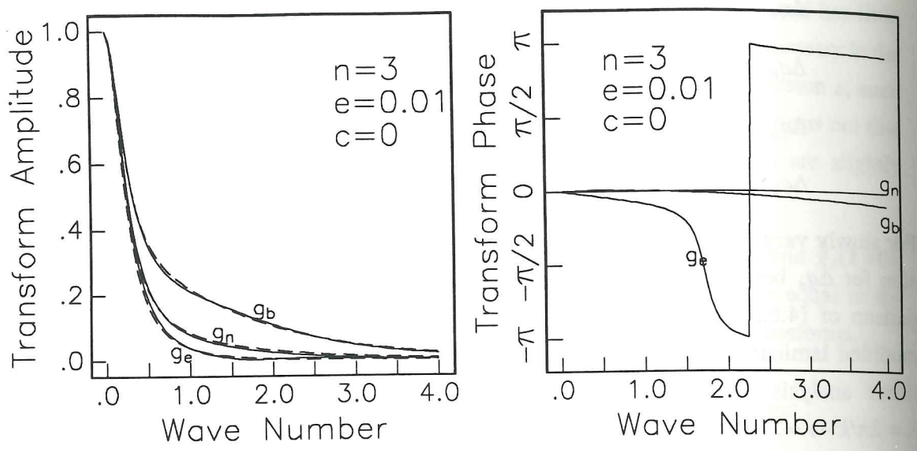

FIGURE 4.6.2: Normalized Fourier transforms $\hat{g}_e(k)$, $\hat{g}_n(k)$ and $\hat{g}_b(k)$ of flux filters computed numerically for non-linear rheology with $n = 3$, $e = 0.01$ and no basal sliding ($c = 0$). The figures shows the amplitude (left) and the phase (in radians) (right) of the complex Fourier transforms. The amplitude curves are normalized with the value of the Fourier transforms at $k = 0$. Solid curves show the results of the numerical computations. Dashed amplitude curves show the results of a simplified analysis, which will be discussed in the next subsection.

independent of the values of the parameters n, e, c and m. The slow decay of $\hat{g}_b(k)$ compared to $\hat{g}_n(k)$ and $\hat{g}_e(k)$ can be explained in the same way as in the case of linear rheology (*cf.* subsection 4.5.6) and turns out to be crucial for the transfer of bedrock undulations to the ice surface. The slow decay of $\hat{g}_b(k)$ with k leads to a relatively narrow peak in the flux filter $g_b(x)$ at $x = 0$ (Fig. 4.6.3). The width of the narrow peak in $g_b(x)$ is approximately 2 ice thicknesses. There is an indication of a similar but much lower peak in $g_n(x)$ at $x = 0$. Outside the peaks in $g_b(x)$ and $g_n(x)$, *i.e.* for $|x| \gtrsim 1$–2, the filters decay slowly to zero. The shape of this slow decay is similar for the three filters. These features in the shape of the filters are qualitatively the same, independent of the values of the parameters n, e, c and m. Changing the parameters changes the relative height of the narrow peak in $g_b(x)$ and the length-scale of the slow decay of the filters for $|x| \gtrsim 1$–2.

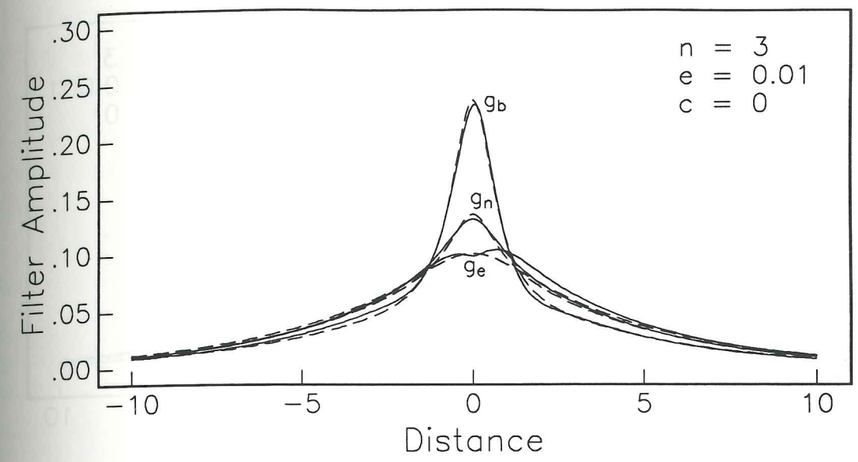

FIGURE 4.6.3: Normalized flux filters $g_e(x)$, $g_n(x)$ and $g_b(x)$ computed numerically for non-linear rheology with $n = 3$, $e = 0.01$ and no basal sliding ($c = 0$). The curves are normalized with the value of the corresponding Fourier transforms at $k = 0$ so that the area of each filter is equal to 1. Solid curves show the results of the numerical computations. Dashed curves show the results of a simplified analysis, which will be discussed in the next subsection.

Figure 4.6.2 (right) shows that the phase of $\hat{g}_n(k)$ is equal to zero and that the phase of $\hat{g}_b(k)$ is close to zero. Thus, $g_n(x)$ and $g_b(x)$ are almost symmetric in x (*cf.* Fig. 4.6.3). The phase of $\hat{g}_e(k)$ shows considerable variation with k, but most of this variation takes place after the amplitude of $\hat{g}_e(k)$ is almost zero. Therefore, the resulting asymmetry in $g_e(x)$ (*cf.* Fig. 4.6.3) is not great. It turns out that $g_e(x)$, $g_n(x)$ and $g_b(x)$ are almost symmetric in x independent of the values of the parameters n, e, c and m. This suggests that the effect of the viscosity component η_3 on the ice flow is not important (see the discussion earlier in this subsection).

Figure 4.6.4 shows that the normalized ice flux filters become lower and wider when the datum longitudinal extension/compression is lowered to $e = 0.001$. This can be explained by the increased stiffness of the ice in the boundary layer near the ice surface

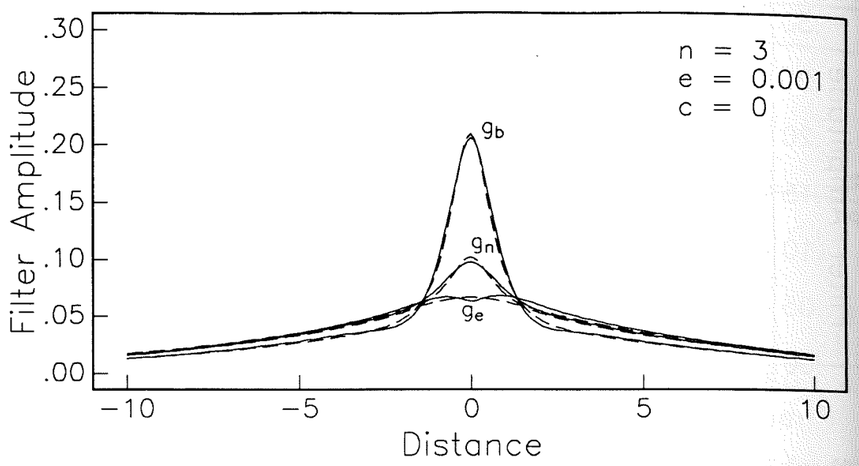

FIGURE 4.6.4: Same as Figure 4.6.3 except that the flux filters in this figure correspond to $e = 0.001$.

when e is lowered. The narrow peak in $g_b(x)$ at $x = 0$ is not affected by the change in e. Making the rheology more non-linear by increasing the flow law power n (not shown) has similar effect on the filters as decreasing e, in addition to lowering the relative height of the narrow peak in $g_b(x)$.

Figure 4.6.5 shows the flux filters for non-zero basal sliding with $c = 0.4$ and $m = 2$. By (4.6.7), the datum ice flux is approximately given by $q_0 \approx 2/(n+2) + c$. Thus, $c = 2/(n+2) = 0.4$ for $n = 3$, corresponds to datum ice flow where the ice flux due to basal sliding is approximately equal to the ice flux due to internal deformation. The parameters $n = 3$ and $e = 0.01$ are the same as in Figure 4.6.3. Comparison with Figure 4.6.3 shows that the flux filters for non-zero sliding are wider than for no sliding, but at the same time the narrow peak in $g_b(x)$ is higher. The width of the narrow peak is approximately the same with and without sliding. Increasing the sliding law power m (not shown) lowers the relative height of the narrow peak in $g_b(x)$ but it has much less effect on the filters than changing the flow law power n.

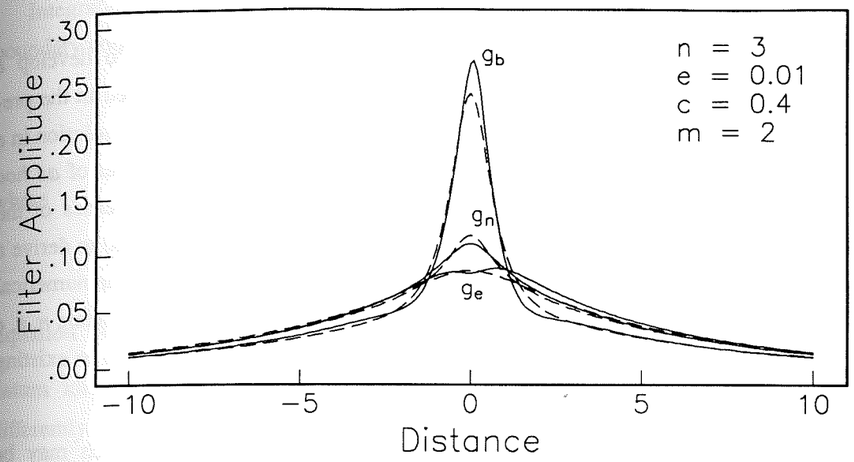

FIGURE 4.6.5: Same as Figure 4.6.3 except that the flux filters in this figure correspond to non-zero basal sliding with $c = 0.4$.

Summarizing, the flux filters $g_e(x)$, $g_n(x)$ and $g_b(x)$ for non-linear rheology are characterized by the following main features.

1. The filters are approximately symmetric in x.
2. The shape of all three filters is almost the same for $|x| \tilde{>} 1$–2, where the filters decay slowly to zero on a length-scale which increases with decreasing $|e|$ and increasing n and c.
3. There is a relatively narrow peak in $g_b(x)$ at $x = 0$ with width approximately equal to 2 independent of n, e, c and m. The relative height of the peak decreases with increasing n and m and increases with c. The height of the peak is relatively independent of e.

The physical meaning of the above numerical results will be discussed in the next subsection after the derivation of a simplified theory which explains much of the shape of the flux filters.

4.6.8 Simplified theory

By introducing a number of simplifying assumptions, it is possible to develop a simplified, semi-analytical theory which reproduces the flux filters computed in the previous subsection fairly well. The purpose is not to compute an accurate flow solution in a rigorous way, since this requires numerical computations. Rather, a number of *ad hoc* modification of the field equations (4.3.13) and (4.3.15), using some properties of the numerically computed solution described in the previous subsection, are used to derive a semi-analytical solution, the validity of which is tested by comparison with the numerical solution. This theory explains the dependence of the flux filters on the parameters n, e, c and m and it clarifies the relation of the theory developed in this dissertation to existing theories of glacier flow.

The derivation of the simplified theory starts by omitting terms, which may be expected to be important for short scale longitudinal flow variations only, from the field equations. The resulting theory turns out to be valid for flow variations on length-scales longer than a few ice thicknesses. A relatively simple *ad hoc* modification, suggested by the numerical computations of the previous subsection, is then used to extend the validity of the theory to flow variations on much shorter length-scales.

Subtracting the $(\partial/\partial x)$ derivative of the force balance equation for the z-direction (4.3.13b) from the $(\partial/\partial z)$ derivative of the force balance equation for the x-direction (4.3.13a), leads to

$$2\frac{\partial^2 \Delta\tau_{xx}}{\partial x \partial z} + \left(\frac{\partial^2}{\partial z^2} - \frac{\partial^2}{\partial x^2}\right)\Delta\sigma_{xz} = 0\,. \qquad (4.6.42)$$

The term $(\partial^2\sigma_{xz}/\partial x^2)$ in (4.6.42) may be expected to be important for short scale longitudinal flow variations only and will therefore be neglected. Omitting $(\partial^2\sigma_{xz}/\partial x^2)$ from (4.6.42) is equivalent to the omission of the T term in theories based on integrated force balance equations. The term $(\partial^2\tau_{xx}/\partial x \partial z)$ in (4.6.42), which will be retained, corresponds to the G term in theories based on integrated force balance equations (*cf.* Collins, 1968; Nye, 1969a; Budd, 1970a; Kamb and Echelmeyer, 1986a,b; Kamb, 1986) (see also section 2.4).

Integration of (4.6.42), with the term $(\partial^2\sigma_{xz}/\partial x^2)$ omitted, using (4.3.13a) and the boundary conditions (4.3.24) at the ice surface, gives

$$-2\int_z^1 \frac{\partial \Delta\tau_{xx}}{\partial x} d\zeta + \Delta\sigma_{xz} = \Delta\sigma_{\substack{xz \\ z=1}} + (\partial\Delta\sigma_{\substack{zz \\ z=1}}/\partial x)(1-z)\,, \qquad (4.6.43)$$

where

$$\Delta\sigma_{\substack{xz \\ z=1}} = \Delta z_s + 2(\partial\Delta z_s/\partial x)\,|e|^{1/n}\mathrm{sign}(e)\,, \quad \Delta\sigma_{\substack{zz \\ z=1}} = -\cot\alpha_0 \Delta z_s\,. \qquad (4.6.44)$$

Equation (4.6.43) shows that the stress perturbations $\Delta\sigma_{\substack{xz \\ z=1}}$ and $(\partial\Delta\sigma_{\substack{zz \\ z=1}}/\partial x)$ at the datum ice surface affect the shear stress perturbation $\Delta\sigma_{xz}$ below the ice surface differently. The shear stress perturbation due to $\Delta\sigma_{\substack{xz \\ z=1}}$ is independent of depth, whereas the shear stress due to $(\partial\Delta\sigma_{\substack{zz \\ z=1}}/\partial x)$ increases linearly with the ice depth. This difference turns out to explain the different shapes of the flux filters $g_e(x)$ and $g_n(x)$ which was observed in the numerical computations in the previous subsection (*cf.* Figs. 4.6.3, 4.6.4 and 4.6.5).

The flow law equations (4.3.15) give $\Delta\tau_{xx}$ and $\Delta\sigma_{xz} = \Delta\tau_{xz}$ as functions of $\Delta\dot{\varepsilon}_{xx} = (\partial\Delta u/\partial x)$ and $\Delta\dot{\varepsilon}_{xz} = \frac{1}{2}(\partial\Delta u/\partial z + \partial\Delta w/\partial x)$ using the viscosity components η_1, η_2 and η_3. The numerical computations of the previous subsection indicate that the effect of η_3 on the flow is not important and the terms involving η_3 in (4.3.15) will therefore be omitted. Furthermore, the term $(\partial\Delta w/\partial x) = -(\partial^2\psi/\partial x^2)$ in the definition of $\Delta\dot{\varepsilon}_{xz}$ may be expected to be significant compared to $(\partial\Delta u/\partial z) = (\partial^2\psi/\partial z^2)$ for short scale longitudinal flow variations only and it will therefore also be neglected. Finally, the most important contribution to the integral $\int_z^1 \frac{\partial\Delta\tau_{xx}}{\partial x} d\zeta \approx \int_z^1 \frac{\partial(2\eta_1(\partial\Delta u/\partial x))}{\partial x} d\zeta$ will be in the boundary layer near the ice surface (*cf.* Fig. 4.3.2) where $\Delta u \approx \Delta u_{z=1}$. Since the derivative of η_1 with x may be neglected (it is $O(\delta)$), this means that the integral in (4.6.43) can be approximated by $\int_z^1 \frac{\partial\Delta\tau_{xx}}{\partial x} d\zeta \approx 2\int_z^1 \eta_1 d\zeta \frac{\partial^2 \Delta u_{z=1}}{\partial x^2}$. Using all these approximations (4.6.43) can be rewritten as

$$-4\int_z^1 \eta_1 d\zeta \frac{\partial^2 \Delta u_{z=1}}{\partial x^2} + \eta_2 \frac{\partial \Delta u}{\partial z} = \Delta\sigma_{\substack{xz \\ z=1}} + (\partial \Delta\sigma_{\substack{zz \\ z=1}} / \partial x)(1-z) \,. \qquad (4.6.45)$$

Furthermore, the shear stress perturbation at $z = 0$ is by (4.6.43) given as

$$\Delta\sigma_{\substack{xz \\ z=0}} = \Delta\sigma_{\substack{xz \\ z=1}} + (\partial \Delta\sigma_{\substack{zz \\ z=1}} / \partial x) + 4\int_0^1 \eta_1 dz \frac{\partial^2 \Delta u_{z=1}}{\partial x^2} \,. \qquad (4.6.46)$$

For the following derivation, it is convenient to define special notation for various depth integrals of η_1 and η_2.

$$\begin{aligned}
I_1 &= \int_0^1 \frac{1}{\eta_2} dz \approx 2 \,, \\
I_2 &= \int_0^1 \frac{z}{\eta_2} dz \approx \frac{2}{(n+1)} \,, \\
I_3 &= \int_0^1 \frac{1-z}{\eta_2} dz \approx \frac{2n}{(n+1)} \,, \\
I_4 &= \int_0^1 \frac{z(1-z)}{\eta_2} dz \approx \frac{2n}{(n+1)(n+2)} \,, \\
I_5 &= \int_0^1 \frac{(1-z)^2}{\eta_2} dz \approx \frac{2n}{(n+2)} \,,
\end{aligned} \qquad (4.6.47)$$

and

$$l_g^2 = 4\left(\int_0^1 \frac{1}{\eta_2} \int_z^1 \eta_1 d\zeta dz + mc \int_0^1 \eta_1 dz\right) . \qquad (4.6.48)$$

The reason for the notation l_g in (4.6.48) will be explained below. The approximate expressions on the far right of (4.6.47) are found by neglecting the effect of the boundary layer at the surface so that $\eta_2 = (1-z)^{-(n-1)}/(2n)$. The error in the approximations is caused by the datum longitudinal extension/compression e in the boundary layer and is on the order of $|e|^{1+2/n}$. For $|e| = 0.01$ this error is a few parts in 1000.

Integration of (4.6.45) using (4.6.46), (4.6.47) and (4.6.48), and the sliding boundary condition (4.3.26) at the base $z = 0$, together with (4.6.5), gives the following ordinary differential equation for the velocity perturbation $\Delta u_{z=1}$ at the datum ice surface.

$$-l_g^2 \frac{\partial^2 \Delta u_{z=1}}{\partial x^2} + \Delta u_{z=1} = (I_1 + mc)\Delta\sigma_{\substack{xz \\ z=1}} + (I_3 + mc)(\partial \Delta\sigma_{\substack{zz \\ z=1}} / \partial x) - (I_1 + mc)\Delta z_b \,. \qquad (4.6.49)$$

Equation (4.6.49) can be solved analytically in the wave number domain or in the space domain. Let the filter $f(x)$ be defined such that

$$\hat{f}(k) = \frac{1}{1 + l_g^2 k^2} \,, \qquad (4.6.50)$$

which implies

$$f(x) = \frac{1}{2l_g} e^{-|x|/l_g} \,. \qquad (4.6.51)$$

Then the Fourier transform of $\Delta u_{z=1}$ is given by

$$\Delta\hat{u}_{z=1}(k) = \hat{f}(k)((I_1 + mc)\Delta\hat{\sigma}_{\substack{xz \\ z=1}} + (I_3 + mc)(ik\Delta\hat{\sigma}_{\substack{zz \\ z=1}}) - (I_1 + mc)\Delta\hat{z}_b) \,, \qquad (4.6.52)$$

and the space domain solution is of (4.6.49) is therefore

$$\Delta u_{z=1}(x) = f(x) * ((I_1 + mc)\Delta\sigma_{\substack{xz \\ z=1}} + (I_3 + mc)(\partial \Delta\sigma_{\substack{zz \\ z=1}} / \partial x) - (I_1 + mc)\Delta z_b) \,. \qquad (4.6.53)$$

Equation (4.6.53) expresses the surface velocity perturbation $\Delta u_{z=1}$ as an exponentially weighted average of the perturbations $\Delta\sigma_{\substack{xz \\ z=1}}$, $(\partial \Delta\sigma_{\substack{zz \\ z=1}} / \partial x)$ and Δz_b. The length-scale of the weighted average is given by l_g which is defined by (4.6.48). Equation (4.6.53) is similar to expressions for the depth average of the longitudinal velocity in Kamb and Echelmeyer's (1986a) filter theory as will be discussed in a later subsection.

The length-scale l_g, given by (4.6.48), is a measure of the range of longitudinal stress gradients which are expressed by the term $(\partial^2 \tau_{xx} / \partial x \partial z)$ in (4.6.42). This term is related to the G term in theories based on integrated force balance equations as mentioned above, and therefore the subscript "g" is chosen for the length-scale. The length-scale l_g is almost equal to the longitudinal coupling length in Kamb and Echelmeyer's (1986a) filter theory as will be discussed in a later subsection. Equation (4.6.48) predicts that $l_g = O(|e|^{-(n-2)/(2n)})$ for small $|e|$ and $n > 2$. For $n = 3$ this order of magnitude estimate is $l_g = O(|e|^{-1/6})$. Thus, the length-scale l_g increases slowly as the longitudinal extension/compression $|e|$ in the datum flow is reduced, *i.e.* with increasing stiffness of

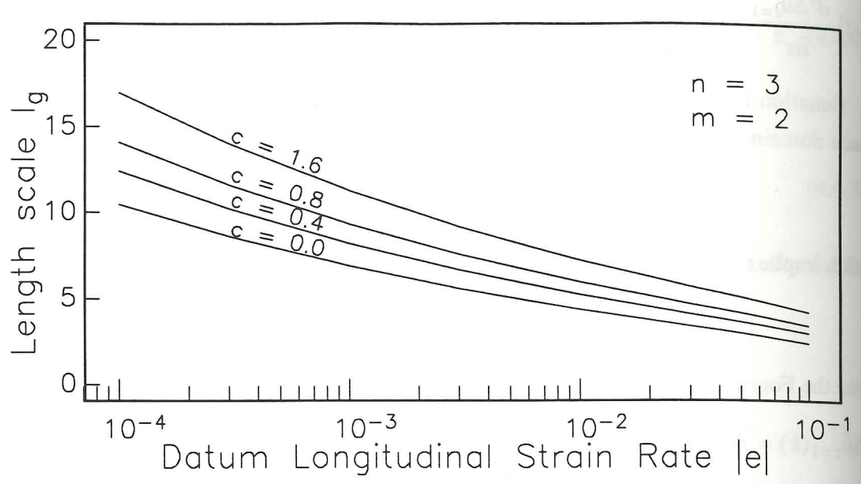

FIGURE 4.6.6: Length-scale l_g of longitudinal stress gradients given by (4.6.48) for $n = 3$ and $m = 2$ plotted as a function of datum longitudinal strain rate $|e|$ for a range of values of the basal sliding parameter c. The curve labeled "c = 0" gives l_g for no basal sliding. $c = 0.4$ corresponds to datum ice flow where the ice flux due to basal sliding is approximately equal to the ice flux due to internal deformation. The curves labeled "c = 0.8" and "c = 1.6" correspond to datum ice flow where the ice flux due to basal sliding is approximately two and four times the ice flux due to internal deformation.

the ice in the boundary layer near the ice surface. By (4.6.48), l_g also increases with increasing c, *i.e.* with increasing importance of basal sliding. l_g furthermore increases with increasing flow law and sliding law exponents n and m. For linear Newtonian rheology ($n = 1, m = 1$) (4.6.48) predicts $l_g = \sqrt{2(1+c)}$, which for no sliding ($c = 0$) becomes $l_g = \sqrt{2}$. Figure 4.6.6 shows l_g computed from (4.6.48) for $n = 3$ and $m = 2$ as a function of $|e|$ for a range of values of the basal sliding parameter c. The figure shows that l_g varies from approximately 4 to over 10 for $0.001 < |e| < 0.01$ and $0 < c < 1.6$.

Using the solution (4.6.53) of (4.6.49), the ice flux perturbation Δq, defined in (4.3.23), can be found by integration of (4.6.45). In order to simplify the result it is

advantageous to approximate the integral $\int_z^1 \eta_1 d\zeta$, for $0 < z < 1$, as $\int_z^1 \eta_1 d\zeta \approx \int_0^1 \eta_1 dz$ during the derivation of Δq from (4.6.45). This approximation arises because the most important contribution to the integral comes from the boundary layer near $z = 1$, so that the integral varies slowly with z below the boundary layer. The error associated with this approximation is small, but it results in considerable simplification in the expression for Δq. Using this approximation and integration by parts to reduce double integrals in z to the integrals defined in (4.6.47), Δq is found to be

$$\begin{aligned} \Delta q &= \int_0^1 \Delta u dz + u_0 \underset{z=1}{} \Delta z_s - u_0 \underset{z=0}{} \Delta z_b = \int_0^1 \Delta u dz + (I_2 + c)\Delta z_s - c\Delta z_b \\ &= (I_2 + c)\Delta z_s + G_e f^* \Delta\sigma_{xz} \underset{z=1}{} \\ &\quad + G_n f^* (\partial \Delta\sigma_{zz} \underset{z=1}{} / \partial x) + T_n (\partial \Delta\sigma_{zz} \underset{z=1}{} / \partial x) - G_b f^* \Delta z_b - T_b \Delta z_b \,, \end{aligned} \tag{4.6.54}$$

where the filter $f(x)$ is defined by (4.6.51) and the constants G_e, G_n, G_b, T_n and T_b are given by

$$\begin{aligned} G_e &= G_b = I_3 + mc \approx \frac{2n}{n+1} + mc \,, \\ G_n &= \frac{(I_3 + mc)^2}{I_1 + mc} \approx \frac{(2n/(n+1) + mc)^2}{2 + mc} \,, \\ T_n &= \frac{I_2(I_3 + mc)}{I_1 + mc} - I_4 \approx \frac{4(n/(n+1) + mc)}{(n+1)(n+2)(2+mc)} \,, \\ T_b &= I_2 + c = u_0 \underset{z=1}{} \approx \frac{2}{n+1} + c \,. \end{aligned} \tag{4.6.55}$$

As in (4.6.47) the approximate expressions on the far right of (4.6.55) are found by neglecting the effect of the boundary layer at the surface and the error is a few parts in 1000 for $|e| = 0.01$. The "G" and "T" notation of the constants in (4.6.54) and (4.6.55) refers to the G and T terms in theories based on integrated force balance equations. The reason for this notation will become clear below.

It is straightforward to interpret (4.6.54) in terms of the ice flux perturbation components Δq_e, Δq_n, Δq_a and Δq_b (*cf.* subsection 4.3.7), and ice flux filters $g_e(x)$, $g_n(x)$ and

$g_b(x)$ (*cf.* subsections 4.5.6, 4.6.4 and 4.6.7). The advection component $\Delta q_a = (I_2 + c)\Delta z_s$ predicted by (4.6.54), agrees exactly with advection component for non-linear rheology given by (4.6.40).

The flux perturbation components Δq_e, Δq_n and Δq_b, predicted by (4.6.54), are combinations of weighted longitudinal averages and local values of the perturbations $\Delta\sigma_{xz}{}_{z=1}$, $(\partial\Delta\sigma_{zz}{}_{z=1}/\partial x)$ and Δz_b. The weighted averages are computed using the filter $f(x)$, defined by (4.6.51). This means that the flux filters $g_e(x)$, $g_n(x)$ and $g_b(x)$, predicted by the simplified analysis, are given as a linear combination of the filter $f(x)$ and the delta function $\delta(x)$, *i.e.*

$$g_e(x) = G_e f(x)\,, \quad g_n(x) = G_n f(x) + T_n\delta(x)\,, \quad g_b(x) = G_b f(x) + T_b\delta(x)\,. \qquad (4.6.56)$$

Since $\int_{-\infty}^{\infty} f(x)dx = \int_{-\infty}^{\infty} \delta(x)dx = 1$, the areas of the filters given by (4.6.56) can be derived from (4.6.55) as

$$\int_{-\infty}^{\infty} g_e(x)dx = G_e = I_3 + mc\,, \quad \int_{-\infty}^{\infty} g_n(x)dx = G_n + T_n = I_5 + mc\,, \quad \int_{-\infty}^{\infty} g_b(x)dx = G_b + T_b = I_1 + mc\,.$$

The above expressions for the areas of the filters agree exactly with (4.6.39), which is derived from an analytical solution of the full field equations (4.6.14) in the wave number domain in the limit $k = 0$.

The above simplified analysis thus predicts the correct advection flux perturbation component, and flux filters with the correct areas, but a part of the areas of the predicted flux filters $g_n(x)$ and $g_b(x)$ is contained in delta spikes at $x = 0$. The reason for the delta spikes in $g_n(x)$ and $g_b(x)$, predicted by the simplified analysis, is the omission of the term $(\partial^2\sigma_{xz}/\partial x^2)$ from (4.6.42) and the omission of the term $(\partial\Delta w/\partial x)$ from the strain rate component $\dot{\varepsilon}_{xz}$. In the full flow equations, these terms lead to smoothing of the flow field on short longitudinal length-scales and the delta spikes are replaces by the relatively narrow peaks which are seen in the numerically computed flux filters determined from the full field equations (*cf.* Figs. 4.6.3, 4.6.4 and 4.6.5). The areas of the narrow peaks in $g_n(x)$ and $g_b(x)$, predicted by a solution of the full flow equations, turn out to be

accurately predicted by the constants T_n and T_b in the approximation (4.6.56) of $g_n(x)$ and $g_b(x)$. There is no narrow peak in $g_e(x)$, predicted by a solution of the full flow equations, and this is reflected by the absence of a delta function term in the expression for $g_e(x)$ in (4.6.56).

The numerical computations of the previous subsection suggest two *ad hoc* modifications of the flux filters given by (4.6.56). First, the numerical computations indicate that the width of the narrow peak in $g_n(x)$ and $g_b(x)$ is approximately equal to 2 ice thicknesses, independent of the parameters n, e, c and m. Since the areas of the narrow peaks in $g_n(x)$ and $g_b(x)$ are approximately given by T_n and T_b, respectively, replacing the delta functions in (4.6.56) by a suitable filter with unit area and a width between 1 and 2 ice thicknesses, should lead to much more realistic filters. Second, the filter $f(x)$ defined by (4.6.51) has a break in the slope at $x = 0$ which is not observed in the flux filters predicted by a solution of the full equations. This suggests replacing $f(x)$ by a new filter which is smooth at $x = 0$, but otherwise similar to $f(x)$.

Let the filter that replaces the delta function in (4.6.56) be denoted by $g_t(x)$ and the filter that replaces $f(x)$ by $g_g(x)$. The subscripts "g" and "t" refer to the G and T terms in theories based on integrated force balance equations. They are chosen because the filter $g_g(x)$ is primarily determined by longitudinal stress gradients represented by the term $(\partial^2\tau_{xx}/\partial x\partial z)$ in (4.6.42), which corresponds to the G term. The filter $g_t(x)$, on the other hand, represents the effect of the term $(\partial^2\sigma_{xz}/\partial x^2)$, which was omitted from (4.6.42), and corresponds to the T term. After some trial and error the filters $g_g(x)$ and $g_t(x)$ where defined by the following equations.

$$\hat{g}_g(k) = \frac{1}{1 + l_g^2\sinh^2 k}\,, \quad \hat{g}_t(k) = \frac{1}{\cosh(\pi l_t k/2)}\,, \qquad (4.6.57)$$

and

$$g_g(x) = \frac{1}{2\sqrt{l_g^2+1}}\,\frac{\sinh((\pi/2 - \sin^{-1}(1/l_g))|x|)}{\sinh(\pi|x|/2)}\,, \quad g_t(x) = \frac{1}{\pi l_t\cosh(x/l_t)}\,, \qquad (4.6.58)$$

where l_g is given by (4.6.48) and $l_t = 0.5$. These definitions were chosen because the filters lead to good approximations of the flux filters $g_e(x)$, $g_n(x)$ and $g_b(x)$ and because they have relatively simple analytical expressions in both the wave number and the space

domain. The expression for $\hat{g}_g(k)$ is a modification of the expression (4.6.50) for $\hat{f}(k)$ and guaranties smoothness of $g_g(x)$ at $x = 0$. The filter $g_t(x)$ has a shape that is close to the shape of the narrow peak of the numerically computed flux filters. It has the same form in both the wave number and the space domain. The filter $g_t(x)$ reaches the value e^{-1} at $x \approx 1.66 \cdot l_t = 0.83$. This value is an appropriate estimate the half width of $g_t(x)$.

The expression for $g_t(x)$ in (4.6.58) can be found in many tables of Fourier transforms. The expression for $g_g(x)$ in (4.6.58) can be derived by inverting $\hat{g}_g(k)$ given by (4.6.57) using (3.3.4a) and summing an infinite series of residues on the imaginary axis in the complex plane. The requirement $l_g > 1$ is necessary for the expression for $g_g(x)$ to be valid.

Replacing $f(x)$ and $\delta(x)$ in (4.6.56) by the filters for $g_g(x)$ and $g_t(x)$ leads to the following approximation of the flux filters $g_e(x)$, $g_n(x)$ and $g_b(x)$.

$$g_e(x) = G_e g_g(x)\,, \quad g_n(x) = G_n g_g(x) + T_n g_t(x)\,, \quad g_b(x) = G_b g_g(x) + T_b g_t(x)\,. \tag{4.6.59}$$

This approximation is shown as dashed curves in figures 4.5.1, 4.5.2, 4.6.2, 4.6.3, 4.6.4 and 4.6.5, both in the wave number and the space domain for linear Newtonian and non-linear rheologies. Figures 4.5.1 and 4.5.2 show that the approximate filters given by (4.6.59) are not unrealistic for linear Newtonian rheology. This is perhaps surprising because the boundary layer approximations, which were used in the simplified analysis, are not accurate for linear rheology. Figures 4.6.2, 4.6.3, 4.6.4 and 4.6.5 show that the approximate filters are considerably more accurate for non-linear rheology than for linear rheology, as was to be expected. The slow decay of the filters for $|x| \tilde{>} 1$–2 is well predicted by $g_g(x)$ and the length-scale l_g, derived from the simplified analysis. Similarly, the relative size of the narrow peaks in $g_n(x)$ and $g_b(x)$ is well predicted by the simplified analysis. It has been checked that the difference between the numerically computed filters for non-linear rheology and the approximate filters given by (4.6.59) is similar as indicated in these figures for the parameter ranges $0.0001 < e < 0.1$, $2 < n < 4$, $0 < c < 1.2$ and $1 < m < 3$, except that the narrow peak at $x = 0$ in the approximation of the filter $g_b(x)$ becomes slightly too low (10 - 20%) for the higher values of the sliding parameter c.

The simplified analysis makes it possible to interpret the numerical results of the previous subsection as follows.

1. The slow decay of the flux filters for $|x| \tilde{>} 1$–2 is caused by longitudinal stress gradients involving the stress component τ_{xx} (*i.e.* the G term) with a range $2l_g$ where l_g is given by (4.6.48). l_g is primarily determined by the datum longitudinal strain rate $|e|$ in the boundary layer near the ice surface. Variation in the length-scale of the decay of the flux filters with the parameters n, e, c and m is accurately predicted by variations in l_g computed from (4.6.48).
2. The narrow peaks in $g_n(x)$ and $g_b(x)$ are caused by longitudinal stress gradients involving the stress component σ_{xz} (*i.e.* the T term). The range of these stress gradients is approximately $2 \cdot 1.66 \cdot l_t = 1.66$ ice thicknesses independent of the parameters n, e, c and m. The reason for this behavior is that vertical shearing of the ice (the T term primarily represents longitudinal variation in shearing along vertical planes) is not sensitive to the relatively thin boundary layer of stiff ice near the surface, nor to sliding at the base. Variation in the relative importance of the narrow peaks with the parameters n, e, c and m is accurately predicted by the constants T_n and T_b given by (4.6.55).

The small difference between the approximate filters given by (4.6.59) and the numerically computed filters indicates that the approximate filters can be used without introducing significant error in studies of steady state ice surface undulations and for the formulation of ice flux in terms of glacier geometry in numerical ice flow models.

4.6.9 Length-scales for longitudinal flow variations

Based on the simplified analysis in the previous subsection, a number of length-scales for longitudinal flow variations may be identified. These scales can be defined in terms of the widths of the filters $g_g(x)$ and $g_t(x)$ defined by (4.6.58), or in terms of wavelengths or wave numbers of harmonic flow variations based on the Fourier transforms $\hat{g}_g(k)$ and $\hat{g}_g(k)$ given by (4.6.57).

Balise and Raymond (1985) and Balise (unpublished) analyzed the transfer of velocity variations at the base to the surface of a glacier assuming linear Newtonian rheology. They identified four longitudinal scales of differing behavior.

Long $\lambda > 10$. Basal velocity anomalies appear at the surface unattenuated.

Intermediate $5 < \lambda < 10$. Surface velocity has nearly the same spatial pattern as the velocity at the base, but the amplitude is reduced.

Short $1 < \lambda < 5$. Longitudinal velocity at the surface is reduced in amplitude and has the opposite direction as the longitudinal velocity at the base.

Very short $\lambda < 1$. Essentially no response at the surface.

The reversal in the direction of the velocity anomaly at the short scale is caused by recirculation in the perturbation ice flow.

Balise and Raymond's scales for linear Newtonian rheology can be interpreted in terms of the Fourier transforms $\hat{g}_g(k)$ and $\hat{g}_t(k)$ and applied to non-linear rheology by adjusting the boundary between the intermediate and the long scale. The boundary between the intermediate and the long scales can be identified as the wave number $k \approx 1/l_g$ where $\hat{g}_g(k)$ starts falling off. This is the length-scale where longitudinal stress gradients in the flow (*i.e.* the G term) become important. This transition takes place at longer wavelengths for non-linear rheology than for linear rheology because of the increased range of longitudinal stress gradients for non-linear rheology. The boundary between the intermediate and the short scales can be identified as the wave number $k \approx 1$–2 where $\hat{g}_t(k)$ starts falling off. This is the length-scale where longitudinal shear stress gradients in the flow (*i.e.* the T term) become important. This transition takes place at the same wavelength for non-linear and linear rheologies as discussed in the previous subsection. Finally, the boundary between the short and the very short scales can be identified as the wave number $k \approx (1\text{–}2)\pi$ where $\hat{g}_t(k)$ (and $\hat{g}_g(k)$) has become essentially zero. Flux variations caused by harmonic perturbations in $\Delta\sigma_{xz}\big|_{z=1}$, $(\partial\Delta\sigma_{zz}\big|_{z=1}/\partial x)$ and Δz_b may therefore be interpreted in terms of the four longitudinal scales defined by Balise and Raymond for transfer of velocity anomalies from the base to the surface. In terms of flux perturbations the definition of the longitudinal scales is as follows.

Long $k < 1/l_g$, $\lambda > 2\pi l_g$. Flux perturbations are well predicted by the laminar flow approximation, *i.e.* they are determined by local ice thickness and local surface slope.

Intermediate $1/l_g < k < 1\text{–}2$, $(1\text{–}2)\pi < \lambda < 2\pi l_g$. Longitudinal stress gradients dominate the flow and lead to damping of flux perturbations compared to the flux predicted by the laminar flow approximation.

Short $1\text{–}2 < k < (1\text{–}2)\pi$, $1\text{–}2 < \lambda < (1\text{–}2)\pi$. The perturbation flow field is dominated by recirculation which extends through the thickness of the ice. The flux perturbation Δq_b is significant, but Δq_n and especially Δq_e are small.

Very short $k > (1\text{–}2)\pi$, $\lambda < 1\text{–}2$. Essentially no flux variations. Recirculation in the perturbation flow is limited to thin layers close to the surface and the base.

It has some advantages to view the above classification in the space domain. Flux variations determined from (4.6.22) and (4.6.59) are a linear combination of weighted longitudinal averages of the perturbations $\Delta\sigma_{xz}\big|_{z=1}$, $(\partial\Delta\sigma_{zz}\big|_{z=1}/\partial x)$ and Δz_b using the filters $g_g(x)$ and $g_t(x)$. The widths of $g_g(x)$ and $g_t(x)$ in the space domain are approximately $2l_g$ and 1.66 ice thicknesses, respectively. If the length-scale of a perturbation is much longer than a filter which is used for computing a weighted average, then the weighted average is essentially equal to the local value of the perturbation. This leads to the following classification of scales for longitudinal flow variations.

Long length-scale $> 2l_g$. Weighted averages computed using both $g_t(x)$ and $g_g(x)$ are approximately equal to the corresponding local values. Flux perturbations are well predicted by the laminar flow approximation.

Intermediate $1.66 <$ length-scale $< 2l_g$. Weighted averages computed using $g_t(x)$ are approximately equal to the corresponding local values, but averages computed using $g_g(x)$ are damped by longitudinal stress gradients.

Short length-scale < 1.66. Weighted averages computed using $g_t(x)$ are damped by longitudinal shear stress gradients, but averages computed using $g_g(x)$ are essentially equal to zero. Δq_b is the only significant flux perturbation.

Very short length-scale $\ll 1.66$. Weighted averages computed using both $g_t(x)$ and $g_g(x)$ are essentially equal to zero and consequently there are no flux variations.

Finally, a very long scale may be defined from l_1 given by (4.4.4). Very long flux variations on a length-scale longer than l_1 are determined by local thickness perturbations

only. The laminar flow approximation predicts perfect transfer of bedrock undulations to the surface (*cf.* (4.4.8)) on the very long scale.

The above classification of length-scales may be used to clarify the distinction between the datum long scale flow (*cf.* section 4.2) and the short scale flow (*cf.* section 4.3). The datum long scale solution given in subsections 4.2.5 and 4.3.4 is essentially equivalent to the laminar flow solution. From the above discussion, the datum long scale solution and the short scale solution are equivalent on length-scales longer that $2l_g$. The datum long scale solution will therefore be valid if longitudinal variations in the datum geometry are on length-scales longer that $2l_g$. If this condition is fulfilled then longitudinal gradients in the viscosity components η_1, η_2 and η_3 will also be small which is a condition for the validity of the short scale analysis (*cf.* subsection 4.6.3). There is of course no unique way to define a datum geometry that satisfies this condition. However, different possibilities will differ on length-scales longer that $2l_g$ only, where there is no difference between the long scale and the short scale solutions. The total flux, which is computed by adding the datum long scale flux and the flux perturbation found by the short scale analysis, will therefore be the same. In extreme circumstances (*e.g.* close to ice falls) the definition of a slowly varying datum geometry will lead to so large perturbations in the geometry that the short scale analysis breaks down. In such circumstances, the full non-linear flow equations must be solved and the theory developed in this dissertation does not apply.

4.6.10 Total flux

In some applications (*e.g.* in the specification of ice flux in terms of glacier geometry in numerical ice flow models) an expression for the total ice flux is needed rather than an expression for the flux perturbations Δq_e, Δq_n, Δq_a and Δq_b. It is possible to use the approximate theory of the previous subsection to compute the total flux directly from weighted longitudinal averages of the geometry of the glacier. This is convenient since the computation of perturbations in the geometry, using an explicitly defined datum geometry and an associated datum ice flow, can then be omitted. The total flux computation is based on the following assumptions and approximations.

1. A datum geometry $z_{s\,0}$ and $z_{b\,0}$ can be defined which varies so slowly in x that longitudinal averages computed with the filters $g_g(x)$ and $g_t(x)$, given by (4.6.58), can be replaced with local values. This datum geometry does not need to be explicitly defined.
2. The flux filters $g_e(x)$, $g_n(x)$ and $g_b(x)$ can be approximated by the flux filters given by (4.6.59).
3. The constants G_e, G_n, G_b, T_n and T_b in (4.6.59) can be replaced by the approximate expressions on the far right of (4.6.55).
4. The term $2(\partial\Delta z_s/\partial x)\,|e|^{1/n}\mathrm{sign}(e)$ in the definition (4.6.15) of $\Delta\sigma_{xz\,z=1}$ can be omitted. The ratio of the flux perturbation associated with this term relative to Δq_n, which is also proportional to $(\partial\Delta z_s/\partial x)$, is $O(|e|^{1/n}\tan(\alpha_0))$. This ratio is very small for the low slopes which are observed on ice caps and glaciers.
5. The surface slope α, $\sin\alpha$ and $\tan\alpha$ can all be approximated by $\alpha_0 - (\partial z_s/\partial x)$. In a coordinate system with a vertical z-axis α may be approximated by $(-\partial z_s/\partial x)$.

Define the following weighted longitudinal averages of the surface and bedrock geometry.

$$\begin{aligned} <z_s> &= (G_e g_g * z_s + u_{0\,z=1}\, z_s)/(G_e + u_{0\,z=1}), \\ <z_b> &= (G_b g_g * z_b + T_b g_t * z_b)/(G_b + T_b), \\ <h> &= <z_s> - <z_b>, \end{aligned} \tag{4.6.60}$$

$$<\alpha> = \gamma - (G_n g'_d * z_s + T_n g'_t * z_s)/(G_n + T_n), \tag{4.6.61}$$

where $\gamma = \alpha_0$, is the angle that the z-axis makes with the vertical at $x = 0$, the filters $g_g(x)$ and $g_t(x)$ are given by (4.6.58), and the constants G_e, G_n, G_b, T_n and T_b are given by (4.6.55). The definition of $<\alpha>$ uses longitudinal derivatives of the filters $g_g(x)$ and $g_t(x)$ (denoted by the prime mark) to compute a longitudinal average of $(-\partial z_s/\partial x)$, using the mathematical relation $f(x)*g'(x) = f'(x)*g(x)$, which follows from the properties of the convolution operation. This avoids the explicit computation of point values of the surface slope, which are often difficult to compute for real data because of noise. Note that $G_b = G_e$ and $T_b = u_{0\,z=1}$.

Equations (4.6.60) and (4.6.61) automatically lead to smoothing of noise which is always present in real data. This smoothing is a consequence of the dynamics of the ice flow, which is a considerable advantage over other methods for handling noise in the data.

Using (4.6.60) and (4.6.61) the total ice flux $q = q_0 + \Delta q$ may, for any valid choice of the datum long scale geometry, be computed by the equation

$$q = \frac{2}{(n+2)} <\alpha>^n <h>^{n+2} + c <\alpha>^m <h>^{m+1} \qquad (4.6.62)$$

to first order in the perturbations. This equation follows from (4.3.20), (4.3.27), (4.6.20), (4.6.22), (4.6.55), (4.6.58) and (4.6.59), using the assumptions and approximations listed above. It has the same form as (3.7.3), which gives the ice flux predicted by the laminar flow approximation, with the modification that the local ice thickness and surface slope in (3.7.3) are replaced by the longitudinal weighted averages defined in (4.6.60) and (4.6.61).

Equation (4.6.62) still depends on the datum geometry in the sense that it is expressed in the non-dimensional short scale coordinate system (*cf.* subsection 4.3.2), which is aligned parallel to the surface at one particular point on the datum surface profile where the datum ice thickness is put equal to 1. An estimate of the datum ice thickness is therefore required to establish a unit of length for the x- and z- coordinates. The datum surface slope α_0, at $x = 0$, also enters in the definition of $<\alpha>$ through the term γ. Furthermore, the non-dimensional parameters e and c (*cf.* subsection 4.3.2 and 4.3.4), which are required for the determination of the flux filters, depend on the datum ice thickness and datum surface slope. However, the validity of equation (4.6.62) is not restricted to this coordinate system. It may be shown that (4.6.62) is also valid in a general coordinate system where the z-axis makes any small angle $\gamma \ll 1$, with the vertical. In particular, it is valid in a coordinate system with a horizontal x-axis and a vertical z-axis, where $\gamma = 0$. The datum ice thickness and surface slope in such a coordinate system will vary along the x-direction. Therefore, the short scale non-dimensionalization, which is described in subsection 4.3.2, must be modified to use appropriate scales for the ice thickness and surface slope instead of $\tilde{h}_0$ and $\sin\alpha_0$. An explicit specification of the datum geometry is still needed for using (4.6.62) because it requires that at each point x, where q is to be

computed, the correct datum ice thickness at x must be used as the unit of length for the computation of the weighted longitudinal averages defined in (4.6.60) and (4.6.61). Also, correct non-dimensional values of e and c at x must be used for the definition of the flux filters. A relatively crude approximation of the datum ice thickness is sufficiently accurate for these computations ($g_g * (z_s - z_b)$ is good enough). Furthermore, e and c are only known as rough estimates in practice and they can just as well be estimated directly rather that starting from rough estimates of the corresponding dimensional physical parameters. This means that (4.6.60), (4.6.61) and (4.6.62) can be used together with a crude estimate of the datum ice thickness and estimates of the non-dimensional parameters e and c, to compute q at any point x.

Equation (4.6.62) incorporates the effect of longitudinal stress gradients (*i.e.* the G term) and longitudinal shear stress gradients (*i.e.* the T term) on the ice flux to a first approximation. It can for example be used for the specification of ice flux in terms of glacier geometry in numerical ice flow models. It is a substantial improvement over flux expressions based on local or arbitrarily averaged ice thickness and surface slope which are often used in such models (*e.g.* Budd and Jenssen, 1975; Bindschadler, 1982; Waddington, unpublished; Bindschadler's model uses a longitudinal average of the surface slope, but this average is not theoretically derived).

It was mentioned previously (*cf.* subsection 4.2.6) that surface slope variations on ice caps and glaciers are often equal to or larger than the long scale average slope. A useful theory of longitudinal ice flow variations must be able to handle such variations in the surface slope. Equations (4.6.60), (4.6.61) and (4.6.62) lead to a criterion for the validity of the theory of flux variations which has been developed in the previous subsections. Assuming that a long scale datum geometry has been explicitly defined, the longitudinal average of the surface slope defined in (4.6.61) may be rewritten as $<\alpha> = \gamma + (-\partial z_s/\partial x)_0 + <\Delta\alpha>$, where $<\Delta\alpha> = -(G_n g'_d * \Delta z_s + T_n g'_t * \Delta z_s)/(G_n + T_n)$. In order for (4.6.62) to be valid, the weighted *longitudinal average* $<\Delta\alpha>$ of the slope perturbation $(\partial \Delta z_s/\partial x)$ must be small compared to the datum surface slope $\gamma + (-\partial z_s/\partial x)_0$. If this requirement is not satisfied, then velocity and flux perturbations will not be small compared to the datum ice flow solution and the theory is invalid. Furthermore, the non-

dimensional perturbations Δz_s, and Δz_b, and their derivatives with respect to x, must be small compared to 1. However, neither the surface nor the bedrock slope perturbations $(-\partial \Delta z_s/\partial x)$ and $(-\partial \Delta z_b/\partial x)$, need to be small compared to the datum surface slope $\gamma + (-\partial z_s/\partial x)$. This means that the above theory of flux variations can be valid for large variations in the surface slope compared to the datum surface slope $\gamma + (-\partial z_s/\partial x)$, if the length-scale of the surface undulations is so short that the longitudinal average $<\Delta\alpha>$ is small compared to $\gamma + (-\partial z_s/\partial x)$.

4.6.11 Relation to previous work

As previously mentioned, the theory which has been developed in the previous subsections, is partly based on the boundary layer theory of Johnson and McMeeking (1984) and on Hutter's (1983) mathematical and numerical formulation of two-dimensional glacier flow. Equations (4.2.20) and (4.3.19), which were used for the computation of the viscosity components η_1, η_2 and η_3, are essentially equivalent to corresponding equations in Johnson and McMeeking's (1984) boundary layer analysis and Nye's (1957) analysis of the distribution of stress in glaciers. Similar equations have also been used by Dahl-Jensen (1985) and by Kamb and Echelmeyer (1986a) in order to take the effect of longitudinal stress gradients on glacier flow into account. With the exception of Kamb and Echelmeyer's theory, the results of the abovementioned authors cannot be directly compared to the flux filters obtained above.

Kamb and Echelmeyer's filter theory (*cf.* section 2.6) is derived from a differential equation for the depth average $\bar{u}$ of the longitudinal velocity. This equation is formally similar to (4.6.49) for the velocity perturbation $\Delta u_{z=1}$ at the datum ice surface, when $\Delta\sigma_{xz\,z=1}$ and $(\partial\Delta\sigma_{zz\,z=1}/\partial x)$ are expressed in terms of Δz_s. The solution of their equation (*cf.* (2.6.3), (2.6.4) and (2.6.5)) is formally similar to the solution (4.6.53) of (4.6.49), and the filter lengths given by (2.6.5) and (4.6.48) close to each other although they are not exactly equal. The reason that $\Delta u_{z=1}$ appears in the above simplified theory, rather than $\bar{u}$ as in Kamb and Echelmeyer's theory, is that the stiff ice in the boundary layer near the ice surface makes the surface velocity much more important for the determination of longitudinal stress gradients than the velocity at depth.

The main difference between Kamb and Echelmeyer's theory and the theory developed here, is that their theory makes no distinction between the effect of perturbations in the surface geometry, on one hand, and perturbations in the bedrock geometry, on the other, on the ice flux. The effect of both perturbations is represented by their effect on the ice thickness. Therefore, local values of both Δz_s and Δz_b affect the ice flux perturbation predicted by Kamb and Echelmeyer's theory. This is in contrast to the filter theory developed here, which predicts an advection term $\Delta q_a = u_{0\,z=1}\,\Delta z_s$, involving the local value of Δz_s, but Δz_b is predicted to affect the flux through the filter $g_b(x)$ only. Kamb and Echelmeyer's theory is almost, but not exactly, equivalent to replacing the narrow peak in $g_b(x)$ at $x = 0$ (*cf.* Figs. 4.6.3, 4.6.4 and 4.6.5) by a delta function. This is not unexpected since the narrow peak may be viewed as a consequence of the T term, which is ignored in Kamb and Echelmeyer's theory, but included in the theory developed here. This difference turns out to be essential for the analysis of steady state ice surface undulations, but it is much less important for the computation of longitudinal variations in the velocity of glaciers which was the primary purpose of Kamb and Echelmeyer's theory.

4.7 NON-LINEAR FLOW — PERTURBATIONS IN THE STEADY STATE SURFACE GEOMETRY

4.7.1 General

The steady state ice surface geometry Δz_s, corresponding to specified bedrock undulations Δz_b, is determined by the steady state equation (4.3.30) using the advective flux component Δq_a given by (4.6.20) or (4.6.40) and the flux filters $g_e(x)$, $g_n(x)$ and $g_b(x)$ defined by (4.6.22) and determined numerically as described in subsection 4.6.5. In the space domain the equation determining Δz_s is

$$g_e*(\Delta z_s + 2(\partial\Delta z_s/\partial x)\,|e|^{1/n}\mathrm{sign}(e)) + g_n*(-\partial\Delta z_s/\partial x)\cot\alpha_0 + u_{0\,z=1}\,\Delta z_s - g_b*\Delta z_b = 0\,, \quad (4.7.1)$$

where $u_{0\,z=1} = \hat{g}_b(k=0) - \hat{g}_e(k=0)$ by (4.6.40).

The wave number representation of this equation is

$$(\hat{g}_e(k) + \hat{g}_b(0) - \hat{g}_e(0) - ik(\hat{g}_n(k)\cot\alpha_0 - 2|e|^{1/n}\text{sign}(e)\hat{g}_e(k)))\Delta\hat{z}_s = \hat{g}_b(k)\Delta\hat{z}_b \ . \quad (4.7.2)$$

The term $2|e|^{1/n}\text{sign}(e)\hat{g}_e(k)$, which arises from non-zero τ_{xx} at the datum ice surface, is much smaller than $\hat{g}_n(k)\cot\alpha_0$. The effect of this term is hardly noticeable on plots of Δz_s and it will therefore be neglected for simplicity in the following. With this modification, equation (4.7.2) can be written

$$(\hat{g}_e(k) + \hat{g}_b(0) - \hat{g}_e(0) - ik\hat{g}_n(k)\cot\alpha_0)\Delta\hat{z}_s = \hat{g}_b(k)\Delta\hat{z}_b \ . \quad (4.7.3)$$

Equation (4.7.3) is formally almost identical to (4.5.22) for linear Newtonian rheology and it determines a transfer function $t(k)$ (*cf.* subsection 3.3.3) for the steady state transfer of bedrock undulations to the ice surface, *i.e.* $\Delta\hat{z}_s = t(k)\Delta\hat{z}_b$. Just as for linear Newtonian rheology, the transfer function may be inverted using (3.3.4a) to yield the Green's function $g(x)$ (*cf.* subsection 3.3.4), such that $\Delta z_s = g(x)*\Delta z_b$ satisfies (4.7.1).

In the limit of asymptotically long waves (*i.e.* when $k\to 0$, $\lambda\to\infty$), equations (4.7.2) and (4.7.3) predict that $\lim_{k\to 0} t(k) = 1$ as expected from the discussion in subsection 4.4.4 on the laminar flow approximation.

Equation (4.7.3) shows that flux filters, which have been computed numerically for certain values of the parameters n, e, c and m, can be used to compute transfer functions and Green's functions for many different values of the long scale surface slope α_0. In dimensional variables, the non-dimensional parameter e represents the ratio of datum longitudinal strain rate at the ice surface to the datum shear strain rate at the bed, while the non-dimensional parameter c represents the relative importance of basal sliding in the datum flow (the ratio of sliding flux to deformation flux in the datum flow $r_0 = q_s/q_d$, is given by $r_0 = c(n+2)/2$). The non-dimensional perturbations Δz_b and Δz_s represent the size of perturbations in the geometry of the glacier relative to the ice thickness. Thus, the above theory of the formation of short and intermediate scale glacier landscape is formulated in terms of *relative* perturbations with respect to the datum ice flow and it does not depend on (very uncertain) absolute values of the dimensional rheological and sliding parameters A and C (*cf.* subsections 3.4.3 and 3.5.4). It only depends on the datum surface slope α_0, the flow law and sliding law powers n and m, and on the *relative*

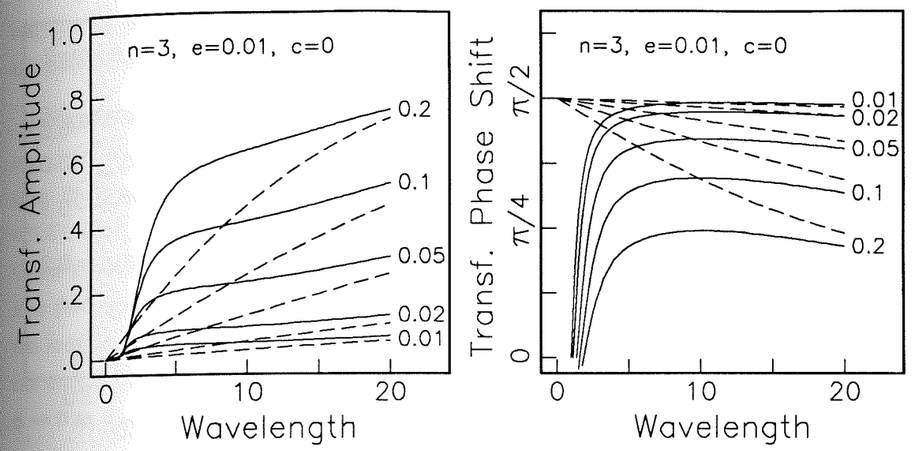

FIGURE 4.7.1: The transfer amplitude $|t|$ (left) and phase shift ϕ (right) for the transfer of bedrock undulations to the ice surface predicted for non-linear rheology with $n = 3$ and $e = 0.01$ for no basal sliding ($c = 0$) (solid curves). The transfer is shown for a range of long scale surface slopes $\tan\alpha_0$. $|t|$ and ϕ are plotted as functions of dimensionless wavelength $\lambda = 2\pi/k$. Dashed curves are the corresponding transfer amplitude and phase shift predicted by the laminar flow approximation (4.4.7). The curves are labeled with $\tan\alpha_0$.

importance of certain features in the datum ice flow, *i.e* longitudinal strain rate at the ice surface and basal sliding. This is quite different from theories of the long scale shape of ice caps and glaciers, as discussed in the introduction (section 1.1).

4.7.2 Transfer functions

Figure 4.7.1 shows the transfer amplitude (left) and phase shift (right) predicted for non-linear rheology with $n = 3$ and $e = 0.01$ for no basal sliding ($c = 0$) (solid curves). The figure also shows the transfer amplitude and phase shift predicted by the laminar flow approximation (4.4.7) (dashed curves) for comparison. The curves have qualitatively the same shape as the transfer function curves shown in Figure 4.5.3 for linear Newtonian rheology, but the increased transfer amplitude with respect to the laminar

amplitude at a wavelength approximately equal to 2 ice thicknesses is that $\hat{g}_b(k)$ decays abruptly to zero for wave numbers corresponding to wavelengths below 2 ice thicknesses.

4.7.3 Green's functions

The relatively complicated transfer functions which are shown in Figures 4.7.1 and 4.7.2 correspond to considerably simpler Green's functions in the space domain, as was found before for the laminar flow approximation and for linear Newtonian rheology. Therefore, the formation of steady state glacier landscape for non-linear rheology will be primarily discussed in terms of Green's functions in the following.

The Green's function $g(x)$ for the formation of steady state landscape is found by inverting $\hat{g}(k) = t(k)$ given by (4.7.3). The Green's function describes the ice surface geometry corresponding to a sharp spike in the bedrock geometry. Since $t(k=0) = 1$, the area under the Green's function is equal to 1. Consequently, the total volume of ice in the surface perturbations is equal to the total volume of the bedrock perturbations.

Figure 4.7.3 compares the Green's function predicted by non-linear rheology with $n = 3$ and $e = 0.01$ for no basal sliding ($c = 0$) with the one-sided exponential Green's function predicted by the laminar flow approximation (4.4.9) and shown in Figure 4.4.2. The figure shows a scaled Green's function as a function of scaled distance as described in the discussion of Figure 4.5.5 in subsection 4.5.9 on linear Newtonian rheology. The Green's functions for non-linear rheology are similar in shape to the one-sided exponential Green's function predicted by the laminar flow approximation, except for a "standing wave" near $x = 0$. The wavelength of the standing wave is approximately the same as for linear rheology (*cf.* Fig. 4.5.5), but its amplitude is much higher. For $|x| \tilde{>} 2$–3 ice thicknesses, there is little difference between the Green's function predicted by non-linear rheology and the exponential Green's function predicted by the laminar flow approximation.

The long exponential tail of the Green's functions shown in Figure 4.7.3 is problematic for the application of the Green's functions to real data, especially for low values of the datum slope $\tan\alpha_0$. The tail decays to zero on the length-scale l_1 defined by (4.4.4), which is proportional to $\cot\alpha_0 = 1/(\tan\alpha_0)$. For $n = 3$, $\tan\alpha_0 = 0.01$ and no basal

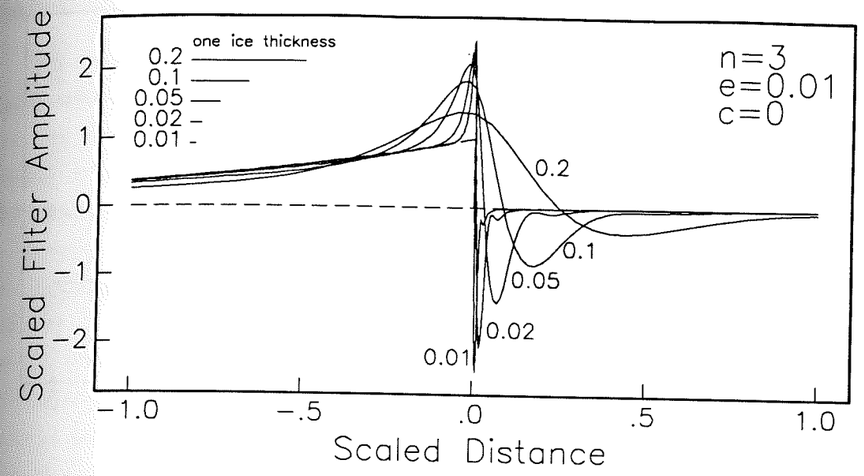

FIGURE 4.7.3: Green's functions predicted by non-linear rheology with $n = 3$ and $e = 0.01$ for no basal sliding ($c = 0$) (solid curves) compared to the one-sided exponential Green's function predicted by the laminar flow approximation with $n = 3$ (4.4.9) (barely visible dashed curve). The curves are scaled both horizontally and vertically and labeled with $\tan\alpha_0$. Length-scales corresponding to one ice thickness for each value of $\tan\alpha_0$ are shown in the upper left corner (for explanation, see text).

sliding the length-scale l_1 is given by (4.4.4) is $l_1 = 60$ ice thicknesses. The Green's function $g(x)$ is derived on the assumption that deviations in the datum surface and bedrock geometry from a parallel slab geometry are negligible (*cf.* subsection 4.3.6). This is unlikely to be true over the length-scale l_1 for low values of $\tan\alpha_0$. The Green's functions can be used for real data for relatively high datum slopes (*i.e.* for $\tan\alpha_0 \tilde{>} 0.05$). For lower slopes, problems arising from the long tail in the Green's functions can be partly overcome by working with *slope filters* (see below) instead of the Green's functions shown in Figure 4.7.3. The slope filters have a relatively small amplitude outside the standing wave at $x = 0$ (*i.e.* for $|x| \tilde{>} 2$–3). In spite of practical problems arising from the long tail of the Green's functions derived from (4.7.3) for low

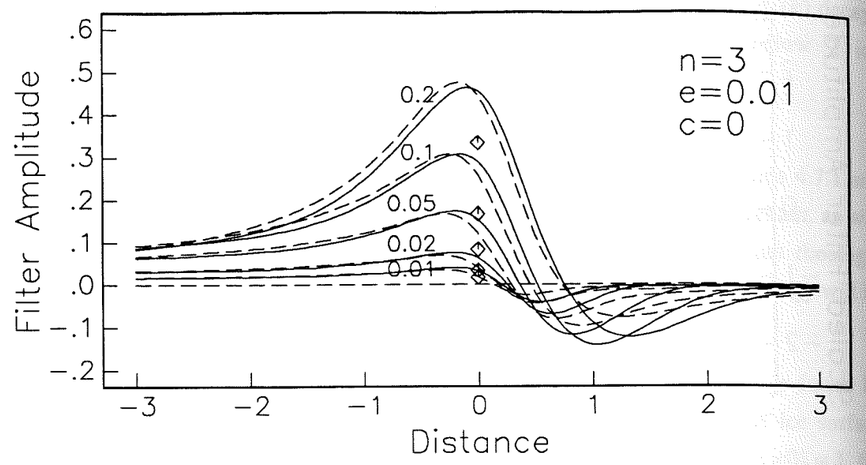

FIGURE 4.7.4: Green's functions predicted by non-linear rheology with $n = 3$ *and* $e = 0.01$ *for no basal sliding* ($c = 0$) *(solid curves). The Green's functions predicted by the laminar flow approximation are indicated by diamond symbols which are plotted where the tops of the one-side exponentials would be located. The curves are labeled with* $\tan\alpha_0$. *Dashed curves show Green's functions predicted by flux filters derived from the simplified analysis described in subsection 4.6.8.*

datum slopes, the Green's functions provide theoretical understanding of the formation of steady state surface undulations on ice caps and glaciers.

Figure 4.7.4 displays the central part of the Green's functions shown in Figure 4.7.3. The laminar flow Green's functions are indicated by diamond symbols which are plotted where the tops of the one-side exponentials (4.4.9) would be located. The exponentials themselves are not shown. The standing wave, which was observed in Figure 4.7.3, has essentially the same shape as for linear Newtonian rheology. (*cf.* Fig. 4.5.6). The distance between the peak on the upstream side of the basal spike and the trough on the downstream side is between 0.75 and 1.4 ice thicknesses for the range $0.01 \leq \tan\alpha_0 \leq 0.2$. The corresponding distance for linear rheology with no sliding is 1 - 1.5 ice thicknesses (*cf.* Figs. 4.5.5 and 4.5.6). The distance between the peak and the trough for non-linear

rheology corresponds to approximate wavelengths in the range 1.5 - 3 ice thicknesses.

The amplitude of the standing wave is much higher for non-linear rheology than for linear rheology. The reason for this behavior is the increased transfer amplitude for wavelengths between 2 and 10-20 ice thicknesses for non-linear rheology which was discussed in the previous subsection. For linear rheology and no basal sliding, the difference in height between the peak and the trough of the standing wave for $\tan\alpha_0 \leq 0.1$ is between 1.2 and 1.7 times the height of the exponential Green's function predicted by the laminar flow approximation (*cf.* Figs. 4.5.5 and 4.5.6). The corresponding ratio is between 2.7 and 4.8 for non-linear rheology (*cf.* Figs. 4.7.3 and 4.7.4). The relative height of the standing wave, compared to the height of exponential Green's function predicted by the laminar flow approximation, becomes still higher for $\tan\alpha_0 < 0.01$ (not shown) and for non-zero basal sliding (see below). It thus appears that the increased transfer amplitude in the wave number domain for wavelengths between 2 and 10-20 ice thicknesses (*cf.* Figs. 4.7.1 and 4.7.2) primarily results in a higher amplitude of the standing wave compared to linear rheology. The wavelength of the standing wave is not increased even though the increased transfer in the wave number domain extends to longer wavelengths than for linear rheology.

It follows from the above estimates of the height of the standing wave, that slope changes predicted by non-linear rheology for relatively narrow basal mountains are much higher (*i.e.* by a factor on the order of 3-5 for $0.01 < \tan\alpha_0 < 0.1$) than slope changes predicted by the laminar flow approximation. The laminar flow approximation predicts lower slope changes for non-linear rheology than for linear rheology. This arises because the one-sided exponential Green's function predicted from laminar flow is longer and lower for non-linear rheology than for linear rheology. The increased height of the standing wave for non-linear rheology counteracts this tendency of the laminar flow approximation and results in larger slope changes for non-linear rheology than for linear rheology (see below).

It was mentioned in section 2.2 that slope changes predicted by the laminar flow approximation turned out to be much too low along a flow line to the south of Camp Century on the Greenland ice sheet (Robin, 1967). The above results, which are derived for temperate ice, cannot be directly applied to cold ice sheets. One may expect the stiff cold

ice near the surface and the low surface slopes of cold ice sheets to increase the amplitude of the standing wave significantly compared to temperate ice caps. For cold ice sheets with $\tan\alpha_0 < 0.01$, it is therefore likely that the standing wave would lead to slope changes an order of magnitude or more greater that the slope changes predicted by the laminar flow approximation. This is not inconsistent with the data from the Camp Century flow line. Furthermore, the shape of the surface undulations above sharp basal peaks on the Camp Century flow line (at distances approximately equal to 27 *km* and 35 *km* in Robin's (1967) Figure 2) is reasonably predicted by the shape of the standing wave. This is in spite of the fact that the theory developed here places no special emphasis on reversals in the sign of the longitudinal strain rate. Such reversals are discussed by Robin (1967) and he argues that they are important for the formation of surface undulations. This is apparently not the case, which is fortunate because a theory that takes sign reversal in the longitudinal strain rate into account would be much more complicated than the theory developed here.

In the case of purely two-dimensional flow, reversals in the sign of the longitudinal strain rate lead to infinite viscosity at the ice surface at points where the longitudinal strain rate goes through zero. In the neighbourhood of such points, the stiffness of the ice near the ice surface will be determined by the perturbation ice flow rather than by the datum flow and therefore a theory based on a linearization of the non-linear ice flow equations with respect to the datum flow is invalid. As discussed in subsection 4.3.5, all real glacier flow is to some extent three-dimensional. Therefore, one may expect some contribution from the strain rate components τ_{yy} and τ_{xy}, to the ice viscosity where the longitudinal strain rate goes through zero and a singularity in the viscosity distribution is thereby prevented. Nevertheless, the perturbation ice flow may lead to a significant non-linear softening of the ice near the ice surface in areas where the longitudinal strain rate is relatively low compared to the strain rates introduced by the perturbation ice flow. Although this question has not been analyzed in detail, it seems likely that the effect of such softening on the formation of ice surface undulations will be qualitatively the same as specifying an "effective" longitudinal strain rate, somewhat larger than the measured or estimated datum longitudinal strain rate, in the linearized theory which is presented here. It is shown in the next subsection that the linearized theory is not sensitive to the exact

value of the datum longitudinal strain rate. Therefore, the formation of ice surface undulations in areas of relatively low datum longitudinal strain rate should be qualitatively similar to the prediction of the linearized theory for areas where the datum longitudinal strain rate determines the stiffness of the ice near the ice surface.

Dashed curves in Figure 4.7.4 show Green's functions predicted by flux filters derived from the simplified analysis which is described in subsection 4.6.8. The amplitude of the standing wave predicted by the simplified theory is slightly reduced and it is shifted a short distance in the upstream direction. This difference indicates the relative importance of the viscosity component η_3 and the resulting asymmetry in the flux filters (*cf.* subsection 4.6.7), for the formation of surface undulations. The Green's functions predicted by the simplified analysis become more accurate for lower values of e (not shown), but the accuracy becomes worse for non-zero basal sliding (not shown), where the amplitude of the standing wave may be significantly underestimated.

Figure 4.7.5 shows the steady state ice surface geometry Δz_s corresponding to a smooth basal mountain described by a Gaussian bell function (4.5.26) for non-linear rheology (*cf.* Fig. 4.5.8 for linear rheology). The basal mountain has a unit area and an approximate width equal to 2σ. The curves in the figure are drawn for no basal sliding and $\tan\alpha_0 = 0.05$. For basal mountains wider than approximately 2-4 ice thicknesses there is almost no noticeable effect from the standing wave in the Green's function (*cf.* Figs. 4.7.3 and 4.7.4). The standing wave appears abruptly as a surface feature when the width of the basal mountain is reduced below approximately 2-4 ice thicknesses. This implies that the laminar flow approximation will predict realistic steady state ice surface undulations Δz_s if the length-scale of the bedrock undulations Δz_b is longer than 2-4 ice thicknesses. This was previously found to be the case for linear Newtonian rheology (*cf.* subsection 4.5.9 and Figs. 4.5.8 and 4.5.9). Figure 4.7.5 also shows that the wavelength of the standing wave associated with a basal mountain of finite width, is slightly longer than the wavelength of the standing wave in the Green's function.

The standing wave in the Green's function for non-linear rheology explains observations of dominant ice surface features with wavelengths in the range 3 - 4 ice thicknesses, which were discussed in Chapter 2. The standing wave in the Green's function has approximate wavelength in the range 1.5 - 3 ice thicknesses. This wavelength range for

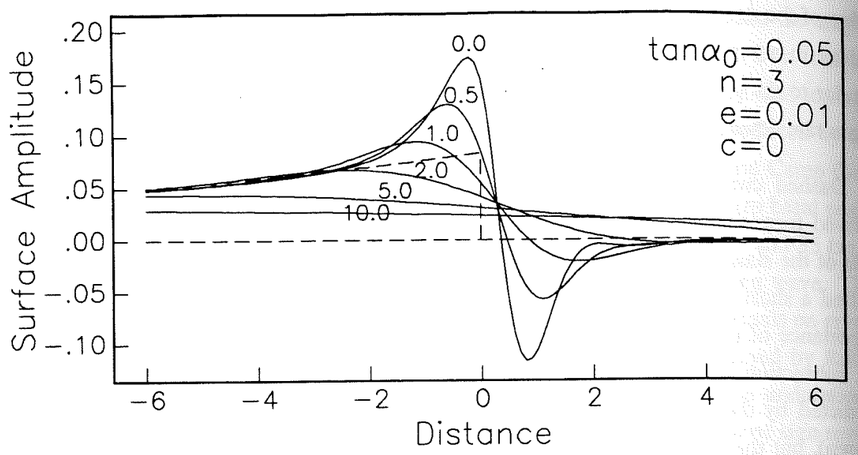

FIGURE 4.7.5: Steady state ice surface geometry predicted by non-linear rheology with $n = 3$ and $e = 0.01$ for no basal sliding ($c = 0$) for a basal mountain given by (4.5.26) for a range of half widths σ (solid curves). The long scale surface slope is $\tan\alpha_0 = 0.05$. The curves are labeled with the values of σ. The curve labeled with "0.0" is the Green's function corresponding to a basal spike. Also shown for comparison is the one-sided exponential Green's function corresponding to the laminar flow approximation (4.4.9) (dashed curve).

the standing wave in the Green's function is consistent with dominant ice surface features with wavelengths in the range 3 - 4 ice thicknesses, when the increase in the wavelength associated with the finite width of features in the basal landscape is taken into account. The standing wave also demonstrates that there is no need for minimum damping (*cf.* Budd, 1970b; Whillans and Johnsen, 1983) at these wavelengths to explain the observations.

The Green's functions shown in Figures 4.7.3 and 4.7.4 predict that the surface of ice caps is very smooth except in the immediate vicinity of sharp bedrock peaks or troughs, where localized undulations with wavelengths between 2 and 4 ice thicknesses are predicted. This is in agreement with the description of Zwally and others (1983) of the

landscape of the Greenland ice sheet which was quoted in Chapter 2.

Based on the Green's functions shown in Figures 4.7.3 and 4.7.4, four different longitudinal scales for the formation of glacier landscape may be identified.

Very long	length-scale > l_1. The length-scale of the basal landscape is longer than the one-sided exponential Green's function predicted by the laminar flow approximation. The basal landscape is perfectly transferred to the ice surface.
Long and intermediate	2–4 < length-scale < l_1. Glacier landscape is reasonably predicted by the laminar flow approximation. Bedrock undulations are damped (by a factor on the order of $\tan\alpha_0$) and shifted (maximum surface slopes above bedrock peaks) as they are transferred to the surface.
Short	0.5–1 < length-scale < 2–4. The standing wave in the Green's function appears above narrow peaks (and troughs) in the bedrock landscape.
Very short	length-scale $\ll 1$. Bedrock undulations have no effect on the ice surface.

The above classification is similar to the classification of longitudinal scales for flow variations described in subsection 4.6.9, except that the distinction between the long and intermediate scales does seem to be important for the formation of glacier landscape. This is because longitudinal stress gradients, which lead to the transition between the long and intermediate scales, have similar effect on all three flux filters $\hat{g}_e(k)$, $\hat{g}_b(k)$ and $\hat{g}_n(k)$ in (4.7.2) and (4.7.3) at $k \simeq 1/l_g \ll 1$ (*cf.* Fig. 4.6.2). Therefore the combined effect on $t(k)$ and thus $g(x)$ is small.

4.7.4 Effect of longitudinal strain rate

The high amplitude of the standing wave in the Green's functions for non-linear rheology is caused by the stiffness of the ice in the boundary layer near the ice surface. Therefore, the amplitude of the standing wave may be expected to increase when the datum longitudinal strain rate at the ice surface e, is lowered, since low e leads to stiff ice near the surface. This is indeed the case as seen in Figure 4.7.6 which shows the Green's functions predicted for $n = 3$ and $e = 0.001$ and no basal sliding ($c = 0$). The increase in the amplitude of the standing wave is, nevertheless, not great and there is little effect on the wavelength of the standing wave.

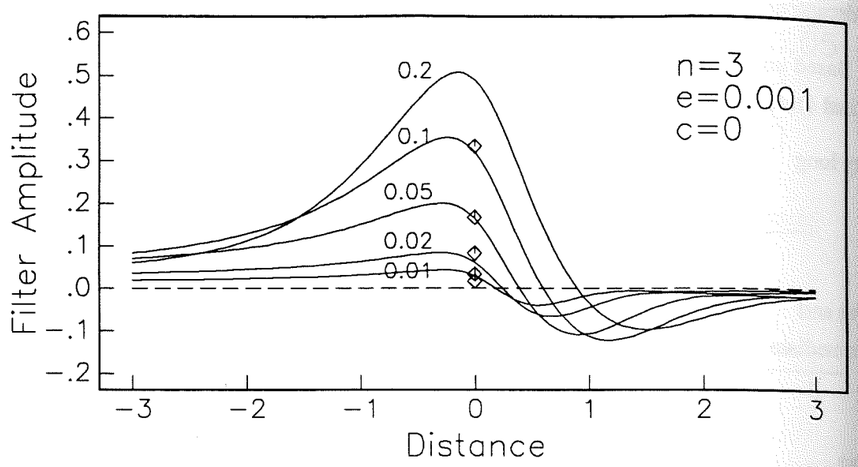

FIGURE 4.7.6: Same as Figure 4.7.4 except that the Green's functions in this figure correspond to a lower datum longitudinal strain rate $e = 0.001$.

4.7.5 Effect of basal sliding

Basal sliding has the effect of increasing the height of the standing wave in the Green's function for linear Newtonian rheology and this can be understood from the shape of the flux filters $g_e(x)$, $g_b(x)$ and $g_n(x)$ (*cf.* subsections 4.5.6, 4.5.8 and 4.5.9). The same arguments apply to non-linear rheology and Figure 4.7.7 shows that the relative importance of basal sliding is greater for non-linear rheology than for linear rheology (*cf.* Fig. 4.5.7). The figure shows the Green's functions predicted for $n = 3$, $e = 0.01$, $c = 0.4$ and $m = 2$. The wavelength of the standing wave is almost the same with and without basal sliding (*cf.* Fig. 4.7.4), but for the range of $\tan\alpha_0$ from 0.01 to 0.2 basal sliding increases the wave amplitude by a factor between 1.3 and 2.

4.7.6 Slope filters

Slope filters $g_\alpha(x)$, defined by (4.5.27) and (4.5.28) in subsection 4.5.10 on linear Newtonian rheology, can be computed from the Green's functions for non-linear rheology. Figure 4.7.8 shows slope filters predicted for non-linear rheology with $n = 3$ and $e = 0.01$ for no basal sliding ($c = 0$). Comparison with Figure 4.5.10 for linear Newtonian rheology shows that slope changes predicted for non-linear rheology are

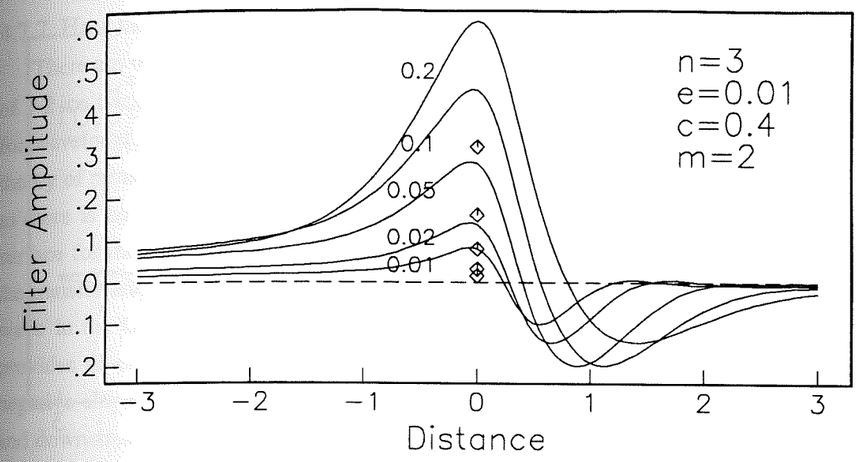

FIGURE 4.7.7: Same as Figure 4.7.4 except that the Green's functions in this figure correspond to non-zero basal sliding with $c = 0.4$ *and* $m = 2$.

larger than for linear rheology, especially for low values of $\tan\alpha_0$. The predicted slope changes become significantly larger for non-zero basal sliding (not shown). The slope filters are relatively symmetric in shape. There is an interval of positive slope perturbation, about 1 ice thickness wide, located downstream of the basal spike, with intervals of negative slope perturbation on each side. Figure 4.7.8 shows that the amplitude of the slope filters is relatively small outside the interval $|x| \tilde{>} 2$–3. This is also true for other values of the datum longitudinal strain e, and for non-zero basal sliding (not shown).

The slope filters in Figure 4.7.8 predict that relatively small basal peaks can lead to substantial surface slope changes. A narrow basal mountain with an area equal to 0.1, *e.g.* a Gaussian bump given by (4.5.26) multiplied by 0.1, with width between 0.5 and 1.0 ice thicknesses (*i.e.* $0.25 \leq \sigma \leq 0.5$) and height between 0.08 and 0.16 ice thicknesses, is associated with slope changes between 20 and 100% of the long scale surface slope $\tan\alpha_0$ for $0.01 \leq \tan\alpha_0 \leq 0.2$. For non-zero basal sliding or lower values of $\tan\alpha_0$, the predicted slope changes are still higher.

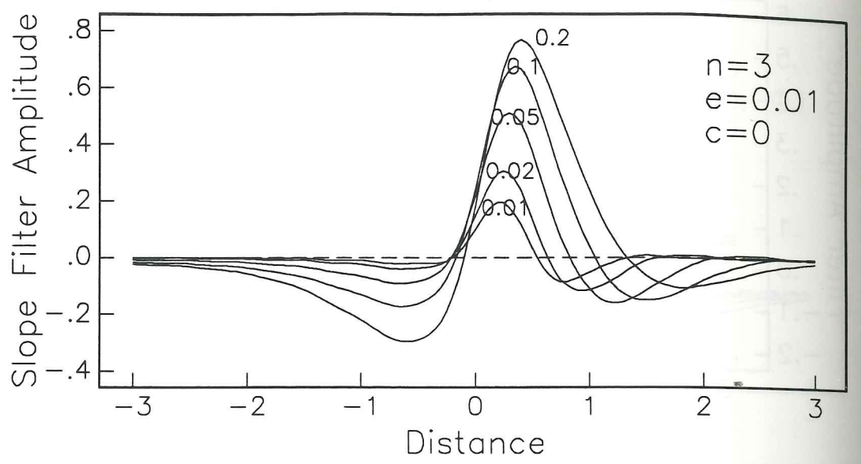

FIGURE 4.7.8: Surface slope filters predicted by non-linear rheology with $n = 3$ *and* $e = 0.01$*, for no basal sliding* ($c = 0$) *and a range of long scale surface slopes* $\tan\alpha_0$*. The curves are labeled with* $\tan\alpha_0$*.*

The slope filter $g_\alpha(x)$ can be used to compute a predicted profile of surface slope fluctuations $\Delta\alpha$ from a profile of measured basal undulations Δz_b. The datum geometry z_{b_0} and z_{s_0}, which must be defined for the computation of Δz_b and in order to compare the predicted $\Delta\alpha$ to measured values, must be slowly varying over the interval where $g_\alpha(x)$ is significantly differently from zero. Since $\int_{-\infty}^{\infty} g_\alpha(x)dx = 0$ and the interval where $g_\alpha(x)$ is significantly differently from zero is relatively narrow, the predicted slope fluctuations are not very sensitive to the specification of the datum bedrock topography z_{b_0}. For low values of the datum slope $\tan\alpha_0$, the slope filter $g_\alpha(x)$ has substantial advantages over the Green's function $g(x)$ for the analysis of real data, because of the long exponential tail of the Green's function (*cf.* Figs. 4.7.3, 4.7.4, 4.7.6 and 4.7.7). The use of $g_\alpha(x)$ and $\Delta\alpha$ instead of $g(x)$ and Δz_s is essentially equivalent to detrending of a non-stationary time series by differencing, which is an often used technique in time series analysis (Chatfield, 1980; Box and Jenkins, 1976).

4.7.7 How far can a glacier flow uphill?

There are observations from ice sheets of ice flowing uphill for distances on the order of 1-2 ice thickness (*cf.* section 2.1). Budd (1970b) used his theory of minimum damping for wavelengths between 3 and 4 ice thicknesses to explain these observations. Budd's theory of minimum damping for wavelengths between 3 and 4 ice thicknesses is not valid as there is not necessarily a maximum in the transfer of bedrock undulations to the ice surface for these wavelength, although there may be a relatively weak local maximum in the transfer amplitude for non-zero basal sliding (*cf.* Figs. 4.7.1 and 4.7.2). The standing wave in the Green's functions computed above (*cf.* Figs. 4.7.3, 4.7.4, 4.7.6 and 4.7.7) provides an explanation of these observations. The standing wave leads to intervals of negative slope perturbation, with lengths between 1 and 2 ice thicknesses both upstream and downstream from a sharp basal peak. Similarly, an interval of negative slope perturbation with length approximately equal to 1 ice thickness occurs above or slightly downstream from a sharp basal trough. These intervals become somewhat longer when the finite width of features in the basal landscape is taken into account. The negative slope perturbation must become larger than the datum slope $\tan\alpha_0$, in order for the ice to flow uphill. This is most likely to occur for non-zero basal sliding and for low values of $\tan\alpha_0$. The standing wave can thus lead to uphill flow for a distance up to approximately 1 - 2 ice thicknesses when negative slope perturbations become larger than the $\tan\alpha_0$. The standing wave implies that the sharpness of peaks and troughs in the basal landscape is more important for the occurrence of uphill flow than the amplitude of the peaks and troughs.

4.7.8 Effect of mass balance variations

The theory developed in the previous subsections can be used to estimate the effect of steady (*i.e.* independent of time) mass balance variations Δb, on the landscape of ice caps and glaciers (*cf.* subsection 4.3.8 and Eq. (4.3.31)). The effect of Δb may be estimated independent of the effect of bedrock undulations Δz_b, on the landscape, because of the linearity of the steady state equation (4.3.31). If needed, the effect of Δb and Δz_b may be added together after they have been determined separately. The ice surface perturbation Δz_s, resulting from mass balance variations Δb, in the absence of bedrock undulations Δz_b, must by the steady state equation (4.3.31) together with (4.6.22) and (4.6.40) satisfy the following equation.

$$g_e*(\Delta z_s + 2(\partial \Delta z_s/\partial x)\,|e|^{1/n}\mathrm{sign}(e)) + g_n*(-\partial \Delta z_s/\partial x)\cot\alpha_0 + u_{0\,z=1}\,\Delta z_s = \int_{-\infty}^{x} \Delta b\, d\xi = \Delta q. \quad (4.7.4)$$

Neglecting the term $2|e|^{1/n}\mathrm{sign}(e)\hat{g}_e(k)$, for the same reason as discussed in subsection 4.7.1, the wave number representation of the above equation is

$$(\hat{g}_e(k) + u_{0\,z=1} - ik\hat{g}_n(k)\cot\alpha_0)\Delta\hat{z}_s = \Delta\hat{q}\ , \quad (4.7.5)$$

where $\Delta\hat{q}$ is the Fourier transform of the flux perturbation $\Delta q = \int_{-\infty}^{x} \Delta b\, d\xi$, which results from variations Δb, in the mass balance.

In order to correctly interpret (4.7.5), an order of magnitude estimate of Δb and Δq in the short scale variables (*cf.* subsection 4.3.2) must be found. As a consequence of the boundary condition (4.2.5), the datum mass balance must satisfy $b_0 = O(\delta)$. This condition arises because b_0 must by (4.2.5) be on the same order as the datum longitudinal flux gradient $(\partial q_0/\partial x)$ and $(\partial q_0/\partial x) = O(\delta)$ because it is a longitudinal derivative of the datum ice flux, which is assumed to be slowly varying in the short scale x-coordinate. It is, furthermore, reasonable to assume that the mass balance perturbation Δb, is on the same order as the datum mass balance b_0, itself or smaller. This leads to the order of magnitude estimate $\Delta b = O(\delta) = 10^{-2}$. Finally, if the wavelength of a harmonic variation in Δq is much shorter that the length of the glacier, *i.e.* if λ is on the order of a few to ten ice thicknesses, then $\Delta q = \int_{-\infty}^{x} \Delta b\, d\xi$ is on the same order as Δb (note that the amplitude of the fluctuations in Δq can be found as the integral of Δb over half a wavelength; thus if λ is equal to ten ice thicknesses then the amplitude of Δq is approximately three times the amplitude of Δb). Therefore, $\Delta q = O(\delta) = 10^{-2}$ for the wavelengths that are of interest for the formation of glacier landscape.

Comparison of (4.7.5) with (4.7.3) shows that a harmonic variation in Δq has in principle a similar effect on the glacier landscape as a harmonic bedrock undulation Δz_b. The main difference between (4.7.5) and (4.7.3) is that $\Delta\hat{z}_b$ in (4.7.3) is multiplied by $g_b(k)$. If λ is on the order of a few to ten ice thicknesses, then a rough estimate of $g_b(k)$ is $g_b(k) \simeq T_b \simeq 2/(n+1) + c = O(1)$ (*cf.* subsection 4.6.8). Thus, a harmonic variation in Δq

(or equivalently Δb), with wavelength on the order of a few to ten ice thicknesses, has roughly a similar effect on the glacier landscape as a harmonic bedrock undulation Δz_b, with the same non-dimensional amplitude. Since the non-dimensional amplitude of Δq and Δb is $O(10^{-2})$, the effect of steady mass balance variations on glacier landscape will be similar in magnitude as the effect of bedrock undulations with an amplitude on the order of 1% of the ice thickness. Bedrock undulations are typically larger than 1% of the ice thickness and thus the effect of steady mass balance variations on glacier landscape may be expected to be considerably less important than the effect of bedrock topography. This conclusion does not apply in the vicinity of ice divides where spatial mass balance variations may lead to substantial ice flux perturbations compared to the (relatively small) datum ice flux.

4.7.9 Relation to previous work

The transfer functions shown in Figures 4.7.1 and 4.7.2 are similar to some of the transfer functions computed by Hutter (1983). Hutter does not take longitudinal strain rate in the datum flow into account and therefore detailed quantitative comparison with his transfer functions is not useful.

The transfer functions in Figures 4.7.1 and 4.7.2 for $\tan\alpha_0 = 0.01$ have a similar shape as the transfer function that Dahl-Jensen (1985) computed for a profile near Dye 3, South Greenland (where mean surface slopes are on the order of 0.004). Dahl-Jenssen's computations include the effect of the datum longitudinal strain rate on the transfer function. The transfer amplitude and phase shift computed by Dahl-Jensen decline sharply to zero in the interval $\lambda = 1$–2 ice thicknesses. Above $\lambda \simeq 2$ ice thicknesses the transfer amplitude rises slowly while the phase shift is approximately equal to $\pi/2$. This is in general agreement with the transfer functions shown in Figures 4.7.1 and 4.7.2. Detailed comparison cannot be made as Dahl-Jenssen's computations are made for cold ice (rheological properties vary with ice depth), but Figures 4.7.1 and 4.7.2 apply to temperate ice. The general agreement between Dahl-Jenssen's results and the transfer functions in Figures 4.7.1 and 4.7.2 for low values of $\tan\alpha_0$, nevertheless indicates that transfer of bedrock undulations to the surface of cold ice sheets is in principle similar to the transfer of bedrock undulations to the surface of temperate ice caps and glaciers. The most important difference is that the datum slope $\tan\alpha_0$ is typically much smaller for cold ice

sheets than for temperate ice caps. Less importantly, cold stiff ice near the surface of cold ice sheets may be expected to increase the transfer amplitude for wavelengths above 2 ice thicknesses and consequently the amplitude of the standing wave in the Green's function for cold ice sheets than for temperate ice caps with the same datum slope $\tan\alpha_0$.

The flux filters $g_e(x)$, $g_b(x)$ and $g_n(x)$, which are used for the derivation of the transfer function $t(k)$ and the Green's function $g(x)$ from (4.7.3), are related to Kamb and Echelmeyer's (1986a) filter theory (*cf.* section 2.6) as discussed in subsection 4.6.11. It is instructive to derive the transfer function $t(k)$ which is predicted by Kamb and Echelmeyer's filter theory, although the theory was not intended for that purpose. Relative ice flux perturbations $\Delta q/q_0$ predicted by (2.6.3) are given by

$$\frac{\Delta q}{q_0} = \frac{\Delta(\bar{u}h)}{\bar{u}_0 h_0} = \frac{\Delta\bar{u}}{\bar{u}_0} + \frac{\Delta h}{h_0} = f*((n+1)\frac{\Delta h}{h_0} + n\frac{\Delta\alpha}{\alpha_0}) + \frac{\Delta h}{h_0}\,, \qquad (4.7.6)$$

to first order in the perturbations. The filter $f(x)$ is defined by (2.6.4) as $f(x) = e^{-|x|/l}/(2l)$. It describes the effect of longitudinal stress gradients on the ice flow. The filter length l is defined by (2.6.5). It is approximately equal to the length-scale l_g, defined by (4.6.48), which was derived from the simplified analysis of glacier flow in subsection 4.6.8. Let h_0 be the unit of length and write $\Delta h = \Delta z_s - \Delta z_b$, $\Delta\alpha = -(\partial\Delta z_s/\partial x)$ and $\alpha_0 = \tan\alpha_0$. Neglecting longitudinal variation in the datum ice flow, the steady state equation (4.3.30) and equation (4.7.6) lead to the following transfer function for the transfer of bedrock undulations to the ice surface.

$$t(k) = \frac{(n+1)\hat{f}(k) + 1}{(n+1)\hat{f}(k) + 1 - ikn\hat{f}(k)\cot\alpha_0}\,, \qquad (4.7.7)$$

where $\hat{f}(k) = 1/(1+l^2k^2)$.

Figure 4.7.9 compares the transfer function predicted by Kamb and Echelmeyer's filter theory (4.7.7) (short-dashed curves) to the transfer function predicted by (4.7.3) (solid curves). The figure shows transfer functions predicted for $n = 3$, $e = 0.01$ and no sliding ($c = 0$). The filter length l for $\hat{f}(k)$ is chosen to be equal to $l_g = 4.34$ so that the transfer functions predicted by (4.7.7) are as close to the transfer functions predicted by

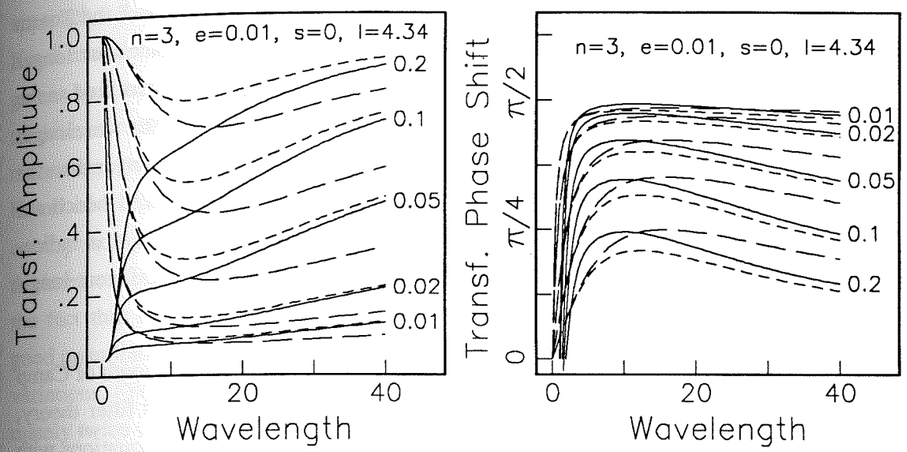

FIGURE 4.7.9: Transfer amplitude (left) and phase shift (right) predicted by (4.7.3) for $n = 3$, $e = 0.01$ and no sliding ($c = 0$) (solid curves, same curves as in Figure 4.7.1), compared to the transfer functions predicted by Kamb and Echelmeyer's (1986a) filter theory (4.7.7) with $l = 4.34$ (short-dashed curves) and transfer functions corresponding to Robin's (1967) analysis of steady state surface undulations (4.7.8) with $l = 4.34$ (long-dashed curves) (for explanation, see text).

(4.7.3) as possible. The filter length l computed from equation (28) in Kamb and Echelmeyer (1986a) is $l \simeq 4.3$ in this case. Figure 4.7.9 shows that the transfer functions predicted by (4.7.7) are relatively close to the correct transfer functions for $\lambda \gtrsim 10$–20, but for shorter wavelengths the transfer amplitude becomes too high and it approaches 1 as $\lambda \to 0$. This failure for short and intermediate wavelengths can be traced to the omission of the T term (*i.e.* longitudinal shear stress gradients ($\partial^2\sigma_{xz}/\partial x^2$)) in Kamb and Echelmeyer's filter theory. The omission of the T term removes all resistance to vertical shearing from the ice flow equations and therefore vertical shearing can extend through the thickness of the ice for basal undulations with arbitrarily short wavelengths. For short wavelengths, the glacier is, therefore, predicted to deform like a deck of cards sliding on its side over the bedrock landscape and this leads to $t(k) \to 1$ as $\lambda \to 0$. Figure 4.7.9 demonstrates the importance of the T term for the formation of steady state ice

surface undulations and it indicates that it is necessary to include the effect of the T term at wavelengths shorter than approximately 10 ice thicknesses. This is somewhat longer than the wavelength $\lambda = 3$–4 ice thicknesses which Budd (1969, 1970a) identified as the transition wavelength below which the T term would become important. The wavelength $\lambda \approx 10$, where the effect of the T term becomes noticeable, is also slightly longer than the transition wavelength $\lambda \approx (1\text{–}2)\pi$ between the intermediate and short scales which are discussed in subsection 4.6.9. The difference between $\lambda \approx 10$ and $\lambda \approx (1\text{–}2)\pi$ is indicative of the approximate nature of the transition wavelengths between the different longitudinal scales which are defined in subsection 4.6.9.

Robin's (1967) analysis of surface undulations along a flow line to the south of Camp Century on the Greenland ice sheet is related to Kamb and Echelmeyer's filter theory, because Robin's analysis is also based on vertically integrated equilibrium equations with the T term omitted (*cf.* section 2.4). Robin computed surface slope fluctuations associated with longitudinal stress gradients and concluded that surface slope fluctuations, computed in this way, explain most of the actual variation in the surface slope along the Camp Century profile. Robin's analysis may be related to (4.7.3) and (4.7.7) by using Kamb and Echelmeyer's filter theory to evaluate the longitudinal stress gradients which are used for computing slope fluctuations. This is actually more accurate than the method used by Robin for evaluating the longitudinal stress gradients. Robin's method is based on (2.4.3a), (2.4.3b) and (2.4.3c) and it ignores depth variation in the longitudinal deviatoric stress. Neglecting longitudinal variation in the datum flow and assuming that slope fluctuations $\Delta\alpha$ arise *exclusively* from longitudinal stress gradients, the following estimate of the transfer function $t(k)$ for the transfer of bedrock undulations to the ice surface may be derived.

$$t(k) = \frac{(n-1)\hat{f}(k) + 1}{(n-1)\hat{f}(k) + 1 - ikn\hat{f}(k)\cot\alpha_0}\,, \tag{4.7.8}$$

where $\hat{f}(k) = 1/(1+l^2k^2)$ is the Fourier transform of the filter $f(x)$ in Kamb and Echelmeyer's filter theory. Equation (4.7.8) is essentially, but not exactly, equivalent to Robin's analysis and it is useful for comparison with (4.7.3) and (4.7.7). Transfer functions predicted by (4.7.8) are plotted in Figure 4.7.9 as long-dashed curves. It is seen that the transfer amplitude computed from (4.7.8), corresponding to Robin's analysis,

approaches 1 as $\lambda \to 0$, just as the transfer amplitude computed from (4.7.7), predicted by Kamb and Echelmeyer's filter theory. For $\lambda \lesssim 10$ ice thicknesses, the transfer functions given by (4.7.7) and (4.7.8) are relatively close to each other, but for $\lambda \gtrsim 10$ ice thicknesses, the transfer function (4.7.8), corresponding to Robin's analysis, deviates more from the correct transfer function than the transfer function (4.7.7), predicted by Kamb and Echelmeyer's filter theory. Figure 4.7.9 shows that the transfer amplitude, corresponding to Robin's analysis, is more than twice too high at wavelengths $\lambda \lesssim 5$ ice thicknesses for datum slopes $\tan\alpha_0 \leq 0.05$. It seems likely that this is the explanation for the fact that Robin needed to reduce his calculated strain rates by half in order to get good quantitative agreement between his calculated slope variations and measured slope variations. Without this correction Robin's predicted slope variations were approximately twice too high. Figure 4.7.9 also explains the need for smoothing of Robin's computed slope variations (*cf.* section 2.4). The transfer amplitude corresponding to Robin's analysis approaches 1 instead of 0 as $\lambda \to 0$. Thus, short wavelength bedrock undulations (and measurement errors) are by his analysis predicted to have much too great effect on the surface slope.

Green's functions and slope filters for the transfer of bedrock undulations to the ice surface have not been used previously by other authors on glacier flow. Therefore, the standing wave in the Green's functions and slope filters derived from the full ice flow equations, and the one-sided exponential Green's function predicted by the laminar flow approximation, cannot be compared directly to results of previous theoretical research on the formation of glacier landscape. However, the standing wave has clear relevance for the interpretation of observations of dominant ice surface features with wavelengths in the range 3-4 ice thicknesses (*cf.* Chapter 2). These observations have been interpreted to indicate that there should be a maximum in the transfer from the bed to the surface at these wavelengths. The absence of such a maximum in correctly derived transfer functions has sometimes been viewed as a failure of current theories of glacier dynamics to explain the observations (*cf.* section 2.8). The analysis presented here shows that transfer functions that increase monotonically with wavelength can indeed explain the observations. The standing wave in the Green's functions leads to the formation of ice surface undulations with wavelengths on the order of 3-4 ice thicknesses in the immediate neighbourhood of sharp peaks and troughs in the bedrock geometry.

The absence of a maximum in the transfer functions from the bed to the surface is related to the limited extension of the standing wave and to the monotonic increase in the transfer from the bed to the surface which is predicted by the laminar flow approximation. A harmonic wave of infinite extension in the Green's functions would lead to a sharp peak in the corresponding transfer functions. The spectral power of a wavelet (a wave with a limited extension), on the other hand, is spread over a range of wavelengths. The standing wave in the Green's functions predicted by the full ice flow equations is superimposed on the one-sided exponential Green's functions predicted by the laminar flow approximation (*cf.* Figs. 4.5.5 and 4.7.3). The transfer function corresponding to the one-sided exponential increases monotonically with wavelength (*cf.* Fig. 4.4.1). The explanation of the absence of a maximum in the transfer functions at wavelengths approximately equal to 3-4 ice thicknesses is that the spectral power of the standing wave is usually not sufficiently concentrated in frequency to lead to a maximum (local or global) when it is superimposed on the monotonically increasing transfer function corresponding to the one-sided exponential.

Observations of glacier landscape have not only shown that undulations with wavelengths around 3-4 ice thicknesses are common on ice sheet and ice caps. The observations have also been used to estimate the wavelength dependent transfer function from the bed to the surface directly and some authors have reported that there is a maximum in the transfer function at wavelengths approximately equal to 3-4 ice thicknesses (Beitzel, 1970; Budd and Carter, 1971). The decaying transfer with decreasing wavelength for undulations shorter than 3-4 ice thicknesses is in good agreement with the theory developed here. The decaying transfer with increasing wavelength for undulations longer than 3-4 ice thicknesses, on the other hand, is in direct contradiction to the theory. As discussed in subsection 4.4.4 it is very difficult to reconcile transfer functions from the bed to the surface that decrease with wavelength for long wavelengths with any reasonable theory of glacier dynamics. The observational evidence for this behavior at long wavelengths is weak and it is possible that the reported decrease in the transfer functions for wavelengths above 3-4 ice thicknesses is caused by inappropriate methods for computing the transfer functions or difficulties associated with detrending or windowing of the data (*cf.* section 2.8).

CHAPTER 5: THREE-DIMENSIONAL THEORY

5.1 INTRODUCTION

This chapter generalizes some of the two-dimensional theory of Chapter 4 to three-dimensional glacier flow. The steady state transfer of bedrock undulations to the ice surface is derived for the laminar flow approximation and for linear Newtonian rheology. The transfer to the surface of bedrock undulations, which are aligned along the direction of the datum flow, is computed and the effect of transverse strain rate $\dot{\varepsilon}_{yy}$, and horizontal shear strain rate $\dot{\varepsilon}_{xy}$, in the datum flow, on the viscosity components η_1, η_2 and η_3 for two-dimensional flow perturbations is estimated.

5.2 DATUM ICE FLOW AND PRELIMINARY ANALYSIS

5.2.1 General

For two-dimensional flow it was found that longitudinal velocity gradients in the datum flow are primarily important for the determination of the datum viscosity components η_1, η_2 and η_3 for the perturbation ice flow (*cf.* subsections 4.3.3 and 4.3.5). Although longitudinal velocity gradients in the two-dimensional datum flow can in most cases be assumed to be small, they must be included in the definition of the ice viscosity in order to prevent singularities in the viscosity components at the ice surface. It may be expected that small transverse velocity gradients (*i.e.* the strain rate components $\dot{\varepsilon}_{yy}$ and $\dot{\varepsilon}_{xy}$) in the datum ice flow have a significant effect on the ice viscosity in addition to the datum longitudinal strain rate $\dot{\varepsilon}_{xx}$, even when the perturbation flow can otherwise be considered to be two-dimensional. This question is analyzed below for ice caps on the basis of a datum long scale ice flow solution for three-dimensional flow.

Following the analysis of the datum long scale ice flow, the steady state equation for three-dimensional ice flow perturbations is presented and the special case of steady state ice flow over bedrock undulations, which are aligned along the direction of the datum flow, is analyzed.

Three-dimensional effects on the flow of valley glaciers, which are traditionally analyzed in terms of a so-called channel-shape factor (Nye, 1965c), are different from three-dimensional effects on the flow of ice caps. The following analysis of three-dimensional ice flow only applies to ice caps and three-dimensional effects on the flow of valley glaciers are not considered.

5.2.2 Non-dimensional variables

The system of non-dimensional variables, defined in subsection 4.3.2 for the short scale analysis of two-dimensional ice flow, will be used for the three-dimensional analysis. In addition to the variables defined in (4.3.1), the non-dimensional transverse coordinate y and transverse velocity v, are defined as $y = \tilde{y}/\tilde{h}_0$ and $v = \tilde{v}/(\tilde{h}_0/\tilde{t}_0)$. The origin of coordinate system is located at the long scale average bedrock, approximately in the middle of the area under consideration. The x-y-plane is parallel to the long scale average ice surface at the origin and the x-axis points in the downslope direction. The long scale average surface slope at the origin is denoted by α_0 and used for the definition of a time-scale and for non-dimensionalization of stresses (*cf.* subsection 4.3.2).

5.2.3 Long scale datum flow

A long scale three-dimensional datum ice flow solution for ice caps can be derived in the same way as for two-dimensional flow (*cf.* section 4.2). To lowest order the datum flow is given by the laminar flow approximation with the modification that the deviatoric stress components $\underset{0}{\tau}_{xx}$, $\underset{0}{\tau}_{yy}$, $\underset{0}{\tau}_{zz}$ and $\underset{0}{\tau}_{xy}$, are found from horizontal velocity gradients in the datum flow using Glen's flow law. The datum flow is assumed to be slowly varying in the horizontal directions, *i.e.* the $(\partial/\partial x)$ and $(\partial/\partial y)$ derivatives in the datum flow are assumed to be $O(\delta)$, where δ is the small ratio of the vertical to the horizontal dimensions of the ice cap. If the same vertical scale cannot be used for the ice thickness and the range of altitudes over the ice cap (*i.e.* for steep ice caps), the parameter δ in the discussions below should be based on a scale for the ice thickness rather than a scale for the altitude. In the non-dimensional variables describe above, the datum stress solution at the origin $x,y = 0$ is given by

$$\underset{0}{\sigma}_{xz} = \underset{0}{\tau}_{xz} = (1-z)\,, \quad \underset{0}{\sigma}_{yz} = \underset{0}{\tau}_{yz} = 0\,, \quad \underset{0}{\sigma}_{zz} = -(1-z)\cot\alpha_0\,, \tag{5.2.1}$$
$$\underset{0}{\sigma}_{xx} = \underset{0}{\sigma}_{zz} + 2\underset{0}{\tau}_{xx} + \underset{0}{\tau}_{yy}\,, \quad \underset{0}{\sigma}_{yy} = \underset{0}{\sigma}_{zz} + 2\underset{0}{\tau}_{yy} + \underset{0}{\tau}_{xx}\,, \quad \underset{0}{\sigma}_{xy} = \underset{0}{\tau}_{xy}\,.$$

The datum velocity u_0, v_0, w_0 and ice flux $\underset{0}{q}_x, \underset{0}{q}_y$ at the origin $x,y = 0$ are determined by the above datum stress field as for two-dimensional flow.

$$u_0 = c + \frac{2}{(n+1)}(1-(1-z)^{n+1})\,, \quad v_0 = 0\,, \quad w_0 = 0\,, \quad \underset{0}{q}_x = c + \frac{2}{(n+2)}\,, \quad \underset{0}{q}_y = 0\,, \tag{5.2.2}$$

The above datum velocity field can be expressed in a fixed coordinate system which makes it possible to compute the strain rates $\underset{0}{\dot{\varepsilon}}_{xx}$, $\underset{0}{\dot{\varepsilon}}_{yy}$, $\underset{0}{\dot{\varepsilon}}_{zz} = -(\underset{0}{\dot{\varepsilon}}_{xx} + \underset{0}{\dot{\varepsilon}}_{yy})$, and $\underset{0}{\dot{\varepsilon}}_{xy}$ associated with the datum velocity field. These strain rates are all computed from horizontal velocity gradients which are assumed to be $O(\delta)$ in the datum flow. They are therefore all $O(\delta)$.

The datum strain rates $\underset{0}{\dot{\varepsilon}}_{xx}$, $\underset{0}{\dot{\varepsilon}}_{yy}$, $\underset{0}{\dot{\varepsilon}}_{zz}$ and $\underset{0}{\dot{\varepsilon}}_{xy}$ can be used to determine the deviatoric stress components $\underset{0}{\tau}_{xx}$, $\underset{0}{\tau}_{yy}$, $\underset{0}{\tau}_{zz}$ and $\underset{0}{\tau}_{xy}$, in the same way as $\underset{0}{\dot{\varepsilon}}_{xx}$ was used to determine $\underset{0}{\tau}_{xx}$ for two-dimensional flow (*cf.* subsections 4.2.3, 4.2.4 and 4.2.5). The effective strain rate $\dot{\varepsilon}$, and the effective shear stress τ, are by (3.4.4) defined as $2\dot{\varepsilon}^2 = \dot{\varepsilon}_{ij}\dot{\varepsilon}_{ij}$ and $2\tau^2 = \tau_{ij}\tau_{ij}$, respectively. Incompressible flow satisfies $\dot{\varepsilon}_{ii} = 0$ and $\tau_{ii} = 0$. Furthermore, $\dot{\varepsilon}_{zy} = 0$ by Glen's flow law, because $\tau_{yz} = 0$ when the x-direction points along the direction of the datum surface slope. This leads to the following expressions for $\dot{\varepsilon}$ and τ for the three-dimensional datum flow.

$$\dot{\varepsilon}_0^2 = \underset{0}{\dot{\varepsilon}}_{xx}^2 + \underset{0}{\dot{\varepsilon}}_{zz}^2 + \underset{0}{\dot{\varepsilon}}_{xx}\underset{0}{\dot{\varepsilon}}_{zz} + \underset{0}{\dot{\varepsilon}}_{xy}^2 + \underset{0}{\dot{\varepsilon}}_{xz}^2\,, \quad \tau_0^2 = \underset{0}{\tau}_{xx}^2 + \underset{0}{\tau}_{zz}^2 + \underset{0}{\tau}_{xx}\underset{0}{\tau}_{zz} + \underset{0}{\tau}_{xy}^2 + \underset{0}{\tau}_{xz}^2\,. \tag{5.2.3}$$

Define $e > 0$ and $\tau'_0 > 0$ by the above expressions for $\dot{\varepsilon}_0$ and τ_0 with the xz terms omitted.

$$e^2 = \underset{0}{\dot{\varepsilon}}_{xx}^2 + \underset{0}{\dot{\varepsilon}}_{zz}^2 + \underset{0}{\dot{\varepsilon}}_{xx}\underset{0}{\dot{\varepsilon}}_{zz} + \underset{0}{\dot{\varepsilon}}_{xy}^2\,, \quad \tau'^2_0 = \underset{0}{\tau}_{xx}^2 + \underset{0}{\tau}_{zz}^2 + \underset{0}{\tau}_{xx}\underset{0}{\tau}_{zz} + \underset{0}{\tau}_{xy}^2\,. \tag{5.2.4}$$

The definition of e only involves strain rates which are $O(\delta)$ in the datum flow. Thus,

$e = O(\delta)$. In dimensional variables e is the ratio of the long scale effective strain rate at the ice surface to the long scale shear strain rate at the bed. From Glen's flow law (3.4.3) it follows that

$$e = (\tau'^2_0 + \tau^2_{xz\,0})^{(n-1)/2}\tau'_0 = (\tau'^2_0 + (1-z)^2)^{(n-1)/2}\tau'_0 \,. \qquad (5.2.5)$$

This implicit equation for τ'_0 corresponds to (4.3.19) which determines $\tau_{xx\,0}$ in the case of two-dimensional flow. When τ'_0 has been found as the solution of (5.2.5), the datum effective shear stress is given as $\tau^2_0 = \tau'^2_0 + \tau^2_{xz\,0} = \tau'^2_0 + (1-z)^2$ and the deviatoric stress components $\tau_{xx\,0}$, $\tau_{yy\,0}$, $\tau_{zz\,0}$ and $\tau_{xy\,0}$ are given by Glen's flow law as

$$\tau_{ij\,0} = \tau_0^{-(n-1)}\dot{\varepsilon}_{ij\,0} \,, \quad ij \neq xz,yz \,. \qquad (5.2.6)$$

As for two-dimensional flow (*cf.* subsection 4.2.5), it is possible to replace the horizontal velocity gradients in (5.2.4), (5.2.5) and (5.2.6) by the values of the gradients at the datum ice surface and the resulting error in the deviatoric stresses will be $O(\delta)$.

Equations (5.2.5) and (5.2.6) describe a similar boundary layer near the ice surface for the three-dimensional datum ice flow as was previously found for the two-dimensional datum flow (*cf.* subsections 4.2.3, 4.2.4 and 4.2.5). The deviatoric stress components determined from (5.2.6) are $O(e^{1/n}) = O(\delta^{1/n})$ near the ice surface and $O(e) = O(\delta)$ away from the surface. The thickness of the layer where the deviatoric stress components are on the order of $e^{1/n}$ may be estimated in a similar way as for two-dimensional flow as the depth d_b below the ice surface where the shear stress $\sigma_{xz\,0} = \tau_{xz\,0} = (1-z)$ reaches the value of τ'_0 at the surface. This gives

$$d_b = e^{1/n} \,. \qquad (5.2.7)$$

As for two-dimensional datum flow, the thickness of the boundary layer is predicted to be a significant fraction (10 - 20%) of the ice thickness.

5.2.4 Datum viscosity for two-dimensional flow perturbations

If bedrock undulations are close to being perpendicular to the datum ice flow, it may be reasonable to assume that the ice flows directly over the bedrock landscape without significant transverse ice flow perturbations. The three-dimensional analysis of Reeh (1987) for linear Newtonian rheology shows that if the transverse width of basal undulations is larger than about 2-3 times their length, then the finite width of the undulations has only minor influence on the perturbation flow, which can be considered two-dimensional to a good approximation. However, even if the *perturbation* ice flow is two-dimensional to a good approximation, it may not be justified to neglect the effect of transverse (*i.e.* three-dimensional) velocity gradients in the *datum* ice flow on the ice viscosity. As discussed in subsection 4.3.5 there is at least one point on each flow line where the datum longitudinal strain rate is equal to zero. Transverse velocity gradients in the datum flow must be important in the neighbourhood of such points. Transverse velocity gradients in the datum flow may also be important at other points along the flow line, depending on the relative size of $\dot{\varepsilon}_{yy\,0}$ and $\dot{\varepsilon}_{xy\,0}$ compared to $\dot{\varepsilon}_{xx\,0}$.

The effect of transverse velocity gradients in the datum flow on two-dimensional ice flow perturbations can be estimated from the three-dimensional datum ice flow solution which is described above. This is done by taking transverse velocity gradients in the datum flow into account during the linearization of Glen's flow law, which is described in subsection 4.3.3 for two-dimensional flow. The field equations (4.3.12) and (4.3.13) and the boundary conditions (4.3.23), (4.3.24), (4.3.25) and (4.3.26) for the perturbation ice flow do not need to be changed, but the flow law field equations (4.3.15) and the definitions (4.3.16) of the viscosity components η_1, η_2 and η_3 have to be modified. From Glen's flow law (3.4.3) and the expressions (5.2.3) for $\dot{\varepsilon}$ and τ for the three-dimensional datum flow, the following expressions for the deviatoric stress perturbations $\frac{1}{2}(\Delta\sigma_{xx} - \Delta\sigma_{zz})$ and $\Delta\sigma_{xz} = \Delta\tau_{xz}$ for two-dimensional flow perturbations can be derived.

$$\tfrac{1}{2}(\Delta\sigma_{xx} - \Delta\sigma_{zz}) = 2\eta_1\Delta\dot{\varepsilon}_{xx} - 2\eta_3\Delta\dot{\varepsilon}_{xz} \qquad (5.2.8a)$$

$$\Delta\sigma_{xz} = \Delta\tau_{xz} = 2\eta_2\Delta\dot{\varepsilon}_{xz} - 2\eta_3\Delta\dot{\varepsilon}_{xx} \,, \qquad (5.2.8b)$$

where

$$\eta_1 = \frac{1}{2n}\tau_0^{-(n+1)}(n\tau_0^2 - (n-1)(\tau_{xx} + \tfrac{1}{2}\tau_{yy})^2)$$
$$\eta_2 = \frac{1}{2n}\tau_0^{-(n+1)}(n\tau_0^2 - (n-1)\tau_{xz}^2) \qquad (5.2.9)$$
$$\eta_3 = \frac{n-1}{2n}\tau_0^{-(n+1)}(\tau_{xx} + \tfrac{1}{2}\tau_{yy})\tau_{xz} ,$$

are viscosity components which arise from a linearization of Glen's flow law and take the effect of transverse velocity gradients in the datum flow into account. The above definition of viscosity components reduces to η_1, η_2 and η_3 as defined by (4.3.16) for two-dimensional datum flow, when $\dot{\varepsilon}_{yy} = \dot{\varepsilon}_{xy} = 0$ and therefore $\tau_{yy} = 0$, $\tau_{xx} = -\tau_{zz}$. The standard viscosity η is given by $\eta = \frac{1}{2}\tau/\dot{\varepsilon} = \frac{1}{2}\tau_0^{-(n-1)}$. As for two-dimensional flow, $\eta = \eta_1 = \eta_2 = \frac{1}{2}$ and $\eta_3 = 0$ for linear Newtonian rheology, *i.e.* for $n = 1$.

Equations (5.2.8) and (5.2.9) can be analyzed in exactly the same way as (4.3.15) and (4.3.16) for two-dimensional datum flow. The only difference between (5.2.8) and (4.3.15) is that $\Delta\tau_{xx}$ in (4.3.15a) is replaced by $\frac{1}{2}(\Delta\sigma_{xx} - \Delta\sigma_{zz}) = \Delta\tau_{xx} + \frac{1}{2}\Delta\tau_{yy}$ in (5.2.8a). This difference has no effect on the stress function formulation of the perturbation stress field (*cf.* subsection 4.6.2) nor on the derivation the simplified theory of subsection 4.6.8. The viscosity components η_1, η_2 and η_3 defined by (5.2.9) have essentially the same shape as the viscosity components defined by (4.3.16) (*cf.* Figure 4.3.2). The main difference is that there is less difference between η_1 and η_2 in the boundary layer near the ice surface when there are significant transverse velocity gradients in the datum flow. The effect of transverse velocity gradients in the datum flow can be accurately described by their effect on the length-scale or range of longitudinal stress gradients l_g, if l_g is computed from (4.6.48) using the viscosity components defined by (5.2.9). In practice, numerical values of transverse velocity gradients in the datum flow are rough estimates and detailed computations of their effect through (5.2.9) are therefore not justified. Rather, the parameter e in the two-dimensional analysis should be estimated such that it incorporates the effect of transverse velocity gradients in the datum flow. Thus, transverse velocity gradients in the datum flow do not lead to fundamental changes in the two-dimensional analysis of Chapter 4.

Finally, it may be mentioned that a non-zero $\dot{\varepsilon}_{xy}$ component in the datum flow will for non-linear rheology lead to a non-zero $\Delta\tau_{xy}$ stress component in the perturbation stress field even when the perturbation flow field is assumed to be two-dimensional. This arises because of cross-interaction between perturbation stress and strain rate components. A non-zero $\Delta\tau_{xy}$ stress component is not compatible with strictly two-dimensional field equations for the perturbation flow field as it leads to a non-zero $(\partial\Delta\tau_{xy}/\partial x)$ force component in the y-direction in the three-dimensional force equilibrium equations. This force component can neither be balanced by $(\partial\Delta\tau_{yy}/\partial y)$ nor $(\partial\Delta\tau_{yz}/\partial z)$ since they are identically equal to zero for a two-dimensional perturbation flow field. Thus, a two-dimensional perturbation flow field determined from (5.2.8) and (5.2.9) is not entirely consistent with the three-dimensional force equilibrium equations. However, the effect of cross-interaction between perturbation stress and strain rate components, brought about by the viscosity component η_3, was not found to be very important for two-dimensional flow (*cf.* subsections 4.6.7 and 4.6.8). Therefore, the abovementioned inconsistency, which only arises in the case of a non-zero $\dot{\varepsilon}_{xy}$ component in the datum flow, is probably not important.

5.2.5 Ice flux perturbations

As in the case of two-dimensional flow, one may view the ice flux perturbation $\Delta\vec{q}$, for three-dimensional flow as arising from four "forcing" functions at the surface and the bedrock, $\Delta\sigma_{xz}|_{z=1}$, $\Delta\sigma_{zz}|_{z=1}$, Δz_s and Δz_b, which determine four flux perturbation components $\Delta\vec{q}_e$, $\Delta\vec{q}_n$, $\Delta\vec{q}_a$ and $\Delta\vec{q}_b$ (*cf.* subsection 4.3.7). The "forcing" functions arise from a linearization of the boundary conditions for three-dimensional flow in a similar way as described in subsections 4.3.6 and 4.3.7 for two-dimensional flow. There is no flux perturbation component corresponding to a transverse shear stress perturbation at the surface because $\Delta\sigma_{yz}|_{z=1} = 0$. This arises because the corresponding datum stress component σ_{yz} is identically equal to zero and therefore $(\partial\sigma_{yz}/\partial z)_{z=1} = 0$ (*cf.* subsection 4.3.6).

The advection component follows directly from the datum flow as

$$\Delta\vec{q}_a = u_{0\,z=1}\,\Delta z_s\vec{a}_x = (2/(n+1)+c)\Delta z_s\vec{a}_x\,. \tag{5.2.10}$$

If the contribution of the boundary layer to the stress at the surface is neglected (this contribution is $O(|e|^{1/n})$), the "forcing" functions $\Delta\sigma_{xz\,z=1}$ and $\Delta\sigma_{zz\,z=1}$ have the same evaluation as for two-dimensional flow, *i.e.* $\Delta\sigma_{xz\,z=1} = \Delta z_s$, $\Delta\sigma_{zz\,z=1} = -\cot\alpha_0\Delta z_s$ (*cf.* the two-dimensional surface stress boundary conditions (4.3.24)).

5.2.6 Steady state ice surface undulations

The steady state equation for ice flow perturbations in three-dimensions is different from the steady state equation (4.3.30) for two-dimensional flow, because ice flow in three dimensions can be diverted *around* bedrock obstacles in addition to flowing directly *over* the bedrock landscape. Ice flux perturbations for three-dimensional flow in the absence of mass balance perturbations, must by (3.6.3) satisfy the following steady state equation.

$$\vec{\nabla}\cdot\Delta\vec{q} = \frac{\partial\Delta q_x}{\partial x} + \frac{\partial\Delta q_y}{\partial y} = 0\,. \tag{5.2.11}$$

This equation states that the steady state ice flux perturbation $\Delta\vec{q}$, for three-dimensional flow in the absence of mass balance perturbations, must be divergence free. This is different from two-dimensional flow where the steady state ice flux perturbation Δq, must by (4.3.30) be identically equal to zero.

5.2.7 Undulations along the direction of the datum flow

An interesting special case that arises in the three-dimensional theory is the steady state transfer to the surface of bedrock undulations, which are aligned along the direction of the datum flow, in the absence of mass balance variations. The datum flow is assumed to be uniform in the x- and y-directions or so slowly varying that the effect of longitudinal and transverse gradients in the datum flow can be ignored. In this case the steady state surface and basal geometries $z = z_s(y)$ and $z = z_b(y)$ can be assumed to be functions of the y-coordinate only. Furthermore, all longitudinal derivatives $(\partial/\partial x)$, in the field equations and boundary conditions are equal to zero by assumption. The assumption of uniform datum flow is equivalent to neglecting the effect of the datum mass balance on the

flow. Since mass balance variations are assumed to be zero, this means that the effect of mass balance on the flow is ignored.

The field equations (3.4.1), (3.4.2) and (3.4.3) and boundary conditions (3.6.3), (3.5.2), (3.5.3) and (3.5.4) for steady state flow can in this special case be written as two systems of field equations and boundary conditions. One system determines the velocity components v and w, and the other determines u. In the dimensionless short scale variables the system determining v and w is as follows.

Field equations:

$$\frac{\partial v}{\partial y} + \frac{\partial w}{\partial z} = 0\,, \tag{5.2.12}$$

$$\frac{\partial\sigma_{yy}}{\partial y} + \frac{\partial\sigma_{yz}}{\partial z} = 0 \tag{5.2.13a}$$

$$\frac{\partial\sigma_{yz}}{\partial y} + \frac{\partial\sigma_{zz}}{\partial z} = \cot\alpha_0\,, \tag{5.2.13b}$$

$$\dot{\varepsilon}_{ij} = \tau^{n-1}\tau_{ij}\,. \tag{5.2.14}$$

Boundary conditions at the surface $z = z_s(y)$ (note that the effect of mass balance is ignored by assumption):

$$\frac{\partial q_y}{\partial y} = 0\,, \tag{5.2.15}$$

$$-\frac{\partial z_s}{\partial y}\sigma_{yy} + \sigma_{yz} = 0 \tag{5.2.16a}$$

$$-\frac{\partial z_s}{\partial y}\sigma_{yz} + \sigma_{zz} = 0\,. \tag{5.2.16b}$$

Boundary conditions at the base $z = z_b(y)$:

$$-v\frac{\partial z_b}{\partial y} + w = 0\,, \tag{5.2.17}$$

$$v_b = c\,|\tau_b|^{m-1}\tau'_b\,, \tag{5.2.18}$$

where v_b is the transverse velocity parallel to the bed, τ_b is the total bed parallel shear

stress and τ'_b is the transverse basal shear stress. v_b and τ'_b are given by

$$v_b = \cos\theta\, v - \sin\theta\, w \tag{5.2.19}$$

and

$$\tau'_b = (\cos^2\theta - \sin^2\theta)\tau_{yz} + 2\sin\theta\cos\theta\tau_{yy}\,, \tag{5.2.20}$$

v_b and τ'_b are transverse velocity and shear stress components in a coordinate system which is rotated about the x-axis by a small angle $\tan\theta = -(\partial z_b/\partial y)$. The above sliding condition is derived on the assumption that the basal sliding velocity is parallel to the direction of the bed parallel shear stress.

The system determining u is as follows.

Field equations:

$$\frac{\partial\sigma_{xy}}{\partial y} + \frac{\partial\sigma_{xz}}{\partial z} = -1\,, \tag{5.2.21}$$

$$\dot\varepsilon_{ij} = \tau^{n-1}\tau_{ij}\,. \tag{5.2.22}$$

Boundary conditions at the surface $z = z_s(y)$:

$$-\frac{\partial z_s}{\partial y}\sigma_{xy} + \sigma_{xz} = 0 \tag{5.2.23}$$

Boundary condition at the base $z = z_b(y)$:

$$u_b = c\,|\tau_b|^{m-1}\tau''_b\,, \tag{5.2.24}$$

where τ''_b is the longitudinal basal shear stress which is given by

$$\tau''_b = \sin\theta\,\tau_{xy} + \cos\theta\,\tau_{xz}\,. \tag{5.2.25}$$

The relations $(\partial u/\partial x) = 0$, $(\partial q_x/\partial x) = 0$, $(\partial z_b/\partial x) = 0$, $\dot\varepsilon_{xx} = (\partial u/\partial x) = 0$, $\tau_{xx} = 0$ and $\tau_{yy} + \tau_{zz} = 0$, were used in the derivation of the above equations. They follow from the assumption that all $(\partial/\partial x)$ derivatives are equal to zero.

The above two systems of field equations and boundary conditions are independent except for coupling through the effective shear stress $2\tau^2 = \tau_{ij}\tau_{ij}$, and the bed parallel

shear stress τ_b, which involve deviatoric stress components from both systems.

Comparison of the above system of equations (5.2.12) to (5.2.18), which determines v and w, with the system (4.3.2) to (4.3.10), which determines u and w for two-dimensional flow, shows that the systems are almost identical when $(\partial z_s/\partial t)$ and b in (4.3.5) are put equal to zero. There are differences in the definition of the effective shear stress and in the basal boundary condition, which do not change the nature of the problem, but the most important difference between the two systems is that -1 on the right hand side of (4.3.3a) is replaced by 0 on the right hand side of (5.2.13a). Since the right hand side of (4.3.3a) represents the downslope component of the gravitational force, this difference implies that the system (5.2.12) to (5.2.18) is essentially equivalent the system (4.3.2) to (4.3.10) for two-dimensional flow, when the effect of the downslope component of the gravitational force is neglected. However, the downslope component of the gravitational force is the only driving force of the ice motion in the two-dimensional ice flow equations. When it is neglected, the steady state ice surface predicted by (4.3.2) to (4.3.10) is flat, independent of the bedrock shape, and the velocity components u and w are equal to zero. Similarly, the steady state ice surface predicted by (5.2.12) to (5.2.18) is flat, *i.e.* $(\partial z_s/\partial y) = 0$, and the corresponding steady state vertical and transverse velocity components v and w are equal to zero. This argument leads to the following solution of equations (5.2.12) to (5.2.18)

$$\frac{\partial z_s}{\partial y} = 0\,,\quad \sigma_{yy} = \sigma_{zz} = -(z_s - z)\cot\alpha_0\,,\quad \sigma_{yz} = 0\,,\quad \dot\varepsilon_{yz} = 0\,,\quad v = w = 0\,,$$

which is easily verified by insertion. The remaining stress, strain rate and velocity components are determined as the solution of (5.2.21) to (5.2.25). Thus, τ_{xy} and τ_{xz} are the only non-zero deviatoric stress components and u, $\dot\varepsilon_{xy} = \frac{1}{2}(\partial u/\partial y)$ and $\dot\varepsilon_{xz} = \frac{1}{2}(\partial u/\partial z)$ are the only non-zero velocity and strain rate components.

The above argument implies that bedrock undulations, which are aligned along the direction of the datum flow, are not transferred to the surface at all in the absence of mass balance variations. This conclusion is independent of the flow law and sliding law powers n and m and of the amount of basal sliding as represented be the sliding parameter c. It is also independent of the length-scale of the basal landscape in the y-direction, *i.e.* arbitrarily wide bedrock undulations aligned along the direction of the datum flow are

not transferred to the surface. This conclusion has important consequences for the shape of the transfer function $t(k_x,k_y)$ for three-dimensional flow as will be discussed below.

5.3 LAMINAR FLOW APPROXIMATION

5.3.1 General

The laminar flow approximation (3.7.1), (3.7.2) and (3.7.3) should provide a good approximation to three-dimensional glacier flow if all horizontal flow gradients are small. Thus, ice surface undulations predicted by the laminar flow approximation for three-dimensional flow may be expected to be reasonable when the bedrock undulations are slowly varying in both the longitudinal and the transverse directions. As in the case of two-dimensional flow (*cf.* Chapter 4), a theory based on the laminar flow approximation should be valid as the long wavelength limit of any theory based on the full ice flow equations, as these equation reduce to the laminar flow approximation in the limit of long wavelengths.

Flux perturbations $\Delta\vec{q} = \Delta q_x\vec{a}_x + \Delta q_y\vec{a}_y$, predicted by the laminar flow approximation (3.7.4) and expressed in the short scale variables, are given by

$$\Delta\vec{q}/q_{\underset{0}{d}} = ((n+2) + r_0(m+1))(\Delta z_s - \Delta z_b)\vec{a}_x \qquad (5.3.1)$$
$$- (n + r_0 m)\cot\alpha_0(\partial\Delta z_s/\partial x)\vec{a}_x - (1 + r_0)\cot\alpha_0(\partial\Delta z_s/\partial y)\vec{a}_y ,$$

where $\vec{a}_x$ and $\vec{a}_y$ are basis vectors in the x- and y-directions, $q_{\underset{0}{d}} = 2/(n+2)$, $q_{\underset{0}{s}} = c$ and $r_0 = q_{\underset{0}{s}}/q_{\underset{0}{d}} = c\,(n+2)/2$. The datum longitudinal velocity at the ice surface is given by $u_{\underset{z=1}{0}} = c + 2/(n+1)$ and the datum transverse velocity at the ice surface is given by $v_{\underset{z=1}{0}} = 0$. Flux perturbation components $\Delta\vec{q}_e$, $\Delta\vec{q}_n$, $\Delta\vec{q}_a$ and $\Delta\vec{q}_b$, predicted by the laminar flow approximation are given by

$$\begin{aligned}
\Delta\vec{q}_e &= (2n/(n+1) + mc)\Delta z_s\vec{a}_x \\
\Delta\vec{q}_n &= (2n/(n+2) + mc)\cot\alpha_0(-\partial\Delta z_s/\partial x)\vec{a}_x \\
&\quad + (2/(n+2) + c)\cot\alpha_0(-\partial\Delta z_s/\partial y)\vec{a}_y \\
\Delta\vec{q}_a &= (2/(n+1) + c)\Delta z_s\vec{a}_x \\
\Delta\vec{q}_b &= -(2 + (m+1)c)\Delta z_b\vec{a}_x .
\end{aligned} \qquad (5.3.2)$$

Transverse flux perturbations are only predicted in the case of $\Delta\vec{q}_n$. The other flux perturbation components $\Delta\vec{q}_e$, $\Delta\vec{q}_a$ and $\Delta\vec{q}_b$, are parallel to the direction of the datum flow.

Ignoring mass balance perturbations and horizontal gradients in the datum flow, the steady state equation for the laminar flow approximation, follows from (5.2.11) and (5.3.1)

$$((n+2) + r_0(m+1))\frac{\partial(\Delta z_s - \Delta z_b)}{\partial x} - (n + r_0 m)\cot\alpha_0\frac{\partial^2\Delta z_s}{\partial x^2} - (1 + r_0)\cot\alpha_0\frac{\partial^2\Delta z_s}{\partial y^2} = 0 .$$

This equation may be rewritten as

$$-l_1\frac{\partial^2\Delta z_s}{\partial x^2} - l_2\frac{\partial^2\Delta z_s}{\partial y^2} + \frac{\partial\Delta z_s}{\partial x} = \frac{\partial\Delta z_b}{\partial x} , \qquad (5.3.3)$$

where the length-scales l_1 and l_2, are defined by

$$l_1 = \frac{n + r_0 m}{(n+2) + r_0(m+1)}\cot\alpha_0 , \quad l_2 = \frac{1 + r_0}{(n+2) + r_0(m+1)}\cot\alpha_0 . \qquad (5.3.4)$$

Equations (5.3.3) and (5.3.4) correspond to equations (4.4.3) and (4.4.4) for two-dimensional flow and the length-scale l_1 given by (5.3.4) is the same as the length-scale l_1 defined by (4.4.4). The length-scale l_2, which is associated with the y-direction as will be seen below, is considerably shorter than l_1 for non-linear rheology ($n > 1$, $m > 1$). For long scale surface slopes $\tan\alpha_0$ between 0.1 and 0.01, $n = 3$ and $m = 2$, the length-scales l_1 and l_2 are in the ranges 6 - 70 and 2 - 30, respectively.

The most important parameter determining the length-scales l_1 and l_2, is the long scale surface slope α_0, as was the case for l_1 for two-dimensional flow (*cf.* subsection 4.4.1). The relative importance of basal sliding as described by r_0, does not have a large effect on l_1 or l_2. The non-linear flow law ($n > 1$) and sliding law ($m > 1$) of ice lead to

an *increase* in l_1 and a *decrease* in l_2 compared to linear behavior for which $n = m = 1$. For $n = 3$ and $m = 2$, l_1 is increased by a factor between 4/3 and 9/5, but l_2 is decreased by a factor between 3/5 and 2/3, compared to $n = m = 1$, depending on the relative importance of basal sliding. In the limit n and $m \rightarrow \infty$, which corresponds to perfectly plastic rheology, the length-scale l_1 becomes $l_1 = \cot\alpha_0$, but $l_2 \rightarrow 0$. Equation (5.3.3) describes how the non-linear rheology and sliding of glaciers determine (long wavelength) ice surface undulations for three-dimensional ice flow through the effect of the flow law and sliding law powers n and m on the length-scales l_1 and l_2 given by (5.3.4).

Equation (5.3.3) is a partial differential equation in x and y which can be solved for Δz_s in terms of the "forcing" function Δz_b. As for two-dimensional flow (*cf.* section 4.4), it is instructive to carry this solution out both in the frequence domain using a transfer function, and in the space domain using a Green's function.

5.3.2 Transfer functions

The two-dimensional Fourier transform (*cf.* subsection 3.3.2) of (5.3.3) is

$$(l_1 k_x^2 + l_2 k_y^2 + ik_x)\Delta\hat{z}_s = ik_x\Delta\hat{z}_b \, .$$

The Fourier transform of the ice surface undulations can therefore be written

$$\Delta\hat{z}_s = t(k_x,k_y)\Delta\hat{z}_b \, , \tag{5.3.5}$$

where the two-dimensional transfer function $t(k_x,k_y)$ (*cf.* subsection 3.3.3) from the base to the surface is given by

$$t(k_x,k_y) = \frac{ik_x}{ik_x + l_1 k_x^2 + l_2 k_y^2} \, . \tag{5.3.6}$$

The transfer amplitude and phase shift are given by

$$|t(k_x,k_y)| = \frac{|k_x|}{\sqrt{k_x^2 + (l_1 k_x^2 + l_2 k_y^2)^2}} \, , \quad \phi(k_x,k_y) = \tan^{-1}((l_1 k_x^2 + l_1 k_y^2)/k_x) \, . \tag{5.3.7}$$

The wave numbers k_x, k_y are defined as $k_x = 2\pi/\lambda_x$ and $k_y = 2\pi/\lambda_y$ where λ_x and λ_y are the wavelengths of harmonic undulations in the x- and y-directions, respectively.

Equations (5.3.5), (5.3.6) and (5.3.7) reduce to the corresponding equations (4.4.5), (4.4.6) and (4.4.7) for two-dimensional laminar flow, *i.e.* when $k_y = 0$, $k_x = k$.

The transfer function given by (5.3.6) and (5.3.7) describes a considerably more complex behavior than the transfer function given by (4.4.6) and (4.4.7) for two-dimensional flow. For harmonic bedrock undulations along the datum flow, *i.e.* when $k_x = 0$, the transfer amplitude given by (5.3.7) is identically equal to zero independent of k_y as long as $k_y \neq 0$. Longitudinal bedrock ridges are therefore not transferred to the ice surface at all, independent of wavelength. As discussed in subsection 5.2.7, this is a generally true for steady state ice flow over longitudinal bedrock landscape. This property of steady state flow over longitudinal bedrock landscape leads to unexpected behavior of the transfer function in the limit $k_x,k_y \rightarrow 0$, *i.e.* in the limit of asymptotically long wavelengths. If this limit is approached along the k_y-axis in the wave number domain, then $t(k_x=0,k_y) \equiv 0$ for all $k_y \neq 0$ and consequently $\lim_{k_y \rightarrow 0} t(k_x=0,k_y) = 0$. On the other hand, if the limit is approached along any line through the origin in the wave number domain other than the k_y-axis, then $\lim_{k_x,k_y \rightarrow 0} t(k_x,k_y) = 1$ and consequently $|t(k_x,k_y)| \rightarrow 1$, $\phi(k_x,k_y) \rightarrow 0$. This means that very long bedrock undulations, which are not aligned along the datum flow, are perfectly transferred to the ice surface, independent of the value of the long scale surface slope or of the relative importance of basal sliding, just as for two-dimensional flow. However, very long bedrock undulations, which are aligned along the datum flow, are not transferred to the surface at all. This implies that the transfer function $t(k_x,k_y)$ is discontinuous at the origin $k_x,k_y = 0$ in the wave number domain. It is difficult to give a meaningful physical interpretation of a discontinuity in $t(k_x,k_y)$ and the discontinuity must therefore reflect an inconsistency in the three-dimensional analysis. This problem is discussed in a separate subsection below.

For shorter wavelengths and $k_x \neq 0$, the transfer function given by (5.3.6) is more like the transfer function given by (4.4.6) for two-dimensional flow. The length-scales l_1 and l_2, are long (*i.e.* $l_1,l_2 = O(\cot\alpha_0)$) for the low values of the surface slope found on glaciers and ice caps. As a consequence, the transfer amplitude given by (5.3.7) for $k_x \neq 0$ is low, *i.e.* $|t(k_x,k_y)| = O(\tan\alpha_0)$, as long as $k_x,k_y = O(1)$, which corresponds to undulation wavelengths on the order of a few to ten ice thicknesses. Furthermore, the transfer

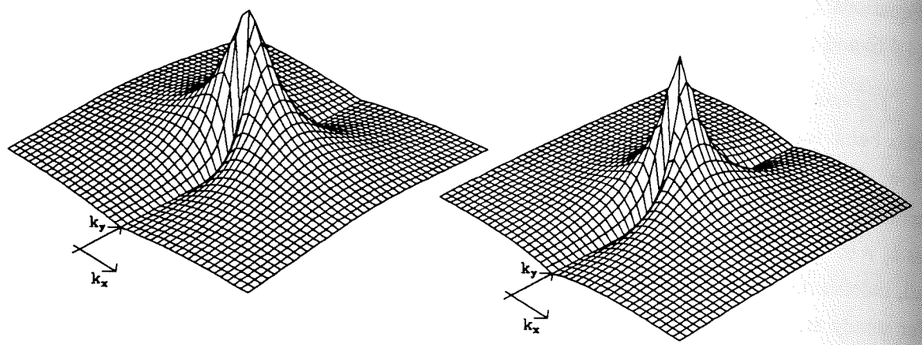

FIGURE 5.3.1: Perspective views of the transfer amplitude $|t(k_x,k_y)|$ predicted by the laminar flow approximation (5.3.7) as a function of k_x,k_y for linear Newtonian rheology ($n = 1$) (left) and non-linear rheology ($n = 3$) (right) for no basal sliding ($c = 0$) and $\tan\alpha_0 = 0.05$. *The perspective views show the area $-1 \le k_x,k_y \le 1$ with grid spacing $\Delta k_x = \Delta k_y = 0.05$. The height of the peak at the origin $k_x,k_y = 0$ is equal to 1.*

phase shift $\phi(k_x,k_y) \simeq \pi/2$ for such undulations.

Figure 5.3.1 shows perspective views of the transfer amplitude $|t(k_x,k_y)|$ predicted by the laminar approximation and given by (5.3.7) for linear Newtonian rheology ($n = 1$) (left) and non-linear rheology ($n = 3$) (right) for no basal sliding ($c = 0$) and $\tan\alpha_0 = 0.05$. The transfer functions reach their maximum value at $k_x,k_y = 0$ where the transfer amplitude is equal to 1. They decay with increasing distance from $k_x,k_y = 0$, which reflects the fact that short wavelength (high values of k_x and k_y) basal undulations are more heavily damped than undulations with longer wavelengths (low values of k_x and k_y). The figure shows that the top in the transfer function at $k_x,k_y = 0$ is wider for linear rheology than for non-linear rheology, which implies that non-linear rheology leads to more damping of basal undulations than linear rheology. Note the narrow "valleys" in the transfer amplitude along the line $k_x = 0$ and the discontinuity at $k_x,k_y = 0$.

5.3.3 Green's functions

The Green's function $g(x,y)$, corresponding to (5.3.3) can be found by inverting the transfer function $t(k_x,k_y) = \hat{g}(k_x,k_y)$, given by (5.3.6) (*cf.* subsection 3.3.4). The Green's function is given by the Fourier integral theorem (3.3.4b), and can be expressed as

$$g(x,y) = \frac{1}{2\pi\sqrt{l_1 l_2}} \frac{\partial}{\partial x} \left[K_0 \left[\tfrac{1}{2}\sqrt{x^2/l_1^2 + y^2/(l_1 l_2)} \right] e^{x/(2l_1)} \right], \qquad (5.3.8)$$

where K_0 is the modified Bessel function of the second kind of order zero (*cf.* Abramowitz and Stegun, 1965). In order to derive (5.3.8), the Fourier integral arising from (3.3.4b) and (5.3.6) is evaluated using residue calculus (Butkov, 1968) and tables of Fourier transforms (Magnus and Oberhettinger, 1949). It can be shown that the integral of $g(x,y)$ given by (5.3.8) along the y-direction, *i.e.* $\int_{-\infty}^{\infty} g(x,y)dy$, is equal to the Green's function $g(x)$ given by (4.4.9) for two-dimensional flow. Thus, the Green's function given by (5.3.8) is consistent with the Green's function (4.4.9) derived from the laminar flow approximation for two-dimensional flow.

The Green's function $g(x,y)$, given by (5.3.8) is the solution of (5.3.3) corresponding to a sharp spike or δ-function in the bedrock geometry. Its shape is a consequence of ice flow both over and around the bedrock obstacle represented by the δ-function at the base. The steady state ice surface geometry Δz_s arising from a general bedrock geometry Δz_b can be expressed as

$$\Delta z_s = \int_{-\infty}^{\infty}\int_{-\infty}^{\infty} g(x-\xi,y-\eta)\Delta z_b(\xi,\eta)d\xi d\eta = g(x,y)*\Delta z_b(x,y)\,. \qquad (5.3.9)$$

Figure 5.3.2 shows perspective views of the Green's function $g(x,y)$ predicted by the laminar flow approximation and given by (5.3.8) for linear Newtonian rheology ($n = 1$) (left) and non-linear rheology ($n = 3$) (right) for no basal sliding ($c = 0$) and $\tan\alpha_0 = 0.05$. The Green's function has an integrable singularity at the origin $x,y = 0$. It can be shown from (5.3.8) that $g(x,y=0) \to \infty$ as $x \to 0$ from the upstream direction, whereas $g(x,y=0) \to -\infty$ as $x \to 0$ from the downstream direction. This singularity is the most pronounced feature of $g(x,y)$ in Figure 5.3.2. The singularity is removed when the full ice flow equations are solved (see below in the case of linear Newtonian rheology).

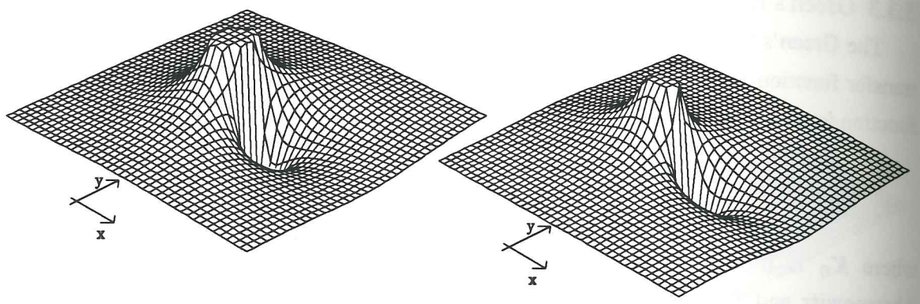

FIGURE 5.3.2: *Perspective views of the Green's function $g(x,y)$ predicted by the laminar flow approximation (5.3.8) for linear Newtonian rheology ($n = 1$) (left) and non-linear rheology ($n = 3$) (right) for no basal sliding ($c = 0$) and $\tan\alpha_0 = 0.05$. The perspective views show the area $-20 \le x,y \le 20$ with grid spacing $\Delta x = \Delta y = 1$. There is a singularity in the Green's function at the origin $x,y = 0$. The Green's functions in the figure are plotted for $|g(x,y)| \le 0.005$. Grid values for which $|g(x,y)| > 0.005$ are replaced by ± 0.005 so that the neighbourhood of the singularity is replaced by a flat surface.*

Apart from the singularity, the figure shows a peak in the glacier landscape upstream from the basal spike and a trough in the downstream direction. The combination of an upstream peak and a downstream trough diverts part of the ice flow around the spike in the bedrock geometry. The peak and trough for non-linear rheology (right), are narrower in the transverse direction and more elongated in the longitudinal direction compared to linear rheology (left). This is a consequence of the dependency of the length-scales l_1 and l_2 on the flow law power n which was discussed above. The length-scale l_1 is a measure of the range of the Green's function along the direction of the datum flow, whereas $\sqrt{l_1 l_2}$ is a similar measure of the range of the Green's function in the transverse direction.

A Green's function with a singularity at the origin and a δ-function in the bedrock geometry cannot as such be considered a realistic model of the geometry of ice caps or glaciers. Furthermore, they are not slowly varying in x and y, which is a condition for the

validity of the laminar flow approximation. As discussed in subsection 3.3.5 and Appendix 1 this does not imply that $g(x,y)$ is invalid. It only means that when $g(x,y)$ is used to compute Δz_s from Δz_b using (5.3.9), then Δz_b, and consequently Δz_s, must be slowly varying in x and y.

5.3.4 Transfer of undulations which are almost aligned with the datum flow

The discontinuity in the transfer function $t(k_x,k_y)$ given by (5.3.6) in the limit $k_x,k_y \to 0$ is not a consequence of the laminar flow approximation. As discussed in subsection 5.2.7, longitudinal bedrock ridges are in general not transferred to the ice surface at all, independent of wavelength. However, the two-dimensional analysis in Chapter 4 shows that transverse bedrock ridges are perfectly transferred to the surface in the long wavelength limit. Therefore, transfer functions for three-dimensional flow will in general be discontinuous in the limit $k_x,k_y \to 0$ in exactly the same way as found above for the laminar flow approximation. Reeh's (1987) transfer function for linear Newtonian rheology without basal sliding has a discontinuity at $k_x,k_y = 0$, and below it will be shown that this is also true for linear Newtonian rheology with non-zero basal sliding. This property of transfer functions for three-dimensional flow leads to both physical and mathematical problems in the application and interpretation of the transfer functions. It reflects a subtle flaw in the three-dimensional analysis which is not encountered in the case of two-dimensional flow. Since this problem arises in the long wavelength limit, it may be analyzed using the laminar flow approximation and the results can be extended to more complete treatments of glacier flow as these reduce to the laminar flow approximation in the long wavelength limit.

The physical problem with the discontinuity at $k_x,k_y = 0$ in transfer functions for three-dimensional flow is the contradiction that the steady state ice surface corresponding to a basal layer of uniform thickness is different depending on whether the layer is viewed as the limit of a transverse basal undulation as $k_x \to 0$ or as the limit of a longitudinal undulation as $k_y \to 0$. This contradiction is of course physically unacceptable. A mathematical problem with the discontinuity is that it is difficult to invert a discontinuous transfer function numerically to find the corresponding Green's function. The reason for the numerical difficulties is that Green's functions corresponding to the discontinuous transfer functions decay very slowly to zero away from the origin (especially in the

downstream direction) and this makes it almost impossible to prevent aliasing when they are computed numerically. This is not a serious problem in the case of the laminar flow approximation, since an analytical solution can be derived in that case as shown above. The slow decay of the Green's functions away from the origin also makes them difficult to use as filters for real data.

The abovementioned problems are related to the fact that the horizontal extent of glaciers and ice caps is limited. This is for the most part ignored in the analysis by the use of Fourier transforms that extend from $-\infty < x,y < \infty$. One may say that the analysis involves an implicit boundary condition at "infinity", where the ice flow "enters" the area under consideration. This condition may or may not be physically acceptable as the wavelength of bedrock undulations goes to infinity. In the case of steady ice flow over longitudinal bedrock ridges, the analysis in subsection 5.2.7 predicts a flat ice surface and an ice flux perturbation component $\Delta q_x(y)$ which varies with y for $-\infty < x < \infty$. Therefore the analysis implicitly assumes that the ice flow "enters" the area under consideration with a flux perturbation component Δq_x, that varies in the y direction in a way consistent with steady flow which is uniform in the x-direction. This is not a physically realistic assumption in the limit of long wavelengths as it requires a specification of non-zero Δq_x far outside the area where the datum ice flow can be considered to be uniform or even outside the area covered by the glacier or ice cap. A more feasible assumption would be to assume that the ice flow "enters" the area under consideration with $\Delta q_x = 0$. In that case the question arises how far the ice needs to flow before transient flow in the y-direction dies out. If this distance is much shorter than the extent of an area within which the datum ice flow solution may be considered to be uniform, then the ice flow analysis in subsection 5.2.7 is valid. If, however, the distance required for the decay of transients is longer than the horizontal extent of the glacier or ice cap, then the analysis is clearly invalid.

In the case of two-dimensional steady flow over transverse bedrock ridges, the ice flux perturbation Δq, is put equal to zero by the steady state equation (4.3.30) for the entire range $-\infty < x < \infty$. Therefore, the two-dimensional analysis assumes that $\Delta q = 0$ as the flow "enters" the area under consideration and it does not require a specification of non-zero Δq outside this area.

The difference between the long wavelength limits corresponding to longitudinal and transverse bedrock ridges, respectively, can thus be traced to different implicit assumptions about the "entering" ice flux perturbation. This incompatibility is the cause of the discontinuity in the transfer function $t(k_x, k_y)$ for three-dimensional flow in the limit $k_x, k_y \to 0$. The only way to completely eliminate this problem is to solve the full three-dimensional non-linear ice flow equations in the space domain over the area covered by the glacier or ice cap with a correct specification of bedrock geometry and mass balance. This approach is much more complicated than the derivation of perturbation equations based on a datum ice flow solution. It also has the drawback that it does not yield the understanding that is provided by the transfer functions and Green's functions that follow from the perturbation approach. Since the problem is associated with the long wavelength limit of the transfer function and since the most interesting feature in the corresponding Green's function (for two-dimensional flow) is the standing wave (*cf.* subsections 4.5.9 and 4.7.3), which has a relatively short wavelength, one might expect that some other solution of this problem is possible.

Another possibility to solve the problem associated with the discontinuity in the transfer functions for three-dimensional flow is to eliminate the discontinuity by brute force based on an analysis of the decay of transient flow predicted by the laminar flow approximation. The length-scales l_1 and l_2 define the horizontal extent of the Green's function (5.3.8) predicted by the laminar flow approximation. Therefore, the area that needs to be considered in order to analyze the flow around a localized disturbance in the bedrock landscape must extent a distance on the order of l_1 or l_2 away from the disturbance. It is natural to *assume* that the effect of a localized bedrock disturbance on the ice flux cannot extent far upstream from this area. This *ad hoc* assumption makes it possible to eliminate the discontinuity in the transfer function as seen below. This assumption is necessarily arbitrary to some extent and there is no way to get around this except to solve the full non-linear ice flow equations as mentioned above. However, the short scale shape of the Green's function (*i.e.* the standing wave) is insensitive to details in the elimination of the discontinuity in the long wavelength limit. Therefore, one may expect that Green's functions, computed from modified transfer functions with the discontinuity at $k_x, k_y = 0$ eliminated, are indicative of the steady state shape of the ice surface in the vicinity of localized bedrock disturbances derived from a solution of the full non-linear

ice flow equations.

Consider ice flow satisfying the steady state equation for the laminar flow approximation (5.3.3). Assume that the ice flows over harmonic bedrock landscape given by $\Delta z_b = e^{i(k_x x + k_y y)}$. Let the flow "enter" at $x = 0$ with $\Delta q_x = 0$ and assume that it approaches the steady state predicted by (5.3.5) and the transfer function (5.3.6) as $x \to \infty$. The above conditions at $x = 0$ and as $x \to \infty$ can be viewed as boundary conditions for (5.3.3) which can be solved as a second order ordinary differential equation by taking a Fourier transform in the y-direction. The solution is

$$\Delta z_s = \frac{1}{ik_x + l_1 k_x^2 + l_2 k_y^2} \left[ik_x e^{i(k_x x + k_y y)} + \frac{2l_2 k_y^2 e^{-(\sqrt{1 + 4l_1 l_2 k_y^2} - 1)x/(2l_1)}}{\sqrt{1 + 4l_1 l_2 k_y^2} + 1} e^{ik_y y} \right] . \quad (5.3.10)$$

The first term in the parenthesis is the steady state solution given by (5.3.5) and (5.3.6). The second term is a transient term which decays exponentially away from $x = 0$. The length-scale of the exponential decay is a function of k_y and is given by

$$l_d = \frac{2l_1}{\sqrt{1 + 4l_1 l_2 k_y^2} - 1} . \quad (5.3.11)$$

The first question that needs to be answered is for what values of k_x and k_y the transient term can be neglected. For transverse undulations, *i.e.* when $k_y = 0$, this transient term is identically equal to zero for all values of k_x. Thus, it does not have to be taken into account for two-dimensional flow. For short wavelength longitudinal undulations, *i.e.* when $k_y \geq 1$, say, the decay of the transient term takes place on a length-scale $l_d = O(1)$ ice thickness. This value of l_d is short compared to $l_1, l_2 = O(\cot\alpha_0)$. The transients will therefore have decayed away before the ice has flowed more than a fraction of the distance across the area that needs to be considered to in order to compute the effect of a localized bedrock disturbance. This implies that the transient term can be ignored in this case. For very long wavelength longitudinal undulations, however, *i.e.* when $k_y < O(l_1^{-1}, l_2^{-1}) = O(\tan\alpha_0)$, the decay of the transient term takes place on a length-scale $l_d \approx (l_2 k_y^2)^{-1}$. Depending on the value of k_y this value of l_d is on the same order as or larger than the length scales l_1, l_2. If the transient term is neglected, the effect of a localized bedrock disturbance on the ice flux will therefore extend much too far away from

the disturbance. Thus, the transient term cannot be neglected for very long wavelength longitudinal undulations. Furthermore, it is clear that it can much less be neglected in the limit $k_y \to 0$ in which case $l_d \to \infty$.

The transient term in (5.3.10) can be used to modify the transfer function given by (5.3.6) so that the discontinuity at $k_x, k_y = 0$ is eliminated. This is done by assuming that the flow "enters" the area under consideration at $x \approx -l_1$ with $\Delta q_x = 0$. The value of the transient term at the origin is then given by (5.3.10) by putting $x = l_1$. For almost longitudinal harmonic bedrock undulations with very long wavelengths in the y-direction, *i.e.* when $k_x \ll k_y$ and $k_y < O(l_1^{-1}, l_2^{-1})$, the transient term varies slowly over a relatively long range in x close to the origin. Furthermore, the variation of the factor $e^{ik_x x}$ with x in the solution (5.3.10), corresponding to a harmonic bedrock undulation $\Delta z_b = e^{i(k_x x + k_y y)}$, is negligible in this case. Therefore, it makes sense to simply add the transient term evaluated from (5.3.10), with $x = l_1$, to the transfer function $t(k_x, k_y)$ for such undulations. There is no need to modify the transfer function except for almost longitudinal undulations, *i.e.* when $k_x \ll k_y$. In order to better prevent an undesirable contribution from the transient term when the $k_x \geq k_y$ for small values of k_y, the transient term will furthermore be multiplied by the factor $e^{-l_1^2 k_x^2}$. The above considerations lead to the following modified transfer function

$$t'(k_x, k_y) = t(k_x, k_y) + \frac{2l_2 k_y^2 e^{-(\sqrt{1 + 4l_1 l_2 k_y^2} - 1)/2 - l_1^2 k_x^2}}{(\sqrt{1 + 4l_1 l_2 k_y^2} + 1)(ik_x + l_1 k_x^2 + l_2 k_y^2)} , \quad (5.3.12)$$

which is denoted by a prime mark to differentiate it from the original transfer function given by (5.3.6).

The above modification of the transfer function is only significant for very long undulation wavelengths where the laminar flow approximation is a good approximation of the solution of the full ice flow equations and it decays exponentially as the undulation wavelength becomes shorter. Thus, the same modification may be applied to transfer functions derived from the full ice flow equations, *e.g.* Reeh's (1987) transfer function for linear Newtonian flow without sliding.

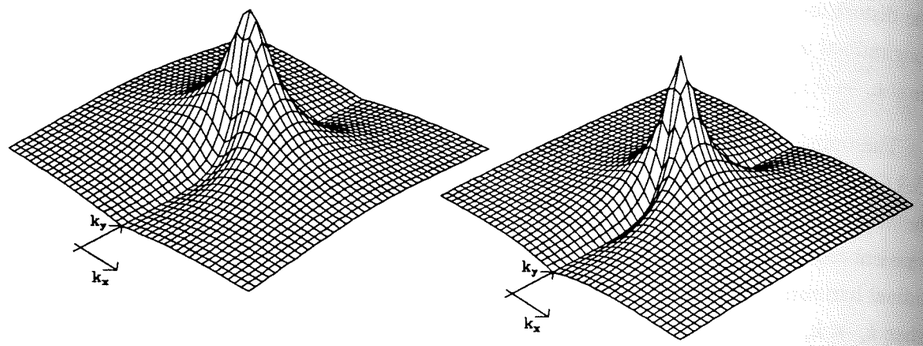

FIGURE 5.3.3: Same as Figure 5.3.1 except that the transfer amplitude is given by the modification $|t'(k_x,k_y)|$ defined by (5.3.12) corresponding to the laminar flow approximation (5.3.6).

This modification of the transfer function is arbitrary in many ways. However, it does make it possible to compute Green's functions numerically from theoretical transfer functions and the short scale shape of the Green's functions is not sensitive to the arbitrariness of the modification.

Figure 5.3.3 shows perspective views of the modified transfer amplitude $|t'(k_x,k_y)|$ given by (5.3.12) corresponding to the laminar flow approximation (5.3.6) for linear Newtonian rheology ($n = 1$) (left) and non-linear rheology ($n = 3$) (right) for no basal sliding ($c = 0$) and $\tan\alpha_0 = 0.05$. The figure shows that the modified transfer amplitude is essentially identical to the unmodified transfer amplitude shown in Figure 5.3.1 except that the "valleys" along the line $k_x = 0$ disappear as the origin is approached and the discontinuity at $k_x,k_y = 0$ has been eliminated. The effect of the modification is limited to the neighbourhood of the line $k_x = 0$ and little effect can be seen at distances further than approximately 5-10 grid spacings away from the origin. These distances correspond to undulation wavelengths shorter than approximately $(4–8)\pi$. Green's functions corresponding to the modified transfer functions in Figure 5.3.3 (not shown) can be computed numerically by applying some smoothing in order to eliminate the singularity at the origin. The modified Green's functions are almost identical to the unmodified Green's functions shown in Figure 5.3.2. The only difference is that the modified Green's

functions decay more rapidly to zero away from the origin in the downstream direction. This difference is so small that it can hardly be seen on plots of the functions. The shape of the singularity at the origin in the modified Green's functions can be investigated both analytically by considering the behavior of the modified transfer functions away from the origin and numerically by varying the smoothing in the numerical computations. The shape of the singularity is essentially identical for the unmodified and modified Green's functions.

5.4 LINEAR NEWTONIAN FLOW

5.4.1 General

Linearized field equations and boundary conditions for three-dimensional flow perturbations and linear Newtonian rheology follow from the general form of the field equations and boundary conditions given in sections 3.4 and 3.5 (*i.e.* (3.4.1), (3.4.2), (3.4.3), (3.5.2), (3.5.3) and (3.5.4)) in a similar way as described for two-dimensional flow in subsections 4.3.3, 4.3.6, 4.5.2, 4.5.3 and 4.5.4. The derivation of the three-dimensional field equations and boundary conditions will only be described where it is different from the two-dimensional derivation.

The long scale datum velocity solution for $n = 1$ is given by

$$u_0 = c + (1-(1-z)^2)\,,\quad v_0 = 0\,,\quad w_0 = 0\,,$$
$$u_{0\,z=0} = c\,,\quad u_{0\,z=1} = c+1\,,\quad (\partial u_0/\partial z)_{z=0} = 2\,,$$
$$q_{x\,0} = c + 2/3\,,\quad q_{y\,0} = 0\,,$$

5.4.2 Stream function for three dimensional flow

A stream function can be defined for three-dimensional incompressible flow perturbations similar to the definition of a stream function for two-dimensional flow described in subsection 4.5.2. A stream function or a vector potential ψ_i, for three dimensional flow is a vector rather than a scalar and is defined by the relation

$$\Delta\vec{u} = \vec{\nabla}\times\vec{\psi}\,, \tag{5.4.1}$$

where the notation $\vec{\nabla}\times$ denotes the *curl* vector operator. It is shown in Appendix 3 that

the stream function may be assumed to be divergence free, *i.e.*

$$\vec{\nabla}\cdot\vec{\psi} = 0\,, \tag{5.4.2}$$

without loss of generality. In component form (5.4.1) becomes

$$\Delta u = \frac{\partial\psi_z}{\partial y} - \frac{\partial\psi_y}{\partial z}\,,\quad \Delta v = \frac{\partial\psi_x}{\partial z} - \frac{\partial\psi_z}{\partial x}\,,\quad \Delta w = \frac{\partial\psi_y}{\partial x} - \frac{\partial\psi_x}{\partial y}\,. \tag{5.4.3}$$

The equation of continuity (3.4.1), is automatically satisfied when the velocity field is expressed by a stream function because of the vector identity $\vec{\nabla}\cdot\Delta\vec{u} = \vec{\nabla}\cdot(\vec{\nabla}\times\vec{\psi}) = 0$.

In the special case of two-dimensional flow (*i.e.* $v = 0$, $(\partial/\partial y) = 0$) the ψ_x and ψ_z components of the three-dimensional stream function are equal to zero and the component ψ_y is equal to the negative of the two-dimensional stream function ψ. The reason for the sign change is that the y-coordinate in the three-dimensional x,y,z coordinate system replaces the z-coordinate in the two-dimensional x,z coordinate system as the second coordinate.

The strain rate $\Delta\dot{\varepsilon}_{ij} = \frac{1}{2}(\partial\Delta u_i/\partial x_j + \partial\Delta u_j/\partial x_i)$, can be written in terms of the stream function ψ_i using the above expressions for the velocity components. Furthermore, the flow law (3.4.3) for linear Newtonian rheology (*i.e.* when $n = 1$) gives the non-dimensional deviatoric stress $\Delta\tau_{ij}$ as

$$\Delta\tau_{ij} = \Delta\dot{\varepsilon}_{ij}\,. \tag{5.4.4}$$

This makes it possible to express all field equations and boundary conditions for three-dimensional flow perturbations in terms of the stream function.

As for two-dimensional flow, the ice flux perturbation $\Delta\vec{q} = q_x\vec{a}_x + q_y\vec{a}_y$, for three-dimensional flow is the sum of the effect of horizontal velocity perturbations through the thickness of the ice plus the effect of perturbations in the surface and bedrock geometries.

$$\Delta\vec{q} = \int_0^1(\Delta u\vec{a}_x + \Delta v\vec{a}_y)dz + (1+c)\Delta z_s\vec{a}_x - c\Delta z_b\vec{a}_x\,. \tag{5.4.5}$$

In terms of the stream function ψ_i, the flux perturbation is given by

$$\Delta\vec{q} = \left[\int_0^1\frac{\partial\psi_z}{\partial y}dz - \psi_{\substack{y\\z=1}} + \psi_{\substack{y\\z=0}} + (1+c)\Delta z_s - c\Delta\hat{z}_b\right]\vec{a}_x + \left[-\int_0^1\frac{\partial\psi_z}{\partial x}dz + \psi_{\substack{x\\z=1}} - \psi_{\substack{x\\z=0}}\right]\vec{a}_y\,. \tag{5.4.6}$$

5.4.3 Field equations

The equation of continuity (3.4.1) is already satisfied by the stream function formulation. The flow law equations (3.4.3) are also automatically satisfied by expressing the deviatoric stresses $\Delta\tau_{ij}$ in terms of the stream function ψ_i using (5.4.3) and (5.4.4). The only field equations left are the force balance equations (3.4.2), which can be written

$$\frac{\partial\Delta\sigma_{ij}}{\partial x_i} = \frac{\partial(\Delta\dot{\varepsilon}_{ij} - \Delta p\,\delta_{ij})}{\partial x_i} = \tfrac{1}{2}\frac{\partial}{\partial x_i}\left[\frac{\partial\Delta u_i}{\partial x_j} + \frac{\partial\Delta u_j}{\partial x_i}\right] - \frac{\partial\Delta p}{\partial x_j} = 0\,.$$

By the equation of continuity, $(\partial\Delta u_i/\partial x_i)$ is equal to zero and the above equation can therefore be rewritten as

$$\tfrac{1}{2}\frac{\partial^2\Delta u_j}{\partial x_i^2} - \frac{\partial\Delta p}{\partial x_j} = 0\,,$$

which in traditional vector notation is given by

$$\tfrac{1}{2}\nabla^2\Delta\vec{u} - \vec{\nabla}\Delta p = 0\,. \tag{5.4.7}$$

Take the curl of the above equation and write $\Delta\vec{u} = \vec{\nabla}\times\vec{\psi}$. Then the vector identities $\vec{\nabla}\times(\vec{\nabla}\Delta p) = 0$, $\vec{\nabla}\cdot\vec{\psi} = 0$, $\vec{\nabla}\times\vec{\nabla}\times\vec{\psi} = \vec{\nabla}(\vec{\nabla}\cdot\vec{\psi}) - \nabla^2\vec{\psi} = -\nabla^2\vec{\psi}$, lead to the three-dimensional biharmonic equation for the stream function $\vec{\psi}$.

$$\nabla^4\vec{\psi} = 0\,. \tag{5.4.8}$$

Written out in full the three-dimensional biharmonic equation is given by

$$\left[\frac{\partial^4}{\partial x^4} + \frac{\partial^4}{\partial y^4} + \frac{\partial^4}{\partial z^4} + 2\frac{\partial^4}{\partial x^2\partial y^2} + 2\frac{\partial^4}{\partial x^2\partial z^2} + 2\frac{\partial^4}{\partial y^2\partial z^2}\right]\psi_i = 0\,. \tag{5.4.9}$$

As for two-dimensional flow the biharmonic equation (5.4.9) replaces all other field equations for the perturbation flow.

The three-dimensional biharmonic equation (5.4.9) can be solved analytically in the wave number domain by taking the Fourier transform in the x- and y-directions. The transformed biharmonic equation is

$$k^4\hat{\psi}_i - 2k^2\frac{\partial^2\hat{\psi}_i}{\partial z^2} + \frac{\partial^4\hat{\psi}_i}{\partial z^4} = 0\,, \tag{5.4.10}$$

where $k^2 = k_x^2 + k_y^2$.

The transformed three-dimensional biharmonic equation for each stream function component ψ_i, is an ordinary differential equation in z and it is identical to the transformed two-dimensional biharmonic equation (4.5.8). It therefore has the same general solution given by (4.5.13), *i.e.*

$$\hat{\psi}_i = (A_i + C_i z)\sinh kz + (B_i + D_i z)\cosh kz\,. \tag{5.4.11}$$

The constants A_i, B_i, C_i and D_i must be determined from the boundary conditions for the flow.

5.4.4 Boundary conditions

Linearized boundary conditions for three-dimensional flow perturbations follow from the general form of the boundary conditions (3.5.2), (3.5.3) and (3.5.4) and the three-dimensional datum solution described in subsection 5.2.3 in essentially the same way as described for two-dimensional flow in subsection 4.3.6. The only part of the derivation of boundary conditions for three-dimensional flow that is significantly different from the two-dimensional derivation is the derivation of the sliding condition at the bed.

In the case of linear Newtonian rheology (*i.e.* $n = m = 1$), the basal boundary condition described in subsection 3.5.4 states that the bed-parallel sliding velocity points in the direction of and is proportional to the bed parallel shear stress. Let a coordinate system with z'-axis perpendicular to the bed be denoted by a prime mark. In such a coordinate system the sliding boundary condition (3.5.4) may be written

$$u' = c\sigma'_{x'z'}\,,\quad v' = c\sigma'_{y'z'}\,.$$

One such coordinate system is given by a rotation about an axis that is tangent to the bedrock and perpendicular to the bedrock gradient. To first order in the bedrock

gradient, the coordinate transformation matrix that describes this rotation is given by

$$A_{ij} = \begin{bmatrix} 1 & 0 & (\partial z_b/\partial x) \\ 0 & 1 & (\partial z_b/\partial y) \\ (-\partial z_b/\partial x) & (-\partial z_b/\partial y) & 1 \end{bmatrix}.$$

The velocity and stress in this rotated coordinate system are given by

$$u'_i = A_{ij}u_j\,,\quad \sigma'_{ij} = A_{ik}A_{jl}\sigma_{kl}\,.$$

The above expressions for u', v' and σ'_{ij} can be used to derive a linearized sliding boundary condition for flow perturbations in the same way as described in subsection 4.3.6 for two-dimensional flow.

The boundary conditions for three-dimensional ice flow perturbations are as follows.

At the datum surface $z = 1$:

$$\Delta\sigma_{xz} - \Delta z_s = 0\,, \tag{5.4.12}$$

$$\Delta\sigma_{yz} = 0\,, \tag{5.4.13}$$

$$\Delta\sigma_{zz} + \cot\alpha_0\Delta z_s = 0\,. \tag{5.4.14}$$

At the datum base $z = 0$:

$$-c\frac{\partial\Delta z_b}{\partial x} + \Delta w = 0\,, \tag{5.4.15}$$

$$\Delta u + 2\Delta z_b = c(\Delta\tau_{xz} - \Delta z_b)\,, \tag{5.4.16}$$

$$\Delta v = c\Delta\tau_{yz}\,. \tag{5.4.17}$$

The stress boundary condition (5.4.14) involves $\Delta\sigma_{zz}$ at the ice surface. $\Delta\sigma_{zz}$ does not follow directly from the stream function and therefore (5.4.14) must be reformulated in order to express it in terms of ψ_i. This can be done in two ways by using the force equilibrium equations to write the $(\partial/\partial x)$ derivative or the $(\partial/\partial y)$ derivative of $\Delta\sigma_{zz}$ as

$$\frac{\partial\Delta\sigma_{zz}}{\partial x} = \frac{\partial\Delta\sigma_{xx}}{\partial x} + \frac{\partial\Delta\tau_{zz}}{\partial x} - \frac{\partial\Delta\tau_{xx}}{\partial x} = -\frac{\partial\Delta\tau_{xy}}{\partial y} - \frac{\partial\Delta\tau_{xz}}{\partial z} + \frac{\partial\Delta\tau_{zz}}{\partial x} - \frac{\partial\Delta\tau_{xx}}{\partial x}\,,$$

or

$$\frac{\partial \Delta\sigma_{zz}}{\partial y} = \frac{\partial \Delta\sigma_{yy}}{\partial y} + \frac{\partial \Delta\tau_{zz}}{\partial y} - \frac{\partial \Delta\tau_{yy}}{\partial y} = -\frac{\partial \Delta\tau_{xy}}{\partial x} - \frac{\partial \Delta\tau_{yz}}{\partial z} + \frac{\partial \Delta\tau_{zz}}{\partial y} - \frac{\partial \Delta\tau_{yy}}{\partial y} ,$$

and replacing the boundary condition (5.4.14) by its $(\partial/\partial x)$ or $(\partial/\partial y)$ derivative. It turns out that both these possibilities for reformulating (5.4.14) lead to the same equation for the determination of the constants A_i, B_i, C_i and D_i in the expression (5.4.11) for the stream function $\hat{\psi}_i$.

The boundary conditions (5.4.12) to (5.4.17) can then be written in terms of the three-dimensional stream function ψ_i as follows.

At the datum surface $z = 1$:

$$\tfrac{1}{2}\left\{\frac{\partial^2\psi_z}{\partial y\partial z} - \frac{\partial^2\psi_y}{\partial z^2} + \frac{\partial^2\psi_y}{\partial x^2} - \frac{\partial^2\psi_x}{\partial x\partial y}\right\} = \Delta\sigma_{\substack{xz\\z=1}} = \Delta z_s , \qquad (5.4.18)$$

$$\tfrac{1}{2}\left\{-\frac{\partial^2\psi_z}{\partial x\partial z} + \frac{\partial^2\psi_x}{\partial z^2} + \frac{\partial^2\psi_y}{\partial x\partial y} - \frac{\partial^2\psi_x}{\partial y^2}\right\} = \Delta\sigma_{\substack{yz\\z=1}} = 0 , \qquad (5.4.19)$$

$$\tfrac{1}{2}\left\{-2\frac{\partial^3\psi_x}{\partial x\partial y\partial z} + \frac{\partial}{\partial z}\left\{3\frac{\partial^2}{\partial x^2} + \frac{\partial^2}{\partial y^2} + \frac{\partial^2}{\partial z^2}\right\}\psi_y \right. \qquad (5.4.20a)$$

$$\left. - \frac{\partial}{\partial y}\left\{\frac{\partial^2}{\partial x^2} + \frac{\partial^2}{\partial y^2} + \frac{\partial^2}{\partial z^2}\right\}\psi_z\right\} = \frac{\partial\Delta\sigma_{\substack{zz\\z=1}}}{\partial x} = -\cot\alpha_0\frac{\partial\Delta z_s}{\partial x} ,$$

$$\tfrac{1}{2}\left\{-\frac{\partial}{\partial z}\left\{\frac{\partial^2}{\partial x^2} + 3\frac{\partial^2}{\partial y^2} + \frac{\partial^2}{\partial z^2}\right\}\psi_x + 2\frac{\partial^3\psi_y}{\partial x\partial y\partial z}\right. \qquad (5.4.20b)$$

$$\left. + \frac{\partial}{\partial x}\left\{\frac{\partial^2}{\partial x^2} + \frac{\partial^2}{\partial y^2} + \frac{\partial^2}{\partial z^2}\right\}\psi_z\right\} = \frac{\partial\Delta\sigma_{\substack{zz\\z=1}}}{\partial y} = -\cot\alpha_0\frac{\partial\Delta z_s}{\partial y} .$$

At the datum base $z = 0$:

$$-c\frac{\partial\Delta z_b}{\partial x} + \frac{\partial\psi_y}{\partial x} - \frac{\partial\psi_x}{\partial y} = 0 , \qquad (5.4.21)$$

$$\frac{\partial\psi_z}{\partial y} - \frac{\partial\psi_y}{\partial z} + 2\Delta z_b = c\left[\tfrac{1}{2}\left\{\frac{\partial^2\psi_z}{\partial y\partial z} - \frac{\partial^2\psi_y}{\partial z^2} + \frac{\partial^2\psi_y}{\partial x^2} - \frac{\partial^2\psi_x}{\partial x\partial y}\right\} - \Delta z_b\right] , \qquad (5.4.22)$$

$$\frac{\partial\psi_x}{\partial z} - \frac{\partial\psi_z}{\partial x} = \tfrac{1}{2}c\left[-\frac{\partial^2\psi_z}{\partial x\partial z} + \frac{\partial^2\psi_x}{\partial z^2} + \frac{\partial^2\psi_y}{\partial x\partial y} - \frac{\partial^2\psi_x}{\partial y^2}\right] , \qquad (5.4.23)$$

As mentioned above it turns out that both (5.4.20a) and (5.4.20b) lead to the same equation for the determination of the constants A_i, B_i, C_i and D_i in the expression (5.4.11) for the stream function $\hat{\psi}_i$. The boundary conditions (5.4.18) to (5.4.23) therefore result in 6 independent equations for the determination of the constants. The expression of the boundary conditions as equations for A_i, B_i, C_i and D_i and the solution of the resulting equations is carried out in Appendix 3.

5.4.5 Ice flux divergence

The divergence of the ice flux perturbation $\vec{\nabla}\cdot\Delta\vec{q}$, appears in the steady state equation (5.2.11) for three-dimensional flow rather than the flux perturbation itself as was the case for the steady state equation for two-dimensional flow (4.3.30). Therefore, the divergence of the ice flux perturbation is the relevant property of the three-dimensional ice flow solution for the formation of steady state ice surface undulations.

The result of the derivation in Appendix 3 is an analytical expression (A3.2) for the Fourier transform of the divergence of the ice flux perturbation. This expression is given by

$$ik_x\Delta\hat{q}_x + ik_y\Delta\hat{q}_y = \frac{1}{k^2K}\left\{i(1+c)k^2k_x\Delta\hat{\sigma}_{\substack{xz\\z=1}} - k(H_c\sinh k - k)\Delta\hat{\sigma}_{\substack{zz\\z=1}}\right. \qquad (5.4.24)$$

$$\left. - ik^2k_x((1+c)H_c + (1+c+c^2k^2)\cosh k)\,\Delta\hat{z}_b\right\}$$

$$+ i(1+c)k_x\Delta\hat{z}_s ,$$

where $K(k)$, $H_c(k)$ and $H_s(k)$ are defined by (4.5.15), and $\Delta\hat{\sigma}_{\substack{xz\\z=1}} = \Delta\hat{z}_s$ and $\Delta\hat{\sigma}_{\substack{zz\\z=1}} = \cot\alpha_0(-\Delta\hat{z}_s)$.

5.4.6 Steady state ice surface undulations

The steady state equation (5.2.11) for three-dimensional flow states that the ice flux perturbation $\Delta\vec{q}$, in the absence of mass balance perturbations, must be divergence free.

Equation (5.4.24) for the Fourier transform of the divergence of the ice flux perturbation therefore determines the steady state transfer of bedrock undulations to the ice surface for three-dimensional Newtonian flow. The transfer function $t(k_x,k_y)$ determined from (5.2.11) and (5.4.24) is given by

$$t(k_x,k_y) = \frac{(1+c)H_c + (1+c+c^2k^2)\cosh k}{(1+c)(1+K) - ik(k/k_x)((H_c\sinh k - k)/k^3)\cot\alpha_0}\,, \qquad (5.4.25a)$$

where $K(k)$, $H_c(k)$ and $H_s(k)$ are defined by (4.5.15). From this expression for $t(k_x,k_y)$ the transfer amplitude $|t(k_x,k_y)|$ and the phase shift $\phi(k_x,k_y)$ are predicted to be

$$|t(k_x,k_y)| = \frac{(1+c)H_c + (1+c+c^2k^2)\cosh k}{((1+c)^2(1+K)^2 + ((H_c\sinh k - k)^2/(kk_x)^2)\cot^2\alpha_0)^{1/2}} \qquad (5.4.25b)$$

$$\tan\phi(k_x,k_y) = \frac{(H_c\sinh k - k)}{(1+c)(1+K)kk_x}\cot\alpha_0\,. \qquad (5.4.25c)$$

The transfer function for three-dimensional flow given by (5.4.25a), is, except for the factor (k/k_x) in the second term in the denominator, formally identical to the transfer function (4.5.23a) for two-dimensional flow. In the special case of two-dimensional flow (*i.e.* $k_y = 0$, $k_x = k$) the three-dimensional transfer function given by (5.4.25a) reduces to (4.5.23a).

The transfer function (5.4.25a) approaches the transfer function (5.3.6) predicted by the laminar flow approximation for $n = m = 1$ in the limit of long wavelengths, *i.e.* as $k_x,k_y \to 0$. The transfer function for longitudinal bedrock ridges, *i.e.* $t(k_x{=}0,k_y)$, is predicted to be equal to zero as expected from the analysis in subsection 5.2.7 and the discussion in subsection 5.3.4. Thus, the transfer function (5.4.25a) needs to be modified as discussed in subsection 5.3.4 for numerical computation of Green's functions.

The transfer function (5.4.25a) is in agreement with Reeh's (1987) results for the transfer of bedrock undulations to the surface for linear Newtonian rheology in the absence of basal sliding ($c = 0$). Reeh discusses the basal boundary conditions for non-zero basal sliding. He concludes that the sliding velocity for three-dimensional flow is ambiguous as a basal velocity vector satisfying the sliding boundary condition can be tangent to the bed for a whole one-parametric family of velocity components. This does

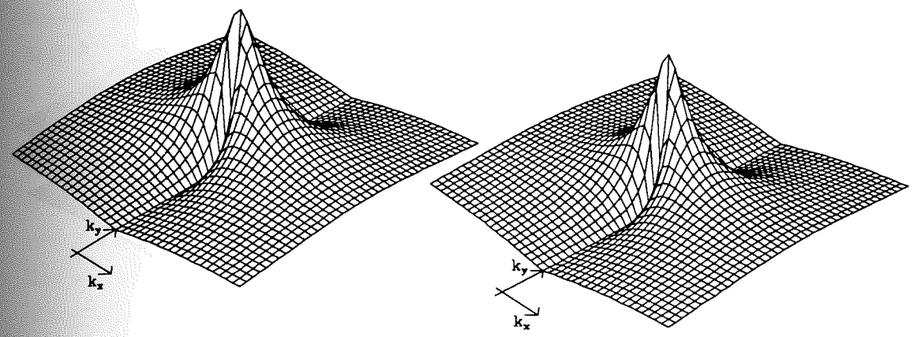

FIGURE 5.4.1: Perspective views of the transfer amplitude $|t(k_x,k_y)|$ predicted by linear Newtonian rheology (5.4.25b) as a function of k_x,k_y for no basal sliding ($c = 0$) (left) and non-zero basal sliding ($c = 2/3$) (right) and $\tan\alpha_0 = 0.05$. The perspective views show the area $-1 \le k_x,k_y \le 1$ with grid spacing $\Delta k_x = \Delta k_y = 0.05$. The height of the peak at the origin $k_x,k_y = 0$ is equal to 1.

not appear to be correct if one makes the assumption that the sliding velocity is parallel to the bed parallel shear stress as is done in the above analysis.

Figure 5.4.1 shows perspective views of the transfer amplitude $|t(k_x,k_y)|$ predicted by linear Newtonian rheology (5.4.25b) for no basal sliding ($c = 0$) (left) and non-zero basal sliding ($c = 2/3$) (right) and $\tan\alpha_0 = 0.05$. The value of the sliding parameter $c = 2/3$ corresponds to datum ice flow where the ice flux from basal sliding and internal deformation are equal. The figure shows that the narrow "valleys" in the transfer amplitude along the line $k_x = 0$ and the discontinuity at $k_x,k_y = 0$ are similar to Figure 5.3.1 for the laminar flow approximation. Close comparison of Figure 5.4.1 (left) with Figure 5.3.1 (left) shows that the solution of the full flow equations for linear Newtonian rheology predicts higher transfer amplitude for $|k_x| \gtrsim ½$ than the laminar flow approximation. This was to be expected from the two-dimensional analysis (*cf.* subsection 4.5.8) and leads to the formation of a standing wave in the space domain (see below). Similar comparison of the two perspective views in Figure 5.4.1 shows that the transfer amplitude is higher for non-zero basal sliding (right) than for no basal sliding (left) in the range

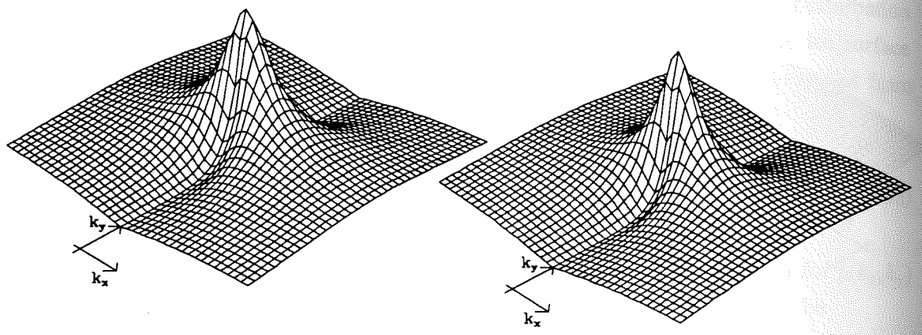

FIGURE 5.4.2: Same as Figure 5.4.1 except that the transfer amplitude is given by the modification $|t'(k_x,k_y)|$ defined by (5.3.12) corresponding to linear Newtonian rheology (5.4.25a).

$|k_x| \tilde{>} ½$. This is as expected from the two-dimensional analysis and leads to a higher amplitude of the standing wave for non-zero basal sliding (see below).

Figure 5.4.2 shows perspective views of the modified transfer amplitude $|t'(k_x,k_y)|$ given by (5.3.12) corresponding to linear Newtonian rheology (5.4.25a) for no basal sliding ($c = 0$) (left) and non-zero basal sliding ($c = 2/3$) (right) and $\tan\alpha_0 = 0.05$. The figure shows that the modified transfer amplitude is essentially identical to the unmodified transfer amplitude shown in Figure 5.4.1 except that the discontinuity at $k_x,k_y = 0$ has been eliminated. As in the case of the laminar flow approximation (*cf.* subsection 5.3.4) the effect of the modification is limited to the neighbourhood of the line $k_x = 0$ close to the origin.

The complex transfer function $t(k_x,k_y)$ for three-dimensional flow given by (5.4.25a) is considerably more difficult to interpret than the transfer function $t(k)$ for two-dimensional flow given by (4.5.23a), because $t(k_x,k_y)$ involves a two-dimensional field of transfer amplitude $|t(k_x,k_y)|$, and phase shift $\phi(k_x,k_y)$. It is easier to interpret the corresponding Green's function $g(x,y)$ (*cf.* subsection 3.3.4) as it is a real function and has the direct physical interpretation that it describes the steady state surface which is formed by ice flow over and around a sharp bedrock peak. The Green function $g(x,y)$,

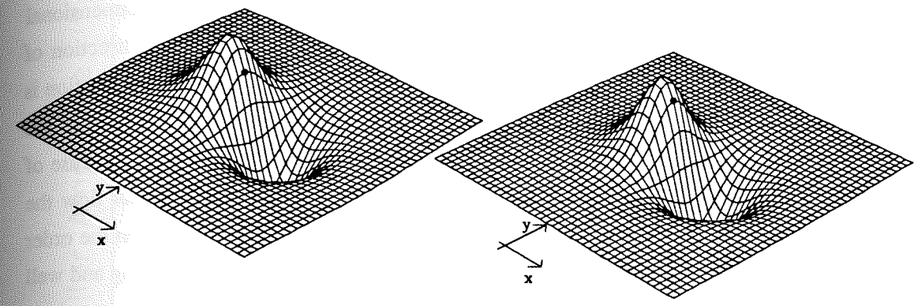

FIGURE 5.4.3: Perspective views of the Green's function $g(x,y)$ predicted by linear Newtonian rheology computed by numerical inversion of the modified transfer function $t'(k_x,k_y)$ given by (5.4.25a) and (5.3.12) for no basal sliding ($c = 0$) (left) and non-zero basal sliding ($c = 2/3$) (right) and $\tan\alpha_0 = 0.05$. The perspective views show the area $-2.5 \le x,y \le 2.5$ with grid spacing $\Delta x = \Delta y = 1/8$. The origin of the coordinate system (i.e. the location of the spike in the bedrock geometry) is indicated with a bullet sign (•). The vertical scaling of the figures is different. The height of the upstream peak is approximately equal to 0.084 in the figure to the left (no basal sliding) but 0.131 in the figure to the right (non-zero basal sliding).

corresponding to the transfer function $t(k_x,k_y)$, given by (5.4.25a), cannot be found directly by numerical inversion of $t(k_x,k_y)$ because of difficulties associated with the discontinuity in $t(k_x,k_y)$ at $k_x,k_y = 0$ as discussed in subsection 5.3.4. These difficulties are overcome by inverting the modified transfer function $t'(k_x,k_y)$ given by (5.3.12).

Figure 5.4.3 shows perspective views of the Green's function $g(x,y)$ predicted by linear Newtonian rheology computed numerically from the modified transfer function $t'(k_x,k_y)$ given by (5.4.25a) and (5.3.12) for no basal sliding ($c = 0$) (left) and non-zero basal sliding ($c = 2/3$) (right) and $\tan\alpha_0 = 0.05$. The figure shows a "standing wave" with a peak on the upstream side of the basal spike and a trough on the downstream side as was expected from the two-dimensional analysis in Chapter 4. Integration of the Green's function $g(x,y)$ along the y-direction is equal to the Green's function $g(x)$ for two-

dimensional flow and this is a good check of the correctness of the three-dimensional computations. The wavelength of the standing wave in Figure 5.4.3 in the direction of the ice flow is between 2 and 3 ice thicknesses and its width in the transverse direction is approximately 2 ice thicknesses. The wavelength of the standing wave is almost the same for non-zero basal sliding as for no basal sliding, but the amplitude for the case of non-zero basal sliding is approximately 50% higher. As for two-dimensional flow the effect of the standing waves is limited to an area with horizontal dimensions on the order of 2 - 3 ice thicknesses. Outside this area the Green's function is slowly varying and well approximated by the Green's function (5.3.8) predicted by the laminar flow approximation (see below), although this cannot be seen from Figure 5.4.3.

Figure 5.4.3 shows a much smaller area (5x5 ice thicknesses) than Figure 5.3.2 (40x40 ice thicknesses), which shows the Green's function predicted by the laminar flow approximation. Outside the area shown in Figure 5.4.3 the amplitude of the Green's functions is relatively low and the Green's functions are slowly varying with x and y. Figure 5.4.4 compares longitudinal and transverse sections through the Green's function $g(x,y)$ predicted by linear Newtonian rheology and computed from (5.4.25a) and (5.3.12) for no basal sliding ($c = 0$) (solid curves) with the analytical Greens function $g(x,y)$ predicted by the laminar flow approximation (5.3.8) (dashed curves). The figure shows that the Green's function predicted by laminar flow is a good approximation to the Green's function predicted by linear Newtonian rheology further away from the origin than approximately 1 - 2 ice thicknesses. Closer to the origin the standing wave in the Newtonian Green's function and the singularity at $x = y = 0$ in the laminar flow Green's function lead to differences between the two Green's functions.

Figure 5.4.5 is identical to Figure 5.4.4 except that the longitudinal and transverse sections are from Green's functions computed for non-zero basal sliding with $c = 2/3$. The figure shows that the amplitude of the standing wave is higher for non-zero basal sliding as was expected from the two-dimensional analysis. The wavelength and the width of the standing wave is approximately the same as for no basal sliding in Figure 5.4.4 and the Newtonian Green's function approaches the laminar flow Green's function at approximately the same distance from the origin as in Figure 5.4.4.

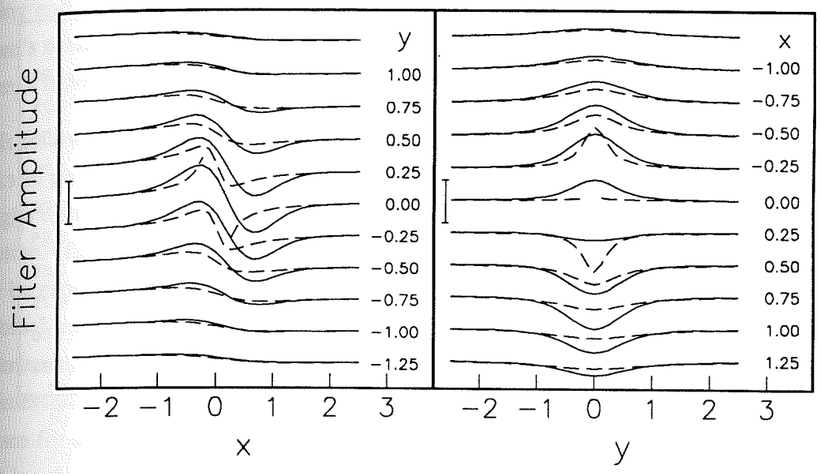

FIGURE 5.4.4: Longitudinal (left) and transverse (right) sections through the Green's function $g(x,y)$ predicted by linear Newtonian rheology for no basal sliding ($c = 0$) (solid curves) computed by numerical inversion of the modified transfer function $t'(k_x,k_y)$ given by (5.4.25a) and (5.3.12). The dashed curves show sections through the analytical Greens function $g(x,y)$ predicted by the laminar flow approximation and given by (5.3.8) for comparison. The sections are shifted vertically to differentiate them from each other. The y-values of the longitudinal sections and the x-values of the transverse sections are indicated to the right in the figures. The scale to the left in the figures indicates the filter amplitude 0.1. The sections through the laminar flow Green's function for $y = 0$ (left) and $x = 0$ (right) are broken at $x = y = 0$ because the Greens function is singular at $x = y = 0$.

Although transfer functions and Green's functions for three-dimensional flow in the case of non-linear rheology have not been computed, it is possible to infer some of their properties by analogy with the two-dimensional analysis in Chapter 4 and the above three-dimensional analysis. It is likely that a standing wave near the origin with a wavelength between 2 and 3 ice thicknesses is the most important feature in the Green's

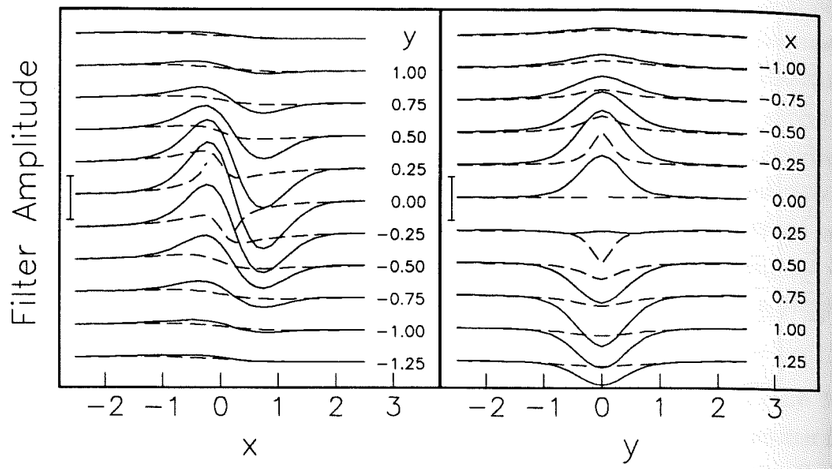

FIGURE 5.4.5: Same as Figure 5.4.4 except that the sections in this figure correspond to non-zero basal sliding with c = 2/3.

function for non-linear rheology for three-dimensional flow. Furthermore, the Green's function (5.3.8) predicted by the laminar flow approximation is likely to be a good approximation of the Green's function predicted by non-linear rheology further away from the origin than approximately 1 - 2 ice thicknesses. Non-zero basal sliding increases the relative importance of longitudinal stress gradients in two-dimensional ice flow in a way which is similar to the increased importance of longitudinal stress gradients caused by non-linear rheology. One of the results of the two-dimensional analysis is that non-zero basal sliding and non-linear rheology both tend to increase the amplitude of the standing wave in the Green's function without changing the its wavelength. The above three-dimensional analysis for linear Newtonian rheology finds that non-zero basal sliding increases the amplitude of the standing wave, but both the wavelength and the width of the standing wave are almost unaltered. This indicates that the wavelength and width of the standing wave in the Green's function for non-linar rheology are relatively constant, and close to the wavelength and width of the standing wave for linear Newtonian rheology. The amplitude of the standing wave, however, is likely to be variable depending on the flow law and sliding law powers n and m and the relative importance of basal

sliding and horizontal strain rate in the datum flow. This implies that the shape of the Green's functions shown in Figure 5.4.3 is indicative of the shape of the corresponding Green's functions for non-linear rheology.

It follows from the above discussion that the surface of ice caps flowing over sharp peaks in the bedrock geometry should have bulges on the upstream side of the peaks and troughs on their downstream side as a consequence of the standing wave in the Green's function. The horizontal extension of the peaks and troughs caused by the standing wave may be expected to be somewhat increased by the finite horizontal extension of peaks in the basal geometry of real ice caps, but it should nevertheless be on the order of 1 - 2 ice thicknesses, which implies an undulation wavelength on the order of 3 - 4 ice thicknesses. The standing wave will not have a noticeable effect on the steady state ice surface for smooth basal features with a horizontal extension greater than approximately 2 - 4 ice thicknesses. This description of the effect of the standing wave in the Green's function is consistent with observations of dominant ice surface features with wavelengths in the range 3 - 4 ice thicknesses and with the description of Zwally and others (1983) of the landscape of the Greenland ice sheet (*cf.* Chapter 2).

CHAPTER 6: TIME-DEPENDENT GLACIER FLOW

6.1 INTRODUCTION

This chapter develops a theory of time-dependent two-dimensional glacier flow over bedrock undulations in order to investigate whether some of the surface landscape of ice caps and glaciers could be a consequence of time-dependent adjustment of the ice flow to changes in the accumulation or ablation rather than a result of the bedrock topography. The main purpose of the theory is to establish a time-scale for the decay of non-steady features with a length-scale of a few ice thicknesses in the landscape of ice caps and glaciers. The theory will also shed some light on the time-dependent adjustment of glaciers to climate changes in general and on the propagation and diffusion of kinematic waves on glaciers.

Nye (1960, 1963a,b, 1965a,b) (see also Paterson (1981) and Hutter (1983)) developed a theory of time-dependent glacier flow based on a linearized treatment of ice motion. He derived the so-called (linearized) kinematic wave equation

$$\frac{\partial \Delta h}{\partial t} + \frac{\partial (C_0 \Delta h)}{\partial x} - \frac{\partial (D_0 (\partial \Delta h / \partial x))}{\partial x} = \Delta b \, . \tag{6.1.1}$$

This equation describes time-dependent evolution of the geometry of a glacier as a combination of propagation, with speed C_0, and diffusion, with diffusion coefficient D_0. Nye's kinematic wave equation is based on the formulation of the ice flux in terms of local ice thickness and surface slope, *i.e.*

$$q = q(h, \alpha) \, . \tag{6.1.2}$$

The kinematic wave velocity C_0, and the diffusion coefficient D_0, are defined as

$$C_0 = \left[\frac{\partial q}{\partial h} \right]_\alpha \, , \quad D_0 = \left[\frac{\partial q}{\partial \alpha} \right]_h \, . \tag{6.1.3}$$

The time-dependent thickness perturbation Δh is defined such that it arises from perturbations in the ice surface geometry only.

Nye's kinematic wave equation predicts that non-steady disturbances in the surface of glaciers should propagate with speed approximately equal to 3-5 times the speed of the ice motion. There are a number of observations of waves on glaciers propagating with approximately the speed predicted by the kinematic wave equation.

The propagation and diffusion of kinematic waves has been analyzed by several authors (for a review of research on this subject, see Hutter (1983)). Commonly, more emphasis is placed on propagation than diffusion of the waves. An example of this is the analysis of Fowler and Larson (1978, 1980) and Fowler (1982) who describe the formation of non-linear shock waves which are predicted by non-linear ice flow dynamics in the absence of a term that leads to the diffusion term in the linearized kinematic wave equation.

6.2 TIME-SCALES FOR GLACIER FLOW

A number of time-scales are involved in time-dependent glacier flow. The memory length or the adjustment time of the glacier $\tilde{\tau}_M$, is, perhaps, the most important of these time-scales. $\tilde{\tau}_M$ is defined to be the time constant in an exponential asymptotic approach to a final steady state after a sudden change in climate to a new constant climate. Jóhannesson and others (1989) derived an estimate of $\tilde{\tau}_M$ in terms of scales for the thickness of the glacier H, and the mass balance at the terminus $(-\tilde{b}_t)$. This estimate is

$$\tilde{\tau}_M = H / (-\tilde{b}_t) \, . \tag{6.2.1}$$

An expression of $\tilde{\tau}_M$ in the short scale non-dimensional notation (*cf.* subsection 4.3.2) is required for the following discussion. For this purpose, assume that $(-\tilde{b}_t)$ can be used as a scale for the mass balance distribution over the area of the glacier and let L be a scale for the horizontal dimensions of the glacier. Then $(-\tilde{b}_t)L/H$ is a scale for the longitudinal velocity $\tilde{u}$ by the equation of continuity. The length-scale $\tilde{h}_0$ in the short scale formulation of the ice flow equations (*cf.* subsection 4.3.2) will be approximately equal to H. This makes is possible to write the non-dimensional memory length τ_M, in the short scale notation, as

$$\tau_M = O(\delta^{-1}) \, , \tag{6.2.2}$$

where $\delta = H/L \ll 1$ is the small ratio of the ice thickness to the horizontal dimensions of

the glacier. This ratio may be roughly estimated as $\delta = O(10^{-2})$. This implies that the time-scale $\tilde{t}_0$ in the short scale formulation is much shorter than the memory length or the adjustment time $\tilde{\tau}_M$ of the glacier as a whole. This was previously mentioned in subsection 4.3.2.

Jóhannesson and others (1989) defined the time-scales $\tilde{\tau}_C$ and $\tilde{\tau}_D$ as the respective times that are needed to propagate or diffuse a disturbance over the full length of the glacier. These time-scales turn out to be shorter than $\tilde{\tau}_M$.

6.3 MODIFIED KINEMATIC WAVE EQUATION

The filter theory, which was developed in Chapter 4, can be used to derive a modified version of the (linearized) kinematic wave equation that takes the effect of longitudinal stress gradients on the flow into account. This equation follows from (4.3.23), (4.3.27), (4.6.15), (4.6.16), (4.6.20) and (4.6.22) and is given by

$$\frac{\partial \Delta z_s}{\partial t} + \frac{\partial}{\partial x}\left[g_e*(\Delta z_s + 2(\partial \Delta z_s/\partial x)\,|e|^{1/n}\mathrm{sign}(e)) + u_{0\,z=1}\,\Delta z_s - \cot\alpha_0 g_n*(\partial \Delta z_s/\partial x)\right] = \frac{\partial (g_b*\Delta z_b)}{\partial x} + \Delta b\,. \tag{6.3.1}$$

For the purpose of the following discussion, it will be assumed that the datum geometry of the glacier is slowly varying in x so that this equation can be considered valid, with the same filters g_e, g_n and g_b, for the entire x-axis. In the absence of time variation, *i.e.* when $(\partial \Delta z_s/\partial t) = 0$, and when $\Delta b = 0$, this equation reduces to the two-dimensional steady state equation (4.7.1). Apart from the term involving Δz_b on the right hand side of (6.3.1), the main difference between (6.3.1) and the traditional kinematic wave equation (6.1.1) is that multiplication with the kinematic wave velocity C_0, and the diffusion coefficient D_0, has been partly replaced by convolutions with the filters g_e and g_n.

It is easier to understand the difference between (6.3.1) and the traditional kinematic wave equation (6.1.1) by transforming (6.3.1) into the wave number domain. The wave number representation of (6.3.1) is

$$\frac{\partial \Delta \hat{z}_s}{\partial t} + (ikC_0(k) + k^2 D_0(k))\Delta \hat{z}_s = ik\hat{g}_b \Delta \hat{z}_b + \Delta \hat{b}\,, \tag{6.3.2}$$

where the wave number dependent kinematic wave velocity $C_0(k)$, and diffusion coefficient $D_0(k)$, are defined as the real and imaginary parts of the factor that multiplies $\Delta \hat{z}_s$ in the Fourier transform of (6.3.1), divided by ik and k^2, respectively. This definition of $C_0(k)$ and $D_0(k)$ gives

$$C_0(k) = Re(\hat{g}_e(k)) + u_{0\,z=1} - 2k\,|e|^{1/n}\mathrm{sign}(e)Im(\hat{g}_e(k)) \approx Re(\hat{g}_e(k)) + u_{0\,z=1} \tag{6.3.3}$$

and

$$D_0(k) = \cot\alpha_0 \hat{g}_n(k) - k^{-1} Im(\hat{g}_e(k)) - 2|e|^{1/n}\mathrm{sign}(e)Re(\hat{g}_e(k)) \approx \cot\alpha_0 \hat{g}_n(k)\,. \tag{6.3.4}$$

The reason for this definition of $C_0(k)$ and $D_0(k)$ is that a harmonic variation in Δz_s with a wave number k will propagate and diffuse with a wave velocity and diffusion coefficient given by (6.3.3) and (6.3.4). The filter theory of Chapter 4 thus predicts a wave number or wavelength dependent kinematic wave velocity and diffusion coefficient. The idea of a wavelength dependent kinematic wave velocity and diffusion coefficient for glacier waves was first introduced by Langdon and Raymond (1978) who based their analysis on numerical computations of the propagation and diffusion of harmonic surface undulations with different wavelengths. The notation $Re(\hat{g}_e(k))$ and $Im(\hat{g}_e(k))$ in (6.3.3) and (6.3.4) refers to the real and imaginary parts of $\hat{g}_e(k)$. The imaginary part of $\hat{g}_n(k)$ is zero and therefore does not have to be considered. The approximations on the far right of (6.3.3) and (6.3.4) arise because $|e|$ and $Im(\hat{g}_e(k))$ are relatively small and $\cot\alpha_0$ is large for the low slopes which are observed on ice caps and glaciers. The error associated with the approximations is hardly noticeable on plots of $C_0(k)$ and $D_0(k)$.

Figure 6.3.1 shows how the kinematic wave velocity $C_0(\lambda)/C_0(\lambda{=}\infty)$, given by the approximation on the far right of (6.3.3), depends on the wavelength $\lambda = 2\pi/k$ for $n = m = 1$, $c = 0$, 2/3 and $n = 3$, $e = 0.01$, $m = 2$, $c = 0$, 0.4. The figure shows that $C_0(\lambda)$ decreases with wavelength and that it has decreased substantially when $\lambda \approx 10$ for $n = 1$ and $\lambda \approx 30$ for $n = 3$. These wavelengths are approximately equal to the transition wavelength $\lambda = 2\pi l_g$ between the long and intermediate length-scales (*cf.* subsection 4.6.8). The transition between the short and intermediate scales is associated with

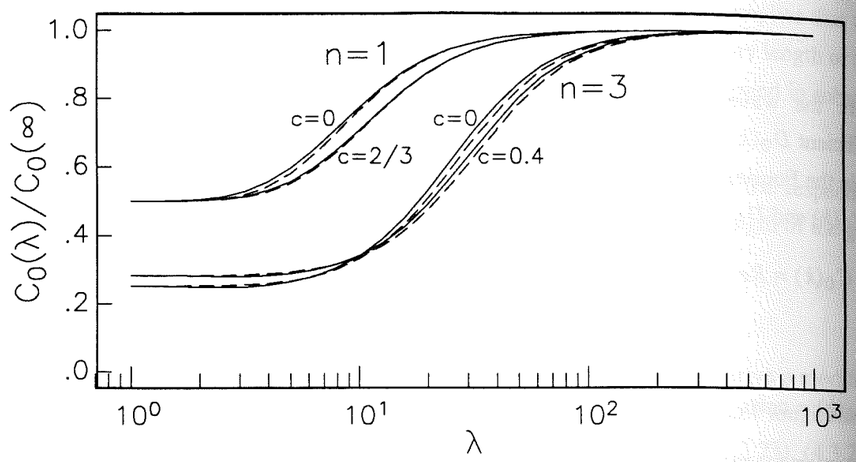

FIGURE 6.3.1: Kinematic wave velocity $C_0(\lambda)/C_0(\lambda=\infty)$, given by the approximation on the far right of (6.3.3), for $n = m = 1$, $c = 0, 2/3$ and $n = 3$, $e = 0.01$, $m = 2$, $c = 0, 0.4$. Dashed curves show the results of the simplified analysis described in subsection 4.6.8.

longitudinal stress gradients and thus the decrease in $C_0(\lambda)$ with decreasing wavelength is caused by the increasing importance of longitudinal stress gradients with decreasing wavelength. The decrease in $C_0(\lambda)$ occurs at slightly longer wavelengths for non-zero basal sliding ($c \neq 0$) than for no basal sliding ($c = 0$) because the range of longitudinal stress gradients increases with increasing basal sliding. The limit of $C_0(\lambda)$ as $\lambda \to 0$ is given by $\lim_{\lambda \to 0} C_0(\lambda) = u_{0\,z=1}$. This means that non-steady short wavelength undulations are predicted to propagate with a velocity almost equal to the datum velocity at the ice surface, *i.e.* they are carried along with the ice.

Figure 6.3.2 shows how the diffusion coefficient $D_0(\lambda)/D_0(\lambda=\infty)$, given by the approximation on the far right of (6.3.4), depends on the wavelength $\lambda = 2\pi/k$ for the same parameters as in Figure 6.3.1. The figure shows that $D_0(\lambda)$ starts decreasing with wavelength at approximately the same wavelengths as $C_0(\lambda)$. The decrease in $D_0(\lambda)$ is also caused by longitudinal stress gradients. The decrease in $D_0(\lambda)$ occurs at slightly

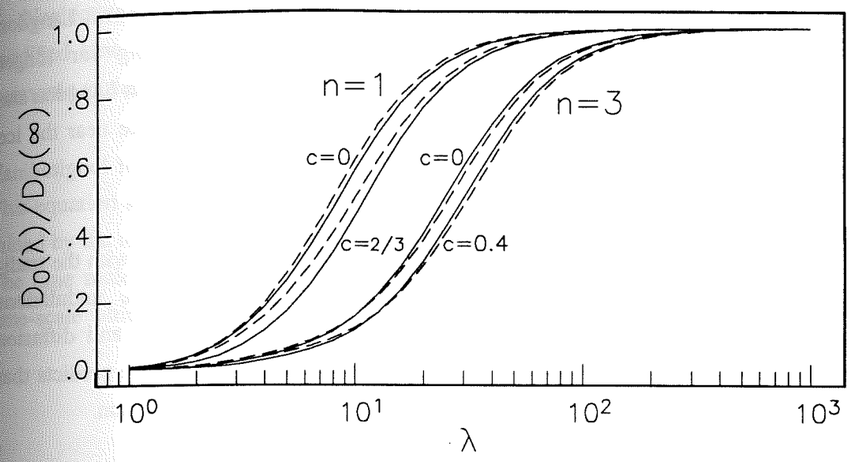

FIGURE 6.3.2: Diffusion coefficient $D_0(\lambda)/D_0(\lambda=\infty)$, given by the approximation on the far right of (6.3.4), for $n = m = 1$, $c = 0, 2/3$ and $n = 3$, $e = 0.01$, $m = 2$, $c = 0, 0.4$. Dashed curves show the results of the simplified analysis described in subsection 4.6.8.

longer wavelengths for non-zero basal sliding compared to no basal sliding as was observed for $C_0(\lambda)$. $D_0(\lambda)$ decreases to zero as $\lambda \to 0$ in contrast to $C_0(\lambda)$ which approaches the limit $u_{0\,z=1}$. This implies that the diffusion at the shortest wavelengths is very much reduced compared to the diffusion predicted by the traditional kinematic wave equation (6.1.1).

Figures 6.3.1 and 6.3.2 also show $C_0(\lambda)$ and $D_0(\lambda)$ predicted by the simplified filter theory which is described in subsection 4.6.8 (dashed curves). The figures show that the simplified filter theory reproduces the wavelength dependence of $C_0(\lambda)$ and $D_0(\lambda)$ fairly well, both for linear ($n = 1$) and non-linear ($n = 3$) rheologies.

Langdon and Raymond (1978) used numerical finite element computations to analyze the effect of longitudinal stress gradients on time-dependent glacier flow. They computed $C_0(\lambda)$ and $D_0(\lambda)$ numerically with a finite element model and obtained results that

are in agreement with the curves shown in Figures 6.3.1 and 6.3.2, except that Langdon and Raymond's $C_0(\lambda)$ and $D_0(\lambda)$ curves for $n = 3$ start decreasing for longer wavelengths. This is because there was no datum longitudinal strain rate in Langdon and Raymond's computations, *i.e.* they assumed $e = 0$. This leads to stiffer ice near the ice surface in the finite element computations and consequently the range of longitudinal stress gradients is longer.

Summarizing, the filter theory developed in Chapter 4 is in agreement with the traditional kinematic wave theory for long wavelength non-steady surface undulations ($\lambda > 2\pi l_s$). For shorter wavelengths both the kinematic wave velocity and diffusion coefficient are predicted to decrease and in the limit $\lambda \rightarrow 0$ the filter theory predicts that non-steady surface undulations are carried along with the ice without diffusion.

6.4 DIFFUSION TIME-SCALE

The purpose of the time-dependent analysis is to estimate the life time of non-steady disturbances in the surface geometry of an ice cap or glacier, which are relatively short compared to the length of the glacier. The memory length or the adjustment time of the glacier as a whole τ_M, defined in (6.2.2), is very long in the short scale variables, *i.e.* $\tau_M = O(\delta^{-1}) \gg 1$. Similarly, the propagation and diffusion time scales τ_C and τ_D defined by Jóhannesson and others (1989) turn out to be long in the short scale variables, because these time-scales are defined for long disturbances with length-scales on the order of the length of the glacier. The traditional kinematic wave equation (6.1.1) predicts that short disturbances should decay much faster by diffusion than longer disturbances. The modified kinematic wave equation (6.3.1) or (6.3.2), however, predicts a wave number or wavelength dependent diffusion coefficient $D_0(k)$ which decays rapidly with decreasing wavelength, (*cf.* Figure 6.3.2). The time-scale of the diffusive decay of relatively short non-steady disturbances with wavelengths on the order of a few ice thicknesses is therefore not clear *a priori*. If this time-scale is on the order of 1 time unit in the short scale variables, then such disturbances will decay rapidly compared to the adjustment time of the ice cap or glacier. This would be in agreement with Nye's (1959c) prediction, which was discussed in section 2.2, that non-steady surface features of the Antarctic ice sheet with length-scales on the order of several ice thicknesses would decay away by diffusion on a time-scale on the order of months.

Neglecting the effect of a non-steady mass balance perturbation Δb for simplicity, the modified kinematic wave equation (6.3.2) predicts that the amplitude of a non-steady harmonic variation in Δz_s with a wave number k decays according to

$$|\Delta z_s| = |\Delta z_s|_{t=0} e^{-k^2 D_0(k) t} = |\Delta z_s|_{t=0} e^{-t/\tau_D(k)} . \tag{6.4.1}$$

This equation applies to non-steady deviations of Δz_s from the steady state shape determined by the term involving the bedrock landscape Δz_b on the right hand side of (6.3.2). The time scale $\tau_D(k)$ in (6.4.1) is a wave number or wavelength dependent diffusion time-scale which is given by

$$\tau_D(k) = \frac{1}{k^2 D_0(k)} \approx \frac{\tan\alpha_0}{k^2 \hat{g}_n(k)} = \frac{\lambda^2 \tan\alpha_0}{(2\pi)^2 \hat{g}_n(k = 2\pi/\lambda)} \tag{6.4.2}$$

If a non-steady harmonic mass balance perturbation Δb with a wave number k is present in (6.3.1) or (6.3.2), then the time-scale $\tau_D(k)$ gives the time span over which a change in the mass balance affects the geometry of the glacier.

The time-scale $\tau_D(\lambda = 2\pi/k)$ can be computed from the curves of $D_0(\lambda)/D_0(\lambda = \infty)$ shown in Figure 6.3.2. For $\tan\alpha_0 < 0.05$, which is reasonable for most ice caps and many glaciers, and for wavelengths in the range $2 < \lambda < 20$ ice thicknesses, it turns out that $\tau_D(\lambda) \tilde{<} 1$; for wavelengths in the range $1\text{–}1.5 < \lambda < 30$ ice thicknesses $\tau_D(\lambda) \tilde{<} 2$. For higher slopes $\tan\alpha_0 < 0.2$ and wavelengths in the range $2 < \lambda < 20$ ice thicknesses, the time-scale satisfies $\tau_D(\lambda) \tilde{<} 4$, but for lower slopes $\tau_D(\lambda)$ can become much smaller than 1 in this wavelength range. The above estimates are valid for both linear ($n = 1$) and non-linear ($n = 3$) rheologies, with and without basal sliding. They are computed for $e = 0.01$, but essentially the same estimates are valid for the entire range $0.001 < |e| < 0.1$. Only for wavelengths shorter that 1 ice thickness do the longitudinal stress gradients lead to diffusion which is slow in the short scale time variable. This means that diffusion of non-steady surface features and mass balance variations takes place on a time-scale on the order of 1 time unit or less in the short scale time variable for all wavelengths which are of interest for the formation of glacier landscape, even when longitudinal stress gradients are taken into account. This conclusion is in accordance with Nye's (1959c) prediction which was mentioned earlier. It is also in accordance with the analysis of Jóhannesson and others (1989) who concluded that

perturbations in ice thickness spread out rather quickly over the glacier length by propagation and diffusion in comparison with the full adjustment time-scale.

The adjustment time of temperate ice caps and glaciers is on the order of $10^1 - 10^2$ years (Jóhannesson and others, 1989). By the above discussion, the ratio of the diffusion time-scale to the adjustment time is $\tau_D(k)/\tau_M = O(\delta) = O(10^{-2})$ for wavelengths in the range $1–2 < \lambda < 20–30$ ice thicknesses. Therefore, the time scale for the decay of non-steady surface features, for wavelengths that are of interest for the formation of glacier landscape, is on the order of a few months to a year. A similar estimate (*i.e.* a diffusion time-scale on the order of a year for $1–2 < \lambda < 20–30$ ice thicknesses) holds true for cold ice sheets because of the low surface slopes which are typically found on ice sheets. Assuming that the modified kinematic wave equation (6.3.1) and (6.3.2) is a valid model of glacier flow, this implies that observed glacier landscape with wavelengths in the range $1–2 < \lambda < 20–30$ ice thicknesses, cannot be a consequence of non-steady ice flow or non-steady mass balance variations. The effect of steady mass-balance variations on glacier landscape was found to be relatively small in subsection 4.7.8, except possibly in the vicinity of ice divides. Glacier landscape must therefore in general be a result of bedrock topography, except where conditions that are not described by (6.3.1) and (6.3.2) are important (*e.g.* surges, variable basal sliding). This conclusion has important consequences for kinematic waves in the wavelength range $1–2 < \lambda < 20–30$ ice thicknesses. They are predicted to decay away on a time-scale of a few months to a year, which does not give them time to propagate very far. The propagation and diffusion of kinematic waves is discussed in more detail in the next section.

The diffusive decay predicted by the traditional kinematic wave equation (6.1.1), which does not take longitudinal stress gradients into account, is much faster for short and intermediate wavelengths than the decay predicted by the modified kinematic wave equations (6.3.1). For $\tan\alpha_0 < 0.05$, the traditional kinematic wave equation predicts $\tau_D(\lambda) \tilde{<} 0.1$ for $\lambda < 2\pi$ ice thicknesses and $\tau_D(\lambda) \tilde{<} 0.01$ for $\lambda < 2$ ice thicknesses, both for linear and non-linear rheologies, with and without basal sliding. For $\tan\alpha_0 < 0.05$, the traditional kinematic wave equation, therefore, predicts that non-steady surface features on temperate ice caps and glaciers with wavelengths shorter than approximately ten ice thicknesses should disappear on a time-scale of weeks or months and features

with wavelengths shorter that two ice thicknesses are predicted to disappear in a few days!

6.5 RELATIVE IMPORTANCE OF PROPAGATION AND DIFFUSION

The diffusion time-scale τ_D defined by (6.4.2) predicts strong diffusion of kinematic waves and the question arises how far the waves can propagate before they disappear. The relative importance of propagation and diffusion predicted by $C_0(k)$ and $D_0(k)$ as defined by (6.3.3) and (6.3.4) can be quantified by the defining a wave number or wavelength dependent parameter $Q(k)$ as the ratio of the real and imaginary parts of the factor that multiplies $\Delta\hat{z}_s$ in (6.3.2).

$$Q(k) = \frac{C_0(k)}{kD_0(k)} \approx \frac{Re(\hat{g}_e(k)) + u_0\big|_{z=1}}{k\cot\alpha_0 \hat{g}_n(k)} = \tan\alpha_0 \frac{Re(\hat{g}_e(k)) + u_0\big|_{z=1}}{k\hat{g}_n(k)} . \qquad (6.5.1)$$

This definition is somewhat analogous to the definition of the "quality factor" in oscillating system, for example in seismology to describe the attenuation of seismic waves (Stacey, 1977; Garland, 1979).

The "quality factor" Q has several equivalent definitions in seismology. It may be defined as the ratio of the real and imaginary parts of the elastic modulus which is then defined as a complex quantity. This definition is analogous to (6.5.1). For small attenuation an equivalent definition is to define $2\pi/Q$ to be equal to the relative energy attenuation over a full cycle in a propagating wave. The energy or the amplitude squared of Δz_s in (6.3.1) and (6.3.2) has no physical meaning and therefore the above definition of Q for glacier waves is based on the amplitude rather than on the amplitude squared.

Let the angular frequency of a harmonic undulation in Δz_s with wave number k be defined as $\omega = kC_0(k)$. The decay in the amplitude of Δz_s predicted by (6.3.2) is then given by

$$|\Delta z_s| = |\Delta z_s|_{t=0} e^{-\omega t/Q(k)} . \qquad (6.5.2)$$

This equation implies that during the propagation of the undulation by one wavelength (*i.e.* when ωt changes by 2π) the amplitude is reduced by the factor $e^{2\pi/Q(k)}$.

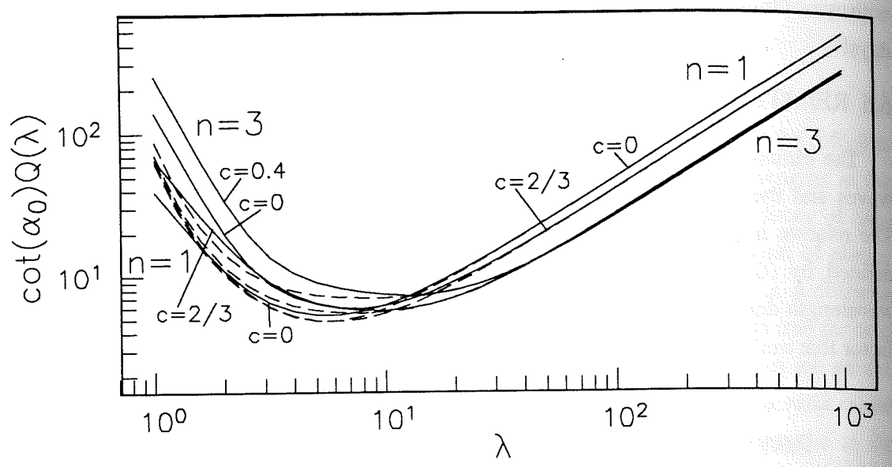

FIGURE 6.5.1: The parameter $Q(\lambda)$ ("quality factor"), given by the approximation on the far right of (6.5.1), for $n = m = 1$, $c = 0$, 2/3 and $n = 3$, $e = 0.01$, $m = 2$, $c = 0$, 0.4. Dashed curves show the results of the simplified analysis described in subsection 4.6.8.

Figure 6.5.1 shows how the parameter $Q(\lambda)$, given by the approximation on the far right of (6.5.1), depends on the wavelength $\lambda = 2\pi/k$ for the same parameters as in Figures 6.3.1 and 6.3.2. The figure shows $\cot\alpha_0 Q(\lambda)$ rather than $Q(\lambda)$ itself because $\tan\alpha_0$ only appears as a multiplying factor on the far right of (6.5.1). The curves in the figure can be multiplied by $\tan\alpha_0$ to yield $Q(\lambda)$ for any value of the datum surface slope α_0. The figure shows that Q reaches a minimum for $\lambda \approx 10$. Q values in a relatively wide range of wavelengths around this minimum are very low. For $\tan\alpha_0 < 0.05$, and wavelengths in the range $3 < \lambda < 40$ ice thicknesses, the curves in Figure 6.5.1 lead to $Q \tilde{<} 1$; for wavelengths in the range $2 < \lambda < 100$ ice thicknesses $Q \tilde{<} \pi$. These estimates are valid for both linear ($n = 1$) and non-linear ($n = 3$) rheologies, with and without basal sliding. The estimates are not sensitive to the value of e as they are valid for the entire range $0.001 < |e| < 0.1$. In the narrower wavelength range $3 < \lambda < 40$ the amplitude of a wave will be reduced by a factor of more than $e^{2\pi} \approx 500$ before it has propagated one wavelength. In the wider range $2 < \lambda < 100$ the amplitude of the wave will be reduced

by a factor of $e^2 \approx 7$ before it has propagated one wavelength. These factors become correspondingly larger for $\tan\alpha_0$ lower than 0.05. Even in the case of relatively steep glaciers, *e.g.* for $\tan\alpha_0$ less than 0.3, Q values for wavelengths in the range $3 < \lambda < 40$ ice thicknesses will satisfy $Q \tilde{<} 2\pi$, and the amplitude of a wave will be reduced by a factor of $e^1 \approx 3$ before it has propagated one wavelength. Waves can hardly be said to propagate in any real sense for such low values of Q. The diffusion slows down for higher or lower values of λ but for relatively low slopes ($\tan\alpha_0 \tilde{<} 0.02$) it is still high for $\lambda \approx 1$.

The Q values predicted by the traditional kinematic wave equation (6.1.1), which does not take longitudinal stress gradients are taken into account, are extremely low for short wavelengths. For $\tan\alpha_0 < 0.05$ and $\lambda < 4$, the traditional kinematic wave equation predicts $Q(\lambda) \tilde{<} 0.1$, both for linear and non-linear rheologies, with and without basal sliding. This corresponds to a reduction in the amplitude of a harmonic wave by a factor of $e^{20\pi} = 2 \cdot 10^{27}$ before it has propagated one wavelength!

Figure 6.5.1 also shows $Q(\lambda)$ as predicted by the simplified filter theory described in subsection 4.6.8 (dashed curves). There is some discrepancy between the simplified theory and the correct curves below $\lambda \tilde{<} 10$, especially for non-linear rheology ($n = 3$).

6.6 DIFFUSION OF WAVE OGIVES

Wave ogives are transverse ice surface undulations which are formed below ice falls on some alpine glaciers (Nye, 1958; Waddington, 1986). The undulations form at the rate of one per year and they are observed to travel downglacier with the surface velocity of the ice. The amplitude of the waves, which is initially on the order of 10 *m*, is usually observed to decay downglacier so that often only 10-20 waves are seen. The decay of the amplitude has been attributed to differential ablation (ablation on the wave crests is sometimes higher than in the troughs) and to diffusion of the waves by differential ice motion (the crests "sink" into the surrounding ice). For a review of previous research on wave ogives, see Waddington (1986).

The formation of wave ogives cannot be analyzed by the linearized filter theory developed in Chapter 4 because the waves are formed as the ice flows through ice falls where the assumption of slowly varying datum flow is not fulfilled. The theory is not

particularly suitable for analyzing the propagation and diffusion of wave ogives below the ice fall after they are formed because longitudinal gradients in the ice flow are typically relatively high below ice falls. However, it is interesting to see whether the strong diffusion of surface undulations predicted by the theory is compatible with observations of wave ogives in a qualitative sense. If the theory predicts that wave ogives should disappear much more rapidly than observed then that would indicate a failure of the theory at short wavelengths although the theory as such is not suitable for detailed quantitative analysis of wave ogives.

The propagation and diffusion of wave ogives can be discussed on the basis of the wavelength or wave number dependent kinematic wave velocity and diffusion coefficient which are defined by (6.3.3) and (6.3.4). The filter theory in its present form is based on two-dimensional ice flow and it does not take three-dimensional effects on the flow of valley glaciers into account (*cf.* Nye, 1965c). The effect of the finite transverse width of valley glaciers is therefore ignored in the discussion below.

The wavelength of wave ogives is equal to the distance that the ice at the ice surface travels in one year. This distance can be roughly estimated from (3.7.2) which predicts a velocity difference between the bed and the ice surface equal to $\tilde{u}_0(\tilde{z}=\tilde{z}_s) - \tilde{u}_0(\tilde{z}=\tilde{z}_b) = (2h_0/(n+1))(\tilde{\tau}_b/B)^n$, where $\tilde{\tau}_b$ is the basal shear stress and $B \approx 1.8 bar\, a^{1/3}$ and $n \approx 3$ are parameters in Glen's flow law (*cf.* subsection 3.4.3). Estimating $\tilde{\tau}_b$ as 0.5-1.5 *bar* (*cf.* Paterson (1981)) and assuming that the sliding velocity $\tilde{u}_0(\tilde{z}=\tilde{z}_b)$, is not much higher than the velocity difference $\tilde{u}_0(\tilde{z}=\tilde{z}_s) - \tilde{u}_0(\tilde{z}=\tilde{z}_b)$, one finds that the wavelength of wave ogives is on the order of one ice thickness or shorter. Equation (6.3.3) and Figure 6.3.1 show that surface undulations with wavelengths on the order of one ice thickness are predicted to propagate with the surface velocity of the ice $u_{0\,z=1}$. This is in accordance with observations of the propagation of wave ogives.

The diffusion of wave ogives is described by (6.5.1) and (6.5.2). As discussed above, undulations with wavelengths in the range 3 to 40 ice thicknesses should decay so rapidly by diffusion ($Q(\lambda) \lesssim 2\pi$ for $\tan\alpha_0 < 0.3$) that they essentially disappear before they have

propagated one wavelength. This conclusion does not apply to wavelengths shorter than 2-3 ice thicknesses, especially not for steep glaciers. Figure 6.5.1 shows that the parameter $Q(\lambda)$ increases rapidly with decreasing wavelength for wavelengths shorter than a few ice thicknesses (note the logarithmic scale for Q in the figure). Figure 6.5.1 is based on $e = 0.01$ which is too low for a discussion of wave ogives as they are often observed in areas of strong compression below the ice fall. Therefore, the value $e = 0.1$ will also be used in the discussion below.

The diffusion of wave ogives is sensitive to the datum slope of the ice surface α_0, because $\tan\alpha_0$ appears as a multiplying factor in (6.5.1) which defines the parameter $Q(k)$. Values of $\tan\alpha_0$ in the range 0.1 to 0.25 will be used below based on observations of wave ogives on Austerdalsbreen, Norway (λ in the range 75 to 240 *m*; $\tan\alpha_0 \approx 0.25$ (Nye, 1959a)) and on the glaciers Morsárjökull ($\lambda \approx 130$ *m*), Kvíárjökull ($\lambda \approx 150$ *m*) and Fjallsjökull ($\lambda \approx 215$ *m*) in Vatnajökull, Iceland (Thórarinsson, 1952, 1953) for which $\tan\alpha_0 \approx 0.1$ is a rough estimate. For non-linear rheology ($n = 3$), $0.01 < |e| < 0.1$ and $0.1 < \tan\alpha_0 < 0.25$, $Q(\lambda=1) \approx 5$–35 in the case of no basal sliding ($c = 0$) and $Q(\lambda=1) \approx 9$–62 in the case of non-zero basal sliding ($c = 0.4$). The above values of Q allow an undulation to propagate between 2 and 20 wavelengths before its amplitude is reduced by e^{-2}, depending mainly on $\tan\alpha_0$ and the relative importance of basal sliding. Shorter undulations can propagate much further and waves with wavelengths shorter than ½ ice thickness can propagate on the order of 30-100 wavelengths before their amplitude is reduced by e^{-2} for $\tan\alpha_0 = 0.25$. Values of $Q(\lambda)$ for longer wavelengths are lower; $Q(\lambda=2) \approx 1$–5 and 2-9 for no basal sliding and non-zero basal sliding, respectively, which corresponds to propagation of less than 3 wavelengths. Wave ogives with wavelengths on the order of one ice thickness or shorter, which is a reasonable estimate a discussed above, are therefore compatible with the theory. Ogives with wavelengths significantly longer than one ice thickness are, however, not compatible with the theory, except for very steep glaciers.

The predicted values of the parameter Q seem to be somewhat too low in the case of the well known wave ogives on Austerdalsbreen, Norway, which were analyzed by Nye (1958, 1959a). Seven or eight crests and troughs can be distinguished below an ice fall on Austerdalsbreen before the waves die away. There is considerable variation in the

undulation wavelength, the ice thickness and the surface slope, but $\lambda \simeq 2$–3 ice thicknesses and $\tan\alpha_0 \simeq 0.25$ can be used as rough estimates based on the figures in Nye's papers. This leads to $Q \tilde{<} 3$–5 if the parameters $e = 0.1$ and $c = 0{,}0.4$ are used. Q becomes higher if basal sliding is more important in the flow, but even for $c = 1.2$ (3/4 of the ice flow is transported by basal sliding) Q is predicted to be lower than approximately 9. Therefore, the wave ogives on Austerdalsbreen are predicted to die away over a distance of less than 1-3 wavelengths. The ice thickness in Nye's analysis (39 to 88 *m*) was calculated from measurements of the ice velocity and one measurement of the ice thickness below the ice fall. Later, the ice thickness has been measured by radio echo sounding (Laumann, personal communication) and found to be more than twice the thickness computed by Nye (the measured thickness is between 160 and 270 *m*). The wavelength of the wave ogives (75 to 240 *m*) relative to the ice thickness is thereby reduced by more than half to $\lambda \tilde{<} 1$ ice thickness and the parameter Q is estimated to be $Q \tilde{>} 13$–23 (again using $e = 0.1$ and $c = 0{,}0.4$). The amplitude of the wave ogives are therefore predicted to be reduced by e^{-2} after more than 4-8 wavelengths which is in reasonable agreement with observation.

In summary the filter theory of Chapter 4 predicts that diffusion of wave ogives is strongly wavelength dependent. The diffusion also depends on the datum slope (less diffusion for steep slopes) and to a lesser degree on the relative importance of basal sliding (less diffusion as basal sliding becomes more important). The above values of Q as a function of undulation wavelength relative to the ice thickness are of course not directly applicable to real valley glaciers with variable ice thickness across a valley cross section, but they indicate that the theory is not inconsistent with the existence of wave ogives on glaciers.

6.7 PROPAGATION OF KINEMATIC WAVES

The kinematic wave equation (6.1.1) has been used to explain observations of propagating waves on glaciers with a speed approximately equal to 3-5 times the speed of the ice motion. The rapid diffusion which is implied by both the traditional kinematic wave equation (6.1.1) and the modified kinematic wave equation (6.3.1), according to the arguments in sections 6.4 and 6.5, calls this explanation of the propagation of waves on glaciers into question. Waves with wavelengths in the range $3 < \lambda < 40$ ice thicknesses

decay so rapidly that there should be no possibility to observe or measure their propagation. The fact that such propagating waves have been observed on glaciers indicates that some physical process, not included in the derivation of kinematic wave equations (6.1.1) or (6.3.1), must be responsible for their propagation. One possibility is that time-dependent changes in the basal water system of the glacier drive the waves, but this will not be further discussed here.

The rapid diffusion of non-steady surface features, predicted by the analysis in the previous sections for $3 < \lambda < 40$ ice thicknesses, indicates that the kinematic wave equations (6.1.1) and (6.3.1) are first and foremost diffusive in nature. It seems that traditional interpretation of the kinematic wave equation (6.1.1) (*e.g.* Paterson 1981; Hutter, 1983) places much too great emphasis on the propagation of kinematic waves. It also seems difficult to justify the surface wave analysis of Fowler and Larson (1978, 1980) and Fowler (1982) who give the (assumed small) diffusion terms in the non-linear ice flow equations the role of defining the structure of propagating non-linear shock waves.

CHAPTER 7: LANDSCAPE OF HOFSJÖKULL

7.1 INTRODUCTION

In this chapter the theory that has been developed in the previous chapters is tested using digital maps of the surface and the bedrock of the Hofsjökull ice cap, Central Iceland. The two-dimensional theory of Chapter 4 is applied to surface and bedrock profiles along approximate flow lines, and the three-dimensional laminar flow theory of Chapter 5 is applied to digital maps of the surface and the bedrock. Finally, the implications of the tests are summarized and discussed.

The theoretical prediction of a "standing wave" in the steady state ice surface corresponding to a sharp peak in the bedrock landscape, is the most interesting result of the analysis in the previous chapters. Much of the following analysis of the data from Hofsjökull is therefore aimed at detecting the effect of the standing wave on the measured landscape of Hofsjökull.

7.2 HOFSJÖKULL

7.2.1 General

Hofsjökull is the third largest ice cap in Iceland with an area of 923 km^2 and a volume of 208 km^3 (Fig. 7.2.1). The surface and bed topography are well known from radio echo sounding and precision barometric altimetry (Björnsson, 1988). The mass balance of the ice cap is, however, relatively poorly known since regular monitoring of accumulation and ablation was not started until 1988.

7.2.2 Geometry

Hofsjökull covers a subglacial volcano, which reaches a maximum altitude of 1500-1600 m a.s.l. close to the center of the nearly circular ice cap. The maximum altitude of the ice surface is 1800 m a.s.l.. The altitude of the ice margin varies from about 900 m a.s.l. on the north side of the ice cap to between 600 and 700 m a.s.l. at the termini of the outlet glaciers that flow to the south. The lowest altitude of the ice margin is about 620 m a.s.l. at the terminus of the outlet glacier Múlajökull. The average thickness of the ice is 225 m. The ice flow is close to being radial from the center. Outside a

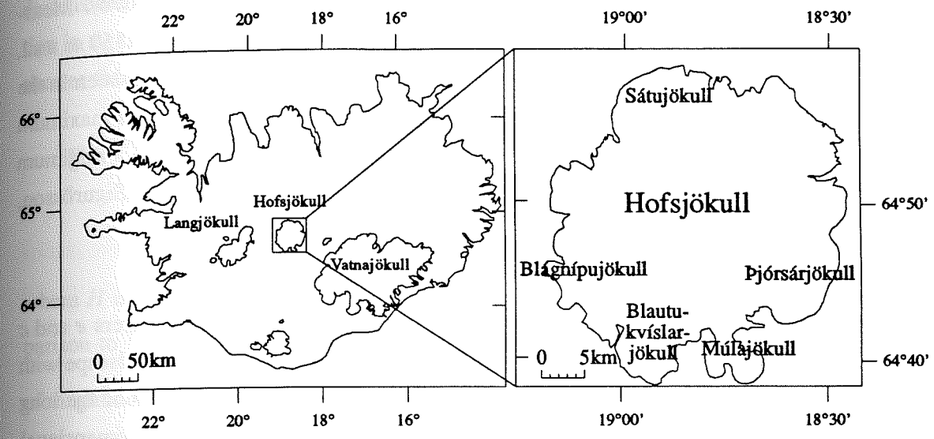

FIGURE 7.2.1: Map showing the location of the Hofsjökull ice cap in Iceland (left) and the location of the outlet glaciers of the ice cap which are mentioned in the text (right).

relatively flat area near the center and away from an ice divide to the northeast from the center, long scale surface slopes on Hofsjökull are typically in the range 0.04 - 0.1, although the slope becomes as high as 0.2 in a few areas.

Using L = 15–20 km as a horizontal scale and H = 200–300 m as a thickness or vertical scale for Hofsjökull, leads to the estimate δ = 0.01–0.02 of the small (dimensionless) ratio of the vertical to the horizontal dimensions of the ice cap (*cf.* subsection 4.2.2). This value of δ determines the accuracy of various approximations and simplifications which are used in the theoretical derivation in the previous chapters. An explicit value of δ is not needed in the following application of the theory to Hofsjökull.

7.2.3 Mass balance

Measurements of the termini of the outlet glaciers of Hofsjökull indicate that the ice cap has been relatively near an equilibrium (steady state) for the last decades (Sigurðsson, 1989a). Long term averages of accumulation and ablation are not available. Regular mass balance measurements were started on the outlet glacier Sátujökull (*cf.* Fig. 7.2.1) in 1988. The measurements are now performed on the outlet glaciers Þjórsárjökull

and Blágnípujökull (*cf.* Fig. 7.2.1) in addition to Sátujökull (Sigurðsson, 1989b). Measured equilibrium line altitudes since 1988 have been between 1000 and 1350 m a.s.l. (higher on the northern part of the ice cap) and the mass balance gradient has been in the range 0.007 to 0.011 $m_{ice}a^{-1}m^{-1}$. The measured mass balance ranges from a maximum on the order of 4 $m_{ice}a^{-1}$ at an altitude of 1800 m a.s.l. near the summit, to a minimum on the order of -4 $m_{ice}a^{-1}$ at 1000 m a.s.l. near the terminus of Sátujökull (Sigurðsson, personal communication).

7.2.4 Datum velocity and strain rate

The datum long scale velocity field determines the dimensionless parameters e and c which are required for the computation of short and medium scale glacier landscape with the theory developed in the previous chapters. The parameter e is the ratio of the long scale longitudinal (for two-dimensional datum flow) or effective (for three-dimensional datum flow) strain rate at the ice surface to the long scale shear strain rate at the bed (*cf.* subsections 4.3.4, 4.3.5 and 5.2.3). The parameter c represents the relative importance of basal sliding compared to internal deformation (*cf.* subsection 4.3.2).

No strain rate measurements and very few velocity measurements have been carried out on Hofsjökull. An order of magnitude estimate of e can be derived from relatively simple considerations, but c must be estimated from observations of basal sliding from other temperate glaciers.

The parameter $e = \tilde{\dot{\varepsilon}}_{0xx}(\tilde{z}=\tilde{z}_{s0})/\tilde{\dot{\varepsilon}}_{0xz}(\tilde{z}=\tilde{z}_{b0})$ can be estimated by deriving separate order of magnitude estimates for $\tilde{\dot{\varepsilon}}_{0xx}(\tilde{z}=\tilde{z}_{s0})$ and $\tilde{\dot{\varepsilon}}_{0xz}(\tilde{z}=\tilde{z}_{b0})$. $\tilde{\dot{\varepsilon}}_{0xx}$ is the longitudinal derivative of u_0. Going down a flow line, u_0 initially increases from zero at an ice divide (or the head of a glacier) to a maximum in the interior and then decreases to near zero at the ice margin. Ignoring depth variation in $\tilde{\dot{\varepsilon}}_{0xx}$, an order of magnitude estimate for $\tilde{\dot{\varepsilon}}_{0xx}(\tilde{z}=\tilde{z}_{s0})$ is therefore given by

$$\tilde{\dot{\varepsilon}}_{0xx}(\tilde{z}=\tilde{z}_{s0}) \approx U/(\tfrac{1}{2}L) ,$$

where U is a scale for the horizontal velocity and L is a scale for the horizontal

dimensions of the ice cap or glacier (the factor ½ in front of L arises because the variation in u_0 from a maximum to a minimum takes place over a distance which is somewhat shorter than L).

$\tilde{\dot{\varepsilon}}_{0xz}$ is (one half of) the vertical derivative of u_0 and it can by (4.3.20) be estimated as

$$\tilde{\dot{\varepsilon}}_{0xz}(\tilde{z}=\tilde{z}_{b0}) \approx (2/(n+1)+c)^{-1}U/H ,$$

where H is a scale for the ice thickness. Neglecting a factor of $2(2/(n+1)+c)$ in comparison to 1, the above estimates for $\tilde{\dot{\varepsilon}}_{0xx}(\tilde{z}=\tilde{z}_{s0})$ and $\tilde{\dot{\varepsilon}}_{0xz}(\tilde{z}=\tilde{z}_{b0})$ lead to the following order of magnitude estimate

$$e = O(H/L) = O(\delta)$$

for the parameter e. This estimate of e is therefore a consequence of the fact that vertical variation in u_0 takes place over a vertical distance on the order of H, whereas horizontal (or longitudinal) variation in u_0 is on a length-scale somewhat shorter than L.

The above order of magnitude estimate for e results in the estimate e = 0.01–0.02, when the scales L = 15–20 km and H = 200–300 m are used as reasonable values for Hofsjökull. The value e = 0.01 will be used in the subsequent computations along approximate flow lines. At points of low longitudinal strain rate, it is assumed that this value of e reflects the effect of transverse strain rate in the datum flow (*cf.* subsection 5.2.4). The effect of the sign of e for two-dimensional flow, which was found to be small in Chapter 4, is neglected. It has been checked that the uncertainty in e does not lead to significant changes in the results of the computations by doing computations for alternative e in the range 0.005 to 0.02 (*cf.* subsection 7.4.10).

Measured sliding speeds on a number of temperate glaciers range from 3% to 90% of the total surface velocity (Paterson, 1981). For n = 3, the corresponding range of the sliding parameter c is 0.01 to 4.5. The value of c is therefore highly uncertain. The effect of this uncertainty in c is much greater than the effect of the uncertainty in e. In the following computations the value of c will be chosen to be c = 0 (no sliding) and $c = 2/(n+2) = 0.4$ for n = 3 (ice flux from basal sliding and internal deformation are

equal). The difference of the results for $c = 0$ and $c = 0.4$ indicates the importance of basal sliding for the formation of glacier landscape.

The flow law and sliding law powers n and m are chosen to be $n = 3$ and $m = 2$ in the following unless stated otherwise.

7.3 DIGITAL MAPS OF HOFSJÖKULL

The data set on the geometry of Hofsjökull was made available for this analysis by Helgi Björnsson at the Science Institute, University of Iceland. The data set consists of a map of the surface of the ice cap obtained by barometric altimetry and a map of the subglacial topography obtained by radio echo sounding. The maps are based on approximately 26,000 data points along 1350 *km* of sounding lines on the glacier. The spacing of the lines is typically 500 to 1000 *m*. The digital maps consist of equally spaced points on a 200x200 *m* grid which were interpolated from the sounding lines. The data acquisition, data reduction and the compilation of the maps are described by Björnsson (1988).

The grid of the digital maps is based on conformal conical Lambert coordinates (standard parallel 65°N, central meridian 18°W, false origin such that the point (18°W,65°N) has the coordinates (500,000;500,000)). The x-axis in this coordinate system points to the west and the y-axis points to the north at the point (18°W,65°N). One unit in the x- and y-coordinates is approximately equal to 1 *m* over the area of Hofsjökull. The map of Hofsjökull to the right in Figure 7.2.1 covers the area $520{,}000 \le x \le 560{,}000$ $460{,}000 \le y \le 500{,}000$. This coordinate system will be used in the following to specify the location of points and lines on the Hofsjökull ice cap.

The uncertainty in the measurements has been estimated by comparing the measurements at crossover points on the sounding lines. The standard deviation of the differences in the ice surface altitude is 5 *m* and the standard deviation of the differences in the bedrock altitude is 20 *m* (Björnsson, 1988). This corresponds to a standard error of about 3.5 *m* for the ice surface measurements and a standard error of about 14 *m* for the bedrock measurements. There are gaps in the measurements in areas of the ice cap which were too dangerous for measuring. The grid values of the digital maps in such areas were estimated manually based on the trend of the landscape in neighbouring areas. These areas are not used in the subsequent analysis as they contain no information about the short and intermediate scale landscape of the ice cap.

The distance between sounding lines is in most cases similar to the wavelength of the standing wave in the Green's function for the transfer of bedrock undulations to the ice surface (*cf.* subsection 4.7.3). Therefore, the spacing between sounding lines is in general too large for resolving the standing wave in the Green's function in detail. The effect of the standing wave on the measured landscape of the ice surface is nevertheless noticeable as will be seen below.

There are problems associated with the interpolation of the data from the sounding lines onto the grid. As a consequence of the relatively large spacing between the sounding lines, the accuracy of the computed altitude at each grid point depends to a large extent on its distance to the nearest sounding line. The error associated with the interpolation and the uncertainty in the measurements themselves may be expected to lead to considerable discrepancy between theoretically computed glacier landscape and the digital maps, especially in areas where the amplitude of the measured ice surface undulations is comparable to or lower than the estimated standard error of the measurements of the ice surface altitude and in areas where the bedrock landscape is rapidly varying.

7.4 ANALYSIS ALONG APPROXIMATE FLOW LINES

7.4.1 General

The landscape along a total of 15 approximate flow lines from the outlet glaciers Blautukvíslarjökull, Þjórsárjökull and Sátujökull was analyzed. The length of the flow lines varies from 10.6 to 14.4 *km*. The lines were chosen from areas away from ice divides and the ice margin. There are no big gaps in the measurements along the lines and variations in the long scale ice thickness and surface slope are relatively slow.

7.4.2 Blautukvíslarjökull

Blautukvíslarjökull is an outlet glacier in the southern part of Hofsjökull (Fig. 7.2.1). Figure 7.4.1 shows perspective views of the bedrock and the surface of a part of Blautukvíslarjökull viewed from the southwest. The figure shows a long and relatively narrow subglacial valley in the bedrock landscape in the lower part of the glacier. The valley is close to being parallel to the direction of the ice flow and has almost no visible effect on the ice surface. This is a confirmation of the theoretical prediction, discussed in Chapter

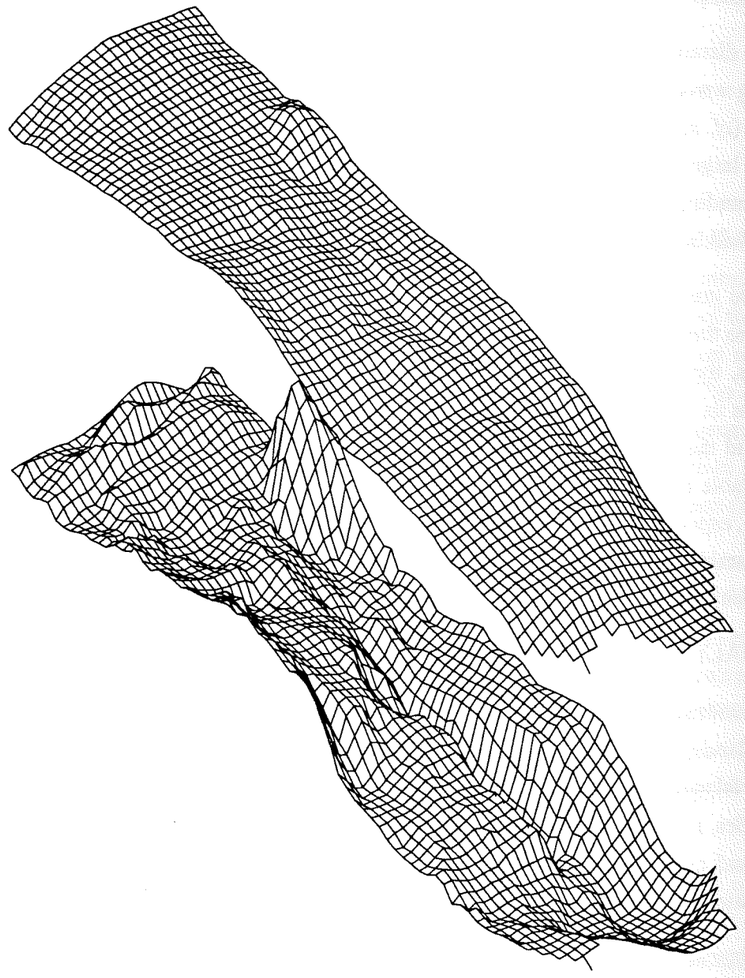

FIGURE 7.4.1: Perspective views of the bedrock (bottom) and surface (top) of a part of the Blautukvíslarjökull glacier outlet viewed from the southwest. The area shown is 14.6x4.8 km and the grid spacing is 200 m. The ice flow is to the south and the ice thickness is between 200 and 300 m over most of the area shown.

5, that bedrock undulations aligned along the direction of the ice flow should not be transferred to the ice surface at all. The figure also shows bulges and troughs on the ice surface which seem to be related to bedrock landscape and will be further discussed below.

The direction of the ice flow on the Blautukvíslarjökull glacier is close to due south. Therefore, profiles along approximate flow lines on the Blautukvíslarjökull glacier can be picked directly from the gridded values in the digital map of Hofsjökull by taking values with a constant x-coordinate. The grid spacing along these flow lines is the same as in the digital map, *i.e.* 200 *m*. Figure 7.4.2 shows profiles along 5 equally spaced parallel flow lines from Blautukvíslarjökull (labeled "a" to "e") separated by 400 *m* from each other. Table 7.4.1 below describes the location of the flow lines and gives the average ice thickness and surface slope for each line. The beginning and end of the flow lines are chosen so that they start some distance away from the subglacial caldera which is near the center of Hofsjökull and do not extend outside the area covered by the sounding lines on the glacier (*cf.* Björnsson, 1988). The easternmost profiles "a" and "b" are shorter than the others because the sounding lines do not extend further to the south in the area where they are located. The flow lines all start at the northern edge of the perspective views from Blautukvíslarjökull which are shown in Figure 7.2.1 and they end 4.0 *km* ("a" and "b") and 2.6 *km* ("c", "d" and "e") from the southern edge of the perspective views. The line labeled "c" lies along the center of the perspective views. Some of the sounding lines on the Blautukvíslarjökull glacier are almost parallel to the ice flow. In order to minimize the effect of interpolation errors, two of the flow lines were chosen close to sounding lines which lie along the 18°57' parallel (profile labeled "e") and 18°56' parallel (profile labeled "c").

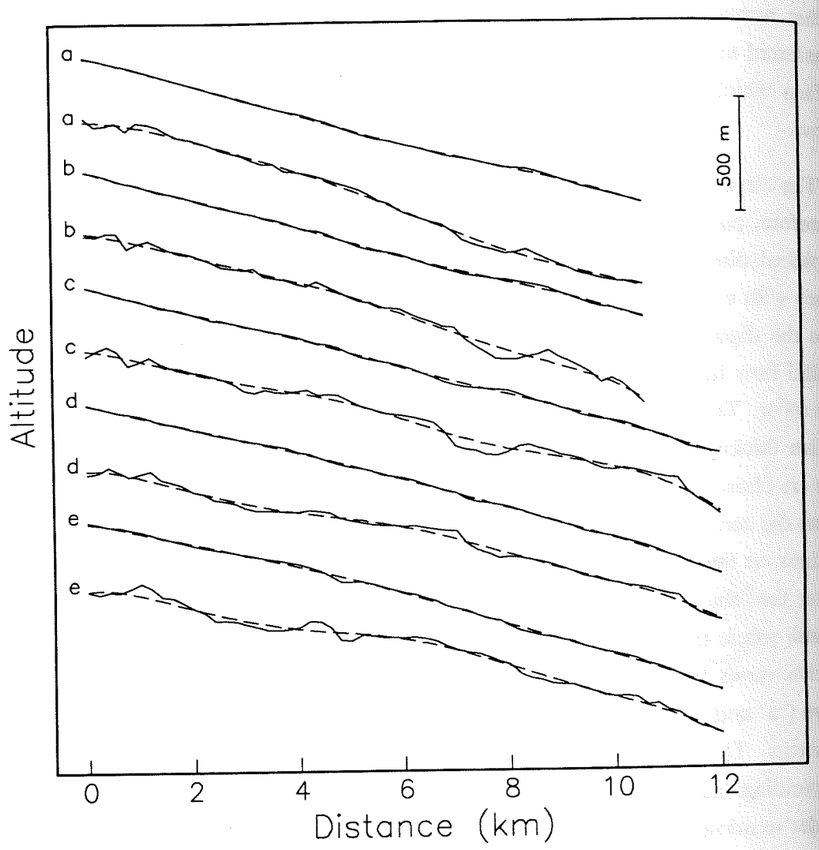

FIGURE 7.4.2: Profiles along 5 approximate flow lines from the Blautukvíslarjökull outlet glacier. The profiles are shown as pairs of solid curves labeled "a" to "e". The upper curve in each pair is the ice surface and the lower curve is the bedrock. The profile labeled "e" is furthest to the west and "a" is furthest to the east. Dashed curves show long scale averages of the ice surface and bedrock profiles which are explained below. The scale near the upper right corner of the figure indicates a vertical distance of 500 m.

TABLE 7.4.1: Flow lines from Blautukvíslarjökull.

Flow line	start		end		length	$\bar{h}$	$\tan\bar{\alpha}$
	x	y	x	y	(km)	(m)	
a	544,000	475,000	544,000	464,400	10.6	298	0.061
b	544,400	"	544,400	"	"	270	0.061
c	544,800	"	544,800	463,000	12.0	232	0.062
d	545,200	"	545,200	"	"	227	0.062
e	545,600	"	545,600	"	"	223	0.062

7.4.3 Þjórsárjökull

Þjórsárjökull is an outlet glacier in the southeastern part of Hofsjökull (Fig. 7.2.1). Figure 1.1.2 in Chapter 1 shows perspective views of the bedrock and surface of a part of Þjórsárjökull viewed from the northeast. As discussed in Chapter 1 the figure shows bulges and troughs in the ice surface which seem to be related to the bedrock landscape. The direction of the ice flow on the Þjórsárjökull glacier is close to southeast. Therefore, profiles along approximate flow lines can be picked directly from the digital map of Hofsjökull by taking values along diagonal lines in the grid. The grid spacing along these flow lines is equal to the grid spacing of the digital map times $\sqrt{2}$, *i.e.* $200\sqrt{2} = 283$ *m*. Figure 7.4.3 shows profiles along 7 equally spaced parallel flow lines from Þjórsárjökull (labeled "a" to "g") separated by 707 *m* from each other. Table 7.4.2 below describes the location of the flow lines and gives the average ice thickness and surface slope for each line. The flow lines "a" and "b" start on the line $x = 535{,}000$. The flow lines "c" to "g" start progressively further to the east in order to stay away from an ice divide. The flow lines "a" and "b" cut across a corner of a gap in the net of sounding lines on Hofsjökull. The gap in flow line "a" extends from a distance approximately equal to 3 *km* to approximately 5 *km*, but the gap in flow line "b" extends from distance 4 *km* to 5 *km*. The distance used in the plotting of the profiles in Figure 7.4.3 and other figures below refers to distance from the line $x = 535{,}000$, although only lines "a" and "b" extend that far to the west. The lines all end on the line $x = 525{,}000$, well away from the ice margin. The flow lines "a" and "b" start at the western edge of the perspective views from Þjórsárjökull which are shown in Figure 1.1.2. The other flow lines start somewhat to the east of the edge. The flow lines all end 1.0 *km* from the eastern edge of

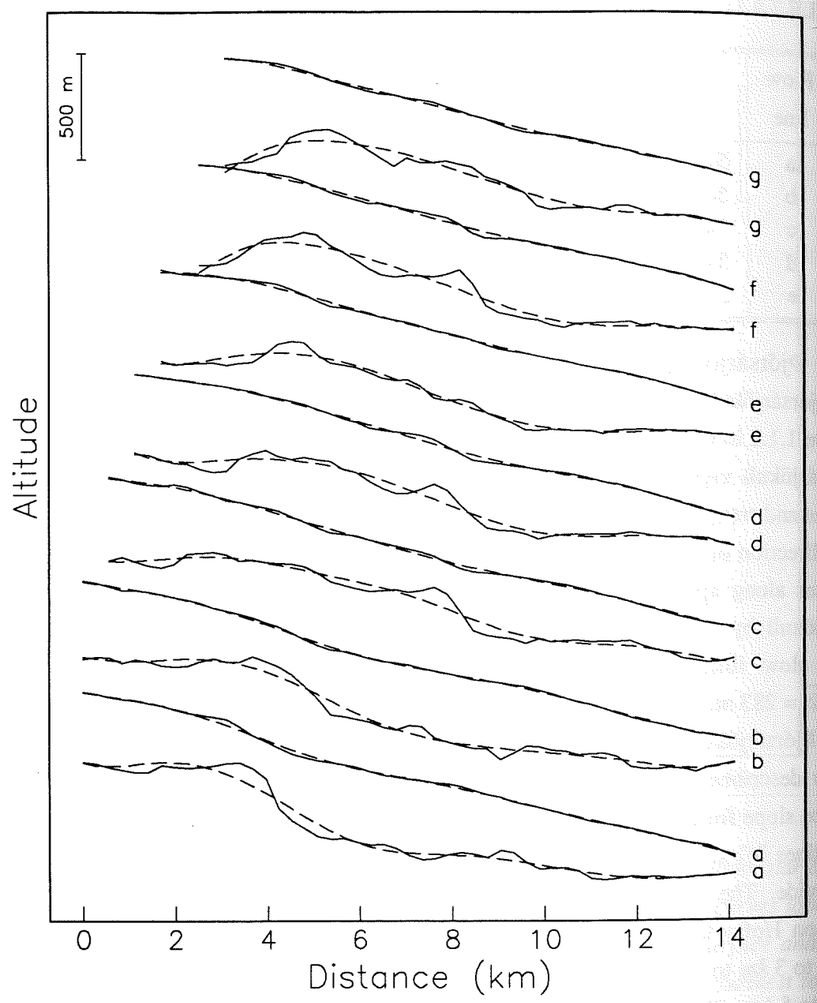

FIGURE 7.4.3: Profiles along 7 approximate flow lines from the Þjórsárjökull outlet glacier. The profiles are shown as pairs of solid curves labeled "a" to "g". The upper curve in each pair is the ice surface and the lower curve is the bedrock. The profile labeled "a" is furthest to the southwest and "g" is furthest to the northeast. Dashed curves show

long scale averages of the ice surface and bedrock profiles which are explained below. The scale near the upper right corner of the figure indicates a vertical distance of 500 m.

the perspective views. The line labeled "c" runs from right to left along the NW-SE diagonal of the perspective views.

TABLE 7.4.2: Flow lines from Þjórsárjökull.

Flow line	start		end		length	$\bar{h}$	$\tan\bar{\alpha}$
	x	y	x	y	(km)	(m)	
a	535,000	480,000	525,000	470,000	14.1	267	0.055
b	"	481,000	"	471,000	"	265	0.055
c	534,600	481,600	"	472,000	13.6	249	0.055
d	534,200	482,200	"	473,000	13.0	271	0.054
e	533,800	482,800	"	474,000	12.4	301	0.053
f	533,200	483,200	"	475,000	11.6	309	0.053
g	532,800	483,800	"	476,000	11.0	304	0.052

7.4.4 Sátujökull

Sátujökull is an outlet glacier in the northern part of Hofsjökull (Fig. 7.2.1). The direction of the ice flow on the Sátujökull glacier is variable, but in general towards north and northwest. Flow lines on Sátujökull were therefore digitized from a map of the flow lines on Hofsjökull published by Björnsson (1988) and profiles along the digitized flow lines were interpolated from the digital map of Hofsjökull. The grid spacing along these flow lines was chosen to be the same as the grid spacing in the digital map, *i.e.* 200 *m*. Figure 7.4.4 shows profiles along 3 flow lines from Sátujökull (labeled "a" to "c"). Table 7.4.3 below describes the location of the flow lines and gives the average ice thickness and surface slope for each line. The beginning of the flow lines is chosen some distance away from the subglacial caldera which is near the center of Hofsjökull and they end a relatively short distance away from the ice margin. The distance between sounding lines is longer than usual (about 1.6 *km*) at two locations on Sátujökull. Interpolation errors may therefore be expected to be larger at these locations in the profiles from Sátujökull than in the profiles from Blautukvíslarjökull and Þjórsárjökull.

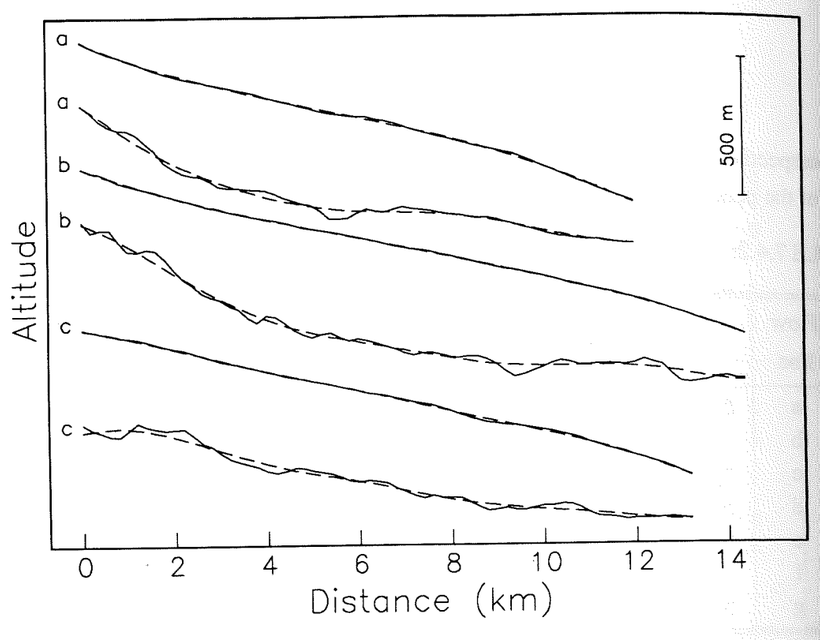

FIGURE 7.4.4: Profiles along 3 approximate flow lines from the Sátujökull outlet glacier. The profiles are shown as pairs of solid curves labeled "a" to "c". The upper curve in each pair is the ice surface and the lower curve is the bedrock. The profile labeled "a" is furthest to the west and "c" is furthest to the east. Dashed curves show long scale averages of the ice surface and bedrock profiles which are explained below. The scale near the upper right corner of the figure indicates a vertical distance of 500 m.

TABLE 7.4.3: Flow lines from Sátujökull.

Flow line	start		end		length	$\bar{h}$	$\tan\bar{\alpha}$
	x	y	x	y	(km)	(m)	
a	540,900	483,800	545,400	494,200	12.0	285	0.044
b	538,800	482,600	544,200	495,400	14.4	300	0.039
c	537,600	484,500	542,800	496,400	13.2	296	0.039

7.4.5 Detrending

The ice surface profiles in Figures 7.4.2, 7.4.3 and 7.4.4 show considerable short scale undulations which are clearly a consequence of peaks and troughs in the bedrock landscape in many places. The relationship between the landscape of the bedrock and the ice surface is as expected from the theoretical development in Chapter 4, *i.e.* the maximum ice surface slopes occur above bedrock peaks and the minimum slopes occur above bedrock troughs.

In order to make a quantitative comparison between theoretical predictions and the measured profiles, short and intermediate scale perturbations in the glacier landscape must be separated from the long scale trend. The "detrending" of the profiles is performed by subtracting a smoothed profile from the actual measured profile. The smoothed profile is computed by fitting a local weighted least squares parabola to the measured profile at each point where a value of the smoothed profile is required. The weight function was chosen to be $w(\xi) = e^{-\xi^2/\sigma_s^2}$, where σ_s is a length-scale of the smoothing and ξ is distance from the point in question. This method for detrending the profiles removes all undulations with length-scales longer than approximately σ_s from the profiles. This method was chosen after some experimenting with global least squares lines and parabolas in addition to local weighted least squares lines.

The dashed curves in Figures 7.4.2, 7.4.3 and 7.4.4 show the smoothed profiles computed as described above with the length-scale of the smoothing chosen to be $\sigma_s = 2.5\ km$. This value of σ_s eliminates all undulations with length-scales longer than approximately 2.5 *km*, which corresponds to approximately 10 ice thicknesses. The effect of varying σ_s is discussed in subsection 7.4.9 below.

7.4.6 Ice surface filters

According to the theory developed in Chapter 4, steady perturbations in the ice surface geometry $\Delta z_s(x)$, can be computed as a convolution of perturbations in the bedrock geometry $\Delta z_b(x)$, with a Green's function or a filter $g(x)$, *i.e.* $\Delta z_s(x) = g(x)*\Delta z_b(x)$. The filter $g(x)$, which can be computed numerically from the ice flow equations (*cf.* Chapter 4), describes the steady state ice surface geometry corresponding to a sharp spike in the bedrock geometry. When this theory is applied to discrete data at equally spaced points $x_i = i\Delta x$, the continuous filter $g(x)$, must be sampled or discretized to yield a discrete filter g_i, which predicts $\Delta z_s(x_i)$ as a discrete convolution, *i.e.* $\Delta z_s(x_i) = \Delta x\, g_i*\Delta z_b(x_i)$. The sampling of a continuous filter $g(x)$, is discussed in Appendix 1 and the discrete filters which are used in the following are computed as described there using (A1.2.7b) and (A1.2.8b). The discrete filter g_i, describes the steady state ice surface perturbation at the points x_i, corresponding to a triangular disturbance in the bedrock geometry with half width equal to Δx.

The discrete filter g_i is uniquely determined by the flow law and sliding law powers n and m, the longitudinal strain rate parameter e, the sliding parameter c, the long scale ice thickness and surface slope, and the grid spacing Δx. Ideally, local values of the long scale ice thickness and surface slope at each point along the flow lines should be used to compute separate filters for each point along the flow lines, because the long scale ice thickness and surface slope vary slowly with distance along the lines. For simplicity, the filters will initially be computed using the average ice thickness and surface slope for each line. Results computed from filters that vary along the flow lines will be discussed in subsections 7.4.11, 7.4.12 and 7.4.13.

Figure 7.4.5 shows examples of discrete filters computed according to the theory of Chapter 4 for selected flow lines on Blautukvíslarjökull (line "c"), Þjórsárjökull (line "c") and Sátujökull (line "b") with (top) and without (bottom) basal sliding. Filters computed from laminar flow theory are shown as circles and filters computed from the full ice flow equations are shown as triangles. The filters are discretized as described in Appendix 1 which leads to a well defined filter value at the origin for the discrete filters derived for laminar flow although the corresponding filter $g(x)$ is discontinuous at the origin (*cf.* Fig. 4.4.2). The laminar flow filters have the shape of a one-sided exponential. They are

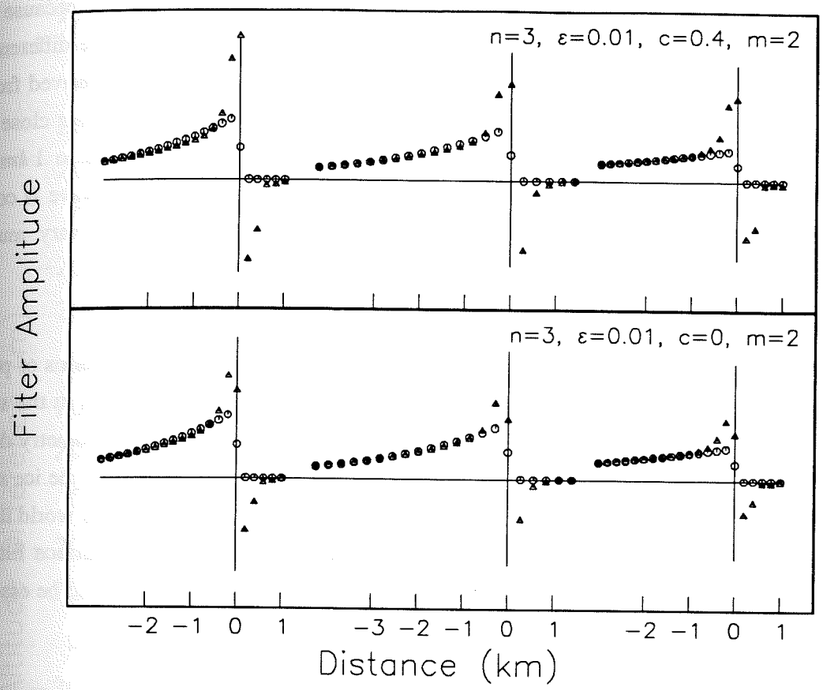

FIGURE 7.4.5: Discrete filters computed for line "c" on Blautukvíslarjökull (left, Δx = 200 m), line "c" on Þjórsárjökull (middle, Δx = 283 m) and line "b" on Sátujökull (right, Δx = 200 m) using the average ice thickness and surface slope for each line (cf. tables 7.4.1, 7.4.2 and 7.4.3). The parameters used for the computation of the filters are given in the figure. The lower part of the figure shows filters computed for no basal sliding (c = 0) and the upper part shows filters for non-zero basal sliding (c = 0.4). Filters computed from laminar flow theory (cf. subsection 4.4.3) are plotted as circles and filters computed from the full ice flow equations (cf. subsection 4.7.3) are plotted as triangles. The filters are discretized as described in Appendix 1. The origin of the filters is indicated with vertical lines.

lower and longer for Sátujökull than for Blautukvíslarjökull and Þjórsárjökull because of the relatively low surface slope on Sátujökull (*cf.* Eq. (4.4.4)). There is little difference between the laminar flow filters with and without basal sliding. The filters derived from the full ice flow equations are almost identical to the laminar flow filters except close to the origin where a standing wave with a wavelength approximately equal to 1 *km* is superimposed on the one-sided exponential. The amplitude of the standing wave is considerably higher for non-zero basal sliding, but the amplitude does not vary much between the three glaciers.

7.4.7 Slope filters

As explained in Chapter 4 it is possible to analyze glacier landscape in terms of perturbations in the ice surface geometry itself Δz_s, or in terms of perturbations in the surface slope $\Delta\alpha$. Both can be computed from perturbations in the bedrock geometry Δz_b, using appropriate filters. It is more direct to work in terms of perturbations in the ice surface geometry Δz_s, and it is easier to relate figures of Δz_s in meters to the real world than figures of $\Delta\alpha$ in radians. Therefore, the following analysis will use ice surface filters rather than slope filters. The results of an analysis based on slope filters would be essentially the same.

7.4.8 Results for laminar flow

The top 4 panels in Figure 7.4.6 show ice surface undulations along flow line "c" on Blautukvíslarjökull computed using the detrending length-scale $\sigma_s = 5$ *km* (solid curves). Flow line "c" is chosen in order to minimize interpolation errors as it lies close to a sounding line on the glacier as mentioned above. The panels also show ice surface undulations predicted by filters derived for laminar flow for different values of the flow law power n, both with (dotted curves) and without (dashed curves) basal sliding. The value of the sliding law power m for non-zero basal sliding is determined from n as $m = (n+1)/2$ (*cf.* Paterson, 1981) and the sliding parameter c for non-zero basal sliding is chosen as $c = 2/(n+2)$ so that one half of the datum ice flux is caused by basal sliding. The filters are computed from the average ice thickness and surface slope along the flow line (the filters for $n = 3$ are shown to the left in Figure 7.4.5). The predicted undulations are uncertain near the upper and lower end of the profiles as no tapering is applied near the ends during the filtering.

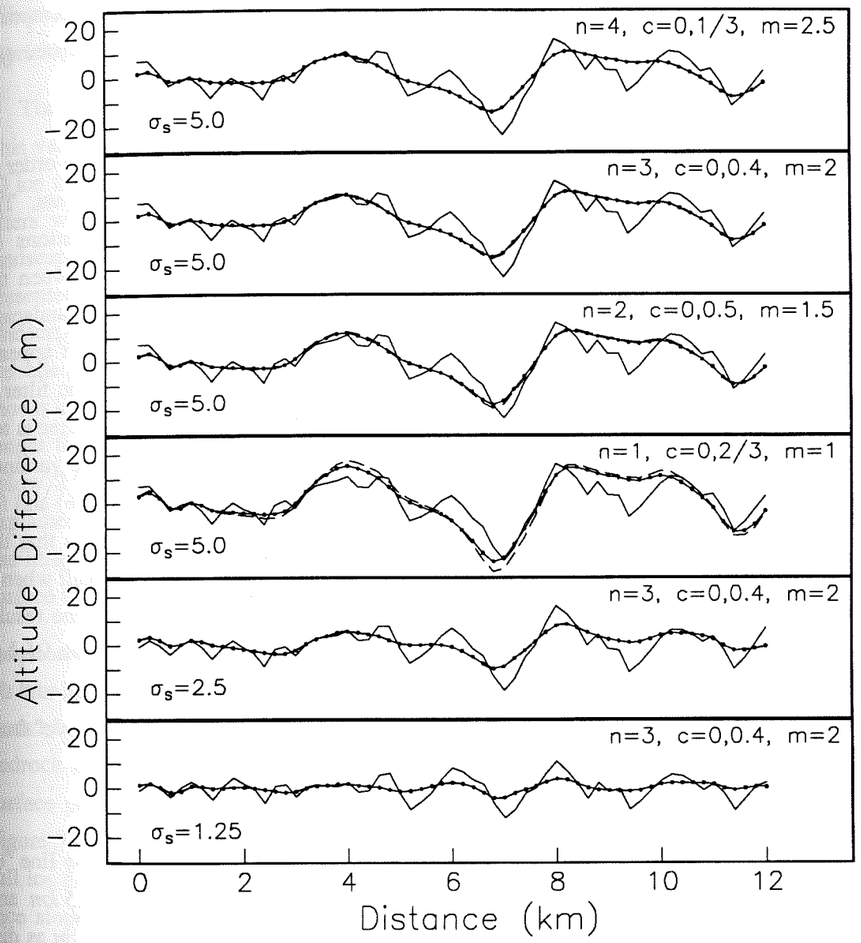

FIGURE 7.4.6: Ice surface undulations predicted by the laminar flow approximation. The solid curves show ice surface undulations along flow line "c" on Blautukvíslarjökull computed from the measured ice surface profile using different detrending length-scales σ_s. The figure also shows predicted ice surface undulations computed from the corresponding basal undulations using filters derived for laminar flow for different values of the flow law power n, both with (dotted curves) and without

(dashed curves) basal sliding. The basal undulations are computed using the same detrending length-scales as for the ice surface (for explanation, see text).

The figure shows ice surface undulations with a maximum amplitude on the order of 20 *m*, which is well above the estimated error of the ice surface measurements. The predicted undulations show considerable similarity to the measured undulations on length-scales longer than approximately 1-2 *km*. There is little difference between the undulations predicted with and without basal sliding and therefore the glacier landscape predicted by laminar flow is primarily determined by the flow law power n. It appears that the amplitude of the predicted undulations using $n = 1$ is too large (*i.e.* the filter is too short) while the predicted undulations using $n = 4$ are too small (*i.e.* the filter is too long). For $n = 3$, the predicted undulations explain approximately 66% of the variance of the measured undulations, which is slightly better than for $n = 2$ (about 65%) and for $n = 4$ (about 65%) and much better than for $n = 1$ (about 50%). This implies that the non-linear flow law of ice ($n > 1$) manifests itself in the landscape of Hofsjökull when it is interpreted using the laminar flow approximation. The difference between the results for $n = 2$, 3 and 4 is small, but the results are consistent with the commonly accepted flow law power $n = 3$. Results for the other flow lines from Blautukvíslarjökull and the flow lines from Þjórsárjökull (not shown) are similar to the above results for line "c" from Blautukvíslarjökull.

7.4.9 Effect of detrending length scale

The bottom 2 panels in Figure 7.4.6 show ice surface undulations along flow line "c" on Blautukvíslarjökull computed using the detrending length-scales $\sigma_s = 2.5$ *km* and $\sigma_s = 1.25$ *km*. The top 4 panels show the undulations corresponding to $\sigma_s = 5$ *km* as discussed in the previous subsection. Reducing σ_s leads to ice surface undulations with shorter length-scales and smaller amplitudes as expected. Ice surface undulations predicted from the bedrock topography (detrended with the same value of σ_s as the surface topography) on the basis of the laminar flow approximation decay sharply with decreasing σ_s and become much smaller than the measured undulations (only shown for $n = 3$). The predicted undulations explain about 51% of the variance of the undulations computed with $\sigma_s = 2.5$ *km* and only about 27% for $\sigma_s = 1.25$ *km*. This indicates a

failure of the laminar flow approximation for landscape features with length scales shorter than approximately 1-2 *km*.

The detrending length-scale σ_s will be chosen to be $\sigma_s = 2.5$ *km* in the following. This value emphasizes landscape features with length scales shorter that approximately 10 ice thicknesses. It is suitable for investigating the effect of the standing wave in the filters which are used here for computing ice surface undulations from the bedrock landscape. The exact value of σ_s is not important for the conclusions which will be presented in the following. If σ_s had been chosen to be longer than 2.5 *km*, then longer landscape features would have been present in the detrended profiles, but such features are adequately explained by filters derived from the laminar flow approximation as shown in the previous subsection. If σ_s had been chosen to be shorter than 2.5 *km* (but longer than approximately 1 *km*), then landscape features with length-scales somewhat below 2.5 *km* would have been reduced, but such features are also to a large extent explained by filters based on the laminar flow approximation. Thus, the exact value of σ_s has little effect on landscape features which are related to the standing wave in the ice surface filters as long as σ_s is well above approximately 1 *km*.

7.4.10 Results for full ice flow equations

The standing wave in the ice surface filters corresponding to the full ice flow equations has considerable effect on the predicted ice surface undulations. Figure 7.4.7 shows bedrock and ice surface undulations along flow line "c" on Blautukvíslarjökull (the ice surface profile is the same as the profile shown in the second panel from the bottom in Figure 7.4.6) together with ice surface undulations predicted by filters derived from the full ice flow equations. The filters are computed from the average ice thickness and surface slope along the flow line for three different values of the strain rate parameter e, both with and without basal sliding (the filters for $e = 0.01$ are shown to the left in Figure 7.4.5). The damping and shifting effect of the filters can be clearly seen by comparing the bedrock undulations to the predicted ice surface undulations.

Figure 7.4.7 shows that filters based on the full ice flow equations lead to an improvement in the predicted ice surface undulations compared to the laminar flow approximation (*cf.* the second panel from the bottom in Figure 7.4.6). For $e = 0.01$, which is a representative value for Hofsjökull, the predicted undulations explain 65% (no sliding)

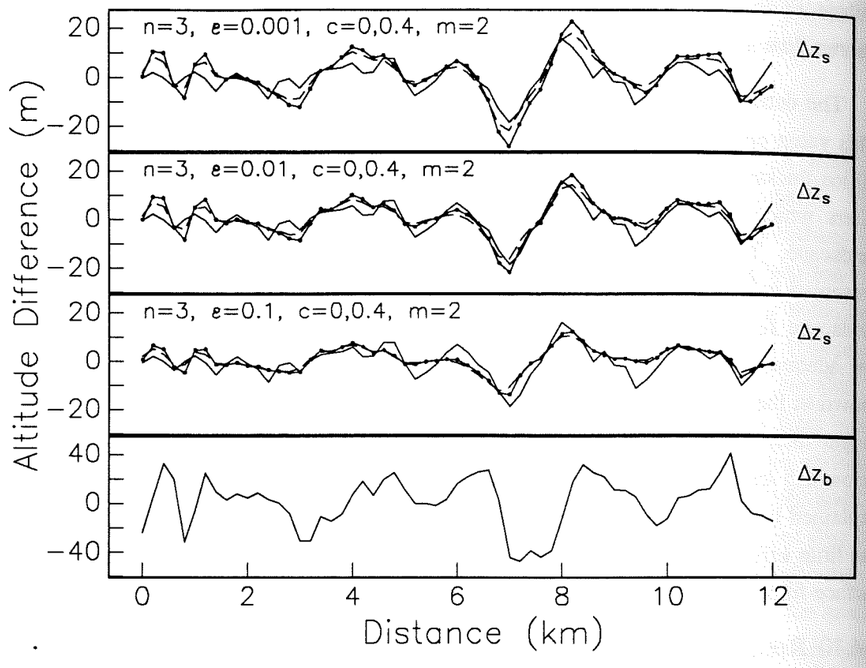

FIGURE 7.4.7: Ice surface undulations predicted by the full ice flow equations. The solid curves show measured bedrock undulations Δz_b (bottom panel), and ice surface undulations Δz_s (top 3 panels), along flow line "c" on Blautukvíslarjökull computed using $\sigma_s = 2.5$ km. The ice surface panels also show predicted ice surface undulations computed by filters derived from the full ice flow equations for $n = 3$ and $m = 2$ both with (dotted curves, $c = 0.4$) and without (dashed curves, $c = 0$) basal sliding. The three ice surface panels show the predicted undulations for three different values of the strain rate parameter e.

and 54% (non-zero sliding) of the variance of the measured undulations. This is an improvement over filters based on the laminar flow approximation where the corresponding ratio is 51%. Visual comparison of Figures 7.4.6 (second panel from bottom) and 7.4.7 (third panel from bottom) shows that the improvement is larger than expected from

the increase in the explained variance alone. The amplitude and phase of the shortest undulations (for example at distances approximately equal to 7 and 8 *km*) is well predicted, considering that the prediction is based on a two-dimensional study of the ice flow which in reality is three-dimensional to some extent. The amplitude of these undulations is significantly underpredicted by the laminar flow filters as discussed above.

In order to investigate the effect of the datum longitudinal strain rate parameter e, Figure 7.4.7 shows the predicted ice surface undulations for $e = 0.1$ and $e = 0.001$ in addition to the undulations computed for $e = 0.01$, which is a reasonable value for Hofsjökull as explained earlier. In spite of the uncertainty in the value of e, it is clear that the value $e = 0.001$ is far too low for Hofsjökull and $e = 0.1$ is far too high. These values were chosen in order to produce visibly different curves compared to $e = 0.01$. As expected, the predicted amplitude of the shortest undulations becomes smaller for $e = 0.1$ (softer ice near the surface) compared to $e = 0.01$ and for $e = 0.001$ (stiffer ice near the surface) the amplitude becomes larger. Although the effect of the changes in e is not large, it seems that predicted amplitude of the ice surface undulations is significantly better for $e = 0.01$ than for either $e = 0.01$ or $e = 0.001$. This is also the case for the other flow lines on Blautukvíslarjökull and Þjórsárjökull (not shown) and indicates that the order of magnitude estimate $e = 0.01$ is indeed valid for Hofsjökull. Furthermore, the relatively small effect of the large changes in e in Figure 7.4.7 shows that incorrect estimates of e by a factor of 2-3 or variation of e along flow lines by a similar factor will have a marginal effect on the predicted ice surface undulations.

Finally, Figure 7.4.7 shows the effect of basal sliding on the predicted ice surface undulations. As expected from Figure 7.4.5, the predicted amplitude of the ice surface undulations is larger for non-zero basal sliding (dotted curves) than for no basal sliding (dashed curves). The increase in the predicted amplitude for $c = 0.4$ compared to $c = 0$ is similar to the increase in the predicted amplitude for $e = 0.001$ compared to $e = 0.01$. Since $c = 0.4$ is not an unrealistic, although highly uncertain, value of c for Hofsjökull, whereas $e = 0.001$ is much too low, this shows that the uncertainty in the basal sliding parameter c is more important for the landscape of Hofsjökull than the uncertainty in the value of the longitudinal strain rate parameter e.

The predicted undulations along flow line "c" on Blautukvíslarjökull for no basal sliding explain a larger fraction (65%) of the variance of the measured undulations than the undulations predicted for non-zero sliding with c = 0.4 (54%). This is the case for some but not all of the other flow lines on Blautukvíslarjökull and Þjórsárjökull as will be discussed further below. It appears that it is not possible to use the data from Hofsjökull to distinguish between no basal sliding and basal sliding described by c=0.4 (one half of the ice flux caused by basal sliding). This may be a consequence of the uncertainty in the measurements, but it may also be a consequence of spatial variation in the basal sliding of Hofsjökull. The amplitude of the predicted undulations for the all flow lines on Blautukvíslarjökull and Þjórsárjökull does, however, become unrealistically large for $c \gg 0.4$ (not shown). Thus, the measured landscape of Hofsjökull is consistent with basal sliding that transports on the order of 50% of the datum ice flux or lower.

7.4.11 Results for Blautukvíslarjökull

For simplicity, the predicted ice surface undulations shown in Figures 7.4.6 and 7.4.7 are computed with filters based on the average ice thickness and surface slope along flow line "c" on Blautukvíslarjökull. An assumption of constant datum ice thickness and datum surface slope is not unrealistic for this flow line (*cf.* Figure 7.4.2), but it is not realistic for some of the other flow lines on Blautukvíslarjökull (*e.g.* flow lines "a" or "e") or for the flow lines on Þjórsárjökull and Sátujökull (*cf.* Figures 7.4.3 and 7.4.4). Therefore, separate filters based on local values of the long scale ice thickness and surface slope are used in the computation of the predicted ice surface undulations at each point along the flow lines in the following.

Figure 7.4.8 shows predicted ice surface undulations along the 5 flow lines on Blautukvíslarjökull (*cf.* Figure 7.4.2) computed from the full ice flow equations in this way. The predicted undulations for flow line "c" are similar to the undulations shown in Figure 7.4.7, which are computed using the same filters for all the points. Using separate filters for each point leads to a slight improvement in the predicted undulations for the other flow lines on Blautukvíslarjökull and for the flow lines on Þjórsárjökull where there is more variation in the long scale ice thickness and surface slope along the flow lines.

The predicted ice surface undulations shown in Figure 7.4.8 are in general in good agreement with the measured ice surface undulations both in amplitude and in phase,

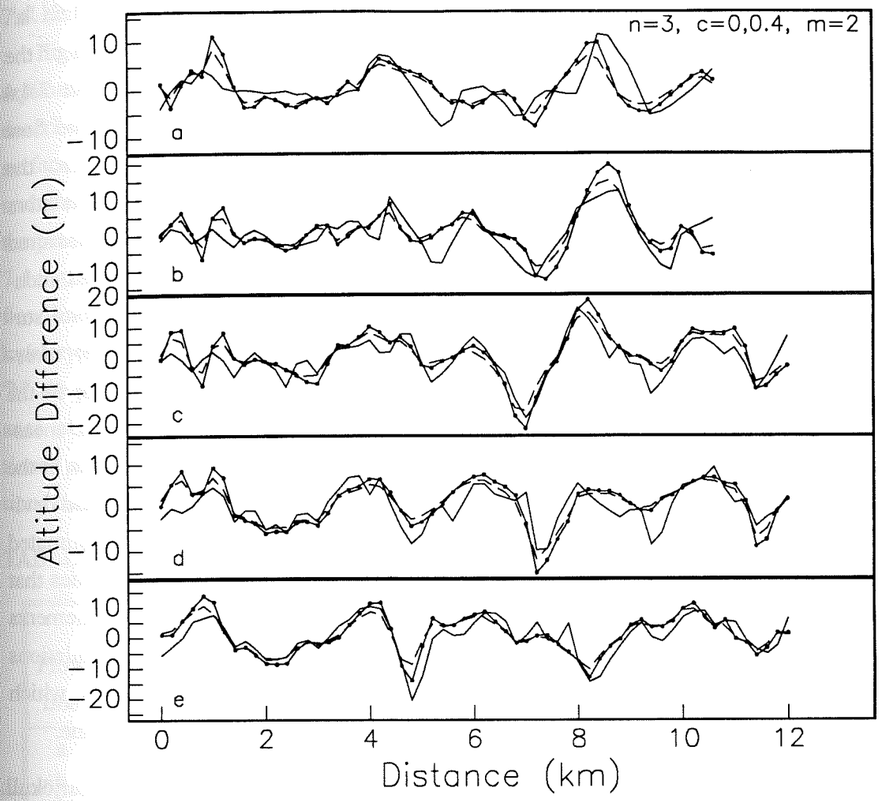

FIGURE 7.4.8: Ice surface undulations on Blautukvíslarjökull predicted by the full ice flow equations. The solid curves show measured ice surface undulations along 5 flow lines labeled "a" to "e" computed using σ_s = 2.5 km. The figure also shows predicted ice surface undulations computed by filters derived from the full ice flow equations for n = 3, e = 0.01 and m = 2, both with (dotted curves, c = 0.4) and without (dashed curves, c = 0) basal sliding. Separate filters based on local values of the long scale ice thickness and surface slope are used for each point along the flow lines. Note the different scales of the y-axes.

although there is considerable discrepancy in many places, especially for flow line "a". The predicted ice surface undulations explain from about 65% of the variance of the measured undulations for flow line "e" to less than 30% for flow line "a". Table 7.4.4 gives the variance of the measured and predicted ice surface undulations for the flow lines on Blautukvíslarjökull. It also gives the variance of the residuals, *i.e.* the differences between the measured and predicted undulations, together with the relative reduction in the variance, *i.e.* one minus the ratio of the residual variance to the measured variance. The main causes of the discrepancy between the measured and predicted undulations are (1) measurement errors both in the measurements of the bedrock and ice surface, (2) interpolation errors in the gridding of the measurements and (3) three-dimensional ice flow around bedrock obstacles which cannot be accounted for in the two-dimensional ice flow analysis. The variance of the differences between the measured and predicted undulations is between 10 and 20 m^2 for all the flow lines, both in the case of no basal sliding and for non-zero basal sliding. The corresponding standard deviation of the residuals is between 3 and 5 m, which is not inconsistent with the estimated standard error of about 3.5 m for the ice surface measurements alone. This implies that the predicted ice surface undulations are within the estimated error of the measurements from the measured undulations. The amplitude of the measured ice surface undulations for flow line "a" is similar to the estimated standard error of the measurements, which explains the relatively low reduction in the variance (27% and 9%) for this flow line.

TABLE 7.4.4: Statistics of ice surface undulations for flow lines from Blautukvíslarjökull.

Flow line	Variance of measurements (m^2)	Predicted/Residual Variance $c = 0$ (m^2)	Predicted/Residual Variance c=0.4 (m^2)	Reduction in Variance $c = 0$ (%)	Reduction in Variance c=0.4 (%)
a	16	10/12	18/15	27	9
b	31	24/15	42/20	52	34
c	39	36/14	56/19	63	51
d	19	18/11	28/13	43	32
e	41	27/15	41/13	62	68

7.4.12 Results for Þjórsárjökull

Figure 7.4.9 shows predicted ice surface undulations along the 7 flow lines on Þjórsárjökull (*cf.* Figure 7.4.3) computed from the full ice flow equations in the same way as described in the previous subsection for Blautukvíslarjökull. The amplitude of the ice surface undulations is larger on Þjórsárjökull than on Blautukvíslarjökull. Therefore, the undulations rise higher above the "noise level" of the measurements and one may expect the predicted undulations to explain a larger fraction of the measured undulations. Table 7.4.5 gives the variance of the measured and predicted ice surface undulations for the flow lines on Þjórsárjökull in the same format as in the previous subsection for Blautukvíslarjökull. The last two columns of the table show that except for flow lines "a" and "b", the predicted undulations explain a larger fraction (up to more than 80%) of the variance of the measured undulations than was the case for Blautukvíslarjökull. As mentioned above, this is a consequence of the higher "signal to noise ratio" for the undulations on Þjórsárjökull.

TABLE 7.4.5: Statistics of ice surface undulations for flow lines from Þjórsárjökull.

Flow line	Variance of measurements (m^2)	Predicted/Residual Variance $c = 0$ (m^2)	Predicted/Residual Variance c=0.4 (m^2)	Reduction in Variance $c = 0$ (%)	Reduction in Variance c=0.4 (%)
a	62	78/31	115/43	50	31
b	32	50/24	72/31	25	2
c	64	51/16	74/15	75	76
d	74	40/19	63/16	74	78
e	44	19/14	33/12	68	73
f	91	58/17	96/16	82	83
g	58	44/11	73/18	81	69

Except for flow lines "a" and "b", the variance of the residuals for Þjórsárjökull is similar to the variance of the residuals for Blautukvíslarjökull, *i.e.* between 10 and 20 m^2 both in the case of no basal sliding and for non-zero basal sliding. The residual variance for flow lines "a" and "b" is somewhat higher (between 24 and 43 m^2). Examination of Figure 7.4.9 shows that the main discrepancy between the measured and predicted ice surface undulations for these flow lines is located at distances between 3 and 5 *km*. Flow

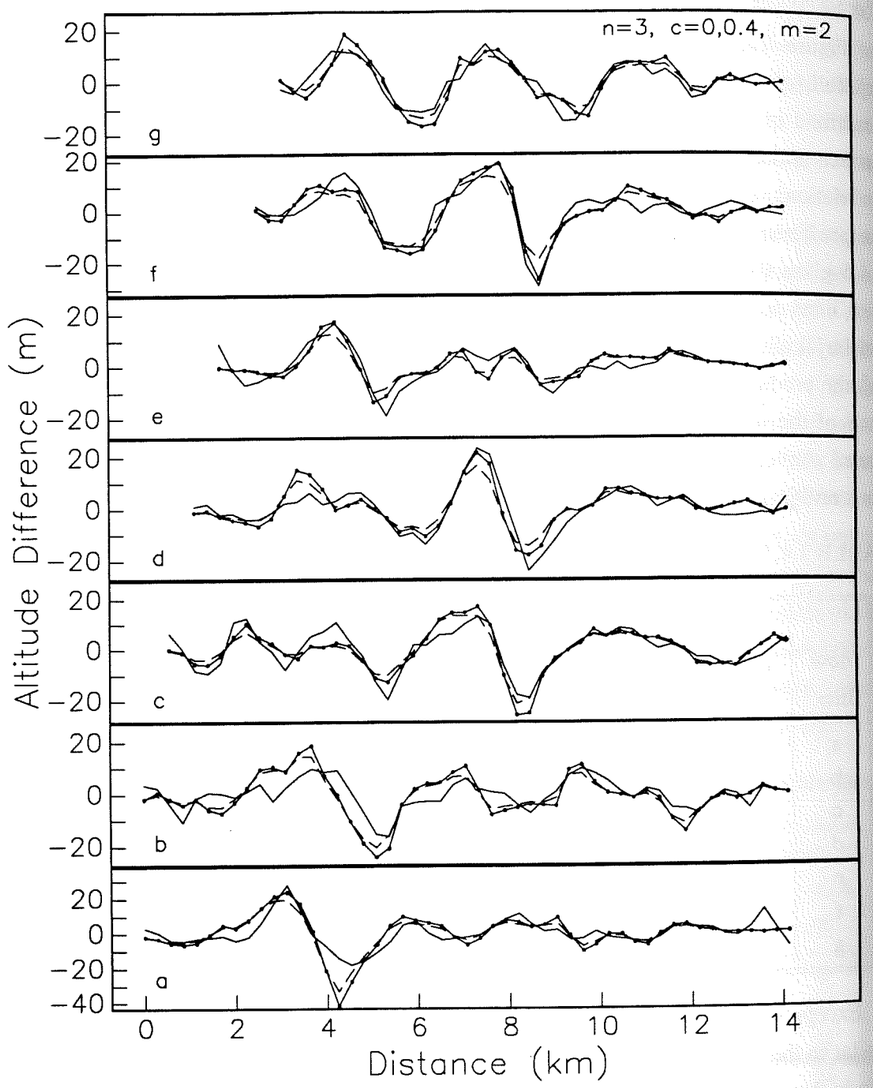

FIGURE 7.4.9: Ice surface undulations for 7 flow lines on Þjórsárjökull predicted by the full ice flow equations (for explanation, see Figure 7.4.8). Note the different scales of the y-axes.

line "a" and "b" cross a gap in the net of the sounding lines on Blautukvíslarjökull at these distances as mentioned earlier. Thus, the discrepancy is most likely caused by interpolation errors in the digital map which arise from the gap in the measurements.

As was the case for Blautukvíslarjökull, the predicted ice surface undulations on Þjórsárjökull are within the estimated error of the measurements from the measured undulations, except for the abovementioned discrepancy at distances between 3 and 5 *km* for flow lines "a" and "b". This is a confirmation of the two-dimensional theory of Chapter 4. Ice surface undulations predicted by the laminar flow approximation for the flow lines from Blautukvíslarjökull and Þjórsárjökull are much smoother than the undulations predicted by the full ice flow equations (compare the second panel from the bottom in Figure 7.4.6 to the third panel from the bottom in Figure 7.4.7). Undulations predicted for laminar flow are not shown here except for flow line "c" on Blautukvíslarjökull. They have the same relation to the undulations predicted by the full ice flow equations as shown above for flow line "c" on Blautukvíslarjökull, *i.e* the laminar flow approximation does not explain the sharpest peaks and troughs which are present in the measured ice surface. The main difference between the ice surface filters based on the laminar flow approximation and the filters based on the full ice flow equations is the "standing wave" close to the origin of the filters (*cf.* Figure 7.4.5). Thus, the existence of a "standing wave" in the steady state ice surface corresponding to a sharp peak in the bedrock landscape is confirmed by the improved predictions of filters based on the full ice flow equations compared to filters based on laminar flow theory.

The fact that ice surface undulations predicted by two-dimensional ice flow theory along flow lines on Blautukvíslarjökull and Þjórsárjökull are within the estimated error of the measurements from the measured undulations, indicates that it is not possible to detect possible effects of three-dimensional flow around bedrock undulations from the digital maps of the bedrock and ice surface of Hofsjökull. Furthermore, it is not possible to estimate the role of basal sliding in the formation of the ice surface undulations in any detail, since the predicted ice surface undulations are within the error of the ice surface measurements both for no basal sliding and for non-zero basal sliding with $c = 0.4$. As mentioned in an earlier subsection, it can nevertheless be concluded that values of the sliding parameter c, which are much higher than $c = 0.4$, are inconsistent with the data

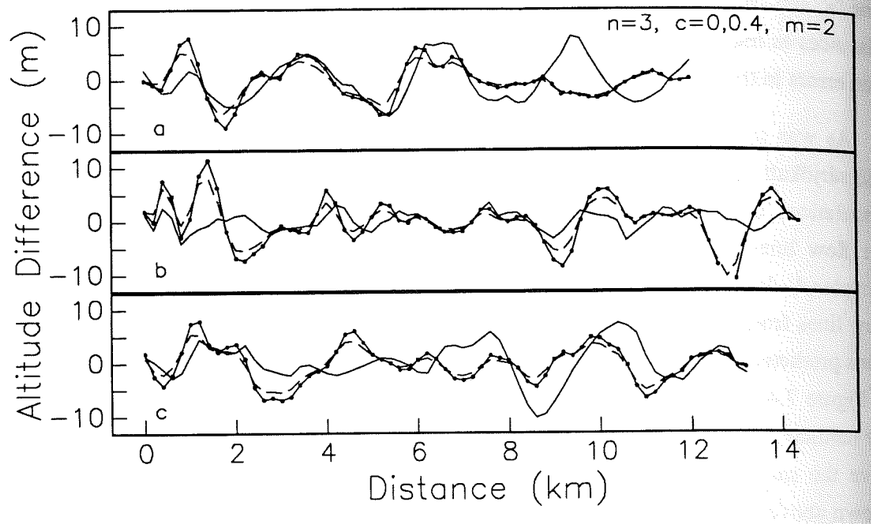

FIGURE 7.4.10: Ice surface undulations for 3 flow lines on Sátujökull predicted by the full ice flow equations (for explanation, see Figure 7.4.8). Note that the scales of the y-axes are different from the scales of y-axes in Figures 7.4.8 and 7.4.9.

from Hofsjökull as they result in an overprediction of the amplitude of short scale ice surface undulations.

7.4.13 Results for Sátujökull

Figure 7.4.10 shows predicted ice surface undulations along the 3 flow lines on Sátujökull (*cf.* Figure 7.4.4) computed from the full ice flow equations in the same way as described above in the subsection for Blautukvíslarjökull. The amplitude of the ice surface undulations is much smaller on Sátujökull than on either Blautukvíslarjökull or Þjórsárjökull. The amplitude is so low that the undulations do not rise above the "noise level" of the measurements and the predicted undulations cannot therefore be expected to explain much of the measured undulations. Table 7.4.6 gives the variance of the measured and predicted ice surface undulations for the flow lines on Sátujökull in the same format as in the earlier subsection for Blautukvíslarjökull. The measured and predicted variance is between 10 and 20 m^2 for all three lines. This is similar to the variance of the

residuals on Blautukvíslarjökull and Þjórsárjökull and comparable to the standard error of the measurements. Thus, it is only natural that the predicted ice surface undulations do not explain much of the variance of the measured undulations (the last two columns of the table).

TABLE 7.4.6: Statistics of ice surface undulations for flow lines from Sátujökull.

Flow line	Variance of measurements (m^2)	Predicted/Residual Variance		Reduction in Variance	
		$c = 0$ (m^2)	c=0.4 (m^2)	$c = 0$ (%)	c=0.4 (%)
a	15	7/13	12/14	15	7
b	3	11/12	19/18	<0	<0
c	13	7/14	12/17	<0	<0

The low amplitude of the ice surface undulations on Sátujökull is in part caused by a relatively low amplitude of the bedrock undulations (*cf.* Figure 7.4.4). It can also be related to the ice surface filters shown in Figure 7.4.5 as the low long scale surface slopes on Sátujökull, compared to Blautukvíslarjökull and Þjórsárjökull, result in longer and lower ice surface filters. Long and low ice surface filters lead to more averaging and consequently lower amplitudes when the filters are applied to bedrock undulations. Thus, the theory of Chapter 4 predicts a lower amplitude of the ice surface undulations on Sátujökull than on Blautukvíslarjökull and Þjórsárjökull.

There are some indications that a part of Sátujökull surged some years before the mapping of Hofsjökull (Björnsson, personal communication). The distance between sounding lines on Sátujökull is also about twice as long as usual at two locations on each flow line as mentioned above, and this could lead to larger interpolation errors at these locations than on Blautukvíslarjökull and Þjórsárjökull. These explanations could account for a part of the discrepancy between the measured and predicted ice surface undulations, but they are not really needed as the measured undulations are so small that they are not significantly different from the estimated standard error of the measurements.

The above analysis of surface undulations on Sátujökull and the earlier experience with flow line "a" on Blautukvíslarjökull and flow lines "a" and "b" on Þjórsárjökull, shows that in order to test the theory of Chapter 4 in a meaningful way the data must contain sufficiently large ice surface undulations (amplitude $\gtrsim 5\ m$ in the case of Hofsjökull) and be from an area with sufficiently dense sounding lines (line spacing $\lesssim 7$–$800\ m$ in the case of Hofsjökull). If either one of these preconditions is not satisfied then no valid conclusions about the formation of short and intermediate scale glacier landscape can be deduced from the data.

7.5 ANALYSIS USING THREE-DIMENSIONAL LAMINAR FLOW THEORY

7.5.1 General

Ice surface undulations in the digital map of Hofsjökull were analyzed using the three-dimensional laminar flow theory of Chapter 5. The "standing wave" in the steady state ice surface corresponding to a sharp peak in the bedrock landscape is not correctly represented in this theory because the theory is based on an approximation and not on a solution of the full ice flow equations. The theory is therefore not valid for the shortest wavelengths in the glacier landscape. It is nevertheless worthwhile to check whether damping and shifting of intermediate length-scale bedrock and ice surface undulations on Hofsjökull is as predicted for laminar flow.

It is not as easy to "hand pick" an area well covered by the sounding lines from the digital maps as it was to choose the location of flow lines in the analysis of the previous section. Areas with ice thickness less than $100\ m$ were excluded from the analysis and also areas close to ice divides with long scale surface slopes less than 0.01. Apart from this the entire digital map of Hofsjökull was used. Predicted ice surface undulations may therefore be expected to be in error close to and inside of gaps in the net of sounding lines on the ice cap.

7.5.2 Detrending

The laminar flow theory is not valid for the shortest wavelengths in the glacier landscape and it must therefore be tested on landscape features with somewhat longer length-scales than the undulations that were used in the analysis along flow lines in the previous section. The detrending of the digital maps was performed in essentially the

same way as described previously for profiles along flow lines, *i.e.* by subtracting a smoothed surface from the values of the digital map at each point. The smoothed surface was computed by fitting a local weighted least squares second degree surface $z = a_{pq}\xi^p\eta^p$, $p+q \le 2$, to the gridded map at each point, where ξ,η are local coordinates in the x and y directions. The weight function was chosen to be $w(\xi,\eta) = e^{-(\xi^2+\eta^2)/\sigma_s^2}$, where σ_s is a length-scale of the smoothing. The length-scale of the smoothing was chosen to be $\sigma_s = 5\ km$. This value of σ_s leads to longer length-scales of the bedrock and ice surface undulations compared to $\sigma_s = 2.5\ km$ which was used in the analysis along flow lines.

7.5.3 Ice surface filters

Predicted ice surface undulations were computed by applying discrete filters g_{ij}, to the measured bedrock undulations, *i.e.* $\Delta z_s(x_i,y_j) = \Delta x \Delta y\ g_{ij} * \Delta z_b(x_i,y_j)$. The discrete filter g_{ij} was computed numerically from the modified transfer function corresponding to laminar flow given by (5.3.6) and (5.3.12) using two-dimensional FFT. The filter was discretized as discussed in Appendix 1 using (A1.3.3b) and (A1.3.5b). This leads to a well defined filter value at the origin for the discrete filter although the corresponding filter $g(x,y)$ is singular at the origin (*cf.* Fig. 5.3.2). The discrete filter g_{ij}, describes the steady state ice surface perturbation at the points x_i,y_j corresponding to a bedrock disturbance with the shape of a pyramid with base widths equal to $2\Delta x$ and $2\Delta y$.

The filter g_{ij} depends on the direction of the long scale ice flow (the ice piles up on the *upstream* side of the origin of the filter, *cf.* Figure 5.3.2). The orientation of the filter was introduced into the computation by a rotation of the transfer function in the Fourier domain (a rotation by a certain angle in the space domain is equivalent to a rotation by the same angle in the wave number domain). Separate filters were computed for each point of the digital map of the ice cap using a long scale ice thickness and a surface slope vector derived from the smoothed bedrock and ice surface.

7.5.4 Results

Figure 7.5.1 shows ice surface undulations predicted by three-dimensional laminar flow with $n = 3$ and no basal sliding for the 7 flow lines on Þjórsárjökull which were used for the flow line analysis in the previous section (*cf.* Figure 7.4.9). The undulations in Figure 7.5.1 are computed using a smoothing length-scale $\sigma_s = 5\ km$ which leads to

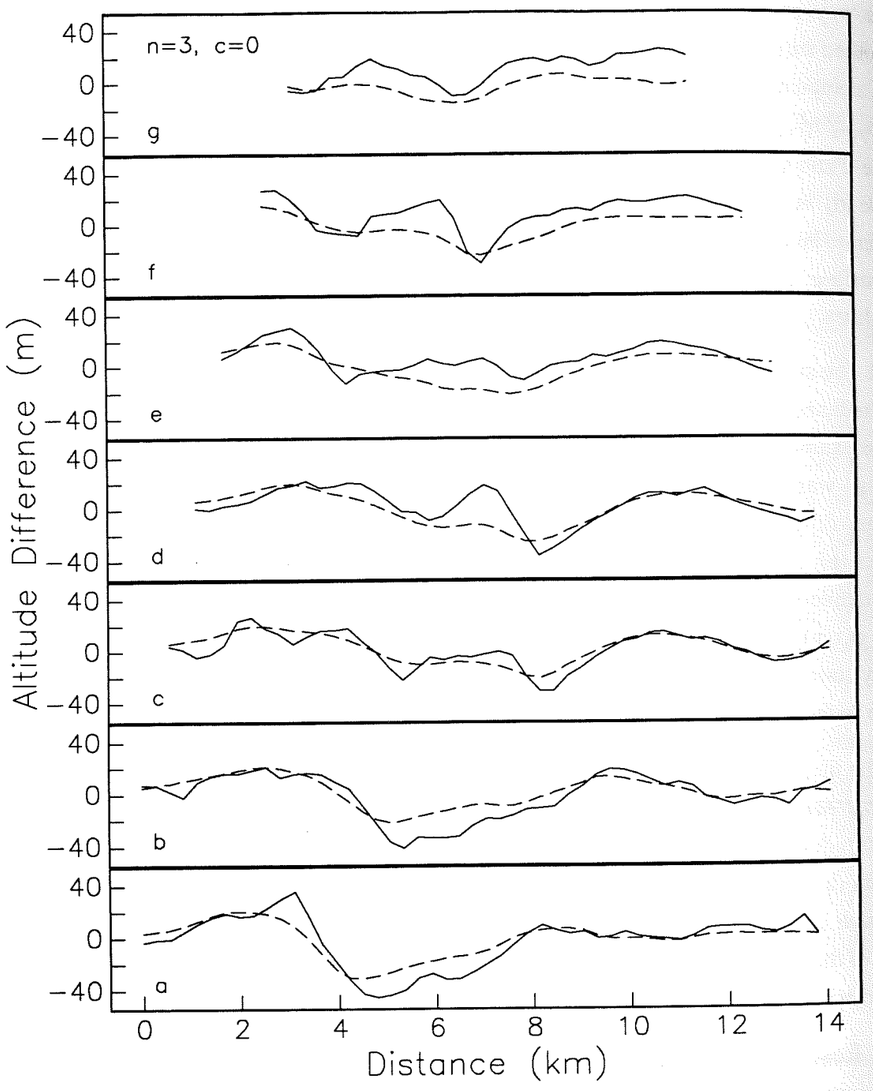

FIGURE 7.5.1: Ice surface undulations on Þjórsárjökull predicted by the laminar flow approximation for three-dimensional flow. The solid curves show measured ice surface undulations computed using σ_s = 5 km along 7 approximate flow lines. The dashed curves show predicted ice surface undulations corresponding to laminar flow for n = 3 for no basal sliding. Separate filters based on local values of the long scale ice thickness and surface slope are used at each point.

longer undulations with larger amplitudes (on the order of 40 *m*) compared to the undulations in the previous section which were computed using σ_s = 2.5 *km*. The undulations computed with non-zero basal sliding are so similar to those predicted with no sliding that only the results for no sliding are shown in Figure 7.5.1.

The predicted ice surface undulations were computed for the entire two-dimensional grid of the digital maps of Þjórsárjökull (excluding areas where the ice thickness is less than 100 *m* or where the long scale surface slope is less than 0.01). This makes it possible to plot and compare the measured and predicted undulations along any line in the *x*,*y*-plane of the digital map, *i.e.* the comparison is not restricted to flow lines. Figure 7.5.2 shows the predicted ice surface undulations along 5 lines (labeled "h" to "l") on Þjórsárjökull which are aligned approximately perpendicular to the direction of the ice flow. The lines strike along SW-NE diagonals in the grid. They start on x = 531,400, at the eastern edge of a gap in the net of the sounding lines and they end on x = 525,000. Line "l" starts at (531,400;476,400) which is at the intersection of flow line "a" and x = 531,400. The other lines start progressively further so the south on x = 531,400 with a spacing of 1 *km*. The lines are all 9 *km* long.

The predicted ice surface undulations are in general in agreement with the measured undulations on length-scales longer than approximately 1-2 *km* although there is considerable disagreement in a number of places, especially in lines "f","g", "k" and "l". Thus, the damping and shifting of bedrock undulations predicted by the laminar flow approximation is in rough agreement with the observations on these length-scales. The agreement between the measured and predicted profiles is similar too although not quite as good as in two-dimensional laminar flow analysis along flow line "c" on Blautukvíslarjökull in subsection 7.4.8. This indicates that the three-dimensional analysis has not produced an essential improvement in the predicted ice surface undulations over two-dimensional analysis along flow lines.

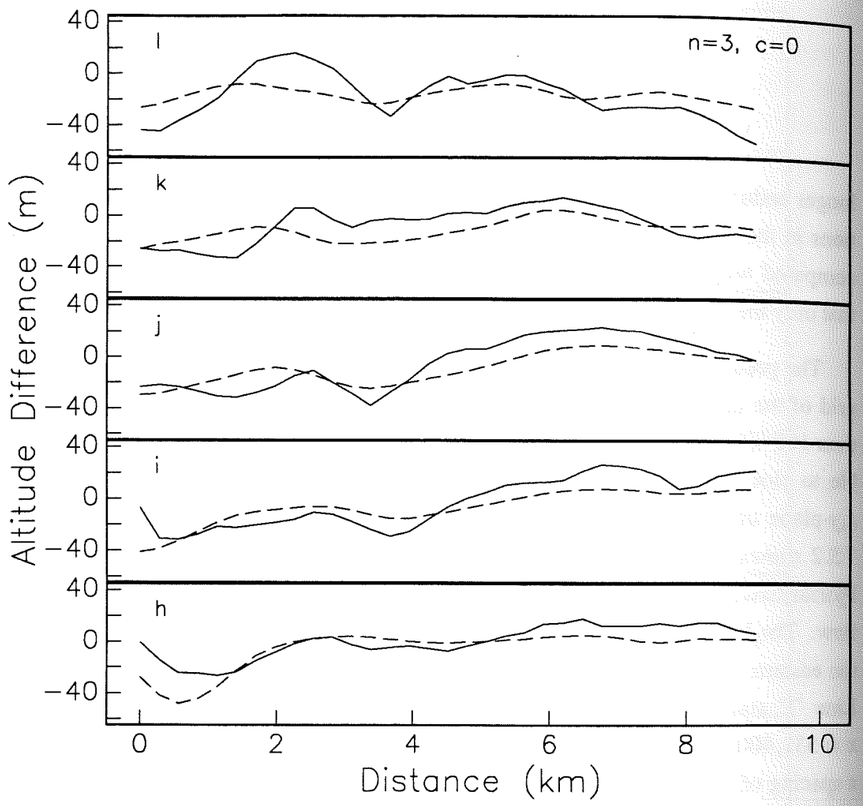

FIGURE 7.5.2: Ice surface undulations on Þjórsárjökull predicted by the laminar flow approximation for three-dimensional flow. The solid and dashed curves show measured and predicted ice surface undulations along 5 lines which are aligned approximately perpendicular to the direction of the ice flow (for explanation, see Figure 7.5.1).

The variance of the measured and predicted ice surface undulations together with the variance of the residuals (*i.e.* the differences between the measured and predicted undulations) may be used as a quantitative measure of the agreement between the measured and predicted undulations. Table 7.5.1 gives the variances for a 57.6 km^2 area on Blautukvíslarjökull which includes flow lines "a" to "e" (essentially the area shown in Figure 7.4.1), a 89.6 km^2 area on Þjórsárjökull which includes lines "h" to "l" and approximately the easternmost 2/3 of flow lines "a" to "g" (essentially the easternmost 2/3 of the area shown in Figure 1.1.2 in Chapter 1), and finally the variances computed from the entire digital map of the ice cap. As mentioned previously, there are some gaps in the net of sounding lines on Hofsjökull. The areas on Blautukvíslarjökull and Þjórsárjökull contain no large gaps. The map of the entire ice cap contains some gaps and also some very rough terrain with a few nunataks where the assumption of small perturbations in the glacier landscape will fail. Therefore, the predicted ice surface undulations for the entire ice cap may be expected to be somewhat worse than in the smaller areas.

TABLE 7.5.1: Statistics of ice surface undulations on Hofsjökull.

Area	Variance of measurements (m^2)	Predicted/Residual Variance (m^2)	Reduction in Variance (%)
Blautukvíslarjökull	452	285/245	46
Þjórsárjökull	390	148/138	65
entire ice cap	755	352/470	38

The variance of the measured undulations computed with $\sigma_s = 5\ km$ is much higher than the variance computed by detrending along flow lines with $\sigma_s = 2.5\ km$ in section 7.4. The variance of the measured undulations in the areas from Blautukvíslarjökull and Þjórsárjökull corresponds to standard deviations of 22 m and 20 m, respectively, while the standard deviation of the undulations for the entire ice cap is 27 m. The predicted undulations explain approximately 46% and 65% of the variance of the measured undulations on Blautukvíslarjökull and Þjórsárjökull, but only 38% in the case of the entire ice cap. The relatively low ratio for the entire ice cap is presumably caused by the gaps in the net of sounding lines and a failure of the theory in areas of very rough terrain.

As in the analysis along flow lines, it is found that ice surface filters corresponding to $n = 1$ (linear rheology) lead to some overprediction of the ice surface undulations (not shown). This reflects the effect of the non-linear flow law of ice on the glacier landscape.

However, there is relatively little difference between the predicted undulations for $n = 2$, 3 and 4 (not shown for $n = 2$ and 4), which implies that it is difficult to use the digital maps to estimate the power n in the ice flow law from the landscape of Hofsjökull. The fact that the standing wave is missing from the filter g_{ij} corresponding to laminar flow is a source of difficulties in this connection. The standing wave has a significant effect on the landscape of Hofsjökull as seen in the previous section. The absence of the standing wave can to some degree be compensated for by using a too low value of n and thereby shortening the length-scale of the filter g_{ij}. Therefore, estimates of n derived from laminar flow theory and the landscape of Hofsjökull will tend to be biased towards too low values. For this reason the data from Hofsjökull will not be used to estimate a precise value of n, but it can be stated that the data are inconsistent with $n = 1$ and consistent with the commonly accepted flow law power $n = 3$. This was also the conclusion of the two-dimensional analysis along flow lines in the previous section.

The three-dimensional laminar flow theory of Chapter 5 predicts that the transverse length-scale l_2, of the Green's function $g(x,y)$, should be considerably shorter for non-linear rheology than the longitudinal length-scale l_1. (*cf.* (5.3.3), (5.3.4) and (5.3.8)). This is the reason for the elongated form of the Green's function for non-linear rheology in Figure 5.3.2. In order to test this particular aspect of the theory, the predicted ice surface undulations where computed using the same length-scale for both the longitudinal and the transverse directions of the Green's function. Two cases were considered: (1) both length-scales equal to l_1 as given by (5.3.4) and (2) both length-scales equal to l_2 as given by (5.3.4). Both cases turned out to lead to dramatically worse predictions. Both length-scales equal to l_2 results in a large overprediction of the undulations, while the reverse is true if both length-scales are equal to l_1.

7.6 DISCUSSION AND SUMMARY OF RESULTS

The analysis of the digital maps of Hofsjökull confirms the theoretical predictions of Chapters 4 and 5. Ice surface undulations predicted from bedrock undulations using theoretically derived discrete filters based on the two-dimensional ice flow equations are in most cases within the estimated error of the measurements from the measured undulations.

Ice surface undulations on length-scales longer than approximately 1-2 *km* or on the order of 4-8 ice thicknesses are reasonably predicted by a relatively simple theory based on the laminar flow approximation. This theory is related to an early theory by Nye (1959b,c) which has been rejected by some researchers on this subject in the past (*cf.* Chapter 2).

The predicted ice surface undulations on length-scales shorter than approximately 1-2 *km* are significantly improved by a more accurate theory based on a solution of the full ice flow equations. The prediction of this theory of a "standing wave" in the steady state ice surface corresponding to a sharp peak in the bedrock landscape is verified by the above analysis of the landscape of Hofsjökull. This theory has only been derived for two-dimensional flow (except for linear Newtonian rheology where an analytical solution exists). The success of the two-dimensional theory along flow lines in explaining the landscape of Hofsjökull indicates that the ice surface undulations are formed by essentially two-dimensional flow *over* the bedrock landscape rather than by three-dimensional flow *around* bedrock obstacles.

The amplitude of the standing wave is primarily a function of the relative importance of basal sliding. The relative magnitude of the datum longitudinal strain rate has little effect on the amplitude of the standing wave. Robin (1967) argued that sign changes in the longitudinal strain rate are important for the formation of glacier landscape. The theory derived here implies that sign changes in the longitudinal strain rate have negligible effect on the formation of ice surface undulations. The theory predicts reasonable ice surface undulations along flow lines where the longitudinal strain rate most likely changes sign from positive values in the accumulation area to negative vales in the ablation area. Therefore, Robin's arguments about the importance of sign changes do not seem to be valid, at least not for Hofsjökull.

The landscape of Hofsjökull is consistent with the commonly accepted flow law power $n = 3$ and with basal sliding that transports on the order of 50% of the datum ice flux or lower. The theory cannot be used to estimate the role of basal sliding in the formation of ice surface undulations on Hofsjökull in detail, nor can it be used to make an independent estimate of the flow law power n based on the data from Hofsjökull.

There are no indications in the data from Hofsjökull that time-dependent glacier flow or spatial variation in basal sliding are significant factors in the formation of the ice surface undulations. The ice surface undulations seem to be primarily formed by steady ice flow over the basal landscape.

The theoretical prediction that the amplitude of the standing wave increases with increasing relative importance of basal sliding in the flow of the glacier, has an interesting consequence for exceptionally fast ice flow, for example during glacier surges, where most of the velocity of the ice is thought to be due to sliding. If a semi-steady state is established in the fast flow of the ice over and around a sharp bedrock obstacle, then the amplitude of the undulation, which is formed in the ice surface directly above the obstacle, should be much higher during a surge than in the quiescent phase between surges. Such undulations have in fact been observed and photographed on a number of Icelandic glaciers during and after surges (Sigurðsson, personal communication). Their shape is quite similar to the Green's function for (linear Newtonian) flow over a spike in the bedrock geometry which is shown in Figure 5.4.3.

CHAPTER 8: SYNOPSIS

The theory developed in this dissertation is a synthesis of the work of several recent authors on glacier dynamics, clarifying the relations of earlier theories to each other and identifying the areas where they need to be improved. The ice flow analysis is based on a linearization of the non-linear ice flow equations using a modification of the boundary layer theory of Johnson and McMeeking (1984) as a datum ice flow solution (*cf.* section 4.2). The mathematical formulation of the linearized ice flow equations and their numerical solution is based on Hutter's (1983) formulation of two-dimensional ice flow (*cf.* section 4.6). The perturbation ice flow satisfying the linearized ice flow equations is analyzed using *ice flux filters* which describe how localized perturbations in the bedrock and ice surface geometries affect the ice flux (*cf.* subsections 4.5.6, 4.6.7 and 4.6.8). The filters express the effect of both longitudinal stress gradients (*i.e.* the G term) and longitudinal shear stress gradients (*i.e.* the T term) on the ice flow (*cf.* subsections 4.6.8 and 4.6.9). The ice flux filters are related to Kamb and Echelmeyer's (1986a) filter theory (*cf.* subsection 4.6.11). The ice flux filters are used to derive steady state ice surface undulations corresponding to given bedrock undulations and also to formulate a time-dependent theory describing non-steady ice flow over bedrock undulations.

Johnson and McMeeking's (1984) boundary layer theory is not suitable for an analysis of glacier landscape because it breaks down for short and intermediate length-scale ice surface undulations. Hutter's (1983) theory does not take the important effect of longitudinal strain rate near the ice surface into account and it can therefore not be applied to the formation of glacier landscape. Kamb and Echelmeyer's (1986a) filter theory does not formulate the effect of longitudinal shear stress gradients (*i.e.* the T term) correctly and this makes it unsuitable for an analysis of short scale glacier landscape. The synthesis of these theories, which is developed in this dissertation, combines Johnson and McMeeking's analysis of the effect of longitudinal strain rate on glacier flow with Hutter's mathematical formulation of the ice flow equations using the filter approach introduced by Kamb and Echelmeyer.

The time-dependent theory is used to define a wavelength dependent kinematic wave velocity and diffusion coefficient which describe the propagation and diffusion of non-steady ice surface undulations (*cf.* sections 6.3 and 6.4). The time-scale for the decay of non-steady ice surface features, for wavelengths that are of interest for the formation of glacier landscape, is predicted to be on the order of a few months to a year. This implies that observed ice surface undulations on temperate ice caps are mainly a result of steady ice flow over the bedrock topography, except where conditions that are not described by the theory are important (*e.g.* surges, variable basal sliding). Time-dependent adjustment to changes in mass balance or spatial mass balance variations are predicted to have small effect on glacier landscape.

The theory implies that the differential equations describing time-dependent glacier flow are first and foremost diffusive in nature and this has interesting consequences for the propagation of kinematic waves (*cf.* sections 6.5 and 6.7). Non-steady glacier waves with wavelengths between 3 and 40 ice thicknesses are in general predicted to disappear by diffusion before they have propagated one wavelength (the wave amplitude is reduced by a factor on the order of 10^1–10^3 over one wavelength depending mainly on the datum surface slope). Propagating waves on glaciers with a speed approximately equal to 3-5 times the speed of the ice motion have traditionally been explained as kinematic waves. The rapid diffusion of glacier waves, which is implied by both the theory developed here and by the traditional kinematic wave equation, calls this explanation of the propagation of waves on glaciers into question. The fact that such propagating waves have been observed on glaciers indicates that some physical process not included in the derivation of the theory must be responsible for their propagation. Much too great emphasis has been placed on the almost non-existing propagation of glacier waves by earlier authors on glacier dynamics. The diffusion slows down for shorter wavelengths so that the theory is consistent with propagation of wave ogives with wavelengths on the order of one ice thickness or shorter with a speed equal to the surface velocity of the ice (*cf.* section 6.6).

Steady ice surface undulations are computed from a filter (Green's function) which describes the ice surface perturbation corresponding to a sharp spike (δ-function) in the bedrock geometry (*cf.* subsection 4.5.9 and section 4.7). This approach is different from previous theories on glacier landscape which have traditionally been formulated in terms

of a wavelength dependent transfer function from the bedrock to the ice surface. For two-dimensional flow, the steady state ice surface perturbation corresponding to a sharp spike in the bedrock geometry is characterized by the following features.

1. There is a "standing wave" in the ice surface directly above the basal spike with a peak on the upstream side and a trough on the downstream side. It's wavelength is approximately 1.5-3 ice thicknesses.
2. There is a long exponentially decaying tail on the upstream side of the standing wave. There is no such tail on the downstream side. The length-scale of the tail is inversely proportional to the long scale average surface slope.
3. The total volume of ice in the ice surface perturbation is exactly equal to the volume of the basal spike.

This implies that the surface of ice caps is predicted to be smooth except in the immediate vicinity of relatively sharp features in the bedrock landscape (*i.e.* features with a length-scale of a few ice thicknesses or shorter) where localized undulations with wavelengths on the order of 3 ice thicknesses are predicted. Although the analysis is focused on temperate ice caps, the above results may also be expected to hold true for ice surface undulations on cold ice sheets.

The standing wave is the explanation of the many observations of ice surface undulations on ice caps and ice sheets with wavelengths on the order of 3-4 ice thicknesses which are reported in the glaciological literature and which have not been adequately explained before. The standing wave arises in spite of the fact that there is in general no maximum (local or global) in the wavelength dependent transfer function from the bedrock to the ice surface at these wavelengths. Such a maximum is evidently not needed to explain the observations.

The prediction that the total volume of ice in the ice surface perturbation corresponding to a sharp basal spike is exactly equal to the volume of the basal spike implies that the wavelength dependent transfer function $t(\lambda)$, from the bedrock to the ice surface approaches unity as the wavelength goes to infinity, *i.e.* $t(\lambda) \rightarrow 1$ as $\lambda \rightarrow \infty$ (*cf.* subsection 4.4.4). This statement has the simple and intuitively obvious physical interpretation that the ice surface geometry of a glacier is predicted to be unaffected by a uniform

vertical uplift of the underlying bedrock. Observations of glacier landscape have by some authors (*e.g.* Beitzel, 1970; Budd and Carter, 1971) been interpreted to indicate that the transfer from the bedrock to the ice surface decays (to zero) with increasing wavelength for wavelengths longer than 3 to 4 ice thicknesses. This interpretation of the observations is in contradiction to the theory developed in this dissertation and it is difficult to reconcile with *any* reasonable theoretical analysis of the problem as it implies that a uniform vertical displacement of the bedrock, which is essentially equivalent to a vertical displacement of the origin of the coordinate system, will not lead to the same displacement of the ice surface. As discussed in section 2.8 and subsection 4.7.9, the observational evidence for a transfer function that decays to zero with increasing wavelength is weak and it appears that this interpretation of the observations is wrong.

The standing wave, on one hand, and the long exponentially decaying upstream tail in the ice surface geometry corresponding to a basal spike, on the other, can be attributed to two different flow regimes in the ice flow over the spike. The long tail is predicted by the laminar flow approximation, which is based on the assumption that the shear stress parallel to the ice surface increases linearly with ice depth from zero at the ice surface and that it is the only non-zero component of the deviatoric stress tensor. The standing wave arises from ice flow which cannot be described by the laminar flow approximation where all components of the deviatoric stress tensor are important.

The wavelength of the standing wave is relatively independent of the long scale average surface slope and other physical parameters that determine the ice flow over the basal spike. The amplitude of the wave, however, increases with the long scale average surface slope and the relative importance of basal sliding and decreases with the magnitude of the longitudinal strain rate in the long scale ice flow.

Three-dimensional analysis in the special case of linear Newtonian rheology sheds some light on how the two-dimensional results are generalized to three-dimensional ice flow (*cf.* section 5.4). A standing wave with a peak on the upstream side and a trough on the downstream side is predicted in the ice surface corresponding to a sharp basal spike. The amplitude of the standing wave increases with the long scale average surface slope and with the relative importance of basal sliding but the wavelength and the transverse width of the wave are relatively independent of the basal sliding and the surface slope.

Glacier landscape along approximate flow lines from the Hofsjökull ice cap, Central Iceland, is in good accordance with the two-dimensional theory. It appears that the geometry of the ice surface is mostly determined by two-dimensional ice flow *over* the bedrock undulations rather than by three-dimensional flow *around* them. Detailed comparison of measured and predicted surface undulations verifies the prediction of a standing wave in the ice surface geometry corresponding to a basal spike.

The theory presented in the dissertation can be further developed in a number of directions. The two-dimensional theory can be improved by taking longitudinal variation in the datum ice flow into account. This may be expected to lead to asymmetry in the ice flux filters when there is significant longitudinal variation in the datum flow over the span of the filters (*cf.* Kamb and Echelmeyer, 1986a).

Channel-shape factors (Nye, 1965c) need to be introduced into the theory before it can be applied to valley glaciers. After that has been done, the expressions for the total ice flux derived in section 4.6.9 can be used as the basis for numerical ice flow modelling. Numerical ice flow models based on ice flux filters can be used to investigate changes in glacier landscape during time-dependent adjustment of the long scale datum ice flow, for example during advance and retreat of the glacier.

The theory can also be modified to take changes in rheological parameters with ice depth into account. This would make the theory suitable for application to cold ice sheets (for example for predicting the distribution of internal velocity and the topography of internal layers).

The three-dimensional theory is not as well developed as the two-dimensional theory. The analysis has only been carried out for two special cases, the laminar flow approximation and for linear Newtonian rheology. Three dimensional analysis for realistic non-linear ice rheology remains to be done.

The application of the theory to Hofsjökull indicates that useful information about the nature of the ice flow is contained in the measured ice surface geometry. The amplitude of the ice surface undulations is sensitive to the relative importance of basal sliding for temperate ice caps and it may be expected to be sensitive to the distribution of temperature and rheological parameters with ice depth on cold ice sheets. This suggests that

accurate and dense measurements of the bedrock and ice surface geometry of ice caps and ice sheets, eventually combined with measurements of the topography of internal layers, can be used to obtain information about the relative importance of basal sliding on temperate ice caps and about the vertical distribution of temperature and rheological parameters with depth on cold ice sheets. Inversion of such measurements would yield averages of the parameters to be found over a relatively large area and they are therefore complementary to more direct measurements in bore holes which can only provide point values at the location of the hole.

LIST OF REFERENCES

Abramowitz, M. and I. A. Stegun. 1965. *Handbook of Mathematical Functions.* New York, Dover Publications, Inc., 1046 pp.

Balise. M. J. Unpublished. *The relation between surface and basal velocity variations in glaciers, with application to the mini-surges of Variegated glacier.* [Ph.D. thesis, University of Washington, 1988, 205 pp.]

Balise, M. J. and C. F. Raymond. 1985. Transfer of basal sliding variations to the surface of a linearly viscous glacier. *Journal of Glaciology,* 31(109), 308-318.

Beitzel, J. E. 1970. The relationship of ice thickness and surface slope in Dronning Maud Land. *AIHS Publication No. 86,* 191-203.

Bindschadler, R. A. 1982. A numerical model of temperate glacier flow applied to the quiescent phase of a surge-type glacier. *Journal of Glaciology,* 28(99), 239-265.

Björnsson, H. 1974. Explanation of jökulhlaups from Grímsvötn, Vatnajökull, Iceland. *Jökull,* 24, 1-26.

Björnsson, H. 1977. The cause of jökulhlaups in the Skaftá river, Vatnajökull. *Jökull,* 27, 71-78.

Björnsson, H. 1988. *Hydrology of Ice Caps in Volcanic Regions.* Reykjavík, Societas Scientarium Islandica, Rit 45, 139 pp.

Bodvarsson, G. 1955. On the flow of ice-sheets and glaciers. *Jökull,* 5, 1-8.

Box, G. E. P. and G. M. Jenkins. 1970. *Time Series Analysis, Forecasting and Control.* San Fransisco, *etc.*, Holden-Day, Inc., 553 pp.

Brockamp, B. and F. Thyssen. 1968. Eine Anwendung der barographisch-topographischen Kurve zur Bestimmung der Bewegung von Inlandeisen. *Polarforschung,* Bd. 6, Jahrg. 37/1967, Ht. 1/2, 125-129.

Budd, W. F. 1968. The longitudinal velocity profile of large ice masses. *AIHS Publication No. 79,* 58-77.

Budd, W. F. 1969. The dynamics of ice masses. *ANARE Scientific Reports. Ser. A (IV). Glaciology. Publication No. 108,* 216 pp.

Budd, W. F. 1970a. The longitudinal stress and strain-rate gradients in ice masses. *Journal of Glaciology,* 9(55), 19-27.

Budd, W. F. 1970b. Ice flow over bedrock perturbations. *Journal of Glaciology,* 9(55), 29-48.

Budd, W. F. 1971. Stress variations with ice flow over undulations. *Journal of Glaciology,* 10(59), 177-195.

Budd, W. F. and D. B. Carter. 1971. An analysis of the relation between the surface and bedrock profiles of ice caps. *Journal of Glaciology,* 10(59), 197-209.

Budd, W. F. and D. Jensen. 1975. Numerical modelling of glacier systems. *IAHS-AISH Publication No. 104,* 257-291.

Butkov, E. 1968. *Mathematical Physics.* Menlo Park, California, Addison-Wesley Publishing Company, 735 pp.

Chatfield, C. 1980. *The Analysis of Time Series: An Introduction (Second Edition).* London, New York, Chapman and Hall, 268 pp.

Collins, I. F. 1968. On the use of the equilibrium equations and flow law in relating the surface and bed topography of glaciers and ice sheets. *Journal of Glaciology,* 7(50), 199-204.

Conte, S. D. and C. de Boor. 1980. *Elementary Numerical Analysis, An Algorithmic Approach (Third Edition).* Aukland etc., McGraw-Hill Book Company, 432 pp.

Dahl-Jensen, D. 1985. Determination of the flow properties at Dye 3, South Greenland, by bore-hole-tilting measurements and perturbation modelling. *Journal of Glaciology,* 31(108), 92-98.

Echelmeyer, K. A. Unpublished. *Response of Blue glacier to a perturbation in ice thickness: theory and observation.* [Ph.D. thesis, California Institute of Technology, 1983, 342 pp.]

Echelmeyer, K. A. and B. Kamb. 1986. Stress-gradient coupling in glacier flow: II. longitudinal averaging in the flow response to small perturbations in ice thickness and surface slope. *Journal of Glaciology,* 32(111), 285-298.

Fowler, A. C. 1982. Waves on glaciers. *Journal of Fluid Mechanics,* 120, 283-321.

Fowler, A. C. and D. A. Larson. 1978. On the flow of polythermal glaciers. I. Model and preliminary analysis. *Proceedings of the Royal Society of London, Ser. A,* 363(1713), 217-242.

Fowler, A. C. and D. A. Larson. 1980. On the flow of polythermal glaciers. II. Surface wave analysis. *Proceedings of the Royal Society of London, Ser. A,* 370(1741), 155-171.

Garland, G. D. 1979. *Introduction to Geophysics.* Philadelphia, *etc.*, W. B. Saunders Company, 494 pp.

Glen, J. W. 1952. Experiments on the deformation of ice. *Journal of Glaciology,* 2(12), 111-114.

Glen, J. W. 1955. The creep of polycrystalline ice. *Proceedings of the Royal Society of London, Ser. A,* 228(1175), 519-538.

Halfar, P. 1981. On the dynamics of ice sheets. *Journal of Geophysical Research,* 86(C11), 11065-11072.

Hindmarsh, R. C. A. 1990. Time-scales and degrees of freedom operating in the evolution of continental ice-sheets. *Transactions of the Royal Society of Edinburg, Earth Sciences,* 81, 371-384.

Hooke, R. LeB. 1981. Flow law for polycrystalline ice in glaciers: comparison of theoretical predictions, laboratory data, and field measurements. *Reviews of Geophysics and Space Physics,* 19(4), 664-672.

Hooke, R. LeB., M. Mellor, W. F. Budd, J. W. Glen, A. Higashi, T. H. Jacka, S. J. Jones, R. C. Lile, R. T. Martin, M. F. Meier, D. S. Russel-Head and J. Weertman. 1980. Mechanical properties of polycrystalline ice: an assessment of current knowledge and priorities for research. *Cold Regions Science and Technology,* 3, 263-275.

Hutter, K. 1980. Time-dependent surface elevation of an ice slope. *Journal of Glaciology,* 25(92), 247-266.

Hutter, K. 1981. The effect of longitudinal strain on the shear stress of an ice sheet: in defence of using stretched coordinates. *Journal of Glaciology,* 27(95), 39-56.

Hutter, K. 1983. *Theoretical glaciology.* Dordrecht, *etc.*, D. Reidel Publishing Company, 510 pp.

Hutter, K., F. Legerer and U. Spring. 1981. First-order stresses and deformations in glaciers and ice sheets. *Journal of Glaciology,* 27(96), 227-270.

Huybrechts, P. and J. Oerlemans. 1988. Evolution of the East Antarctic ice sheet: a numerical study of thermo-mechanical response patterns with changing climate. *Annals of Glaciology,* 11, 52-59.

Jóhannesson, T., C. F. Raymond and E. D. Waddington. 1989. Time-scale for adjustment of glaciers to changes in mass balance. *Journal of Glaciology,* 35(121), 355-369.

Johnson, R. E. and R. M. McMeeking. 1984. Near-surface flow in glaciers obeying Glen's law. *Quarterly Journal of Mechanics and Applied Mathematics*, 37(2), 273-291. [an error in the analysis is corrected in a corrigendum published in the issue 37(4), p. 632]

Kamb, B. 1970. Sliding motion of glaciers: theory and observation. *Reviews of Geophysics and Space Physics*, 8(4), 673-728.

Kamb, B. 1986. Stress-gradient coupling in glacier flow: III. exact longitudinal equilibrium equation. *Journal of Glaciology*, 32(112), 335-341.

Kamb, B. and K. A. Echelmeyer. 1986a. Stress-gradient coupling in glacier flow: I. longitudinal averaging of the influence of ice thickness and surface slope. *Journal of Glaciology*, 32(111), 267-284.

Kamb, B. and K. A. Echelmeyer. 1986b. Stress-gradient coupling in glacier flow: IV. effects of the "T" term. *Journal of Glaciology*, 32(112), 342-349.

Kevorkian, J. and J. D. Cole. 1981. *Perturbation Methods in Applied Mathematics*. New York, *etc.*, Springer-Verlag, 558 pp.

Langdon, J. and C. F. Raymond. 1978. Numerical calculation of adjustment of a glacier surface to perturbations of ice thickness. *Mater. Glyatsiol. Issled. Khron. Obsuzhdeniya*, 32, 233-239.

Lliboutry, L. 1968. General theory of subglacial cavitation and sliding of temperate glaciers. *Journal of Glaciology*, 7(49), 21-58.

Lister, H. 1959. Reports of Discussions: Geophysical discussion of the Royal Astronomical Society on The characteristics of the Antarctic ice sheet (contribution to discussion). *Geophysical Journal of the Royal Astronomical Society*, 2(2), 164-168.

Magnus, W. and F. Oberhettinger. 1949. *Formulas and Theorems of the Special Functions of Mathematical Physics*. Chelsea, 116-120.

Morland, L. W. and I. R. Johnson. 1980. Steady motion of ice sheets. *Journal of Glaciology*, 25(92), 229-246.

Nye, J. F. 1951. The flow of glaciers and ice-sheets as a problem in plasticity. *Proceedings of the Royal Society of London, Ser. A*, 207(1091), 554-572.

Nye, J. F. 1952a. A method of calculating the thicknesses of the ice-sheets. *Nature*, 169(4300), 529-530.

Nye, J. F. 1952b. The mechanics of glacier flow. *Journal of Glaciology*, 2(12), 82-93.

Nye, J. F. 1953. The flow law of ice from measurements in glacier tunnels, laboratory experiments and the Jungfraufirn borehole experiment. *Proceedings of the Royal Society of London, Ser. A*, 219(1139), 477-489.

Nye, J. F. 1957. The distribution of stress and velocity in glaciers and ice-sheets. *Proceedings of the Royal Society of London, Ser. A*, 239(1216), 113-133.

Nye, J. F. 1958. A theory of wave formation in glaciers. *AIHS Publication No. 47*, 139-154.

Nye, J. F. 1959a. The deformation of a glacier below an ice fall. *Journal of Glaciology*, 3(25), 387-408.

Nye, J. F. 1959b. The motion of ice sheets and glaciers. *Journal of Glaciology*, 3(26), 493-507.

Nye, J. F. 1959c. Surface topography of the Antarctic ice sheet. *Nature*, 184(4689), 786-787.

Nye, J. F. 1960. The response of glaciers and ice-sheets to seasonal and climatic changes. *Proceedings of the Royal Society of London, Ser. A*, 256(1287), 559-584.

Nye, J. F. 1963a. On the theory of the advance and retreat of glaciers. *Geophysical Journal of the Royal Astronomical Society*, 7(4), 431-456.

Nye, J. F. 1963b. The response of a glacier to changes in the rate of nourishment and wastage. *Proceedings of the Royal Society of London, Ser. A*, 275(1360), 87-112.

Nye, J. F. 1965a. The frequency response of glaciers. *Journal of Glaciology*, 5(41), 567-587.

Nye, J. F. 1965b. A numerical method of inferring the budget history of a glacier from its advance and retreat. *Journal of Glaciology*, 5(41), 589-607.

Nye, J. F. 1965c. The flow of a glacier in a channel of rectangular, elliptic, or parabolic cross-section. *Journal of Glaciology*, 5(41), 661-690.

Nye, J. F. 1969a. The effect of longitudinal stress on the shear stress at the base of an ice sheet. *Journal of Glaciology*, 8(53), 207-213.

Nye, J. F. 1969b. A calculation on the sliding of ice over a wavy surface using a Newtonian viscous approximation. *Proceedings of the Royal Society of London, Ser. A*, 311(1506), 445-467.

Nye, J. F. 1970. Glacier sliding without cavitation in a linear viscous approximation. *Proceedings of the Royal Society of London, Ser. A*, 315(1522), 381-403.

Orowan, E. 1949. Remarks at a joint meeting of the British Glaciological Society, the British Rheologists' Club and the Institute of Metals. *Journal of Glaciology,* 1(5), 231-236.

Overgaard, S. and N. S. Gundestrup. 1985. Bedrock topography of the Greenland ice sheet in the Dye 3 area. *In* Langway, C. C., Jr., H. Oeschger and W. Dansgaard, *eds. Greenland Ice Core: Geophysics, Geochemistry, and the Environment.* Washington, DC, American Geophysical Union, 49-56. [Geophysical Monograph, 33]

Paterson, W. S. B. 1972. Laurentide ice sheet: estimated volumes during late Wisconsin. *Reviews of Geophysics and Space Physics,* 10(4), 885-917.

Paterson, W. S. B. 1980. Ice sheets and ice shelves. *In* Colbeck, S. C. *ed. Dynamics of Snow and Ice Masses.* New York, Academic Press, 1-78.

Paterson, W. S. B. 1981. *The Physics of Glaciers. Second edition.* Oxford *etc.*, Pergamon Press, 380 pp.

Paterson, W. S. B. and J. C. Savage. 1963. Geometry and movement of the Athabasca glacier. *Journal of Geophysical Research,* 68(15), 4513-4520.

Raymond, C. F. 1980. Temperate valley glaciers. *In* Colbeck, S. C. *ed. Dynamics of Snow and Ice Masses.* New York, Academic Press, 79-139.

Reeh, N. 1982. A plasticity theory approach to the steady-state shape of a three-dimensional ice sheet. *Journal of Glaciology,* 28(100), 431-455.

Reeh, N. 1987. Steady-state three-dimensional ice flow over an undulating base: first-order theory with linear ice rheology. *Journal of Glaciology,* 33(114), 177-185.

Robin, G. de Q. 1967. Surface topography of ice sheets. *Nature,* 215(5105), 1029-1032.

Robin, G. de Q. and D. H. M. Millar. 1982. Flow of ice sheets in the vicinity of subglacial peaks. *Annals of Glaciology,* 3, 290-294.

Robinson, E. S. 1966. On the relationship of ice-surface topography to bed topography on the south polar plateau. *Journal of Glaciology,* 6(43), 43-54.

Schweizer, J. 1989. *Friction at the base of a glacier.* Zürich, VAW, ETH, Mitteilungen 101, 181 pp.

Sigurðsson, O. 1989a. Afkoma Hofsjökuls 1987-1988 (in Icelandic). *Report OS-89005/VOD-02 B.* National Energy Authority, Reykjavík.

Sigurðsson, O. 1989b. Jöklabreytingar 1930-1960, 1960-1980, 1980-1987 og 1987-1988 (in Icelandic). *Jökull,* 39, 108-113.

Stacey, F. D. 1977. *Physics of the Earth, Second Edition.* Chichester, *etc.*, John Wiley & Sons, 414 pp.

Thomson, W. (Lord Kelvin). 1888. Polar ice caps and their influence on changing sea levels. *In* Thomson, W. *Popular lectures and addresses, Vol. 2, Geology and general Physics,* 319-359. London, MacMillan, 1894, 599 pp.

Thórarinsson, S. 1952. Svigður á Morsárjökli. *Jökull,* 2, 22-25.

Thórarinsson, S. 1953. Svigður á Svínafellsjökli í Öræfum. *Jökull,* 3, 39-40.

Vialov, S. S. 1958. Regularities of glacial shields movement and the theory of plastic viscous flow. *AIHS Publication No. 47,* 266-275.

Waddington, E. D. Unpublished. *Accurate modelling of glacier flow.* [Ph.D. thesis, University of British Columbia, 1981, 460 pp.]

Waddington, E. D. 1986. Wave ogives. *Journal of Glaciology,* 32(112), 325-334.

Weertman, J. 1957. On the sliding of glaciers. *Journal of Glaciology,* 3(21), 33-38.

Weertman, J. 1961. Equilibrium profile of ice caps. *Journal of Glaciology,* 3(30), 953-964.

Weertman, J. 1964. The theory of glacier sliding. *Journal of Glaciology,* 5(39), 287-303.

Whillans, I. M., K. C. Jezek, A. R. Drew and N. S. Gundestrup. 1984. Ice flow leading to the deep core hole at Dye 3, Greenland. *Annals of Glaciology,* 5, 185-190.

Whillans, I. M. and S. J. Johnsen. 1983. Longitudinal variations in glacial flow: theory and test using data from the Byrd Station strain network, Antarctica. *Journal of Glaciology,* 29(101), 78-97.

Yosida, Z. 1964. Internal stress and viscous flow of snow covers on sloping ground surfaces. I. Snow cover on wavy ground of mean inclination α. *Teion-kagaku: Low Temperature Science. Ser. A,* 22, 83-100.

Zwally, H. J., R. A. Bindschadler, A. C. Brenner, T. V. Martin and R. H. Thomas. 1983. Surface elevation contours of Greenland and Antarctic Ice Sheets. *Journal of Geophysical Research,* 88(C3), 1589-1596.

Zwally, H. J., R. L. Brooks, H. R. Stanley and W. J. Campbell. 1979. Ice-sheet surface elevation and changes observable by satellite radar altimetry. *Journal of Glaciology,* 24(90), 491-493.

APPENDIX 1: DISCRETE AND CONTINUOUS FILTERS

A1.1 INTRODUCTION

The Green's functions for ice flux and steady state surface geometry which are derived in this dissertation are functions of continuous spatial coordinates because of the continuous nature of the flow of ice caps and glaciers. A Green's function is the solution corresponding to δ-function forcing at the origin and its usefulness lies in the fact that it may be used to derive the solution corresponding to arbitrary forcing by convolving the Green's function with the forcing.

The Green's functions considered here may contain discontinuities or (absolutely) integrable singularities. Although discontinuities and singularities in the Green's functions cannot as such be realized as ice flux or surface geometry of real ice caps, the convolution of the Green's functions with real forcings will lead to realistic solutions. Examples of this phenomenon are the Green's functions for the steady state surface shape over an undulating bed topography derived from the parallel slab approximation for the ice flux (Equations (4.4.9) and (5.3.8)). In one dimension (x), the Green's function is discontinuous but bounded at the origin (Figure 4.4.2). In two dimensions (x and y), the Green's function is unbounded but integrable at the origin (Figure 5.3.2).

Discontinuities and singularities in the Green's functions can, however, lead to problems when the functions are applied to real data which are necessarily discrete in nature. If the application of the Green's function is based on point values at the discrete points of measurement, then it is possible that the Green's function is undefined at some of the points. Furthermore, using point values may lead to considerable loss of accuracy if changes in the Green's function are much more rapid than changes in the data.

Discontinuities and singularities in the Green's function are harmless in the continuos problem because of the continuos convolution with a forcing function. In order to avoid the difficulties associated with undefined values and loss of accuracy in the discrete problem, one must avoid using point values of the Green's function. This can be done by continuous convolution of the Green's function with appropriate smoothing windows to

produce discrete filters which are then applied to the data.

A1.2 ONE DIMENSION

I will first consider the one-dimensional case denoting the forcing function by $f(x)$, the Green's function by $g(x)$ and the corresponding solution by $h(x)$. Then

$$h(x) = g(x)*f(x) = \int g(x-\xi)f(\xi)d\xi\,, \tag{A1.2.1}$$

where continuous convolution is indicated by $g(x)*f(x)$. Let the forcing function be known at the points $x_i = i\Delta x$ for integers i and define $f_i = f(x_i)$, $g_i = g(x_i)$ and $h_i = h(x_i)$. Then, straightforward use of point values leads to

$$h_i \simeq \Delta x\, g_i*f_i = \Delta x \sum_j g_{i-j} f_j\,, \tag{A1.2.2}$$

where discrete convolution is indicated by g_i*f_i.

By this approach each subintegral $\int_{x_j-\Delta x/2}^{x_j+\Delta x/2} g(x_i-\xi)f(\xi)d\xi$ in the continuous convolution is approximated by $\Delta x\, g_{i-j} f_j$. This is equivalent to using the so-called *midpoint rule* for the evaluation of an integral (Conte and de Boor, 1980, Chapter 7) and introduces an error equal to

$$e_p = |d^2(g(x_i-\xi)f(\xi))/d\xi^2|_{\xi=\eta}\,\frac{\Delta x^3}{24} \tag{A1.2.3}$$

for each subintegral, for some η in the interval $x_j-\Delta x/2 \le \eta \le x_j+\Delta x/2$. This error estimate is essentially useless because of the factor $|d^2(g(x_i-\xi)f(\xi))/d\xi^2|_{\xi=\eta}$ which involves $g(x_i-\xi)$ and its first and second derivatives all of which may be singular.

The cause of the above difficulties lies in the discretization of the Green's function. Since it is in principle known for all values of x, some information is unnecessarily thrown away by the discretization. In order to overcome the problems associated with direct discretization of the Green's function it is advantageous to define the function

$$d(x) = \sum_i f_i\,\delta(x-x_i)\,, \tag{A1.2.4}$$

where $\delta(x)$ denotes the continuos δ-function. The function $d(x)$ is a string of δ-functions

located at the points $x = x_i$ for integers i and weighted by f_i. Continuous approximations to $f(x)$ may be defined by appropriate filtering of $d(x)$. Two filters are most convenient to use. The boxcar filter

$$b(x) = \frac{1}{\Delta x} \text{ for } |x| \le \Delta x/2\,,\ b(x) = 0 \text{ for } |x| > \Delta x/2 \qquad \text{(A1.2.5a)}$$

and the triangular filter

$$t(x) = \frac{1}{\Delta x}\left(1 - \frac{|x|}{\Delta x}\right) \text{ for } |x| \le \Delta x\,,\ t(x) = 0 \text{ for } |x| > \Delta x\,, \qquad \text{(A1.2.5b)}$$

both normalized to be of unit area. Then

$$\bar{f}(x) = \Delta x\, d(x) * b(x)$$

and

$$\bar{\bar{f}}(x) = \Delta x\, d(x) * t(x)$$

are two approximations of the forcing $f(x)$, both defined for any value of x. $\bar{f}(x)$ is a step function which intersects $f(x)$ at $x = x_i$, and $\bar{\bar{f}}(x)$ is a piecewise-linear function which intersects $f(x)$ at its breakpoints x_i.

The functions $\bar{f}(x)$ and $\bar{\bar{f}}(x)$ may be used instead of $f(x)$ in (A1.2.1) to define two approximations $\bar{h}(x)$ and $\bar{\bar{h}}(x)$ of the solution $h(x)$. Using the associative and commutative properties of the convolution operation one finds that

$$\begin{aligned}\bar{h}(x) &= g(x) * \bar{f}(x) = \Delta x\, g(x) * (d(x) * b(x)) = \Delta x\, (g(x) * b(x)) * d(x) \\ &= \Delta x\, \bar{g}(x) * d(x) = \Delta x\, \bar{g}(x) * \sum_i f_i\, \delta(x - x_i) = \Delta x \sum_i \bar{g}(x - x_i)\, f_i\,,\end{aligned}$$

where $\bar{g}(x)$ is defined as $g(x) * b(x)$. The values of $\bar{h}(x)$ at $x = x_i$ are then given by

$$\bar{h}_i = \bar{h}(x_i) = \Delta x\, \bar{g}_i * f_i\,, \qquad \text{(A1.2.6a)}$$

where $\bar{g}_i = \bar{g}(x_i)$. Similarly, defining $\bar{\bar{g}}(x) = g(x) * t(x)$ and $\bar{\bar{g}}_i = \bar{\bar{g}}(x_i)$, one finds that

$$\bar{\bar{h}}_i = \bar{\bar{h}}(x_i) = \Delta x\, \bar{\bar{g}}_i * f_i\,. \qquad \text{(A1.2.6b)}$$

In the above derivation, the filtering or smoothing operation, which was used to derive a continuous estimate of the forcing $f(x)$ from its discrete values f_i, has been applied to the Green's function $g(x)$. This amounts to taking the running mean of $g(x)$ by convolution with a boxcar or a triangular filter. This convolution has the convenient property that $\int g(\xi) d\xi = \Delta x \sum_i \bar{g}_i = \Delta x \sum_i \bar{\bar{g}}_i$. Equations (A1.2.6a) and (A1.2.6b) express $\bar{h}_i$ and $\bar{\bar{h}}_i$ as discrete convolutions of the discrete filters $\bar{g}_i$ and $\bar{\bar{g}}_i$ with the discrete measured values of the forcing f_i. The filters $\bar{g}_i$ and $\bar{\bar{g}}_i$ have a simple interpretation. They are the values at the points x_i of the exact solutions corresponding to boxcar and triangular forcings at the origin. Similarly, the approximations $\bar{h}_i$ and $\bar{\bar{h}}_i$ are the values at the points x_i of the exact solutions corresponding to step function forcing and piecewise-linear forcing, respectively. The approximation (A1.2.2), on the other hand, may be interpreted as the exact solution corresponding to a forcing function which consists of a series of δ-spikes (*i.e.* the function $d(x)$ given by (A1.2.4)). The step function forcing or the piecewise-linear forcing are of course much more realistic interpretations of the discrete data under most real circumstances.

Using standard methods for estimating the error of numerical integral approximations (Conte and de Boor, 1980, Chapter 7), the error in the subintegrals leading to $\bar{h}_i$ and $\bar{\bar{h}}_i$ is found to be

$$e_b \le |f''(\eta_1)| \int_{x_j - \Delta x/2}^{x_j + \Delta x/2} |g(x_i - \xi)(\xi - x_j)|\, d\xi$$

for $\bar{h}_i$ and

$$e_t \le \tfrac{1}{2} |f''(\eta_2)| \int_{x_j - \Delta x/2}^{x_j + \Delta x/2} |g(x_i - \xi)(\xi - x_j)(\Delta x - |\xi - x_j|)|\, d\xi$$

for $\bar{\bar{h}}_i$, for some η_1 and η_2 in the interval $x_j - \Delta x/2 \le \eta_1\,,\ \eta_2 \le x_j + \Delta x/2$.

The error estimates e_b and e_t are a large improvement over the estimate e_p given by (A1.2.3). e_b and e_t only involve derivatives of the forcing $f(x)$ and do not depend on derivatives of the Green's function $g(x)$. In fact $g(x)$ only needs to be absolutely

integrable for the error estimates e_b and e_t to be useful. If the Green's function is bounded it may be useful to write these error estimates as $e_b \le |f'(\eta_1)\, g(x_i-\eta_1)|\Delta x^2/4$ and $e_t \le |f''(\eta_2)\, g(x_i-\eta_2)|\Delta x^3/12$. Again these estimates are an improvement over (A1.2.3) because they do not involve derivatives of $g(x)$.

It is possible to interpret the above results in terms of aliasing. In order to prevent aliasing, when sampling a continuous function, the sampling rate must be higher than twice the highest significant frequency which is present in the function. When (A1.2.2) is used to estimate the solution h_i, both the forcing function and the Green's function must be sampled or discretized with the same sampling rate. The restrictions on the sampling rate to prevent aliasing must therefore be based on the frequency distribution of the Green's function in addition to the frequency distribution of the forcing function. This is unfortunate since the Green's function may contain much more power at high frequencies than the forcing function. It is also unnecessary since the Green's function is in principle known for all x and can thus be sampled with an arbitrarily high sampling rate. Using (A1.2.6a) or (A1.2.6b) to estimate h_i does not involve discrete sampling of the Green's function as such and therefore the restrictions on the sampling rate to prevent aliasing only need to take into account the frequency distribution of the forcing function.

It is worth stressing that the use of the filtered Green's functions $\bar{g}_i$ and $\bar{\bar{g}}_i$ in (A1.2.6a) or (A1.2.6b) does not involve an arbitrary approximation. The accuracy of (A1.2.6a) and (A1.2.6b) only depends on how well the step function forcing $\bar{f}(x)$ and the piecewise-linear forcing $\bar{\bar{f}}(x)$ approximate the real forcing $f(x)$. The filtered Green's functions are the appropriate way to express the information contained in the original continuous Green's function in a form suitable for application to discrete measurements.

The Green's functions considered here are typically found from their Fourier transforms. Since convolution in the space domain is equivalent to multiplication in the frequency or wave number domain and since $\bar{g}(x)$ and $\bar{\bar{g}}(x)$ are defined as convolutions of $g(x)$ with $b(x)$ and $t(x)$, it is easiest to determine $\bar{g}_i$ and $\bar{\bar{g}}_i$ from their Fourier transforms. The Fourier transforms of $b(x)$ and $t(x)$ are given by

$$\hat{b}(k) = \frac{1}{\Delta x}\int_{-\Delta x/2}^{\Delta x/2} e^{-ikx}dx = \frac{\sin(k\Delta x/2)}{(k\Delta x/2)} \qquad \text{(A1.2.7a)}$$

and

$$\hat{t}(k) = \frac{1}{\Delta x}\int_{-\Delta x}^{\Delta x} (1-\frac{|x|}{\Delta x})e^{-ikx}dx = \frac{\sin^2(k\Delta x/2)}{(k\Delta x/2)^2} \qquad \text{(A1.2.7b)}$$

From these expressions for $\hat{b}(k)$ and $\hat{t}(k)$ and an already known $\hat{g}(k)$ the Fourier transforms of $\bar{g}(x)$ and $\bar{\bar{g}}(x)$ are given by

$$\hat{\bar{g}}(k) = \hat{g}(k)\hat{b}(k) \qquad \text{(A1.2.8a)}$$

and

$$\hat{\bar{\bar{g}}}(k) = \hat{g}(k)\hat{t}(k)\,. \qquad \text{(A1.2.8b)}$$

The use of (A1.2.8a) and (A1.2.8b) in numerical applications has the advantage that $\hat{\bar{g}}(k)$ and $\hat{\bar{\bar{g}}}(k)$ approach zero more rapidly than $\hat{g}(k)$ as $k \to \pm\infty$. This can lead to substantial computational savings in the computation of $\bar{g}_i$ and $\bar{\bar{g}}_i$ in practice. In general the triangular filter $\bar{\bar{g}}_i$ is easier to compute than the boxcar filter $\bar{g}_i$. Furthermore, Equation (A1.2.6b), which involves $\bar{\bar{g}}_i$, provides better accuracy in the predicted values of the solution at x_i than (A1.2.6a) which uses $\bar{g}_i$.

A1.3 TWO DIMENSIONS

The two-dimensional problem is essentially identical to the one-dimensional one. A solution of a two-dimensional problem may be written as the convolution of a Green's function and a forcing function

$$h(x,y) = g(x,y)*f(x,y) = \iint g(x-\xi,y-\eta)f(\xi,\eta)d\xi d\eta\,, \qquad \text{(A1.3.1)}$$

The forcing function is only known on a grid of points $x = i\Delta x$, $y = j\Delta y$ for integers i, j. The difficulties associated with the discretization of the Green's function may be overcome by filtering it with appropriate smoothing filters. The filtering operation is, just as in the one-dimensional case, based on assumptions about the shape of the forcing function between the known values at the grid points. The smoothing filters are in this case

given by

$$b(x,y) = \frac{1}{\Delta x \Delta y} \text{ for } |x| \le \Delta x/2 \text{ and } |y| \le \Delta y/2 , \qquad \text{(A1.3.2a)}$$
$$b(x,y) = 0 \text{ for } |x| > \Delta x/2 \text{ or } |y| > \Delta y/2$$

and

$$t(x,y) = \frac{1}{\Delta x \Delta y}\left(1 - \frac{|x|}{\Delta x} - \frac{|y|}{\Delta y} + \frac{|xy|}{\Delta x \Delta y}\right) \text{ for } |x| \le \Delta x \text{ and } |y| \le \Delta y , \qquad \text{(A1.3.2b)}$$
$$t(x,y) = 0 \text{ for } |x| > \Delta x \text{ or } |y| > \Delta y ,$$

both normalized to be of unit volume.

The Fourier transforms of $b(x,y)$ and $t(x,y)$ are given by

$$\hat{b}(k_x,k_y) = \frac{1}{\Delta x \Delta y} \int_{-\Delta x/2}^{\Delta x/2} \int_{-\Delta y/2}^{\Delta y/2} e^{-ik_x x} e^{-ik_y y} dx dy = \frac{\sin(k_x \Delta x/2)\sin(k_y \Delta y/2)}{(k_x \Delta x/2)(k_y \Delta y/2)} \qquad \text{(A1.3.3a)}$$

and

$$\hat{t}(k_x,k_y) = \frac{1}{\Delta x \Delta y} \int_{-\Delta x}^{\Delta x} \int_{-\Delta y}^{\Delta y} \left(1 - \frac{|x|}{\Delta x} - \frac{|y|}{\Delta y} + \frac{|xy|}{\Delta x \Delta y}\right) e^{-ik_x x} e^{-ik_y y} dx dy \qquad \text{(A1.3.3b)}$$
$$= \frac{\sin^2(k_x \Delta x/2)\sin^2(k_y \Delta y/2)}{(k_x \Delta x/2)^2 (k_y \Delta y/2)^2}$$

Defining $\bar{g}(x,y) = g(x,y) * b(x,y)$ and $\bar{\bar{g}}(x,y) = g(x,y) * t(x,y)$ and denoting function values at $x = x_i$, $y = y_j$ by the subscript ij, the two-dimensional versions of (A1.2.6a) and (A1.2.6b) are

$$\bar{h}_{ij} = \Delta x \Delta y \, \bar{g}_{ij} * f_{ij} , \qquad \text{(A1.3.4a)}$$

and

$$\bar{\bar{h}}_{ij} = \Delta x \Delta y \, \bar{\bar{g}}_{ij} * f_{ij} , \qquad \text{(A1.3.4b)}$$

The above equations define approximations to the solution $h(x,y)$ at $x = x_i$, $y = y_j$ as discrete two-dimensional convolutions of the filters $\bar{g}_{ij}$ or $\bar{\bar{g}}_{ij}$ with the forcing f_{ij}.

Similarly, the two-dimensional versions of (A1.2.8a) and (A1.2.8b) are

$$\hat{\bar{g}}(k_x,k_y) = \hat{g}(k_x,k_y)\hat{b}(k_x,k_y) \qquad \text{(A1.3.5a)}$$

and

$$\hat{\bar{\bar{g}}}(k_x,k_y) = \hat{g}(k_x,k_y)\hat{t}(k_x,k_y) . \qquad \text{(A1.3.5b)}$$

As in the one-dimensional case the Fourier transforms $\hat{\bar{g}}(k_x,k_y)$ and $\hat{\bar{\bar{g}}}(k_x,k_y)$ are often easier to work with than the original transform $\hat{g}(k_x,k_y)$ because they decay more rapidly as k_x and $k_y \to \pm\infty$.

APPENDIX 2: STREAM FUNCTION FOR LINEAR RHEOLOGY — 2D

This appendix derives a stream function $\hat{\psi}$ in the wave number domain for linear Newtonian flow in two-dimensions satisfying the biharmonic equation (4.5.8) and the boundary conditions (4.5.9), (4.5.10), (4.5.11) and (4.5.12). The stream function is given by (4.5.13)

$$\hat{\psi} = (A + Cz)\sinh kz + (B + Dz)\cosh kz \ .$$

It follows that

$$\frac{\partial \hat{\psi}}{\partial z} = (kA + kCz + D)\cosh kz + (kB + kDz + C)\sinh kz$$

$$\frac{\partial^2 \hat{\psi}}{\partial z^2} = (k^2A + k^2Cz + 2kD)\sinh kz + (k^2B + k^2Dz + 2kC)\cosh kz$$

$$\frac{\partial^3 \hat{\psi}}{\partial z^3} = (k^3A + k^3Cz + 3k^2D)\cosh kz + (k^3B + k^3Dz + 3k^2C)\sinh kz \ .$$

The boundary conditions (4.5.9), (4.5.10), (4.5.11) and (4.5.12) then lead to the following equations for the determination of the constants A, B, C and D.

At the datum surface $z = 1$:

$$(k^2(A + C) + kD)\sinh k + (k^2(B + D) + kC)\cosh k = \Delta\hat{\sigma}_{\substack{xz \\ z=1}} = \Delta\hat{z}_s \ ,$$

$$k^2(A + C)\cosh k + k^2(B + D)\sinh k = i\Delta\hat{\sigma}_{\substack{zz \\ z=1}} = -i\cot\alpha_0\Delta\hat{z}_s \ .$$

At the base $z = 0$:

$$B = -c\Delta\hat{z}_b \ ,$$

$$(kA + D) - ck(kB + C) = -(2 + c)\Delta\hat{z}_b \ .$$

The derivation of A, B, C and D from the above equations is rather tedious and will not be carried out explicitly. The result is

$$A = \frac{1}{k^2K}\left\{-kH_c\Delta\hat{\sigma}_{\substack{xz \\ z=1}} + i(H_c + kH_s)\Delta\hat{\sigma}_{\substack{zz \\ z=1}} - k^2(2(1 + c)k + c^2k^3 - cH_c\sinh k)\Delta\hat{z}_b\right\}$$

$$B = -c\Delta\hat{z}_b$$

$$C = \frac{1}{k^2K}\left\{k(\cosh k - k\sinh k)\Delta\hat{\sigma}_{\substack{xz \\ z=1}} + ik^2\cosh k\ \Delta\hat{\sigma}_{\substack{zz \\ z=1}} + ((2 + c)k^2(\cosh k\sinh k + k) + ck^3(H_c\cosh k + ck^2))\Delta\hat{z}_b\right\}$$

$$D = \frac{1}{k^2K}\left\{(1 + c)k^2\cosh k\ \Delta\hat{\sigma}_{\substack{xz \\ z=1}} - ik(H_c + k\sinh k)\Delta\hat{\sigma}_{\substack{zz \\ z=1}} - ((2 + c)k^2\cosh^2 k + ck^3(H_c\sinh k - k))\Delta\hat{z}_b\right\} ,$$

where

$$K(k) = \cosh^2 k + k^2 + ck(\cosh k\sinh k + k) = H_c\cosh k + (1 + c)k^2$$
$$H_c(k) = \cosh k + ck\sinh k$$
$$H_s(k) = \sinh k + ck\cosh k \ .$$

It follows that the stream function $\hat{\psi}$ is given by

$$\begin{aligned}\hat{\psi} = {} & \frac{1}{k^2K}\left\{-H_ck(1 - z)\sinh(kz) + (1 + c)k^2z\cosh(k(1-z))\right\}\Delta\hat{\sigma}_{\substack{xz \\ z=1}} \\ & + \frac{1}{k^2K}\left\{(H_c + kH_s)\sinh(kz) - H_ckz\cosh(kz) - k^2z\sinh(k(1-z))\right\} i\Delta\hat{\sigma}_{\substack{zz \\ z=1}} \\ & - \frac{1}{k^2K}\left\{((2 + c^2k^2)(1 - z) + c(2 - z))k^3\sinh(kz) + (2 + c)k^2z\cosh k\cosh(k(1-z))\right. \\ & \left. + cH_ck^2(\cosh(k(1-z)) + kz\sinh(k(1-z))) + ck^4(1 - z + c)\cosh(kz)\right\}\Delta\hat{z}_b \ .\end{aligned} \tag{A2.1}$$

The surface and basal values of the stream function are

$$\hat{\psi}_{z=1} = \frac{1+c}{K}\Delta\hat{\sigma}_{\substack{xz\\z=1}} + \frac{H_c\sinh k - k}{k^3 K}(ik\Delta\hat{\sigma}_{\substack{zz\\z=1}}) - \frac{(1+c)H_c + (1+c+c^2k^2)\cosh k}{K}\Delta\hat{z}_b \qquad \text{(A2.2)}$$

and

$$\hat{\psi}_{z=0} = -c\Delta\hat{z}_b \,. \qquad \text{(A2.3)}$$

For linear Newtonian rheology, *i.e.* for $n = 1$, the ice flux perturbation Δq (*cf.* (4.3.23)

$$\Delta q = \int_0^1 \Delta u dz + (1+c)\Delta z_s - c\Delta z_b \,.$$

By the definition of the stream function (4.5.1), $\Delta u = (\partial\psi/\partial z)$. Therefore, $\Delta\hat{q}$ may be expressed as

$$\Delta\hat{q} = \hat{\psi}_{z=1} - \hat{\psi}_{z=0} + (1+c)\Delta\hat{z}_s - c\Delta\hat{z}_b \,.$$

The previously derived expressions for $\hat{\psi}_{z=1}$ and $\hat{\psi}_{z=0}$ and the above expression for $\Delta\hat{q}$ make it possible to identify the ice flux perturbation components Δq_e, Δq_n, Δq_a and Δq_b (*cf.* subsection 4.3.7), predicted by linear Newtonian rheology. Their Fourier transforms are

$$\begin{aligned}
\Delta\hat{q}_e &= ((1+c)/K)\Delta\hat{\sigma}_{\substack{xz\\z=1}}\,, \quad \text{where } \Delta\hat{\sigma}_{\substack{xz\\z=1}} = \Delta\hat{z}_s \\
\Delta\hat{q}_n &= ((H_c\sinh k - k)/(k^3K))(ik\Delta\hat{\sigma}_{\substack{zz\\z=1}})\,, \quad \text{where } \Delta\hat{\sigma}_{\substack{zz\\z=1}} = \cot\alpha_0(-\Delta\hat{z}_s) \qquad \text{(A2.4)} \\
\Delta\hat{q}_a &= (1+c)\Delta\hat{z}_s \\
\Delta\hat{q}_b &= -(((1+c)H_c + (1+c+c^2k^2)\cosh k)/K)\Delta\hat{z}_b \,.
\end{aligned}$$

The above expressions for the flux perturbation components Δq_e, Δq_n, Δq_a and Δq_b are further discussed in subsections 4.5.5 and 4.5.6 of the dissertation.

APPENDIX 3: STREAM FUNCTION FOR LINEAR RHEOLOGY — 3D

This appendix derives a stream function $\hat{\psi}_i$ in the wave number domain for linear Newtonian flow in three-dimensions satisfying the biharmonic equation (5.4.10) and the (Fourier transform of) the boundary conditions (5.4.18) to (5.4.23). The stream function is given by (5.4.11)

$$\hat{\psi}_i = (A_i + C_i z)\sinh kz + (B_i + D_i z)\cosh kz \,.$$

It follows that

$$\begin{aligned}
\frac{\partial\hat{\psi}_i}{\partial z} &= (kA_i + kC_i z + D_i)\cosh kz + (kB_i + kD_i z + C_i)\sinh kz \\
\frac{\partial^2\hat{\psi}_i}{\partial z^2} &= (k^2A_i + k^2C_i z + 2kD_i)\sinh kz + (k^2B_i + k^2D_i z + 2kC_i)\cosh kz \\
\frac{\partial^3\hat{\psi}_i}{\partial z^3} &= (k^3A_i + k^3C_i z + 3k^2D_i)\cosh kz + (k^3B_i + k^3D_i z + 3k^2C_i)\sinh kz \,.
\end{aligned}$$

The above expression for $\hat{\psi}_i$ involves 12 constants, but there are only 6 independent boundary conditions which can be invoked to determine the constants. This situation arises because the stream function corresponding to a given velocity field is not uniquely determined. Any gradient vector can be added to the stream function $\vec{\psi}$, without affecting the velocity field $\vec{u} = \vec{\nabla}\times\vec{\psi}$. A gradient vector is a vector $\vec{f}$, which is the gradient of a potential ϕ, *i.e.* $\vec{f} = \vec{\nabla}\phi$. This property of the stream function follows from the vector identity $\vec{\nabla}\times(\vec{\psi} + \vec{f}) = \vec{\nabla}\times\vec{\psi} + \vec{\nabla}\times(\vec{\nabla}\phi) = \vec{\nabla}\times\vec{\psi}$.

A unique stream function can be determined by imposing constraints on the stream function which leave the corresponding velocity field unaltered. First, the stream function may be assumed to be divergence free, *i.e.* $\vec{\nabla}\cdot\vec{\psi} = 0$, without loss of generality. If the stream function is not divergence free then it may be modified, without changing the corresponding velocity field, by subtracting a gradient vector $\vec{\nabla}\phi$, which satisfies $\nabla^2\phi = \vec{\nabla}\cdot\vec{\psi}$ and the resulting modified stream function will be divergence free. Assuming that the stream function is divergence free, one may write the constants A_z, C_z, B_z

and D_z in the above expression for $\hat{\psi}_i$ in terms of the other 8 constants as

$$A_z = -i\,(k_x(B_x - C_x/k) + k_y(B_y - C_y/k))/k\ ,\quad C_z = -i\,(k_xD_x + k_yD_y)/k\ ,$$
$$B_z = -i\,(k_x(A_x - D_x/k) + k_y(A_y - D_y/k))/k\ ,\quad D_z = -i\,(k_xC_x + k_yC_y)/k\ .$$

Second, any Laplacian gradient vector may be added to the stream function without affecting the corresponding velocity field or the divergence of the the stream function. A Laplacian gradient vector is a gradient vector $\vec{f} = \vec{\nabla}\phi$, which is derived from a potential ϕ, that satisfies Laplace's equation, $\nabla^2\phi = 0$. This property of the stream function follows from the vector identity $\vec{\nabla}\cdot(\vec{\psi} + \vec{f}) = \vec{\nabla}\cdot\vec{\psi} + \vec{\nabla}\cdot(\vec{\nabla}\phi) = \vec{\nabla}\cdot\vec{\psi} + \nabla^2\phi = \vec{\nabla}\cdot\vec{\psi}$. By subtracting a suitable Laplacian gradient vector from the stream function, it is possible to show that the constants A_x and B_x in the above expression for $\hat{\psi}_i$ may be assumed to be equal to zero without loss of generality. This leaves 6 independent constants which are uniquely determined by the 6 boundary conditions.

Taking the Fourier transform of the boundary conditions (5.4.18) to (5.4.23) then leads to the following equations for the determination of the constants C_x, D_x, A_y, B_y, C_y and D_y (note that (5.4.20a) and (5.4.20b) result in the same equation).

At the datum surface $z = 1$:

$$(-k_x^2(A_y + C_y) + k_xk_yC_x - kD_y)\sinh k + (-k_x^2(B_y + D_y) + k_xk_yD_x - kC_y)\cosh k = \Delta\hat{\sigma}_{\substack{xz\\z=1}} = \Delta\hat{z}_s\ ,$$

$$(-k_xk_y(A_y + C_y) + k_y^2C_x + kD_x)\sinh k + (-k_xk_y(B_y + D_y) + k_y^2D_x + kC_x)\cosh k = \Delta\hat{\sigma}_{\substack{yz\\z=1}} = 0\ ,$$

$$k(-k_x(A_y + C_y) + k_yC_x)\cosh k + k(-k_x(B_y + D_y) + k_yD_x)\sinh k = i\Delta\hat{\sigma}_{\substack{zz\\z=1}} = -i\cot\alpha_0\Delta\hat{z}_s\ .$$

At the base $z = 0$:

$$B_y = c\Delta\hat{z}_b\ ,$$

$$-(k_x^2/k)A_y - (k_xk_y/k^2)D_x - (1 + k_y^2/k^2)D_y + c(k_x^2B_y + kC_y) = -(2 + c)\Delta\hat{z}_b\ ,$$

$$-(k_xk_y/k)A_y + (1 + k_x^2/k^2)D_x + (k_xk_y/k^2)D_y + c(k_xk_yB_y - kC_x) = 0\ .$$

The constants C_x, D_x, A_y, B_y, C_y and D_y determined from the above equations are given by

$$C_x = \frac{1}{k^2K}\left\{-k_xk_y(\sinh k + k/\cosh k + cL)\Delta\hat{\sigma}_{\substack{xz\\z=1}} + ikk_y\cosh k\ \Delta\hat{\sigma}_{\substack{zz\\z=1}} + k_xk_y((2 + c)L\cosh k + ck(H_c\cosh k + ck^2))\,\Delta\hat{z}_b\right\}$$

$$D_x = \frac{1}{k^2K}\left\{k_xk_y(\cosh k + cM)\Delta\hat{\sigma}_{\substack{xz\\z=1}} - ik_y(H_c + k\sinh k)\Delta\hat{\sigma}_{\substack{zz\\z=1}} - k_xk_y((2 + c)M\cosh k + ck(H_c\sinh k - k))\,\Delta\hat{z}_b\right\}$$

$$A_y = \frac{1}{k^2K}\left\{kH_c\Delta\hat{\sigma}_{\substack{xz\\z=1}} - i(k/k_x)(H_c + kH_s)\Delta\hat{\sigma}_{\substack{zz\\z=1}} + k^2(2(1 + c)k + c^2k^3 - cH_c\sinh k)\,\Delta\hat{z}_b\right\}$$

$$B_y = c\Delta\hat{z}_b$$

$$C_y = \frac{1}{k^2K}\left\{-(k(1 + k_y^2/k^2)\cosh k - k_x^2\sinh k - 2(k_y^2/k)M)\Delta\hat{\sigma}_{\substack{xz\\z=1}} - ikk_x\cosh k\ \Delta\hat{\sigma}_{\substack{zz\\z=1}} - ((2+c)(k^2\cosh k\sinh k + kk_x^2 - k_y^2M\sinh k) + ckk_x^2(H_c\cosh k + ck^2))\,\Delta\hat{z}_b\right\}$$

$$D_y = \frac{1}{k^2K}\left\{-((k_x^2 + ck^2)\cosh k - ck_y^2M)\Delta\hat{\sigma}_{\substack{xz\\z=1}} + ik_x(H_c + k\sinh k)\Delta\hat{\sigma}_{\substack{zz\\z=1}} + ((2 + c)(k^2\cosh^2 k - k_y^2M\cosh k) + ckk_x^2(H_c\sinh k - k))\,\Delta\hat{z}_b\right\},$$

where

$$K(k) = \cosh^2 k + k^2 + ck\,(\cosh k\sinh k + k) = H_c\cosh k + (1 + c)k^2$$
$$H_c(k) = \cosh k + ck\sinh k$$
$$H_s(k) = \sinh k + ck\cosh k$$
$$L(k) = (2k + \cosh k\sinh k - k^2\tanh k)/(H_c + \cosh k)$$
$$M(k) = (\cosh^2 k - (1+c)k^2)/(H_c + \cosh k)\ .$$

In the case of two-dimensional flow (*i.e.* $k_y = 0$, $k_x = k$) the above constants A_y, B_y, C_y and D_y reduce to the negative of the constants A, B, C and D which were derived in Appendix 2 for two-dimensional flow, but C_x and D_x are equal to zero. As mentioned in subsection 5.4.2, the reason for the sign change is that the y-coordinate in the three-dimensional x,y,z coordinate system replaces the z-coordinate in the two-dimensional x,z coordinate system as the second coordinate. When this change in the sign is taken into account, the above values of the constants are consistent with the two-dimensional analysis in Appendix 2.

The ice flux perturbation $\Delta\vec{q}$, is by (5.4.5) defined as

$$\Delta\vec{q} = \int_0^1 (\Delta u\vec{a}_x + \Delta v\vec{a}_y)dz + (1+c)\Delta z_s\vec{a}_x - c\Delta z_b\vec{a}_x ,$$

and by (5.4.6) $\Delta\vec{q}$ may be expressed in terms of the stream function as

$$\Delta\vec{q} = \left[\int_0^1 \frac{\partial\psi_z}{\partial y}dz - \psi_{\substack{y\\z=1}} + \psi_{\substack{y\\z=0}} + (1+c)\Delta z_s - c\Delta\hat{z}_b\right]\vec{a}_x + \left[-\int_0^1 \frac{\partial\psi_z}{\partial x}dz + \psi_{\substack{x\\z=1}} - \psi_{\substack{x\\z=0}}\right]\vec{a}_y .$$

Furthermore, the divergence of the ice flux perturbation $\vec{\nabla}\cdot\Delta\vec{q}$ is given by

$$\vec{\nabla}\cdot\Delta\vec{q} = \frac{\partial\Delta q_x}{\partial x} + \frac{\partial\Delta q_y}{\partial y} = \frac{\partial}{\partial x}\left[-\psi_{\substack{y\\z=1}} + \psi_{\substack{y\\z=0}} + (1+c)\Delta z_s - c\Delta\hat{z}_b\right] + \frac{\partial}{\partial y}\left[\psi_{\substack{x\\z=1}} - \psi_{\substack{x\\z=0}}\right].$$

The surface and basal values of $\hat{\psi}_x$ and $\hat{\psi}_y$, and the depth integral of $\hat{\psi}_z$ can be determined from the above expressions for the constants C_x, D_x, A_y, B_y, C_y and D_y. This makes it possible to identify the Fourier transforms of the ice flux perturbation components $\Delta\hat{\vec{q}}_e$, $\Delta\hat{\vec{q}}_n$, $\Delta\hat{\vec{q}}_a$ and $\Delta\hat{\vec{q}}_b$ (*cf.* subsection 4.3.7), predicted by linear Newtonian rheology as follows

$$\Delta\hat{\vec{q}}_e = \left\{\frac{(1+c)k_x}{k^2K}(k_x\vec{a}_x + k_y\vec{a}_y) + \frac{2k_y}{k^4}\left(1 - \frac{2}{H_c + \cosh k}\right)(k_y\vec{a}_x - k_x\vec{a}_y)\right\}\Delta\hat{\sigma}_{\substack{xz\\z=1}}$$

$$\Delta\hat{\vec{q}}_n = \left\{\frac{H_c\sinh k - k}{k^3K}(ik_x\vec{a}_x + ik_y\vec{a}_y)\right\}\Delta\hat{\sigma}_{\substack{zz\\z=1}} \qquad \text{(A3.1)}$$

$$\Delta\hat{\vec{q}}_a = (1+c)\vec{a}_x\Delta\hat{z}_s$$

$$\Delta\hat{\vec{q}}_b = -\left\{\frac{k_x((1+c)H_c + (1+c+c^2k^2)\cosh k)}{k^2K}(k_x\vec{a}_x + k_y\vec{a}_y) + \frac{2(2+c)k_y\sinh k}{k^3(H_c+\cosh k)}(k_y\vec{a}_x - k_x\vec{a}_y)\right\}\Delta\hat{z}_b ,$$

where $\Delta\hat{\sigma}_{\substack{xz\\z=1}} = \Delta\hat{z}_s$ and $\Delta\hat{\sigma}_{\substack{zz\\z=1}} = \cot\alpha_0(-\Delta\hat{z}_s)$.

The long wavelength limit (*i.e.* $k_x, k_y \to 0$) of the above expressions for the flux perturbation components are consistent with the laminar flow approximation (5.3.2) for three-dimensional flow in the case of linear Newtonian rheology (*i.e.* for $n = m = 1$).

The expressions for $\Delta\hat{\vec{q}}_e$ and $\Delta\hat{\vec{q}}_b$ in (A3.1) are the sum of two terms each, one proportional to $(k_x\vec{a}_x + k_y\vec{a}_y)$ and the other proportional to $(k_y\vec{a}_x - k_x\vec{a}_y)$. The terms proportional to $(k_x\vec{a}_x + k_y\vec{a}_y)$ are similar to the expressions for $\Delta\hat{q}_e$ and $\Delta\hat{q}_b$ in (A2.4) for two-dimensional flow. The terms proportional to $(k_y\vec{a}_x - k_x\vec{a}_y)$ have no counterparts in two-dimensional flow and arise from horizontal circulation in the flow. The flux perturbation described by these terms is divergence free. Since the steady state equation for three-dimensional flow (5.2.11), only involves the divergence of the flux perturbation, these terms have no effect on the formation of steady state ice surface undulations.

The expression for $\Delta\hat{\vec{q}}_n$ in (A3.1) is identical to the expression for $\Delta\hat{q}_n$ in (A2.4) for two-dimensional flow, except that $(ik\Delta\hat{\sigma}_{\substack{zz\\z=1}})$ in (A2.4) is replaced by $(ik_x\vec{a}_x + ik_y\vec{a}_y)\Delta\hat{\sigma}_{\substack{zz\\z=1}}$ in (A3.1). Since multiplication by $(ik_x\vec{a}_x + ik_y\vec{a}_y)$ in the wave number domain corresponds to the gradient operator in the space domain, the flux perturbation $\Delta\hat{\vec{q}}_n$ for three-dimensional flow is a horizontal weighted average of $\vec{\nabla}\Delta\hat{\sigma}_{\substack{zz\\z=1}} = \cot\alpha_0(-\vec{\nabla}z_s)$ in the same way as the flux perturbation Δq_n for two-dimensional flow is a longitudinal weighted average of the derivative $(\partial\Delta\hat{\sigma}_{\substack{zz\\z=1}}/\partial x) = \cot\alpha_0(-\partial z_s/\partial x)$.

The advective term $\Delta\hat{\vec{q}}_a$ in (A3.1) always points in the direction of the long scale datum flow. It is identical to the advective term $\Delta\hat{q}_a$ in (A2.4) for two-dimensional flow.

The Fourier transform of the divergence of the ice flux perturbation follows from (A3.1) and is given by

$$ik_x\Delta\hat{q}_x + ik_y\Delta\hat{q}_y = \frac{1}{k^2K}\left\{i(1+c)k^2k_x\Delta\hat{\sigma}_{\substack{xz\\z=1}} - k(H_c\sinh k - k)\Delta\hat{\sigma}_{\substack{zz\\z=1}}\right. \tag{A3.2}$$
$$\left. - ik^2k_x((1+c)H_c + (1+c+c^2k^2)\cosh k)\,\Delta\hat{z}_b\right\}$$
$$+ i(1+c)k_x\Delta\hat{z}_s\,.$$

The above expression for the divergence of the ice flux perturbation is further analyzed in subsections 5.4.5 and 5.4.6 of the dissertation.

VITA

Tómas Jóhannesson

Born: August 31, 1957, Reykjavík, Iceland

Cand. mag. University of Oslo, 1982

M.Sc. University of Washington, 1984

1 141WW1 TH 1012
5/92 31365